

**The infection biology of the Brassicaceae
smut fungus *Thecaphora thlaspeos* & Mg²⁺
transport and its role for virulence in the
smut fungus *Ustilago maydis***

Inaugural Dissertation

For the attainment of the title of doctor
in the Faculty of Mathematics and Natural Sciences
at the Heinrich Heine University Düsseldorf

presented by

Lesley Ann Plücker

from Bad Arolsen, Germany

Düsseldorf, September 2022

from the Institute for Microbiology
in the Faculty of Mathematical and Natural Sciences
of the Heinrich Heine University Düsseldorf

Published by the permission of the
Faculty of Mathematics and Natural Sciences at
Heinrich Heine University Düsseldorf

Supervisor: Prof. Dr. Michael Feldbrügge
Institute for Microbiology
Heinrich Heine University Düsseldorf

Co-supervisor: Prof. Dr. Laura Rose
Institute for Population Genetics
Heinrich Heine University Düsseldorf

Date of examination: 14th of November 2022

The research detailed in this thesis was conducted from February 2018 until September 2022 in Düsseldorf at the Heinrich Heine University Düsseldorf in the Institute for Microbiology under the supervision of Prof. Dr. Michael Feldbrügge.

Parts of this thesis are published in:

Plücker, L.; Bösch, K.; Geißl, L.; Hoffmann, P.; Göhre, V. Genetic Manipulation of the Brassicaceae Smut Fungus *Thecaphora thlaspeos*. *J. Fungi* **2021**, *7*, 38.

<https://doi.org/10.3390/jof7010038>

Content

Content	IV
Summary	VI
Zusammenfassung	VIII
Abbreviations	XI
1 Introduction	15
1.1 The versatility of plant-microbe interactions	15
1.2 Infection biology of biotrophic fungi	16
1.3 Challenges in modern agriculture	17
1.4 Smut fungi and their scientific and economic relevance	18
1.5 The life cycle of <i>U. maydis</i>	19
1.6 The lifecycle of <i>T. thlaspeos</i>	20
2 Aims of this thesis	22
3 Results and Discussion	23
3.1 Microscopic characterization of <i>T. thlaspeos</i> infection biology	23
3.1.1 <i>Background</i>	23
3.1.2 <i>Results</i>	25
3.1.3 <i>Discussion</i>	37
3.2 <i>Thecaphora thlaspeos</i> Pit1 complementation analysis in <i>Ustilago maydis</i>	44
3.2.1 <i>Background</i>	44
3.2.2 <i>Results</i>	45
3.2.3 <i>Discussion</i>	70
3.3 Magnesium transport in the smut fungus <i>Ustilago maydis</i>	75
3.3.1 <i>Background</i>	75
3.3.2 <i>Results</i>	79
3.3.3 <i>Discussion</i>	114
4 Conclusions and Outlook	128
5 Material and Methods	133
5.1 Material	133

5.1.1	<i>Solutions, media, enzymes, kits and chemicals</i>	133
5.1.2	<i>Oligonucleotides</i>	140
5.1.3	<i>Plasmids</i>	143
5.1.4	<i>Strains/Lines</i>	148
5.2	Microbiologic, cell biologic and genetic methods.....	151
5.2.1	<i>Escherichia coli</i>	151
5.2.2	<i>Saccharomyces cerevisiae</i>	152
5.2.3	<i>T. thlaspeos</i>	154
5.2.4	<i>U. maydis</i>	156
5.2.5	<i>Zea mays</i>	159
5.2.6	<i>Arabidopsis thaliana/ Ar. hirsuta / Ar. alpina</i>	159
5.3	Molecular biologic methods.....	161
5.3.1	<i>Isolation of nucleic acids</i>	161
5.3.2	<i>Working with nucleic acids</i>	162
5.3.3	<i>Southern Blot analysis</i>	166
5.3.4	<i>DNA sequence analysis</i>	169
5.4	Microscopy and image processing.....	169
5.4.1	<i>Microscopes</i>	169
5.4.2	<i>Cell Tracker™ blue (CMAC) staining</i>	170
5.4.3	<i>Latrunculin A</i>	170
5.5	Inductively coupled plasma mass spectrometry	170
5.6	Computer programs and bioinformatics.....	172
5.6.1	<i>Analysis of DNA and amino acid sequences</i>	172
5.6.2	<i>Data analysis, writing and graphical design</i>	173
6	References.....	174
7	Supplements	199
8	Acknowledgements.....	218
	Statutory declaration	219
	Eidesstattliche Erklärung.....	219

Summary

Detailed understanding of a plant pathogen's life cycle and interaction with its host is essential for the establishment of model pathosystems in basic research as well as the development of targeted drugs and treatments in applied research. Smut fungi are a group of plant pathogenic fungi that infect mostly grasses, including essential crop plants like barley, maize, oats, wheat, sugar cane and sorghum. An important representative is *Ustilago maydis*, a fungus that served the last decades as a scientific model for DNA recombination and repair, signalling pathways, translational and posttranslational regulation, cell cycle regulation as well as mating, morphogenesis and pathogenicity. *Thecaphora thlaspeos* on the other hand, is a dicot-infecting smut fungus of the *Thecaphora*-clade, related to the model smut *U. maydis*. While the grass smut fungi infect crop plants, *T. thlaspeos* infects Brassicaceae plants, in which it establishes a symptomless, systemic and long-lasting biotrophic interaction, and overwinters with perennial hosts as an endophyte. Under lab conditions this includes colonization of the model plant *Arabidopsis thaliana*, which allows to utilize its vast genetic resources available for smut fungi research.

In this work I provide a novel insight into the infection biology of *T. thlaspeos* with a detailed microscopic analysis of the infection structures formed during the early infection phase. This allowed the identification of specific appressoria-like penetration structures on the plant root as well as the leaf surface, which are conserved in the hosts *Arabis alpina* and *Arabis hirsuta* but also in *A. thaliana*. Appressoria-like structures are formed on the root surface, occasionally resulting in rhizodermis cells filled with fungal hyphae, although this colonization does not seem to be essential for successful infection via the roots. On the leaf surface of cotyledons and true leaves, I observed that hyphae of germinated *T. thlaspeos* teliospores form either appressoria-like structures on epidermal cells, on the guard cells or growth directly through the stoma. In contrast to other plant-pathogenic fungi, the guard cells are subsequently colonized before *T. thlaspeos* continues to grow further intracellularly towards the vasculature. These colonized guard cells seem to die during the process. These observations set the foundation for the analysis of tissue resolved molecular infection processes in the future.

Additionally, a putative virulence factor of *T. thlaspeos*, the protein THTG_00998, was characterized in *U. maydis* based on homology to the *U. maydis* virulence factor Pit1. While *Ttpit1* cannot complement the *pit1*Δ deletion phenotype in *U. maydis*, a role for Pit1 in Mg²⁺ transport was suggested. Subsequent analysis of this hypothesis in *U. maydis* could not show that Pit1 functions as a Mg²⁺ transporter, but my experimental data to support the hypothesis of Pit1 functioning as transporter. Together with new structural information on Pit1 supporting a role as receptor, this now provides a new angle to approach the question and sets the foundation for further studies to elucidate its function. Alongside this project a transformation protocol for *T. thlaspeos* protoplasts was developed and published in Journal of Fungi. In the future this will allow the analysis of interesting genetic targets directly in *T. thlaspeos* without the need of a surrogate system.

Besides the hypothesized connection of Pit1 to Mg²⁺ transport in this thesis, a previous study already made an interesting observation with regard to Mg²⁺ homeostasis in *U. maydis* infected maize tissue: It was shown, that Mg concentration is reduced in *U. maydis* infected maize tissue although these are sink tissues with increased phloem flow. To gain first insights into Mg²⁺ homeostasis in *U. maydis* and its potential contribution to virulence an inventory of Mg²⁺ transporters in *U. maydis* was generated. In difference to *S. cerevisiae*, transporter candidates from several different families could be identified, including the well characterized CorA-type Mg²⁺ transporter family. Further analysis of two CorA-type Mg²⁺ transporter candidates identified in *U. maydis*, Alr1 and Mnr2 revealed that both share features typical for plasma membrane and well as vacuole localized Mg²⁺ transporters. While Alr1 appeared indispensable for Mg²⁺ uptake into the cell, both Alr1 and Mnr2 seem equally important to maintain WT-like intracellular Mg²⁺ levels. Based on my data I propose that Alr1 and Mnr2 operate as heterooligomers, while the composition of the heterooligomer determines localization either to the vacuole or the plasma membrane. Furthermore, deletion of *alr1* in *U. maydis* results in a filamentation defect which blocks infection on the plant surface. In contrast, deletion of *mnr2* resulted only in a very slight decrease in virulence, that did not affect the overall Mg reduction in the infected leaf in comparison to the WT. While it is not clear if *U. maydis* interferes with its host Mg²⁺ homeostasis, I hypothesize that Mg²⁺ transporters could contribute to *U. maydis* virulence by taking up Mg²⁺ at the points of cell-cell passage to weaken the plant cell wall and at the infection site to redirect sugar partitioning. In the future,

a better understanding of the role of Mg^{2+} for infection might set the basis to develop new approaches in crop protection like broad spectrum fungicides that target common traits of the pathogens Mg^{2+} homeostasis.

Taken together, the results presented in this thesis greatly contribute to our knowledge on the *T. thlaspeos* infection biology set the foundation to gain further insights on the molecular level of the interaction with the host in the future. The technical advances in the transformation protocol have biggest impact on *T. thlaspeos* research to establish it as a model system in the field. Additionally, the extensive knowledge about *U. maydis* is expanded with an initial characterization of Mg^{2+} homeostasis, a field not yet investigated in this fungus.

Zusammenfassung

Genaueres Verständnis vom Lebenszyklus von Pflanzenpathogenen und der Interaktion mit ihrer Wirtspflanze ist entscheidend, um Modell-Pathogen-Systeme in der Grundlagenforschung zu etablieren und zielgerichtete Pflanzenschutzmittel und Behandlungen in der angewandten Forschung zu entwickeln. Brandpilze sind eine Gruppe pflanzenpathogener Pilze, die hauptsächlich Gräser infizieren, unter anderem wichtige Nutzpflanzen wie Gerste, Mais, Hafer, Weizen, Zuckerrohr und Hirse. Ein wichtiger Vertreter ist *Ustilago maydis*, ein Pilz, der in den letzten Dekaden als wissenschaftliches Modell für DNA Rekombination und – Reparatur, Signalwege, translationale und post-translationale Regulation, Zellzyklus Regulation sowie Paarung, Morphogenese und Pathogenität gedient hat. Auf der anderen Seite ist *Thecaphora thlaspeos* ein Dikotyledone-infizierender Brandpilz der *Thecaphora*-Klade, der verwandt mit dem Modellbrandpilz *U. maydis* ist. Während Gräser-infizierende Brandpilze Nutzpflanzen befallen, infiziert *T. thlaspeos* Brassicaceen, mit denen er eine symptomlose, systemische und langanhaltende biotrophe Interaktion eingeht und als Endophyt mit seinen mehrjährigen Wirtspflanzen überwintert. Unter Laborbedingungen wird ebenfalls die Modellpflanze *Arabidopsis thaliana* kolonisiert, wodurch deren enorme genetische Ressourcen für die Brandpilzforschung nutzbar werden.

Dieser Arbeit bietet neue Einblicke in die Infektionsbiologie von *T. thlaspeos* mit detaillierten mikroskopischen Analysen der Infektionsstrukturen, die während der frühen Phase der Infektion gebildet werden. Dies ermöglichte die Identifikation

spezifischer Appressorien-ähnlicher Strukturen, die auf der Wurzeloberfläche gebildet werden und gelegentlich zur vollständigen Kolonisierung einzelner Rhizodermiszellen mit Pilzhypen führen, wobei diese Kolonisierung für die erfolgreiche Infektion über die Wurzeln nicht essentiell scheint. Auf der Blattoberfläche von Kotyledonen und echten Blättern konnte gezeigt werden, dass Hyphen von keimenden *T. thlaspeos* Teliosporen entweder Appressorien-ähnliche Strukturen auf Epidermiszellen oder Schließzellen bilden oder direkt durch das Stoma wachsen. Im Gegensatz zu anderen pflanzenpathogenen Pilzen werden die Schließzellen anschließend kolonisiert bevor *T. thlaspeos* intrazellulär weiter in Richtung Vaskulatur wächst. Die Schließzellen scheinen durch den Prozess der Kolonisierung zu sterben. Diese Beobachtungen bilden die Grundlage für die zukünftige gewebebezogene Analyse des Infektionsprozesses auf molekularer Ebene.

Zusätzlich wurde ein potentieller Virulenzfaktor von *T. thlaspeos*, das Protein THTG_00998, basierend auf seiner Homologie zum Virulenzfaktor Pit1 aus *U. maydis* in *U. maydis* charakterisiert. Obwohl *Ttpit1* den *pit1Δ* Deletionsphänotyp nicht komplementieren konnte, wurden Hinweise für eine Rolle von Pit1 im Mg^{2+} Transport gefunden. Die anschließende Analyse dieser Hypothese in *U. maydis* konnte zwar nicht zeigen, dass Pit1 als Mg^{2+} Transporter fungiert, doch die experimentellen Daten unterstützen die Hypothese, dass Pit1 als Transporter fungiert. Zusammen mit neuen Informationen zur Struktur von Pit1, die eine Funktion als Rezeptor suggerieren, stellt dies einen neuen Ansatzpunkt dar, um die Funktion von Pit1 zu untersuchen und bildet die Basis für weitere Studien. Parallel dazu wurde ein Transformationsprotokoll für *T. thlaspeos* Protoplasten entwickelt und im Journal of Fungi publiziert. In Zukunft wird es dadurch möglich sein, interessante Gene direkt in *T. thlaspeos* zu untersuchen, ohne dass auf ein Modellsystem zurückgegriffen werden muss.

Neben einer hypothetischen Verbindung von Pit1 zum Mg^{2+} Transport in dieser Arbeit, wurde in einer früheren Studie eine interessante Beobachtung bezüglich der Mg^{2+} Homöostase in *U. maydis* infiziertem Maisgewebe gemacht: Es wurde gezeigt, dass die Mg^{2+} Konzentration in *U. maydis* infiziertem Gewebe reduziert ist, obwohl diese Sink-Gewebe mit verstärktem Phloem-Import darstellen. Um erste Einblicke in die Mg^{2+} Homöostase von *U. maydis* und deren potenziellem

Beitrag zur Virulenz zu gewinnen, wurde ein Mg^{2+} Transporter-Inventar für *U. maydis* erstellt. Im Gegensatz zu *Saccharomyces cerevisiae*, konnten Transporter Kandidaten von mehreren Familien, einschließlich der gut charakterisierten CorA Mg^{2+} Transporter, identifiziert werden. Die weitere Analyse der CorA Mg^{2+} Transporter Kandidaten aus *U. maydis*, Alr1 und Mnr2 zeigte, dass beide typische Eigenschaften für Plasmamembran- sowie Vakuolenmembran-lokalisierte Mg^{2+} Transporter besitzen. Während Alr1 unentbehrlich für die Aufnahme von Mg^{2+} in die Zelle zu sein scheint, scheinen Alr1 und Mnr2 beide gleich wichtig zu sein, um Wildtyp-typische Mg^{2+} Level in der Zelle aufrecht zu erhalten. Basierend auf diesen Daten stelle ich die Hypothese auf, dass Alr1 und Mnr2 als Heterooligomere fungieren, während die Zusammensetzung des Heterooligomers die Lokalisation in der Vakuolenmembran oder Plasmamembran bestimmt. Außerdem führt die Deletion von *alr1* in *U. maydis* zu einem Defekt in der Filament-Induktion, der die Infektion der Pflanze bereits auf ihrer Oberfläche stoppt. Im Gegensatz dazu, resultiert die Deletion von *mnr2* nur in einer leicht verminderten Virulenz, die insgesamt die Reduktion der Mg Konzentration im infizierten Blatt im Vergleich zum Wildtyp nicht beeinflusst. Ich stelle die Hypothese aus, dass Mg^{2+} Transporter zur Virulenz von *U. maydis* beitragen, indem sie Mg^{2+} an den Punkten, an denen der Pilz von einer Zelle zur nächsten Zelle wächst, aufnehmen, um die pflanzliche Zellwand an dieser Stelle zu schwächen und um den Assimilat-Transport in der Pflanze zur Infektionsstelle umzuleiten. In Zukunft könnte ein besseres Verständnis der Rolle von Mg^{2+} für die Infektion die Basis bilden, um neue Ansätze zum Pflanzenschutz, wie Breitspektrum Fungizide, die gemeinsame Merkmale der pathogene Mg^{2+} Homöostase angreifen, zu entwickeln.

Zusammenfassend tragen die Ergebnisse aus dieser Arbeit in großem Maße zu unserem Verständnis der *T. thlaspeos* Infektionsbiologie bei und bilden die Grundlage, zukünftig weitere Einblicke auf molekularem Level in die Interaktion mit der Wirtspflanze zu gewinnen. Der technische Fortschritt mit dem Transformationsprotokoll hat größten Einfluss auf die *T. thlaspeos* Forschung, um *T. thlaspeos* als Modellsystem zu etablieren. Zusätzlich, wird das breite Wissen über *U. maydis* mit der initialen Charakterisierung der Mg^{2+} Homöostase ergänzt, die in diesem Pilz vorher noch nicht untersucht wurde.

Abbreviations

°C	degree Celsius
μE	microeinstein
μl	microliter
μM	micromolar
aa	amino acid
ACDP	Ancient conserved domain protein
ad	fill up to final volume
ALR1	Aluminum resistance 1
AM	Arbuscular Mycorrhizal
ATP	Adenosine triphosphate
BB	Bad Berneck
BLAST	Basic Local Alignment Search Tool
bp	base pairs
cAMP	cyclic adenosine monophosphate
CaMV35S	35S promoter of Cauliflower Mosaic Virus
CBS	cystathionine-β-synthase domain
CCTOP	Consensus Constrained TOPology prediction web server
cDNA	complementary DNA
CDS	coding sequence
cGMP	cyclic guanosine monophosphate
CM	complete medium
CMAC	7-Amino-4-Chlormethylcumarin
CNGCs	cyclin-nucleotide-gated nonselective ion channels
CNNM	cyclin M-type divalent metal cat- ion transport mediators
Col-0	Columbia
COLORFUL-PDF1.2apro	COLORFUL reporter line of the jasmonic acid/ethylene inducible promoter PDF1.2a (PLANT DEFENSIN 1.2a)
COLORFUL-PR1pro	COLORFUL reporter line of the salicylic acid inducible promoter PR1
COLORFUL-VSP2pro	COLORFUL reporter line of the jasmonic acid inducible promoter VSP2 (VEGETATIVE STORAGE PROTEIN 2)
CorA	Cobalt resistance A
CorB	Cobalt resistance B
C-terminal	carboxy-terminal
DAMPs	damage-associated molecular patterns
DF	downstream flank
DIC	differential interference contrast
DNA	Desoxyribonucleic acid
dpi	days post infection
DUF21	Domain of unknown function 21
EB	Eselsburg
EDS1	enhanced disease susceptibility1
eGFP	enhanced GFP
EMS	Ethyl methanesulfonate
ER	endoplasmic reticulum
et al.	and other
ETI	Effector triggered immunity

FET3	multicopper ferroxidase
FRE1	ferric reductase
FRET	fluorescence resonance energy transfer
gDNA	genomic DNA
GEF	guanine nucleotide exchange factor
GFP	green fluorescent protein
GIPF	germination inducing plant factor
GPRC	G-protein-coupled receptors
h	hour
H2O _{bid.}	twice distilled water
HL	Hohe Leite
<i>Hpa</i>	<i>Hyaloperonospora arabidopsidis</i>
HR	hypersensitive response
<i>hsp70</i>	heat shock protein 70
ICP-MS	Inductively Coupled Plasma- Mass Spectrometry
IMP1	Mitochondrial inner membrane protease subunit 1
<i>IP</i>	succinate dehydrogenase-encoding gene locus
ITS	internal transcribed spacer
kb	kilo base
KC	Kaitlyn Courville
l	litre
LF1	<i>T. thlaspeos</i> strain LF1
LF2	<i>T. thlaspeos</i> strain LF2
LP	Lesley Plücker
LPE10	Magnesium transporter LPE10
LRR	leucine-rich-repeat
<i>LTl6b</i>	low temperature induced protein 6b
m	mass
M	molar (mol/l)
MAM3	ACDP-tape Mg transporter
MAPK	Mitogen-activated protein kinase
MDPI	Multidisciplinary Digital Publishing Institute
mGFP	monomeric GFP
MgtE	Magnesium transporter E
min	minute
ml	millilitre
mM	millimolar
MNR2	Manganese resistance 2
mRNA	messenger RNA
MRS2	magnesium transporter MRS2
MSN	Murashige & Skoog medium incl. Nitsch Vitamins
<i>N7</i>	nuclear localization signal
NB-LRR	nucleotide binding, leucine rich repeat
NCBI	National Center for Biotechnology Information
NCBI	National centre for Biotechnology Information
NIPA	nonimprinted in Prader-Willi/Angelman syndrome
NM	Nitrate medium
NRAMP	Natural resistance-associated macrophage proteins
NRMTs	NRAMP- related magnesium transporters

N-terminal	amino terminal
OD	optical density
ORF	open reading frame
PAD4	phytoalexin deficient4
PAMP	Pathogen associated molecular pattern
PBS	Phosphate buffered saline
PCR	polymerase chain reaction
PCWDEs	plant cell wall degrading enzymes
PEG	Polyethylene glycol
Pep1	Protein essential during penetration 1
PFAM	Protein Families
PI	propidium iodide
Pit1	protein(s) important for tumours 1
PKA	Protein kinase A
POX12	maize peroxidase
<i>PR1</i>	pathogenesis-related 1
PRESTO-Tango	parallel receptorome expression and screening via transcriptional output - Tango
PRRs	pattern recognition receptors
PTI	PAMP triggered immunity
R protein	Resistance protein
RH	relative humidity
RH	Ronheim
RK	Ronny Kellner
RNA	Ribonucleic acid
RNAi	RNA interference
RNAseq	RNA sequencing
RPM	revolutions per minute
<i>rps28</i>	ribosomal protein 28
RT	room temperature
SA	salicylic acid
SAG101	Senescence Associated Gene101
sec	second(s)
SLC11	Solute carrier 11
SLC41	Solute carrier 41
SP	signal peptide
T-DNA	transfer DNA
Tin2	Tumour inducing 2
TM	transmembrane domain
TMHMM	TransMembrane prediction using hidden Markov models
TMRE	Tetramethylrhodamine, ethyl ester
<i>Tt</i>	<i>T. thlaspeos</i>
U	unit (enzyme activity)
<i>UBQ10</i>	POLYUBIQUITIN 10 promoter
UF	upstream flank
<i>Um</i>	<i>U. maydis</i>
UPR	Unfolded protein response
V	volume
v/v	volume per volume

Abbreviations

w/v	weight per volume
WGA	Wheat germ agglutinin
wpi	weeks post infection
WT	wild type
x g	acceleration of gravity
YL	YEPSlight
ZmMGT10	<i>Zea mays</i> Magnesium transporter 10
ZmMGT4	<i>Zea mays</i> Magnesium transporter 4
ZmMGT6	<i>Zea mays</i> Magnesium transporter 6
ZmTTK1	<i>Zea mays</i> Tin2-targeting kinase 1
Δ	delta, symbolizes a deletion
μm	micrometer

The infection biology of the Brassicaceae smut *Thecaphora thlaspeos* & Mg²⁺ transport and its role for virulence in the smut fungus *Ustilago maydis*

1 Introduction

1.1 The versatility of plant-microbe interactions

In their natural environment plants are in constant contact with a multitude of microbes comprising bacteria, archaea, fungi, oomycetes and protists (Hassani, Durán and Hacquard, 2018; Park *et al.*, 2018). The nature of these interactions ranges from mutualistic to parasitic. Prominent mutualistic relationships include phosphate providing mycorrhizal fungi or nitrogen-fixing rhizobial bacteria (Dolatabadian, 2021), while diseases like bacterial speck and cankers caused by *Pseudomonas syringae* pathovars or rice blast disease caused by *Magnaporthe oryzae* are of great ecological and scientific importance (Dean *et al.*, 2012; Mansfield *et al.*, 2012). Corresponding to their infection strategy microbial pathogens are divided in necrotrophic, biotrophic and hemi-biotrophic. The necrotrophic lifestyle has the most severe effect on the plant since the pathogen kills the plant tissue to feed on the remnants. Prominent examples are *Sclerotinia sclerotiorum* causing white mould disease or *Botrytis cinerea* causative agent of grey mould disease (Lo Presti *et al.*, 2015). This life style often results in a big host range of the pathogens (Doehlemann *et al.*, 2017). In contrast, biotrophs are characterized by their ability to infect their host without killing it, resulting in genetic adaptation and specialization to their host (Spanu and Kämper, 2010). Well known representatives are *Blumeria graminis* causative agent of powdery mildew or crown gall disease caused by *Agrobacterium tumefaciens*. Hemibiotrophs reside within the spectrum as they initially grow biotrophic to then later switch to necrotrophic growth (Spanu and Panstruga, 2017). Examples include the already mentioned *P. syringae* or *M. oryzae* (Lo Presti *et al.*, 2015). Independent of their life style, the life cycles of plant pathogenic fungi generally follow the same principle: dispersal of infectious particles (mostly spores), attachment to the host and host recognition, penetration, colonization and reproduction/ production of new infectious particles (Meng *et al.*, 2009).

In order to prevent infection, plants have evolved a complex multi-layered innate immunity (Wiermer, Feys and Parker, 2005). Years of coevolution between plants and pathogens resulted in molecularly complex recognition and response mechanisms (Feys *et al.*, 2001; Asai and Shirasu, 2015). In a first basal layer of resistance, defence responses are triggered if plant pattern recognition receptors (PRRs) recognize conserved pathogen-associated molecular patterns (PAMPs), a process called PAMP-triggered immunity (PTI). To overcome PTI pathogens deliver effector proteins to the infection site which increase their virulence. In turn, those effector proteins can be recognized by corresponding plant resistance (R) proteins that mediate an enhanced defence reaction including accumulation of reactive oxygen species, activation of mitogen-activated protein kinases (MAPKs), callose deposition, transcriptional reprogramming, salicylic acid accumulation and often cell death caused through hypersensitive response (HR). This layer of defence is known as effector-triggered immunity (ETI) (reviewed in (Jones and Dangl, 2006; Dodds and Rathjen, 2010). Recently, this initial model of plant immunity was replaced with the concept of cell surface- and intracellular immunity, based on the immune receptors involved. Cell surface receptors (previously PRRs) recognize PAMPs (or broader: microbe-associated molecular patterns (MAMPs)) or damage-associated molecular patterns (DAMPs) that result from the presence of pathogens and initiate an appropriate cellular immune response (previously PTI). Intracellular immune receptors on the other hand recognize signs of adapted pathogens like translocated proteins (intracellular effectors) to initiate immune responses previously summarized as ETI (reviewed in Bentham *et al.*, 2020).

1.2 Infection biology of biotrophic fungi

Within plant pathogens, biotrophic interactions are the most complex ones as they require to constantly evade plant immune responses and manipulate the host plant metabolism to ensure sufficient nutrient supply and keeping damage to plant at a minimum at the same time (Koeck, Hardham and Dodds, 2011; Jaswal, Kiran, *et al.*, 2020). The initial infection is characterized by attachment to the plant surface and formation of germ tubes, followed by differentiation of infection structures called appressoria or hyphopodia (Lo Presti *et al.*, 2015). In difference to hemibiotrophs and necrotrophs, appressoria of biotrophic fungi penetrate the plant surface by applying turgor pressure in combination with secretion of plant cell-wall degrading enzymes

(O'Connell and Panstruga, 2006). By either intracellular growth or development of haustoria/arbuscules in the host cell, biotrophic fungi create a tight biotrophic interphase that allows exchange with host plant e.g. effector secretion and nutrient uptake/exchange (Lo Presti *et al.*, 2015).

Biotrophic fungi comprise the powdery mildews like *B. graminis* (Wicker *et al.*, 2013), downey mildews like *Hyaloperonospora arabidopsidis* (Coates and Beynon, 2010), rust fungi like *Uromyces appendiculatus* (Qi *et al.*, 2019) and smut fungi like *Ustilago maydis* (Vollmeister *et al.*, 2012) or *Thecaphora thlaspeos* (Frantzeskakis *et al.*, 2017). In difference to smut fungi, powdery mildews, downey mildews and rust fungi are obligate biotrophs in a sense that they are unable to grow outside their host and thus cannot be cultivated in axenic cultures (Spanu and Panstruga, 2017). Smut fungi on the other hand can be considered as facultative biotrophs or naturally obligate biotrophs as they can be grown under axenic conditions, but to complete their lifecycle they have to infect their host, while growth in a natural environment other than the host plant was not reported so far (Brefort *et al.*, 2009; Lo Presti *et al.*, 2015; Spanu and Panstruga, 2017).

1.3 Challenges in modern agriculture

Modern agriculture has been facing several challenges over the last decades: A growing world population and increased living standards generate an increasing demand for safe and diverse food (He, Zhan and Xie, 2016). This is contrasted with a limited production potential through competition for and exhaustion of land, depletion of resources and higher risk of disease epidemics through monocultures, while climate change creates additional environmental challenges (He, Zhan and Xie, 2016; Timmusk *et al.*, 2017). Until today, the estimated global yield losses due to pathogens and pests are still 21.5 % in wheat, 30 % in rice, 22.5 % in maize, 17.2 % in potato and 21.4 % in soybean (Savary *et al.*, 2019). Plant crop disease protection is thus one important means which can contribute to meet the future production needs. Previously disease control consisted of applying fungicides and insecticides (Jeger *et al.*, 2021) which is contrasted by the rapid adaptation of pathogens to our modern agrosystems (Savary *et al.*, 2019). In the future the techniques of crop protection will be extended by microbial biocontrol agents, manipulation of the microbiome and plant defence elicitors (Jeger *et al.*, 2021). Therefore, understanding

plant-microbe interactions is key to develop new tools and breeding strategies for agriculture.

1.4 Smut fungi and their scientific and economic relevance

Smut fungi are a group of plant pathogenic fungi characterized by powdery dark brown or black teliospores that are released at the end of their lifecycle (Begerow, Stoll and Bauer, 2006) and which are comprised in the *Basidiomycota* subphylum *Ustilaginomycotina* (Wang *et al.*, 2015). About 1500 smut species infect mostly angiosperms mainly of the families *Poaceae* and *Cyperaceae* including economically important crops such as barley, maize, oats, wheat, sugar cane and sorghum (Martínez-Espinoza, García-Pedrajas and Gold, 2002; Begerow, Stoll and Bauer, 2006). The yield losses in agriculture due to smut fungi infection are considerable, which is why they are well studied (Martínez-Espinoza, García-Pedrajas and Gold, 2002). In general the life cycle of grass smut fungi is characterized through a saprotrophic haploid yeast-like phase and a biotrophic dikaryotic phase (Begerow, Stoll and Bauer, 2006). The most intensively studied fungus and model within the smuts is *Ustilago maydis* the causative agent of maize smut disease (Kahmann and Kämper, 2004). Over the years of research *U. maydis* was a model for studying DNA recombination and - repair, signalling pathways, translational and posttranslational regulation, cell cycle regulation as well as mating, morphogenesis and pathogenicity (Bölker, 2001; Feldbrügge *et al.*, 2004, 2008; Kahmann and Kämper, 2004; Bakkeren, Kämper and Schirawski, 2008; Vollmeister *et al.*, 2012). Also it is the first smut fungus where the complete genome was sequenced (Kämper *et al.*, 2006). Although pathogenic development during smut fungi infection was studied extensively on the fungal side (Vollmeister *et al.*, 2012; Lanver *et al.*, 2017) complete understanding of plant responses is hindered by the genetic complexity of their host plants (Frantzeskakis *et al.*, 2017). On the plant side the model organism is *Arabidopsis thaliana* (Koornneef and Meinke, 2010) due to its good molecular and genetic properties, like a small genome size, the availability of its sequence, a huge mutant collection and an established transformation technique (Andargie and Li, 2016). Combining the knowledge of *A. thaliana* immunity and smut fungal virulence for our understanding of plant-pathogen interactions would be highly valuable (Frantzeskakis *et al.*, 2017). The only known smut fungus infecting *Brassicaceae* so far, is the recently described *T. thlaspeos*, infecting at least 15 species, including

Arabidopsis hirsuta and *Arabidopsis alpina* (Frantzeskakis *et al.*, 2017). Although infection of *A. thaliana* was never observed in nature, colonization under lab conditions is possible (Frantzeskakis *et al.*, 2017), which is why there is much potential for *T. thlaspeos* and *A. thaliana* to become a new model pathosystem.

1.5 The life cycle of *U. maydis*

As described above, a diphasic lifecycle is a characteristic for smut fungi. In accordance, the life cycle of *U. maydis* (Figure 1-1) starts off with teliospores that form a promycelium upon germination (Steinberg, 2007). Haploid sporidia of opposite mating types bud off from this promycelium after meiosis (Steinberg, 2007). Those sporidia are a pathogenic, haploid, saprotrophic and reproduce yeast-like through budding (Bölker, 2001). In order to form an infectious dikaryon, mating of two

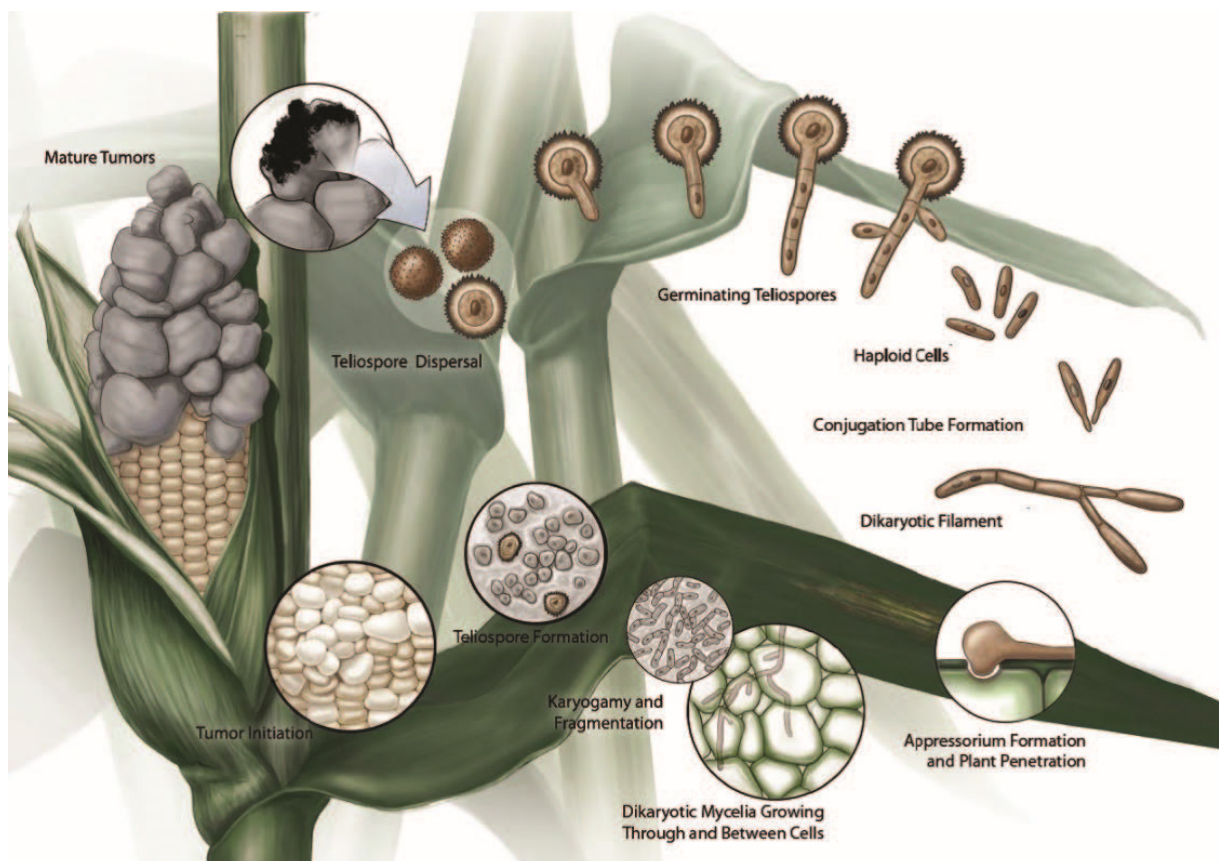


Figure 1-1 The lifecycle of *Ustilago maydis* (Saville, Donaldson and Doyle, 2012): Teliospores are released into the environment and give rise to haploid sporidia. Upon recognition of a compatible mating partner through a pheromone-receptor system conjugation tubes are formed that fuse at their tip to form a dikaryotic filament. The infectious filament forms an appressorium-like structure to penetrate the plant surface. Subsequent proliferation and branching inside the plant finally results in the formation of lobed structures and tumours as shown for the maize cob in the middle. Karyogamy and hyphal fragmentation lead to the formation of black teliospores (ruptured tumour on the maize cob).

compatible sporidia is required (Kahmann and Kämper, 2004). A pheromone-receptor system triggers the formation of conjugation hyphae that grow towards each other along a pheromone gradient until they finally fuse at the tip to form a dikaryon (Vollmeister *et al.*, 2012). Establishing biotrophy is now obligatory to further proceed in development (Bölker, 2001). To infect the plant, *U. maydis* forms special appressoria-like infection structures that penetrate the plant surface and allow *U. maydis* to colonize subjacent tissue (Kahmann and Kämper, 2004). During the biotrophic phase a result of the strong proliferation of *U. maydis* inside its host plant is the formation of tumours in all aerial parts of the plant (Vollmeister *et al.*, 2012). Inside the tumours the characteristic black diploid teliospores are formed through fragmentation and karyogamy of the hyphae (Vollmeister *et al.*, 2012). Rupture of the tumours releases the teliospores into the environment where they germinate under favourable conditions and undergo meiosis to form haploid sporidia again (Donaldson and Saville, 2008).

1.6 The lifecycle of *T. thlaspeos*

While the lifecycle of *T. thlaspeos* is similar to the lifecycle of *U. maydis* in a lot of aspects, like the pheromone-receptor system, the formation of appressoria-like structures to penetrate leaf tissue, the mycelial growth *in planta* or the propagation as teliospores, there are on the other hand some distinctive features that separate *T. thlaspeos* from *U. maydis*. First, diploid teliospores of *T. thlaspeos* germinate only in the presence of a yet unknown plant signal, while *U. maydis* teliospores germinate upon imbibition. Second, after germination a filament emerges from *T. thlaspeos* teliospores that is able to penetrate the host plant directly via roots or leaves without the need of mating (Figure 1-2). On the other hand, conservation of the mating locus and the possibility of cell fusion of compatible mating partners under lab conditions raise the question about the role of mating for *T. thlaspeos* infection. Third, once inside the plant, *T. thlaspeos* grows systemically along the vasculature of the whole plant, while infection of *U. maydis* is local and limited to the aerial parts of the plant (Figure 1-2). There are no visible infection symptoms but when the plant sets seeds these will be covered or replaced with teliospores inside the silique (Figure 1-2). When the siliques open, teliospores are released into the environment. (The paragraph is summarized from Frantzeskakis *et al.* (2017).) *T. thlaspeos* is a biotrophic plant pathogen (Frantzeskakis, 2016) and the symptomless growth of *T.*

thlaspeos inside its host plants resembles endophytic growth and therefore probably requires additional specific adaptations to balance virulence (Frantzeskakis *et al.*, 2017).

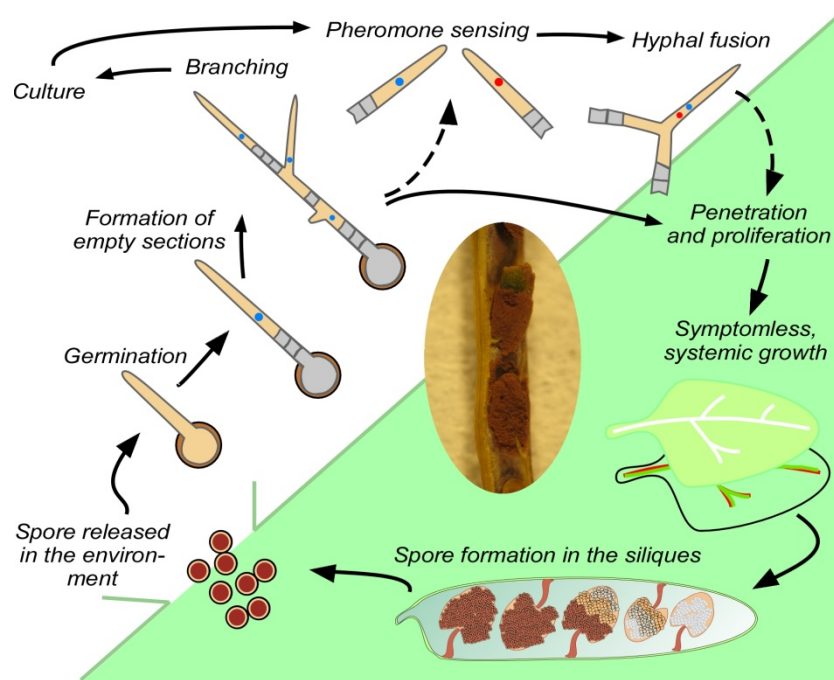


Figure 1-2 Lifecycle of *Thecaphora thlaspeos* (reprinted with permission from Frantzeskakis, L. *et al.* (2017) 'The plant-dependent life cycle of *Thecaphora thlaspeos*: a smut fungus adapted to Brassicaceae', *Mpmi*, 30(4), pp. 272–282): Teliospores are released into the environment where they germination upon recognition of a unknown plant signal. The emerging filament inserts empty sections at its basal pole and continues to grow and branch. The filament can be either cultivated axenically or is readily infectious. In culture, mating of opposite mating types (represented by red and blue nuclei) was observed presumably regulated through the conserved mating loci. After successful infection of the root tissue *T. thlaspeos* proliferates systemically and symptomless along the vasculature. Finally, spores are formed in the siliques where they cover or replace the seeds.

2 Aims of this thesis

The focus of this thesis is on two aspects of smut fungi research: The infection biology of *T. thlaspeos* and Mg^{2+} transport in *U. maydis*. To this end this thesis is structured in three chapters, where the first two deal with the infection biology of *T. thlaspeos* and the third with Mg^{2+} transport in *U. maydis*.

1. Chapter: The life cycle of *T. thlaspeos* was initially described in Frantzeskakis et al (2017) and opened up further questions outlined in the next chapter, especially since the life cycle differs from the model smut fungus *U. maydis*. These questions regard the penetration structures and infection patterns formed during the early infection stages, the formation of an interaction zone with plant as well as the host range of *T. thlaspeos*. Answers to these questions should provide a more detailed understanding of the infection stages, the individual colonized tissues and the different hosts. To address them, this study aimed at a detailed microscopic characterization of *T. thlaspeos* infection biology. The focus was to compare the phase of initial infection (plant penetration and initial growth *in planta*) with the long-lasting phase of established biotrophy in leaf and root tissue between the different hosts *Ar. hirsuta*, *Ar. alpina* and *A. thaliana*, which can be colonized under lab conditions.

2. Chapter: Following the initial characterization of *T. thlaspeos* the publication of the genome and a transcriptome study of systemically infected *Ar. hirsuta* provided detailed insights into the *Ar. hirsuta* - *T. thlaspeos* interaction (Courville *et al.*, 2019). Besides several unique effector candidates a potential virulence factor THTG_00998 was identified (Courville *et al.*, 2019). As genetic modifications were not yet possible for *T. thlaspeos*, THTG_00998 was characterized here in a complementation analysis in comparison to its homologue UMAG_01374 (Pit1) in *U. maydis*. In parallel, a transformation protocol for *T. thlaspeos* was established to allow characterization of THTG_00998 directly in *T. thlaspeos* in the future.

3. Chapter: The third part of this thesis dealt with Mg^{2+} homeostasis in *U. maydis* and a potential contribution of the virulence factor Pit1 (UMAG_01374) to it. The comparison of THTG_00998 and Pit1 revealed a putative connection of Pit1 to Mg^{2+} transport. Further analysis included a first characterization of Mg^{2+} transport in *U. maydis* and a complementation analysis of a Mg^{2+} dependent growth defect with Pit1.

3 Results and Discussion

3.1 Microscopic characterization of *T. thlaspeos* infection biology

3.1.1 Background

T. thlaspeos infection biology

In the first description of *T. thlaspeos* life cycle, it was shown, that *T. thlaspeos* hyphae penetrate *Ar. hirsuta* or *A. thaliana* either via appressoria on leaves or infect via roots to then spread along the vasculature in root or leaf tissue in both species (Frantzeskakis *et al.*, 2017). In *Ar. hirsuta* it was further shown, that *T. thlaspeos* colonizes all organs of its host during the whole life cycle of the plant appearing either in a continuous or fragmented hyphal pattern along the vasculature (Frantzeskakis *et al.*, 2017). This initial description provides already a valuable insight into the infection biology and also raises additional questions like:

Does penetration via appressoria on leaves also result in systemic infection and does it occur also naturally? It is important to answer this question in order to judge the relevance of this infection strategy. The formation of appressoria on the leaf surface was already described for *T. thlaspeos* (Frantzeskakis *et al.*, 2017), but it is not clear if this ability is productive for infection or a remnant feature that is not yet lost. If leaf infection does not result in systemic infection or does not occur naturally because the spores are distributed with the seeds and do not naturally come into contact with leaves, it is irrelevant to further study this infection strategy, because *T. thlaspeos* is not able to fulfil its life cycle applying it.

Does *T. thlaspeos* grow intra- or only intercellularly and does it form feeding structures like haustoria? The formation of feeding structures as well as intracellular growth allows the formation of a tight interaction zone with the plant, a biotrophic interphase, important for nutrient uptake as well as effector secretion (O'Connell and Panstruga, 2006). Answers to these questions provide basic information of the *T. thlaspeos* infection biology that is the prerequisite to gain further insights into the molecular interaction with the host plant. In the long term this knowledge can be applied to identify common traits in comparison to other

plant pathogenic fungi with a similar life style and select targets for fungicide development or genetically introduced disease resistance. This goal leads directly to the next question:

How does the plant respond to the early infection stage? The generation of disease resistant plant lines of course also requires knowledge of the plant response to the infection. To this end, the extension of the transcriptome dataset of systemically infected *Ar. hirsuta* leaves (Courville *et al.*, 2019) with data on the early infection stage is needed.

What is the host range of *T. thlaspeos* spores between different described host plant species and different ecotypes of one host plant species? In comparison to other smut fungi the reported host range of *T. thlaspeos* is bigger than expected (van der Linde and Göhre, 2021), while the fund locations of *T. thlaspeos* infections are across several countries (Vanky, 2004; Frantzeskakis *et al.*, 2017; Kruse *et al.*, 2018; Denchev and Denchev, 2019). The identification of *T. thlaspeos formae speciales* could provide the opportunity to study host adaptation and possibly the process of speciation and how this is manifested on the genome level. Since smut fungi are characterized by a narrow host range, species adaptation usually needs to be studied by comparing several closely related pathosystems (Benevenuto *et al.*, 2018). For example, *U. maydis* infects only maize and its ancestor Teosinte (Bölker, 2001) while *Sporisorium reilianum* has two *formae speciales* that infect maize and sorghum (Poloni and Schirawski, 2016), respectively.

Do the infection structures look similar on the other host species? This question is related to the previous one, but focuses on visible differences between the *T. thlaspeos* spore isolate and different host plants. If the two *S. reilianum formae speciales* are for example combined with their respective non-favoured hosts, fungal proliferation is less than in the compatible host and the interaction zone with the plant differs (Poloni and Schirawski, 2016). Thus differences in the colonization of *T. thlaspeos* between the host species would indicate host species adaptation already in these infection stages.

To analyse the infection biology of *T. thlaspeos* I worked with different infection techniques depending on the infection stage of interest. To examine the early infection stages I used sterile infection setups on plate or liquid. For leaf infection, plants were grown on ½ MSN plates and sterile *T. thlaspeos* spore solution was applied to the leaves of the seedling while for root infection sterile seeds and spores were co-germinated in liquid ½ MSN medium in well plates. Both setups allow to sustain the plants only for a few weeks. To examine the phase of established biotrophy, *T. thlaspeos* spore-coated seeds were germinated on soil to allow long-term maintenance of the plants.

The ability of *T. thlaspeos* to colonize *A. thaliana* under lab conditions is very valuable to study the infection biology, as it offers the possibility to utilize mutants and reporter lines. Great tools are the COLORFUL reporter lines developed by Dr. Hassan Ghareeb from the Institute of Prof Dr. Volker Lipka at the University Göttingen. These lines were generated with the multigene assembly system COLORFUL-Circuit, a cloning platform that allows to combine and express several fluorescent organelle markers (Ghareeb, Laukamm and Lipka, 2016). The reporter line used in this thesis was the COLORFUL-PR1pro (Ghareeb *et al.*, 2020) that consists of a reporter module *PR1-VENUS-N7*, a reference module *UBQ10-mKATE2-N7* and a membrane marker *CaMV35S-EGFP-LTI6b*. In an unchallenged plant the plasma membrane marker and nuclear reference marker will be expressed (Figure 3-5 MOCK). Only if an immune response is triggered either artificially by application of an elicitor or the plant hormone salicylic acid or naturally by infection with a pathogen the reporter module will be activated, changing the colour of the nuclei from red to yellow in the overlay (Figure 3-5 SA and Flagellin).

3.1.2 Results

This chapter aims to describe the infection biology of *T. thlaspeos* microscopically. The early infection stage describes the initial colonization of the plant until the fungus reaches the vasculature. Whereas the stage of fully established biotrophy comprises the time frame of systemic infection that lasts several months. The first can only be investigated under sterile conditions that allow to sample all parts of the plant. However, the second requires infection in an unsterile soil-based setup, that allows to grow the plants for many weeks.

3.1.2.1 *T. thlaspeos* forms appressoria on cotyledons and true leaves of *Ar. hirsuta*, *Ar. alpina* and *A. thaliana*

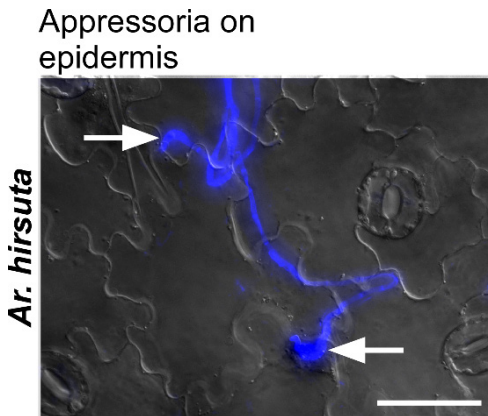


Figure 3-1 Appressoria formation of *T. thlaspeos* spores on the epidermis of *Ar. hirsuta* cotyledons. The appressorium is a bulbous structure formed at the hyphal tip between two adjacent epidermal cells. Below the appressorium a hook like penetration peg is visible. The image was taken at 10 dpi and hyphae were stained with Calcofluor White. Depicted is a maximum projection overlay of the DAPI channel to visualize the whole structure of the appressorium with a single plane of the DIC channel (for clarity) to visualize the plant surface. The scale bar equals 50 μ m.

This section refers to the first and the last question asked above “Does penetration via appressoria on leaves also result in systemic infection and does it occur also naturally?” and “Do the infection structures look similar on the other host species?”, respectively. Initially, the previously described appressoria formation on cotyledons of *Ar. hirsuta* needed to be confirmed (Frantzeskakis *et al.*, 2017). To this end, spores were dropped on cotyledons and true leaves of *Ar. hirsuta*, *Ar. alpina* as well as *A. thaliana* and appressoria formation was analysed microscopically. Spore germination and appressoria formation was confirmed on *Ar. hirsuta* cotyledons and also on *Ar. alpina* and *A. thaliana* cotyledons as well as true leaves (*Ar. alpina* and *A. thaliana*).

Interestingly, formation of appressoria was not only observed on epidermal cells, as reported before, but even more frequently on stomatal guard cells. Altogether, three penetration events could be distinguished: appressoria formation on epidermal cells, on guard cells, hyphal growth through the stomatal opening and subsequent colonization of the guard cells (Figure 3-1 and Figure 3-2). In comparison, appressoria of *U. maydis* are also formed either on epidermal cells or guard cells of the maize leaf and although not quantified, there seems to be no preference if the appressorium is formed on the centre or the edge of the cell underneath (Snetselaar and Mims, 1992; Fernández-Álvarez *et al.*, 2012). In contrast, appressoria of *T. thlaspeos* were so far only observed over the junction between two cells, while the

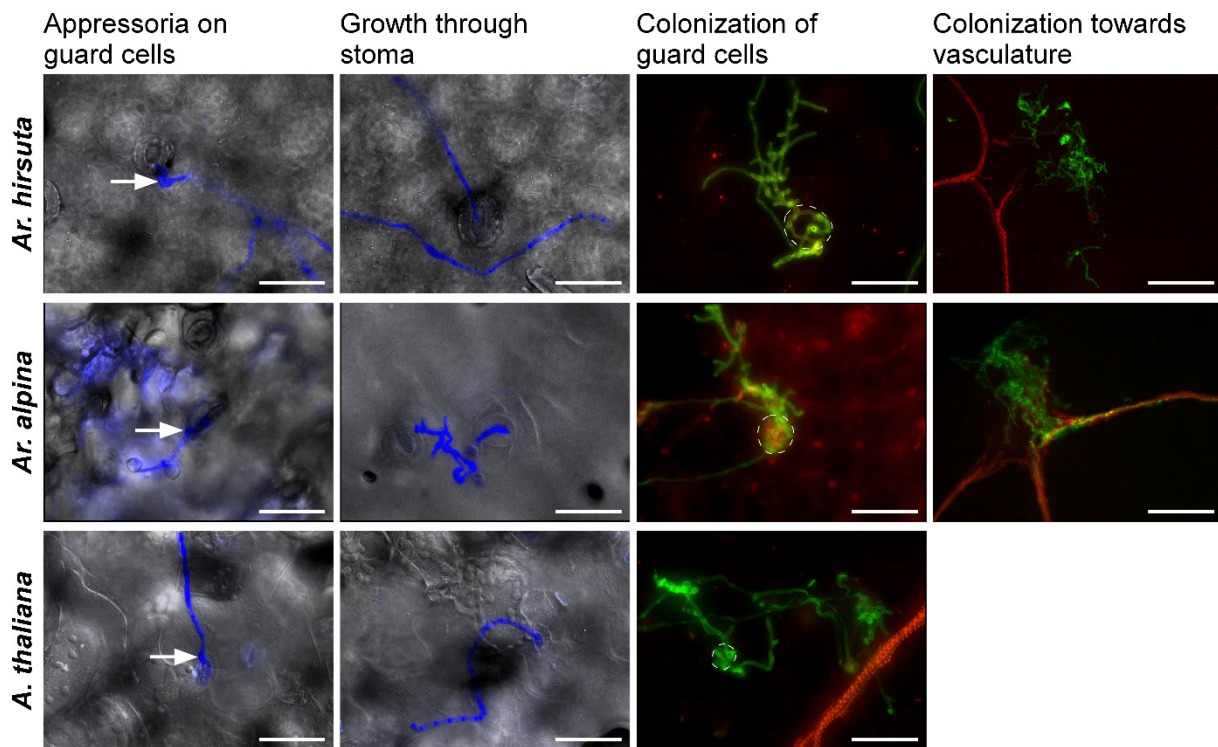


Figure 3-2 Penetration and subsequent colonization of stomata by *T. thlaspeos* is identical in the two host plant species *Ar. hirsuta* and *Ar. alpina* as well as in *A. thaliana* Col-0. Column 1 shows the formation of appressoria-like structures on guard cells by *T. thlaspeos*. Column 2 shows growth of hyphae through the stoma. The hyphae were stained with CalcofluorWhite. Depicted is a maximum projection overlay of the DAPI channel to visualize the whole structure of the appressorium with a single plane of the DIC channel (for clarity) to visualize the plant surface. Column 3 shows the colonized guard cells and growth of hyphae into the adjacent tissue (the outline of the colonized guard cells is indicated as dashed with line). Column 4 shows fungal proliferation towards vasculature after initial penetration. Hyphae were stained with WGA-FITC and the plant tissue was counter-stained with propidium iodide. Images of column 3 are maximum projection overlays of the GFP and PI channel. All images were taken at 12-14 dpi; column 1-4 from left to right; scale bar equals 50µm in column 1-3 and 200 µm in column 4.

growth through the stoma is also not described for *U. maydis*, which could indicate that among others the surface topography plays a role in appressoria differentiation in *T. thlaspeos*.

Occasionally, intensive colonization of the penetrated guard cells was observed, a finding so far not reported in other fungi (Figure 3-3 left). While this does not seem to be necessary for successful infection, it is not yet clear, if this has a specific purpose or if this occurs also naturally or is merely an artefact of the artificial infection conditions a sterile growth setup entails. The first step to gain further insights would be to show the colonization of guard cells under more natural growth conditions e.g. ambient humidity and unsterile or at least semi-sterile conditions. If under such conditions the colonization could be observed as well, it would be interesting to

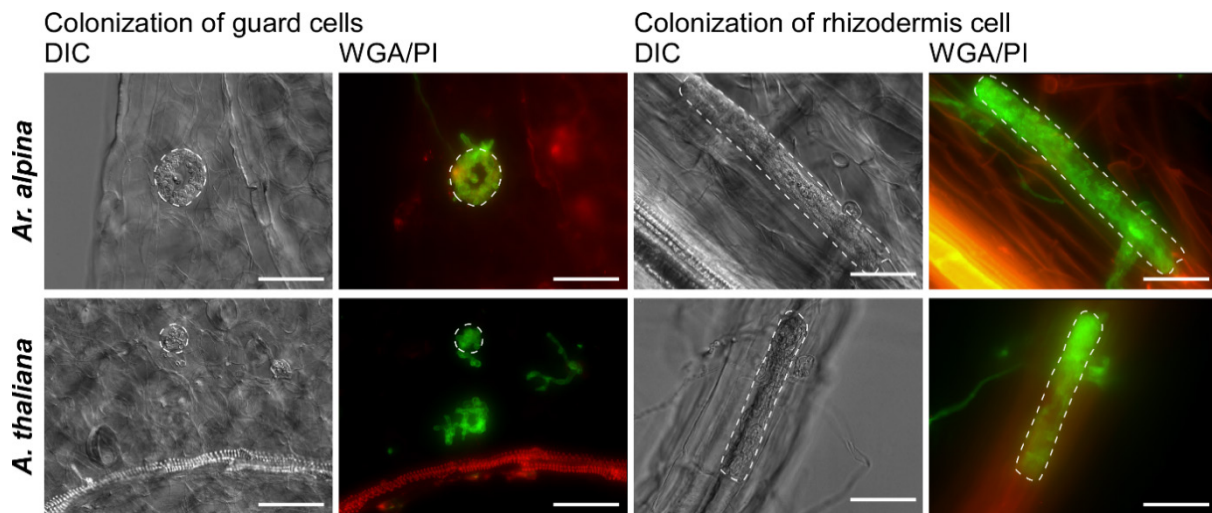


Figure 3-3 Intensive colonization of guard and rhizodermis cells in *Ar. alpina* and *A. thaliana*. Occasionally, the intensive colonization of the cell below the appressorium on leaves and roots was observed. The images show the DIC image and the corresponding maximum projection overlay of the WGA-FITC propidium iodide channel of colonized guard/rhizodermis cells (the outline of the colonized guard/rhizodermis cells is indicated as dashed with line). Pictures were taken 12-14 dpi and hyphae were stained with WGA-FITC and plant tissue was counter-stained with propidium iodide; the scale bar equals 50 μ m.

isolate these structures in comparison to stomata that are only slightly colonized and compare the transcriptome, proteome and metabolome of the plant and the fungus to obtain indications on its purpose and gain in depth insights into the early responses of the plant towards infection.

The infection of leaves was observed not only after spore application on leaves, but also after co-germination of seeds and spores in liquid infection experiments in *Ar. alpina* and *Ar. hirsuta*. Here it was shown for the first time, that after successful initial colonization, *T. thlaspeos* grows through adjacent cells and starts to branch. Like this, *T. thlaspeos* colonizes a broader area of the leaf until it reaches the vasculature. Along the vasculature, *T. thlaspeos* grows towards the leaf base in the typical pattern already described in roots (Frantzeskakis *et al.*, 2017) (Figure 3-2). In contrast to this broad initial colonization, *T. thlaspeos* seems to grow exclusively around the vasculature tissue, once reached. In *A. thaliana* this was not observed yet (Figure 3-2). The reasons for this are likely the lower infection rates of *A. thaliana* in liquid infections and the increased stress of *A. thaliana* caused by this setup in comparison to *Ar. alpina* and *Ar. hirsuta* (see also chapter 3.1.2.4 for a more detailed description of the results from the liquid infection assays). While this does not answer if leaf infection occurs naturally in *T. thlaspeos* infection it gives a first indication, that infection via appressoria on leaves likely results in systemic infection.

3.1.2.2 *T. thlaspeos* forms comparable infection structures on leaves and roots

To microscopically analyse the infection of *T. thlaspeos* spores via root tissue, liquid infection time course experiments over the course of 2-8 weeks were performed in *Ar. hirsuta*, *A. thaliana* and *Ar. alpina*. Corresponding to leaf infection, it was observed that *T. thlaspeos* seems to form special appressoria-like infection structures also on root tissue, likely also between cell junctions (Figure 3-4). Occasionally, root cortex cells were massively colonized by hyphae, similar to guard cells on leaves. Again, this does not seem to be required for successful infection. Upon successful infection *T. thlaspeos* hyphae grow towards and along the vasculature to reach the aerial parts of the plant. It was shown before, that all aerial parts of the host *Ar. hirsuta* are colonized systemically (Frantzeskakis *et al.*, 2017). For the leaf tissue of infected plants this means infection in the majority of the leaves.

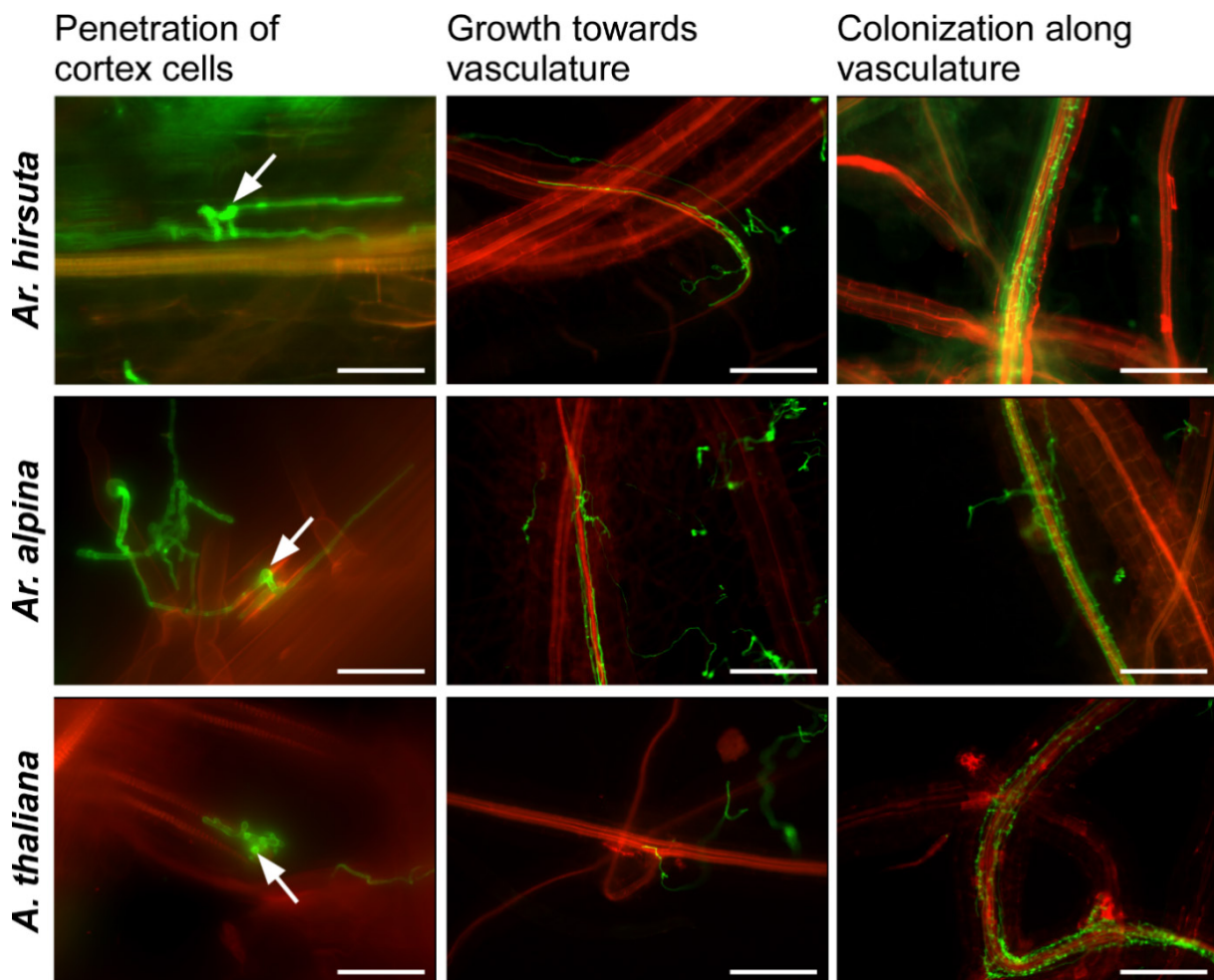


Figure 3-4 Penetration and subsequent colonization of roots by *T. thlaspeos* is identical in the two host plant species *Ar. hirsuta* and *Ar. alpina* as well as in *A. thaliana* Col-0 in liquid infection experiments. The column 1 shows the formation of appressoria-like structures on rhizodermis cells by *T. thlaspeos*. Column 2 shows growth of hyphae through the root cortex towards the vasculature. Column 3

shows the typical growth pattern of *T. thlaspeos* hyphae along the vasculature tissue. Images are maximum projection overlays of the GFP and PI channel and were taken 2-6 wpi. Hyphae were stained WGA-FITC and plant tissue was counter-stained with propidium iodide; scale bar equals 50µm in column 1 and 200 µm in column 2-3. The experiment was performed once for *A. thaliana* and *Ar. hirsuta* and twice for *Ar. alpina*.

In liquid infection assays in *Ar. hirsuta*, *Ar. alpina* and *A. thaliana* over the course of 8 weeks, colonization of the complete root system was not observed. Instead, the infection seems to spread “upwards” from smaller to bigger roots to reach the stem, thus only a small proportion of the root tissue was infected in this setup (Figure 3-4).

Comparing leaf and root infection the observed structures are of striking resemblance. Considering the structural differences of root and leaf tissue, e.g. the composition of the epidermal and rhizodermal cell wall or the presence or absence of stomata this is remarkable.

3.1.2.3 Plant responses to early infection

This part of the first chapter deals with two of the aforementioned questions. Appressoria formation experiments using the COLORFUL-PR1pro reporter line (kindly provided by Hassan Ghareeb, University Göttingen (Ghareeb *et al.*, 2020)) allowed on the one hand to investigate if *T. thlaspeos* grows inter- or intracellularly after penetration of the plant surface and on the other hand to monitor the response of the plant with regard to SA-mediated defense signalling.

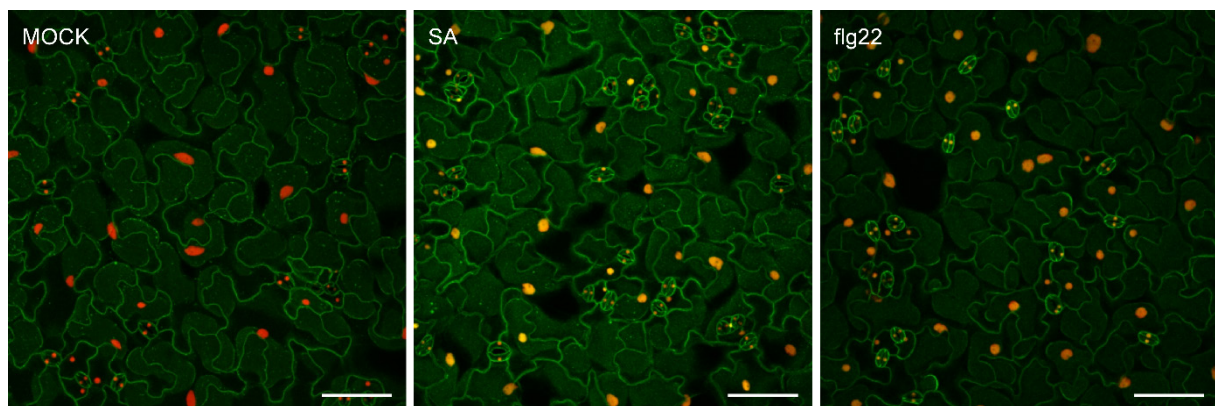


Figure 3-5 The COLORFUL-PR1pro reporter line: Artificial induction of an immune response in 12 days old seedlings with salicylic acid (SA) or the bacterial elicitor peptide flg22 from the motor protein flagellin for 24h. The plant plasma membrane is visualized in green, plant nuclei appear red in the MOCK treated seedling because only the reference marker *UBQ10-mKATE2-N7* is expressed and yellow in the SA or flagellin treated seedlings because both the reference marker *UBQ10-mKATE2-N7* and the immune response marker *PR1-VENUS-N7* are expressed. The images were taken with a confocal microscope and are maximum projection overlays of the Venus, GFP and mKate channel showing the epidermal cell layer and the first subsequent mesophyll cell layer; the scale bar equals 100 µm.

The plasma membrane marker allows to indirectly verify viability of the colonized cells, while the *PR1-VENUS-N7* marker allows to monitor recognition of the fungus

by the plant immune system. Initially, the response of the reporter line towards infection, the colour-switch in the nuclei from red to yellow, was tested by artificial induction of an immune response using salicylic acid (SA) or the bacterial elicitor peptide flg22 (Figure 3-5) and confirmed the functionality of the reporter line for my experimental setup.

In an leaf infection experiment with *T. thlaspeos* spores (Figure 3-6) several observations were made: First, guard cells can die during the colonization process, but the surrounding cells remain alive (Figure 3-6 lower left image). This fits to the observation of occasional intensive colonization of these cells, that might mutually depend on host cell death. In comparison the guard cells remained alive in other penetration events and showed slight intracellular colonization (Figure 3-6 upper right image). Additional leaf infection experiments will be required to distinguish, if guard cell death is an immune response of the plant to block infection, *T. thlaspeos* failed to suppress, followed by subsequent intensive colonization of the cells or a result of the fungal proliferation in the cells. Second, the visualization of the plant plasma membrane in the epidermal cells via the GFP marker showed that invading hyphae are surrounded by plant plasma membrane, forming a biotrophic interphase for extensive exchange between plant and fungus (Figure 3-6 upper two and lower left images). Third, the expression of the *PR1-VENUS-N7* marker (yellow nuclei) showed that independent of where the appressorium is formed on the leaf surface, the plant is responding to infection with an immune response in heavier colonized tissue (Figure 3-6 upper images), while initial colonization is not yet recognized, indicated by red nuclei (Figure 3-6 lower left image).

In comparison to the already published characterization of the *T. thlaspeos* infection biology (Frantzeskakis *et al.*, 2017) by our group, the microscopic analysis presented here shows, that *T. thlaspeos* penetrates leaves via appressoria formation on guard cells or by growth through stomata additionally to the previously described formation of appressoria on epidermal cells. Although further infection experiments will be necessary to clarify, *T. thlaspeos* hyphae grow towards and along the vasculature after leaf penetration which is a good indicator that systemic infection is possible via this infection strategy. In the future it remains to be seen if leaf infection also occurs under natural conditions. Leaf infections with the COLORFUL-PR1pro reporter line revealed for the first time, that *T. thlaspeos* grows intracellularly after penetration and

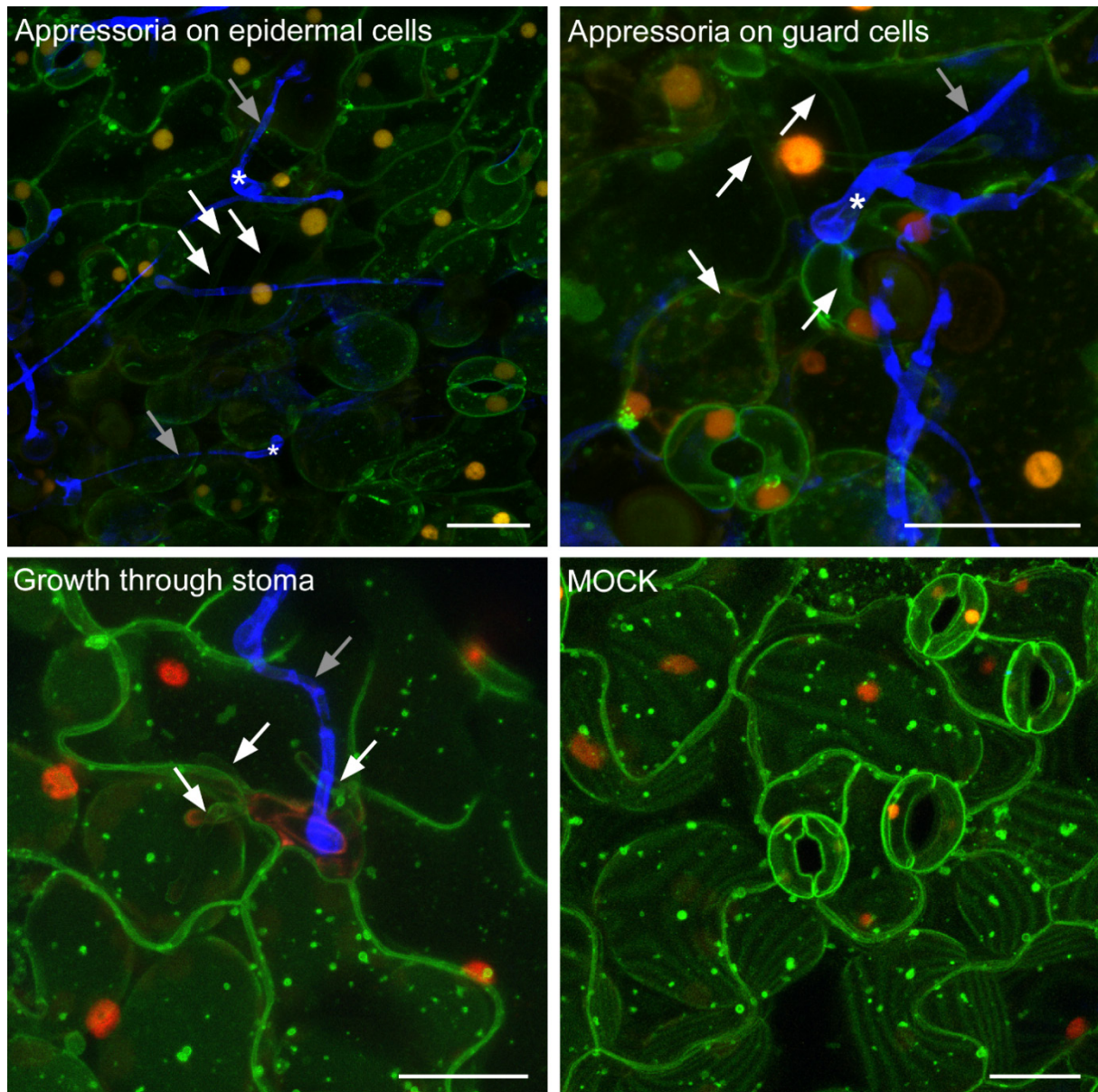


Figure 3-6 Appressoria formation of germinated *T. thlaspeos* spores on COLORFUL-PR1pro reporter line true leaves: Epiphytic hyphae are stained with CalcofluorWhite (blue). Depicted are representative images of the three infection strategies (Appressoria on epidermal cells, on guard cells, or growth through the stoma). Appressoria are marked with *, epiphytic hyphae with a grey arrow and intracellular hyphae with a white arrow. Note, that the outlines of the intracellular hyphae are visualized by the surrounding plant plasma membrane, that contains the GFP marker. The plant nuclei appear yellow in the upper images indicating a plant immune response against the fungus by the expression of *PR1-VENUS-N7* marker. In the lower images the nuclei appear red indicating only the reference marker *mcherry-N7* is expressed. In the image of growth through the stoma, the nuclear reference marker as well as the GFP marker is lost indicating the guard cells are dead. The images were taken with a confocal microscope and are maximum projection overlays of the Venus, GFP, mcherry and DAPI channel showing the epidermal cell layer and the first subsequent mesophyll cell layer; the scale bar equals 25 μm .

is surrounded by plant plasma membrane which creates a biotrophic interphase for exchange with the plant. During this phase of infection *A. thaliana* responds with a salicylic acid signalling-based immune response indicated by PR1 upregulation in the COLORFUL-PR1pro reporter line. This is in line with PR1 upregulation detected in the transcriptome of *T. thlaspeos* infected *Ar. hirsuta* leaves (Courville *et al.*, 2019).

Similar to leave infection my data shows for the first time that penetration structures are formed similarly on the root surface. The subsequent colonization is similar to leaf infection and here I could show that penetration structures as well as initial colonization via leaf and root tissue is similar in *Ar. hirsuta* and *Ar. alpina* as well as in *A. thaliana*. With regard to the host range this indicates that a potential adaptation of *T. thlaspeos* towards different hosts is not visible at this stage of infection within the species compared.

3.1.2.4 What is the host range of *T. thlaspeos* spores between different described host plant species and different ecotypes of one host plant species?

The compatibility of *Arabis alpina* with *Ar. hirsuta*-derived *T. thlaspeos* spores in comparison to *Ar. hirsuta* and *A. thaliana*

To investigate the host range of *T. thlaspeos* spores, soil infection experiments were performed with *Ar. hirsuta* infection-derived *T. thlaspeos* spores in combination with *Ar. alpina* Pajares or *Ar. hirsuta* seeds, since this infection setup resembles the natural infection conditions the most and allows to maintain the plants until seed development. While systemic infection of the plant should be observable within weeks already, the formation of spores in the siliques, that proves completion of *T. thlaspeos* life cycle, is the only indicator that host species and *T. thlaspeos* spore isolates are truly compatible.

Table 3-1 Summary of *Ar. alpina* and *T. thlaspeos* soil infections from current and previous members of the Göhre lab. For spore batches that were collected in Germany, the location and year of the collection are given (BB = Bad Berneck, RH= Rohnheim, HL=Hohe Leite, EB= Eselsburg, Frantzeskakis *et al.*, 2017). For lab spore batches that originated from lab infections the producer and the year are given (KC=Kaitlyn Courville, RK=Ronny Kellner, LP=Lesley Plücker). Grey shading indicates the infection was done by myself, otherwise the infections were done by other lab members; the infection rate for each combination is given.

<i>Ar. alpina</i>	Spore batch	Lab spore batch	infection rate
WT	<i>T. thlaspeos</i> BB 2013		0.0 %
		<i>T. thlaspeos</i> KC 2015	0.0 %
		<i>T. thlaspeos</i> RK 2018	0.0 %
		<i>T. thlaspeos</i> LP 2021	0.0 %
		<i>T. thlaspeos</i> HL 2015	0.0 %
		<i>T. thlaspeos</i> EB2015	0.0 %
pep 1	<i>T. thlaspeos</i> BB 2013		0.0 %
		<i>T. thlaspeos</i> KC 2015	0.0 %
		<i>T. thlaspeos</i> HL 2015	0.0 %

To obtain infected *Ar. alpina* plants, six replicates of soil infections with *Ar. hirsuta*-derived *T. thlaspeos* spores with a total of 215 plants were analysed, but

unexpectedly no infection in leaves was observed (Table 3-1). By contrast, in *Ar. hirsuta* colonization is already visible in leaf samples four weeks after infection (wpi). To find out if and when infection in *Ar. alpina* reaches the leaves, liquid infection assays were performed over the course of eight weeks twice. While the infection rate in roots with 50 % on average was very good, it was observed that *T. thlaspeos* did not reach the leaves even after eight weeks. Furthermore, infection was progressing in the roots only for the first six weeks, but seemed less pronounced after eight weeks (Figure 3-7). For comparison, similar liquid infection assays were also performed once for *Ar. hirsuta* and *A. thaliana*. In line with previous experiences in the lab, the infection rates for *Ar. hirsuta* and *A. thaliana* were with 10-20 % considerably lower. For *A. thaliana* it was not possible to keep the plants for eight weeks as they started to develop massive chlorosis after four weeks. Thus all *A. thaliana* plants were harvested at five wpi.

Overall the development of disease was comparable in *Ar. alpina* and *A. thaliana*: For the first six weeks the infection symptoms increased in *Ar. alpina* while the same was observed in *A. thaliana* for the first four weeks. After that, the fungal proliferation seemed to decrease again (Figure 3-7). In *Ar. hirsuta* the infection progress seemed unchanged between three and eight wpi, likely due to the smaller sample size and lower infection rate no significant differences between the time points were found (Figure 3-7). In *Ar. hirsuta* soil infections, *T. thlaspeos* is usually detectable in most rosette leaves after four weeks, while the infection in the liquid system was limited to a few roots of the root system and did not reach the leaves in all three species. The liquid infection setup results in good infection rates for *Ar. alpina*, but an even longer timeframe to observe fungal proliferation *in planta* is necessary to determine how the infection of *Ar. hirsuta*-derived *T. thlaspeos* spores progresses in *Ar. alpina*. Additionally, the lower infection rates with *Ar. hirsuta* and *A. thaliana* require large sample sizes to obtain robust data. Thus alternative infection setups like a semi-sterile setup on sand should be tested in the future, aiming to improve infection rates in *Ar. hirsuta* and possibly *A. thaliana*, monitor the fungal proliferation in all plant tissues during the whole life cycle and create infection conditions closer to the natural situation.

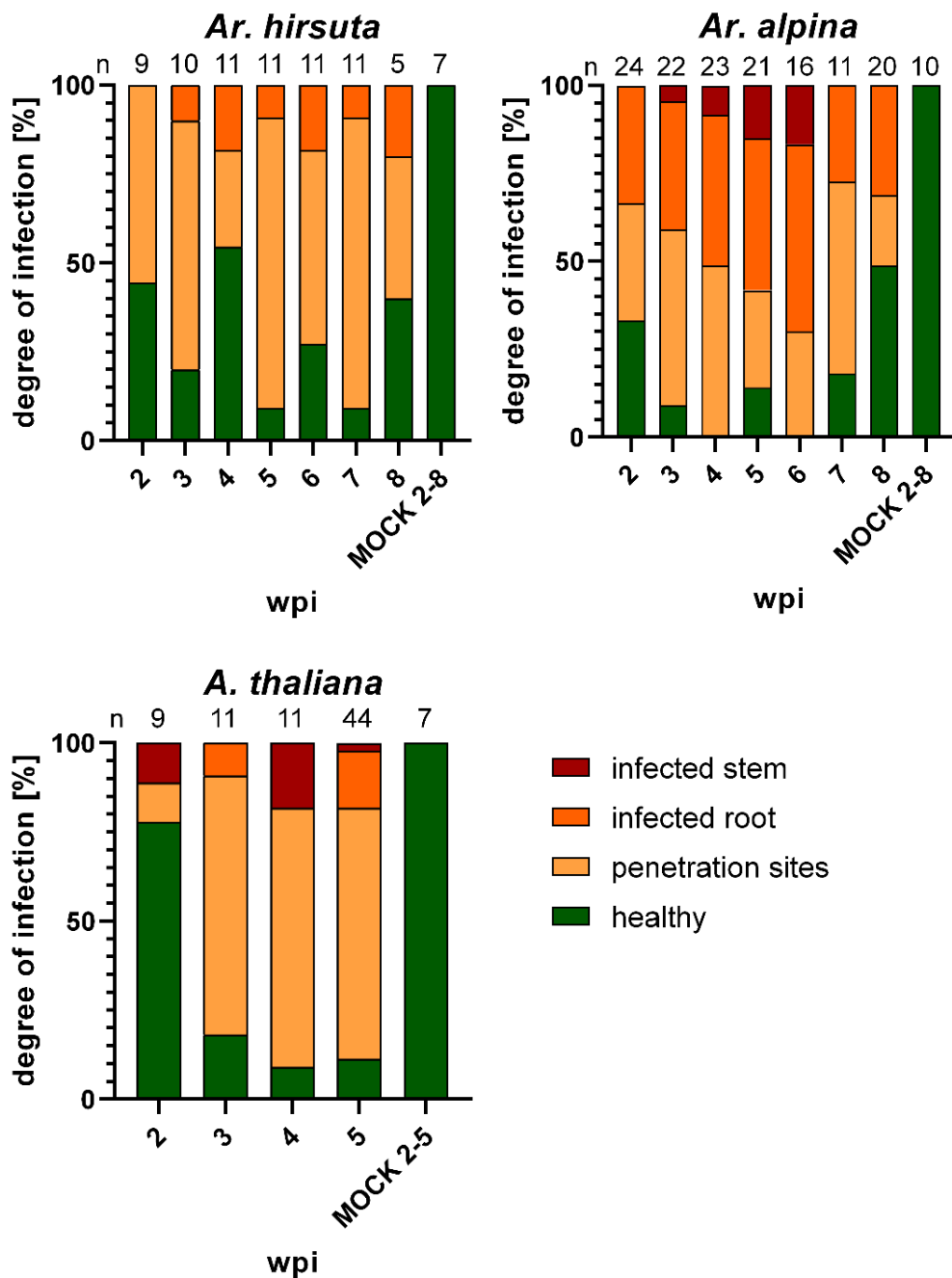


Figure 3-7 Documentation of the progression of *T. thlaspeos* spore infection in liquid infection assays with *Ar. hirsuta*, *Ar. alpina* or *A. thaliana* over the course of 8 weeks. The progression of the infection was scored as follows: healthy: only extraradical hyphae are found surrounding the roots; penetration sites: penetration of the rhizodermis cell layer (because it is impossible to distinguish if the hyphae are truly inside, these plants were not considered as infected yet); infected root: the hyphae grow along the vasculature of the root in the pattern typical for *T. thlaspeos* infection; infected stem: the hyphae grew along the vasculature of the roots and reached the stem vasculature. The *Ar. alpina* infections of two replicates show an increase of infection progression over the first 6 weeks and afterwards the infections seem less progressed. In *Ar. hirsuta* the infection seems unchanged between three and eight wpi, but the data set is less meaningful in comparison to the dataset from *Ar. alpina* because of the smaller sample size (one replicate) and the lower infection rate of *Ar. hirsuta* in the liquid infection system in general. In *A. thaliana* the infection seems to progress for the first four weeks and seems slightly less progressed at five wpi. But also here the data set is less meaningful in comparison to the dataset from *Ar. alpina* because of the smaller sample size (one replicate) and the lower infection rate of *A. thaliana* in the liquid infection system.

Since further growth of the plants in liquid is not possible in the current experimental setup, six possibly infected *Ar. alpina* plants were transferred to soil to see if spores were formed in siliques. Sadly, no spores were found. Finally, one additional soil infection experiment with *Ar. alpina* was performed where the plants were not sampled after four weeks but allowed to flower. Again, no spores were found in the siliques. Reviewing *Ar. alpina* soil infections performed by previous lab members revealed that no infected *Ar. alpina* plant could be obtained so far (Table 3-1). Although it is not possible to determine if *Ar. hirsuta*-derived *T. thlaspeos* spores are able to infect *Ar. alpina* roots in a soil infection setup similar to the liquid infection system, the fact that neither systemic infection nor spore formation was observed in any infection experiment so far, strongly indicates that *Ar. hirsuta*-derived *T. thlaspeos* spores are incompatible with *Ar. alpina* and possibly the existence of *T. thlaspeos formae speciales*.

3.1.2.5 The compatibility of *Ar. hirsuta* ecotypes with *Ar. hirsuta*-derived *T. thlaspeos* spores

The possible incompatibility of *Ar. hirsuta*-derived *T. thlaspeos* spores with *Ar. alpina* suggests a smaller host range of *Ar. hirsuta*-derived *T. thlaspeos* than initially expected based on the reported host plant species. To investigate the host range of *Ar. hirsuta*-derived *T. thlaspeos* spores further, soil infections with several *Ar. hirsuta* ecotypes were performed. Interestingly, infections of the ecotypes *Ar. hirsuta* Slovenia with *T. thlaspeos* Ronheim spores (Lab spore batch RK 2018) did not result in infected plants (160 plants in 4 replicates; Table 3-2). But if *T. thlaspeos* Ronheim spores (spore batches RH 2015, RH 2018 and lab spore batch RK 2018) were used to infect *Ar. hirsuta* Ronheim infection rates of 39 %, 53 % and 60 % were achieved (Table 3-2). In comparison, spores from the same infected plant (Lab spore batch RK 2018) were not able to infect *Ar. alpina* (Table 3-1). Although it cannot be excluded, that the spores used in all *Ar. alpina* infections were simply not infectious, because *Ar. alpina* and *Ar. hirsuta* were not infected with the same spores in parallel, the results further support an incompatibility of *Ar. hirsuta*-derived *T. thlaspeos* spores with *Ar. alpina*.

With regard to the host range of *T. thlaspeos* within *Ar. hirsuta*, the results of previous infections in our lab suggest, that plant-pathogen compatibility is better the closer ecotype locations of *Ar. hirsuta* and *T. thlaspeos* are together (Table 3-2). To test this

hypothesis, parallel infections of the *Ar. hirsuta* ecotypes Slovenia, Hohe Leite, Ronheim and Bad Berneck and *Ar. alpina* Pajares were conducted in three replicates. Unfortunately, the only available spore batch *T. thlaspeos* LP 2021 (after propagating the seeds of the various ecotypes) was unable to infect any of the *Arabis* species. This was unexpected, because previously, the viability of these spores was verified in a germination assay. Thus, the infection experiment needs to be repeated once infectious spores are available.

Taken together, I showed that *T. thlaspeos* spores can infect leaves and roots of *Ar. hirsuta*, *Ar. alpina* and *A. thaliana* in a very similar manner under sterile conditions. To penetrate the root or leaf surface *T. thlaspeos* forms appressoria-like structures which on leaves were frequently formed on stomata as entry points. On the other hand, soil infections hint on a species- and ecotype-dependent incompatibility of *T. thlaspeos* spores with its host.

Table 3-2 Summary of *Ar. hirsuta* and *T. thlaspeos* soil infections from current and previous members of the Göhre lab. For spore batches that were collected in the wild the location and year of the collection are given (BB = Bad Berneck, RH= Rohnheim, HL=Hohe Leite, EB= Eselsburg in Germany). For lab spore batches that originated from lab infections the producer and the year are given (KC=Kaitlyn Courville, RK=Ronny Kellner, LP=Lesley Plücker). Grey shading indicates the infection was done by myself, otherwise the infections were done by other lab members; the infection rate for each combination is given.

<i>Ar. hirsuta</i>	Spore batch	Lab spore batch	infection rate
Slovenia	<i>T. thlaspeos</i> BB 2013		40.0 %
		<i>T. thlaspeos</i> KC 2015	4.5 % (2016)
		<i>T. thlaspeos</i> KC 2015	0.0 % (2019)
		<i>T. thlaspeos</i> RK 2018	0.0 %
		<i>T. thlaspeos</i> LP 2021	0.0 %
Ronheim	<i>T. thlaspeos</i> BB 2013		0.0 %
	<i>T. thlaspeos</i> RH 2015		53.0 %
	<i>T. thlaspeos</i> RH 2018		39.1 %
		<i>T. thlaspeos</i> RK 2018	60.0 %
		<i>T. thlaspeos</i> LP 2021	0.0 %
Hohe Leite		<i>T. thlaspeos</i> LP 2021	0.0 %
	<i>T. thlaspeos</i> HL 2015		30.0 %
	<i>T. thlaspeos</i> EB2015		22.5 %
Bad Berneck		<i>T. thlaspeos</i> LP 2021	0.0 %

3.1.3 Discussion

Important open questions in the field of plant-microbe interaction focus on understanding plant-microbe interactions on a more holistic level. Understanding how

the interactions between plant and microbe are shaped by the microbial community as well as abiotic factors and how the plant balances beneficial and pathogenic interactions and transferring this basic knowledge to applied crop research, will be important goals for the scientific community in the years to come (Harris *et al.*, 2020). *T. thlaspeos* harbours special potential in this regard. As it is the only Brassicaceae smut fungus known (Frantzeskakis *et al.*, 2017), it can link the immense knowledge and tools gained in *A. thaliana* on plant- microbe interactions of the past decades (Provart *et al.*, 2016) with the knowledge of the well-studied smut fungi (Brefort *et al.*, 2009) to link basic research and applied crop science. While this means shifting the focus from binary interactions to engage more in microbiome studies, the former is the prerequisite for the latter. The results presented here provide further insights into the basic infection biology of *T. thlaspeos* and open up new perspectives for future investigations.

Stomata as entry ports for *T. thlaspeos*

Stomata represent a natural opening of the plant surface many plant pathogens utilize for infection (Niks and Rubiales, 2002). Here I show, that leaf infection on cotyledons as well as true leaves is achieved via appressoria formation on epidermal cells or preferably on guard cells of stomata or hyphal growth through the stoma in *T. thlaspeos*. Subsequently, the guard cells are colonized with intracellular hyphae. In both cases the appressorium was formed between the junction of two cells. Appressoria are infection structures typically formed by biotrophic fungi in order to infect the host plant and minimizing damage to the plant (Mendgen and Hahn, 2002). In *U. maydis* hyaline terminal appressoria are formed on the cuticle of epidermal or guard cells to penetrate the surface and subsequently to grow either through the underlying cell wall or to grow initially between epidermal cells (Emmett and Parbery, 1975; Snetselaar and Mims, 1992; Snetselaar, 1993; Fernández-Álvarez *et al.*, 2012). In contrast, growth of *U. maydis* through the stoma was not observed, although sporidia accumulate in depressions surrounding stomata (Snetselaar and Mims, 1992). In rust fungi on the other hand, appressoria are formed in response to topographical features of the leaf (Mendgen and Hahn, 2002). In the bean rust fungus *Uromyces appendiculatus* for example it was shown that appressoria differentiation is induced over the stoma by the leaf surface topography allowing the fungus to recognize the height of the stomatal lip (Hoch *et al.*, 1987). In comparison,

the rust fungus *Phakopsora pachyrhizi* also responds to ridge heights but in this case appressoria are formed between the junctions of epidermal cells (Allen *et al.*, 1991), similar to *T. thlaspeos*. But in difference to rust and other smut fungi *T. thlaspeos* does not seem to be restricted to a special structure for appressoria formation, but can use the whole leaf surface as entry sites. Several modes of penetration on stomata and epidermis are also found in necrotrophic fungi like *Sclerotinia sclerotiorum* (Garg *et al.*, 2010) or *Phaeoacremonium spp* (Feliciano and Gubler, 2001). But the subsequent colonization of the guard cells has not been shown in any fungus so far. This seems counter intuitive at first, as the fungus passed already the stoma, but maybe this is a mechanism to suppress early host immune responses. In *Phytophthora infestans* it was for example recently shown, that guard cell death and stomatal closure are part the host plant immune response, which the fungus counteracts (Yang *et al.*, 2021). Thus it seems possible, that the colonization of the guard cells to suppress early immune responses or for example to keep the stomata open is important for *T. thlaspeos* to establish infection.

The sterile conditions of this infection setup entail very humid growth conditions under which the stomata are usually open. Besides, high humidity affects also plant defence responses like the EDS1 pathway that is regulated through abiotic stresses (Wiermer, Feys and Parker, 2005). Various studies have shown that EDS1/PAD4-dependent responses are suppressed under high humidity (RH>95 %) (Jambunathan, Siani and McNellis, 2001; Zhou *et al.*, 2004; Xiao *et al.*, 2005). In the future it will therefore be essential to show appressoria formation also under natural growth conditions, to ensure that the observations are not artefacts. The powdery mildew fungus of barley *Blumeria graminis f. sp. hordei* for examples requires rather dry conditions for appressoria formation and maturation (Sugai *et al.*, 2020) while powdery mildew of tomato *Leveillula taurica* requires humid conditions for efficient spore germination (Guzman-Plazola, Davis and Marois, 2003). Pretests with soil grown plants were so far not successful to study *T. thlaspeos* appressoria formation either because of other contaminating microbes or lack of spore germination. A semi-sterile infection system on sand might be sufficient to study appressoria formation under more natural conditions. Once this is established it will be intriguing to investigate the plant response as well as the fungal response in spatio-temporal resolution. So far the low and unreproducible rate of appressoria formation on the leaf surface, despite numerous optimization attempts, prevented to analyse the early

infection stages of *T. thlaspeos* on a molecular level via RNA-seq. Now there might be a new approach: Protoplastation of *U. maydis* infected maize tissue showed, that *U. maydis* hyphae sometimes appear to be firmly attached to a maize protoplast (Seomun Kwon personal communication). Using the COLORFUL-PR1pro reporter line it might be possible to sort plant protoplasts with attached hyphae as well as cells that induced an immune response after fixation and protoplasting via fluorescence activated cell sorting and analyse these using single cell RNAseq. If additionally, *T. thlaspeos* appressoria could be induced on an artificial surface like the induction of *U. maydis* appressoria on parafilm (Mendoza-Mendoza *et al.*, 2009), it would even be possible to distinguish the stage of appressoria formation from the initial invading hyphae in *T. thlaspeos*. Differences can for example be expected with regard to the secretome, since the penetration of the plant surface likely requires the secretion of plant cell wall degrading enzymes (PCWDEs) (Lanver *et al.*, 2014), while after penetration the secretion of effectors to counteract the plants immune response is important (Heimel, Freitag, Hampel, Ast, *et al.*, 2013; Hampel *et al.*, 2016). This approach would have the advantage that data on both the fungal and plant side of the interaction could be obtained in spatial resolution. While detection of transcriptomic changes towards infection in whole leaf tissues is possible, the hormone signalling output analysis of *Hyaloperonospora arabidopsidis* with *A. thaliana* CORLORFUL-PR1pro, -VSP2pro and PDF1.2apro revealed distinct hormone responses depending on presence of and distance to *H. arabidopsidis* at the cellular level, underlining the coordinated and spatio-temporally controlled manner of the plants immune system (Ghareeb *et al.*, 2020) Considering, that the portion of *T. thlaspeos* reads in a systemically colonized leaf represents only 0.28 % at most (Courville *et al.*, 2019), and the low and unreproducible rates of appressoria formation, a single-cell based approach is needed to investigate the interaction with *T. thlaspeos* during this early infection stage.

Another way in - appressoria on the root surface

Besides the infection via leaf tissue, *T. thlaspeos* teliospores can also infect their host via the roots (Frantzeskakis *et al.*, 2017), similar to *Sporisorium reilianum* (Martinez *et al.*, 2000, 2002), a close relative of *U. maydis*, while other described smut fungi of the *Thecaphora* clade like *T. frezii* (Rago *et al.*, 2017) or *T. solani* (Andrade *et al.*, 2004) seem to infect underground reproductive organs directly (gymnosporium/peg in

peanut and tubers/stolons and underground stems in potato (Arias *et al.*, 2021)). In which parts leaf and root infection in *T. thlaspeos* occur in nature is not clear and not possible to investigate, but since seeds and spores are sometimes distributed together (Frantzeskakis *et al.*, 2017), root infection can be considered an important infection strategy. In *T. frezii* and *T. solani* it is described that teliospores can overwinter in the soil remaining dormant up to several years until host plant factors induce germination (Arias *et al.*, 2021). As *T. thlaspeos* also only germinates upon perception of a plant signal (Frantzeskakis *et al.*, 2017) a similar scenario seems likely. I showed that *T. thlaspeos* infects roots by forming appressoria-like swollen structures, likely also between cell junctions similar to leaves. In *S. reilianum* no infection structures for root infection were observed (Martinez *et al.*, 2000, 2002) while in arbuscular mycorrhiza fungi, hyphopodia are appressoria-like, well described infection structures formed by AM-hyphae on the root surface (Gutjahr and Parniske, 2013). In *Medicago truncatula* it was shown that hyphopodia formation of AM-fungi as well as appressoria formation of *Phytophthora palmivora* on roots is specifically induced by plant cutin monomers (Wang *et al.*, 2012). Cutin and suberin are lipid plant polymers that form hydrophobic barriers of the cell wall (Pollard *et al.*, 2008). While cutin is mostly part of areal plant tissues, it was recently shown that primary roots also form a cuticle root cap (Berhin *et al.*, 2019). In comparison, cutin and suberin clearly differ in their macromolecular structure but share similarities in their building blocks. For example, both contain ω -Hydroxy fatty acids (Pollard *et al.*, 2008), that were shown to induce appressoria formation in *P. palmivora* (Wang *et al.*, 2012). In many pathogenic fungi, cutin monomers, such as ω -Hydroxy fatty acids, are important signalling molecules to induce appressoria formation on the leaf surface (Gutjahr and Parniske, 2013), including *U. maydis* (Mendoza-Mendoza *et al.*, 2009) and the rust fungus *B. graminis* (Tsuba *et al.*, 2002). Although it is also possible that the appressoria observed on roots and leaves of *T. thlaspeos* are entirely different structures, that differentiate upon perception of different molecules, it seems intriguing that they might be induced by the same fatty acid monomer allowing the fungus to infect all plant tissues via a conserved mechanism, which might be as old as the evolution of land plants (Murray *et al.*, 2013). This hypothesis could be easily tested with germination assays using well plates in presence of different hydroxyl fatty acids or for example by coating the bottom of the well plates with cuticle waxes, similar to an approach by Hansjakob and colleagues (Hansjakob *et al.*, 2010).

Another feature present in leaf and root tissue that could contribute to appressoria differentiation in *T. thlaspeos* is the surface topography, since appressoria of *T. thlaspeos* seem to be formed always between cell junctions that present ridges of a certain height. Similar to experiments in rust fungi a potential contribution of the surface topography to appressoria differentiation in *T. thlaspeos* could be tested with growth assays on artificial surfaces with defined topographies or polystyrene replica of leaf surfaces (Allen *et al.*, 1991).

How to dine inside

One of the initially asked questions addressed the formation of feeding structures in *T. thlaspeos* infection. Haustoria are specialized feeding structures, formed by many biotrophic and hemibiotrophic pathogens like rusts (Garnica *et al.*, 2014), powdery mildews and oomycetes (O'Connell and Panstruga, 2006) but also the smut fungus *U. hordei* forms haustoria-resembling lobed structures (Ökmen *et al.*, 2018). Leaf infection assays using the COLORFUL-PR1pro reporter line revealed, *T. thlaspeos* forms a biotrophic interphase during initial intracellular growth. In this initial data set as well as in all root infections investigated so far no formation of specialized haustoria-like feeding structures was observed. This is similar to *U. maydis* and *S. reilianum* where such structures were also not observed yet (van der Linde and Göhre, 2021).

One spore to infect them all?

Another one of the questions this thesis aimed to address regards the host range of different spore isolates. In total at least 15 different host species are described for *T. thlaspeos* (Frantzeskakis *et al.*, 2017) and recently a new host was reported in North Africa, *Arabis pubescens* (Denchev and Denchev, 2019). For smut fungi this is a slightly broader host range than usual (van der Linde and Göhre, 2021). The comparison of *T. thlaspeos* infections with different host species and ecotypes revealed that *T. thlaspeos* might exist in various *formae specialis*. Although parallel infection data to unequivocally prove this hypothesis is missing yet a decade of unsuccessful *Ar. alpina* soil infection strongly argues in favour of this hypothesis. This is in contradiction with the observation that *Ar. alpina* roots are highly susceptible in our liquid infection system. Unfortunately, the root tissue of soil grown plants is hardly analysable as most of the root tissue is lost during preparation, making it impossible

to directly compare both infection systems. Although the fungal infection pattern observed for *Ar. hirsuta*, *Ar. alpina* and *A. thaliana* in liquid infection resembles the pattern observed for soil infected *Ar. hirsuta* leaf tissue, the observation that *T. thlaspeos* does not reach the leaves in the liquid system in any of the species points out, that a closer resemblance of the natural infection conditions is needed that allows to sample all plant tissues and allows to follow infection over time. Again, a semi-sterile infection setup using sand might be the solution. To test the hypothesis of different *T. thlaspeos* f. spec., the collection of additional *T. thlaspeos* and host samples would be ideal. Recently, *T. thlaspeos* infected *Ar. hirsuta* as well as *Ar. ciliata* were reported from Bavaria, Germany (Kruse *et al.*, 2018). Spores from both plants would be a great opportunity to compare *T. thlaspeos* strains possibly adapted to different hosts with our existing strains for example to identify host specific effectors. It was already shown that *Thecaphora* effector THTG_4398 is found only in the *Ar. hirsuta* spore isolate LF1 but not LF2 (Courville *et al.*, 2019), thus more differences could be expected from isolates of different host plant species.

Collecting basic knowledge about pathosystems is needed to discover conserved mechanisms between species as these are good targets for new broad spectrum fungicides. A very recent example is the elucidation of the Stp complex function in *U. maydis*, a complex consisting of five effector proteins and two membrane proteins that protrudes from the fungal plasma membrane into the host cell and is crucial for fungal virulence to suppress host plant defence responses and might be involved in effector translocation (Ludwig *et al.*, 2021). This protein complex seems to be conserved in smut fungi and led to a recently filed patent for new anti-fungal compounds that are effective against *U. maydis* and even a rust fungus (Max Planck Society, 2021). In comparison to smut fungi, research in rust fungi is limited for they are obligate biotrophs and transformation protocols are lacking, thus the investigation of candidate effectors requires surrogate systems. As proposed by Jaswal and colleagues (Jaswal, Rajarammohan, *et al.*, 2020), smut fungi might be a good model system to study rust effector proteins. With a transformation protocol for *T. thlaspeos* recently established (Plücker *et al.*, 2021) and a culture infection protocol currently being established in our lab, this could in the future also include *T. thlaspeos*.

3.2 *Thecaphora thlaspeos* Pit1 complementation analysis in *Ustilago maydis*

3.2.1 Background

3.2.1.1 *Thecaphora thlaspeos* THTG_00998 a putative virulence factor, highly upregulated during infection

In phytopathology the ability of a pathogen to cause disease is defined as pathogenicity, while the degree of damage caused is referred to as virulence (Sacristán and García-Arenal, 2008; Rauwane *et al.*, 2020). To do so, pathogens utilize virulence factors that enable them to colonize, manipulate and feed from their host (Rauwane *et al.*, 2020). In this context secreted effector proteins play a fundamental role and thus were intensively studied over the last years (Toruño, Stergiopoulos and Coaker, 2016). While the definition of effector proteins is rather narrow, the arsenal of weapons pathogens deploy to promote virulence is not limited to secreted proteins. Except effector proteins, secondary metabolites, small RNAs or membrane proteins for example do also contribute to virulence (Wolpert, Dunkle and Ciuffetti, 2002; Weiberg *et al.*, 2013). For example, in *U. maydis*, the contribution of sugar transporters (Wahl *et al.*, 2010; Schuler *et al.*, 2015), the membrane protein Pit1 (Doehlemann *et al.*, 2011) or the recently identified virulence-associated membrane proteins Vmp1 and Vmp2 (Weiland and Altegoer, 2021) to virulence highlights their importance for pathogenicity.

One possibility to identify virulence factors is to identify genes specifically upregulated during infection in transcriptomic datasets, a classic approach that is also applied in effector prediction. To identify effector protein candidates in *T. thlaspeos*, an RNA-Seq analysis was conducted by our group with *T. thlaspeos* culture and *T. thlaspeos* infected *A. hirsuta* plants, revealing a list of *T. thlaspeos* genes highly upregulated during infection (Courville *et al.*, 2019). Among the top 132 genes upregulated during infection compared to culture is the gene THTG_00998 (position 23 with a 132,51-fold induction). Orthology analysis identified it as an orthologue of *pit1* in *U. maydis* (Courville *et al.*, 2019). While the function of *U. maydis* Pit1 remains elusive, it was identified as a virulence factor essential for tumour formation in *U. maydis* infected maize plants (Doehlemann *et al.*, 2011).

3.2.1.2 The *pit* cluster of *U. maydis*

In *U. maydis* effector genes are arranged in gene clusters that are upregulated during infection (Kämper *et al.*, 2006). One of those clusters, that was identified, is the *pit* (protein(s) important for tumours) cluster (Doehlemann *et al.*, 2011). This cluster contains four genes named *pit1-pit4*. While deletion mutants of *pit3* or *pit4* are not affected in their virulence, deletion mutants of *pit1* or *pit2* are impaired in tumour formation. Further analysis revealed upregulation of *pit1* and *pit2* during all stages of pathogenic development. But while tumour formation is almost abolished in *pit1* as well as *pit2* mutants, epidermal penetration and proliferation during the early phase of pathogenic development were unaffected. Later on, further colonization is impaired and hyphae fail to proliferate in the mesophyll layers. Subsequent analysis of Pit2 revealed that it is a cysteine protease inhibitor that is secreted into the apoplast during infection (Mueller *et al.*, 2013). In contrast, Pit1 is predicted to be a membrane protein with seven transmembrane domains and *pit1::gfp* fusions showed, that Pit1-Gfp localizes to the plasma membrane of hyphal tips, vesicular structures along the hyphae and early endosomes. A molecular function of Pit1 is unknown so far, but the authors speculate because of its localization that Pit1 has either a function in the plasma membrane or mediates the uptake of an unknown compound into the cell via receptor-mediated endocytosis. (summarized from Doehlemann *et al.* 2011)

3.2.2 Results

3.2.2.1 The *pit* locus is conserved among *T. thlaspeos* and members of the *Ustilaginales*

Initially, homology of *T. thlaspeos* THTG_00998 and *U. maydis* Pit1 was confirmed by manual BLAST search and protein sequence alignment with an overall homology of 23 % (linear scoring matrix). To gain confidence in the relation of THTG_00998 to *U. maydis* Pit1 the *pit* loci of several smut fungi were analysed in more detail. On a genomic level, orthologues for all genes of the *U. maydis pit* cluster (*pit1 – pit4*) including five flanking genes to the right and left except *UMAG_11315* and *pit2* were found in *T. thlaspeos* (Figure 3-8, Table 3-3). Overall the Pit2 sequence is poorly conserved in smut fungi, except for a 14 amino acid motif, that is crucial for function (Mueller *et al.*, 2013). No such motif could be identified in the proteome of *T. thlaspeos*, further supporting the absence of Pit2 in *T. thlaspeos*.

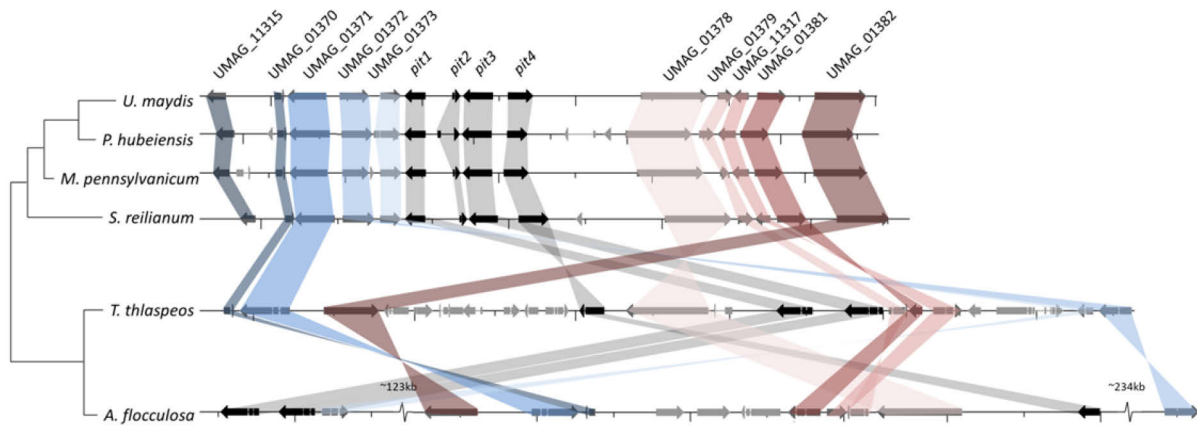


Figure 3-8 Inter-species synteny of the *pit* locus of *U. maydis*, *P. hubeiensis*, *M. pennsylvanicum*, *A. flocculosa* and *T. thlaspeos*. In black shades are genes of the *pit* locus, blue shades represent upstream flanking genes, red shades downstream flanking genes. The phylogenetic tree is based on a multiway DNA alignment including genes for 18S rRNA, ITS1, 5.8S rRNA, ITS2 and 28S rRNA (partial and complete sequence).

A comparison of the grass smuts *U. maydis* and *Sporisorium reilianum*, the anamorphic yeasts *Pseudozyma hubeiensis*, which is the closest sequenced relative of *U. maydis*, and *Anthracoystis flocculosa*, which is the closest sequenced relative of *T. thlaspeos*, as well as the dicot smut *Melanopsichium pennsylvanicum*, that evolved from the grass smuts through a host jump (Sharma *et al.*, 2014), with *T. thlaspeos* revealed that the genomic context of the *pit* locus is conserved only in the smut fungi closely related to *U. maydis* (Figure 3-8). In these closely related smut fungi *U. maydis*, *P. hubeiensis*, *M. pennsylvanicum* and *S. reilianum* (Um group), there is perfect synteny of the *pit* locus, while the genes are arranged differently in the more distantly related *T. thlaspeos* and *A. flocculosa* (Tt group) (Figure 3-8). Conservation of the *pit* locus is also reflected on the protein level with usually similar protein lengths between the orthologues and an overall high percentage level of amino acid identity in the Um group (Table 3-3). The Tt group on the other hand differs from the Um group. For example, the *pit1* or *UMAG_01378* orthologues in the Tt group are bigger than in the Um group. While there is no intron in the *pit* orthologues of the Um group, both orthologues of the Tt group contain two introns and a similar intron exon structure (Figure 3-8). Furthermore, amino acid comparison in this cluster reflects phylogeny (Table 3-3). Finally, the two genes *UMAG_11315* and *pit2* both do not have orthologues in *T. thlaspeos* or *A. flocculosa* (Figure 3-8). In summary, *T. thlaspeos* possesses a *pit1* orthologue as well as the majority of the flanking genes but in a rearranged genomic context.

Table 3-3 Comparison of the *U. maydis* pit locus (including five flanking genes to each side) with the corresponding orthologues in *P. hubeiensis*, *M. pennsylvanicum*, *A. flocculosa* and *T. thlaspeos* based on global-reference protein alignments. Listed are the amino acid lengths for all proteins and their amino acid identity compared to *U. maydis*. Additionally, in *A. flocculosa* the identity compared to *T. thlaspeos* is written behind the corresponding value for *U. maydis*. Conserved domains or functions as far as listed in NCBI are mentioned below for each protein.

Organism Protein	UMAG_11315		UMAG_01370		UMAG_01371		UMAG_01372		UMAG_01373	
	Length	Identity	Length	Identity	Length	Identity	Length	Identity	Length	Identity
<i>U. maydis</i>	407 aa	100 %	151 aa	100 %	825 aa	100 %	656 aa	100 %	423 aa	100 %
<i>P. hubeiensis</i>	393 aa	61 %	145 aa	70 %	863 aa	85 %	658 aa	83 %	517 aa	67 %
<i>M. pennsylvanicum</i>	358 aa	56 %	146 aa	71 %	814 aa	86 %	557 aa	68 %	437 aa	74 %
<i>S. reilianum</i>	323 aa	49 %	141 aa	72 %	856 aa	84 %	675 aa	79 %	430 aa	75 %
<i>T. thlaspeos</i>	-	-	133 aa	40 %	920 aa	46 %	650 aa	48 %	288 aa	33 %
<i>A. flocculosa</i>	-	-	142 aa	49 % 59 %	914 aa	50 % 72 %	687 aa	49 % 71 %	467aa	40 % 46 %
Conserved domains / function	-		Thioredoxin-like superfamily		RRN3 RNA polymerase I specific transcription initiation factor		GTPase		vacuolar membrane protein	

Organism Protein	Pit1		Pit2		Pit3		Pit4	
	Length	Identity	Length	Identity	Length	Identity	Length	Identity
<i>U. maydis</i>	435 aa	100 %	118 aa	100 %	635 aa	100 %	532 aa	100 %
<i>P. hubeiensis</i>	444 aa	69 %	150 aa	29 %	632 aa	67 %	427 aa	51 %
<i>M. pennsylvanicum</i>	452 aa	64 %	109 aa	29 %	624 aa	61 %	522 aa	50 %
<i>S. reilianum</i>	423 aa	69 %	117 aa	32 %	614 aa	66 %	636 aa	51 %
<i>T. thlaspeos</i>	671 aa	23 %	-	-	733 aa	37 %	457 aa	30 %
<i>A. flocculosa</i>	738 aa	22 % 39 %	-	-	699 aa	39 % 56 %	454 aa	32 % 49 %
Conserved domains / function	TM domains, unknown function		Cys protease inhibitor, SP		Cap-Gly, LRR		Expansin, endo-glucanase-like	

Organism Protein	UMAG_01378		UMAG_01379		UMAG_11317		UMAG_01381		UMAG_01382	
	Length	Identity	Length	Identity	Length	Identity	Length	Identity	Length	Identity
<i>U. maydis</i>	1430 aa	100 %	313 aa	100 %	306 aa	100 %	615 aa	100 %	1114 aa	100 %
<i>P. hubeiensis</i>	1417 aa	76 %	304 aa	69 %	371 aa	71 %	608 aa	69 %	1107 aa	73 %
<i>M. pennsylvanicum</i>	1426 aa	71 %	171 aa	30 %	438 aa	68 %	598 aa	69 %	1132 aa	64 %
<i>S. reilianum</i>	1431 aa	73 %	312 aa	68 %	308 aa	81 %	615 aa	67 %	1102 aa	68 %
<i>T. thlaspeos</i>	1769 aa	38 %	305 aa	42 %	268 aa	50 %	513 aa	39 %	1100 aa	34 %
<i>A. flocculosa</i>	1824 aa	38 % 57 %	350 aa	41 % 56 %	415 aa	51 % 45 %	603 aa	43 % 47 %	1142 aa	36 % 60 %
Conserved domains / function	RhoGEF		IMP1 protease		Cis (Z)- Isoprenyl Diphosphate Synthase		-		-	

In comparison *TtPit1* is 236 aa longer than *UmPit1*. The predicted gene model for *Ttpit1* was confirmed via amplification from cDNA previously (Plücker, 2017). A protein alignment of all Pit1 orthologues showed that there is conservation in the N-terminal part of *TtPit1* (Supplementary Figure 7-1) and a putative elongation at the *TtPit1* C-terminus. Predicted transmembrane domains in *TtPit1* and *UmPit1* are located in the N-terminal part roughly within the first 300 aa, suggesting that the

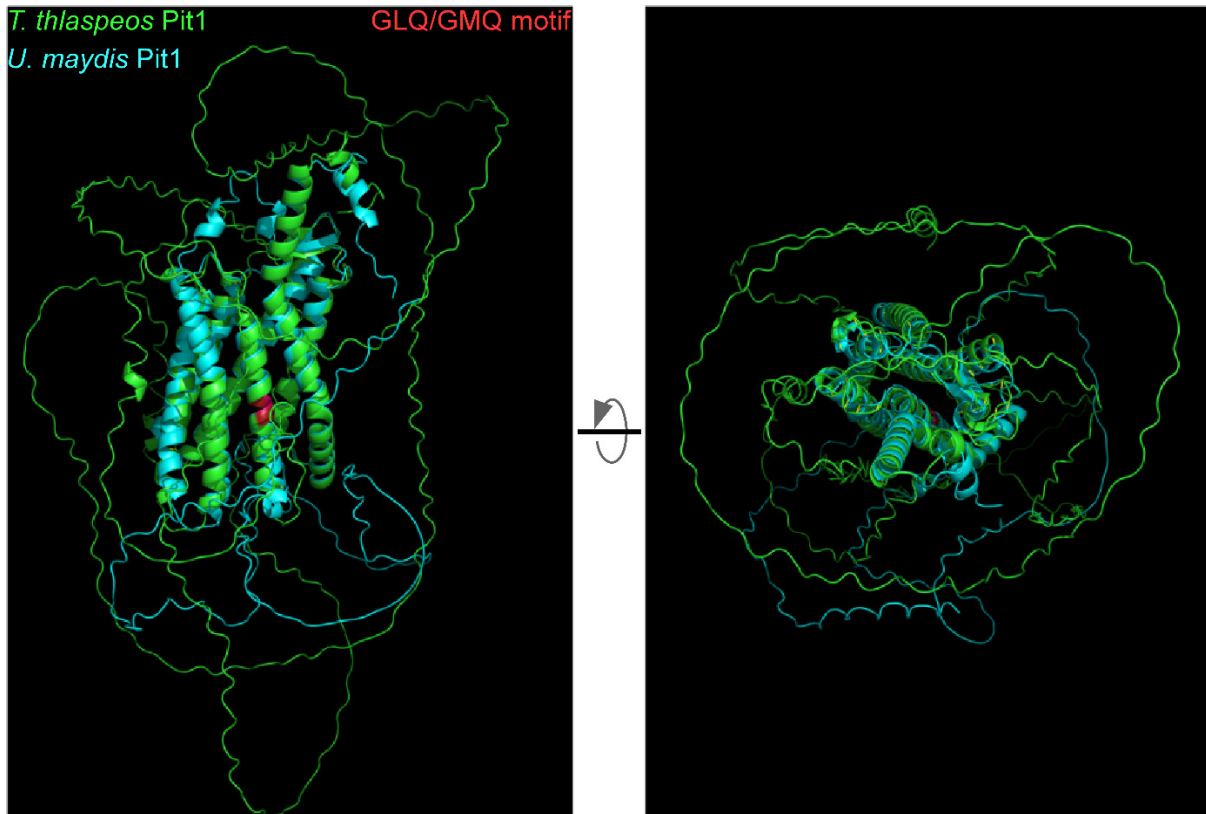


Figure 3-9 Overlay of the structure prediction of *T. thlaspeos* and *U. maydis* Pit1 shows significant overlap in the membrane spanning region (RMSD=0.923 for 1402 of 1681 atoms). Green: *T. thlaspeos* Pit1; blue: *U. maydis* Pit1; red: GMQ/GLQ motif. Left: side view; left: top view. Both Pit1 proteins have seven predicted TM-domains.

region which is integrated into the plasma membrane is conserved while the C-terminal domain is different. Depending on the prediction tool 3-8 TM domains for *UmPit1* and 3-7 TM domains for *T. thlaspeos* were predicted (CCTOP prediction tool (Dobson, Reményi and Tusnady, 2015)), which are in the same region in the protein.

The protein structure prediction tool AlphaFold (Jumper *et al.*, 2021), that became available only recently, confirmed the originally suggested (Doehlemann *et al.*, 2011) seven transmembrane domains for *UmPit1* and similarly for *TtPit1*. Also the overlay of the two proteins fits very nicely in the highly structured regions of the transmembrane domains further supporting that THTG_00998 is a Pit1 orthologue (Figure 3-9).

Additionally, *UmPit1* carries a functionally essential C-terminal O-mannosylation site characterized by a 40 amino acid long stretch consisting of ≥ 40 % serine or threonine (Fernandez-lvarez *et al.*, 2012). In *TtPit1* also a 40 amino acid stretch with 42.5 % Ser/Thr at the C-terminus was found, suggesting that *TtPit1* also has an O-

mannosylation site. In summary these results so far support that *TtPit1* is functional orthologue of *UmPit1*.

3.2.2.2 *T. thlaspeos pit1* is specifically upregulated during infection

The next step to investigate the function of *pit1* was to confirm upregulation during infection of the RNA-Seq dataset (Courville *et al.*, 2019). To this end, *pit1* was amplified from cDNA of a healthy *Ar. hirsuta* plant, a *T. thlaspeos* infected *Ar. hirsuta* plant as well as *T. thlaspeos* culture, confirming that *pit1* is only expressed during plant infection but not in axenic culture (Figure 3-10). This is similar to *pit1* of *U. maydis* (Doehlemann *et al.*, 2011) and supports a function during biotrophic development of the fungus. The next step in investigating the functionality of *TtPit1* would be to analyse the virulence phenotype of the corresponding deletion mutant (Lanver *et al.*, 2017). As a transformation protocol for *T. thlaspeos* was not yet established a complementation analysis of *Ttpit1* in *U. maydis* was done. This experimental strategy was applied successfully to the *T. thlaspeos* effector Pep1 previously (Courville *et al.*, 2019) and thus represents a promising approach here.

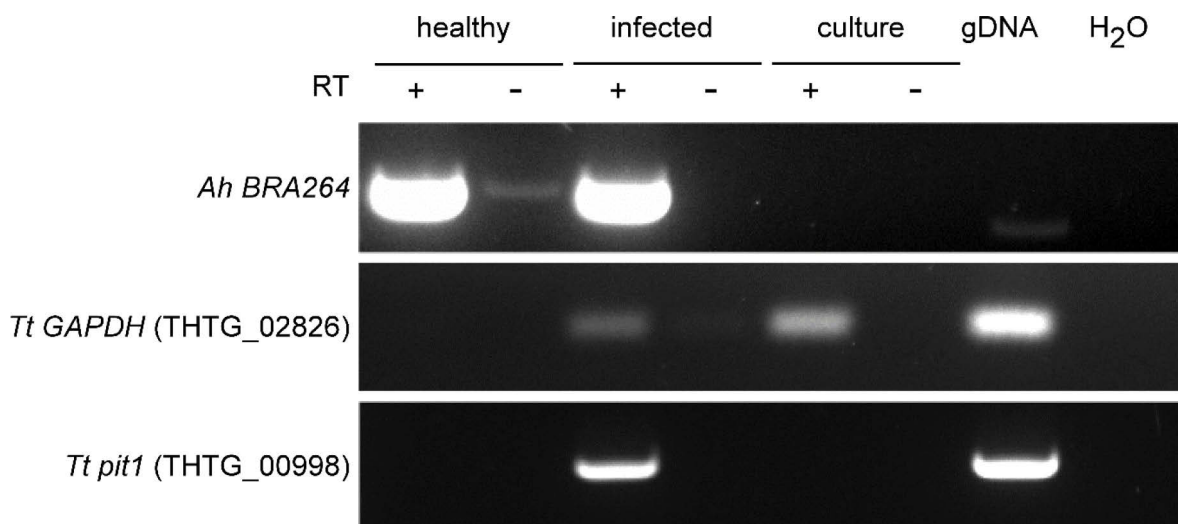


Figure 3-10 *T. thlaspeos pit1* is only expressed during infection but not in axenic culture. PCRs were performed on cDNA generated from RNA of healthy or *T. thlaspeos* infected *Ar. hirsuta* rosette leaves or *T. thlaspeos* culture. Symbols (+) and (-) indicate if the RT reaction was performed in presence or absence of reverse transcriptase, respectively. *Ah BRA264* was amplified as plant marker gene (Stockenhuber *et al.*, 2015), while *Tt GAPDH* was used as marker for *T. thlaspeos*. As positive control the PCRs were also performed on *T. thlaspeos* gDNA.

3.2.2.3 *T. thlaspeos pit1* does not complement the *pit1Δ* phenotype in *U. maydis*

To analyse if *Ttpit1* complements the SG200*pit1Δ* phenotype in *U. maydis* two strains were generated in the SG200*pit1Δ* background. As positive control *Umpit1-gfp* was reinserted into the endogenous locus via homologous recombination and confirmation using Southern Blot, to ensure native gene expression conditions (SG200*pit1Δ-Umpit1-gfp* hereafter referred to as *Umpit1-gfp*). In the second strain *Ttpit1-gfp* (*Ttpit1* open reading frame) was inserted also in the native *pit1* locus via homologous recombination and confirmation using Southern Blot (SG200*pit1Δ-Ttpit1-gfp* #1 and SG200*pit1Δ -Ttpit1-gfp* #2 hereafter referred to as *Ttpit1-gfp* #1 and *Ttpit1-gfp* #2).

Complementation was analysed in three independent infections experiments using the *Zea mays* cultivar Amadeo. The *pit1Δ* phenotype was first described in *Zea mays* Early Golden Bantam infections (Doehlemann *et al.*, 2011). Although the cultivar Amadeo appears to be more resistant towards *U. maydis* infection (general lab observation) the *pit1Δ* phenotype could be confirmed (Figure 3-11 A and B). In comparison, *Umpit1-gfp* regained virulence almost to the degree of the fully virulent SG200_*P_{otef3}xgfp*, while the *Ttpit1-gfp* strains did not complement the mutant phenotype (Figure 3-11). To the contrary, they are even less virulent. Confocal microscopy of infected maize leaves could confirm *U. maydis* Pit1-Gfp expression, but unfortunately not for *T. thlaspeos* Pit1-Gfp indicating that if expressed, expression levels were probably below the detection limit (Figure 3-11).

The native *pit1* promoter induces strongest gene expression between two and eight dpi (14,869 fold induction at 2 dpi (Lanver *et al.*, 2018), still the membrane localization of *U. maydis* Pit1-Gfp is hardly visible *in planta*, while under our conditions it was only possible to see the accumulation of Pit1-Gfp in vacuolar structures (Doehlemann *et al.*, 2011), Figure 3-11 C).

In comparison, plasma membrane localization of the hexose transporter *UmHxt1-Gfp* (Schuler *et al.*, 2015) is nicely visible under our microscopy conditions (Natascha Heßler, personal communication), although *hxt1* expression is maximum half of *pit1* (Lanver *et al.*, 2018), probably indicative of a high turnover rate for Pit1.

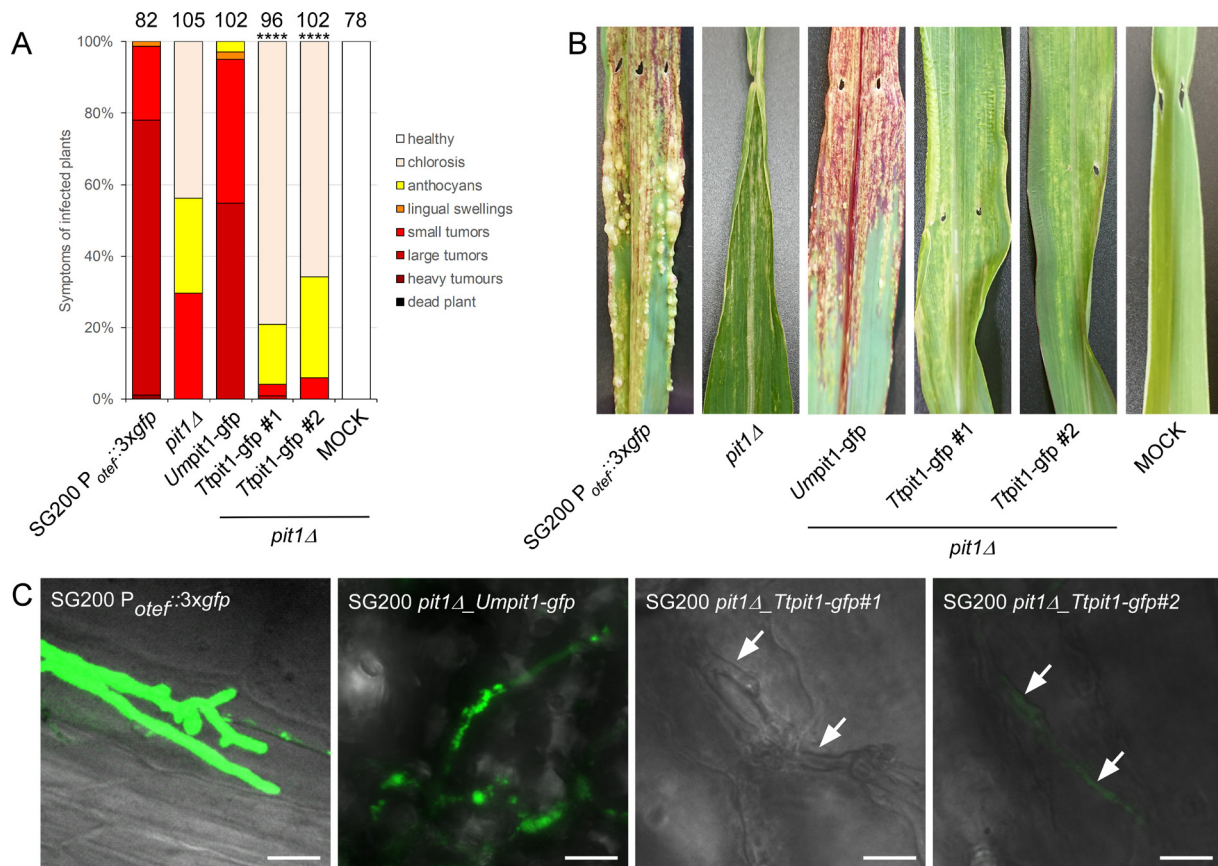


Figure 3-11 *T. thlaspeos pit1* does not complement the *pit1Δ* phenotype in *U. maydis* if expressed under the native *U. maydis pit1* promoter.

A: Disease rating of Amadeo maize plants 12 dpi with *U. maydis* strains as indicated below. The numbers above the bars indicate the total number of plants infected in three independent experiments. Both *Ttpit1-Gfp* complementation strains #1 and #2 do not complement the *pit1Δ* phenotype in *U. maydis* and differ significantly in virulence from both SG200 and *pit1Δ* (Mann-Whitney U test, only the comparison to *pit1Δ* is indicated in the figure).

B: Representative images of maize leaves harvested at 12 dpi with the *U. maydis* strains indicated below. Plants infected with SG200 or *Umpit1-gfp* show chlorosis, anthocyanin formation and tumour formation while the strains *pit1Δ* as well as *Ttpit1-gfp #1* and #2 show predominantly chlorosis.

C: Confocal images of *U. maydis* infected maize leaves 4 dpi. *U. maydis* Pit1-Gfp accumulates in vesicular structures as described in Doehlemann et al (2011). Membrane localization is not visible under these conditions. In comparison *Ttpit1-Gfp #1* and #2 are not detectable *in planta*. Arrows mark *U. maydis* hyphae. The scale bar equals 10µm. Microscopy was performed once.

To improve *T. thlaspeos* Pit1-Gfp expression *in planta* and allow localization in sporidia, *Umpit1-gfp* and *Ttpit1-gfp* (*Ttpit1* coding sequence) were expressed under the artificial constitutive P_{otef} promoter in the *IP* locus. For each construct a strain with a single (*Umpit1-gfp #1* and *Ttpit1-gfp #1*) and multiple (*Umpit1-gfp#2* and *Ttpit1-gfp#2*) insertion of the expression cassette in the *IP* locus was analysed, to cover a range of gene expression levels. Similar to the expression of the fusion constructs under the native promoter, with the constitutive P_{otef} promoter *Umpit1-gfp #1* and #2

regained virulence comparable the fully virulent SG200_*P_{oter}:3xgfp*, while the *Ttpit1*-gfp #1 and #2 strains did not complement the mutant phenotype (Figure 3-12 A,B).

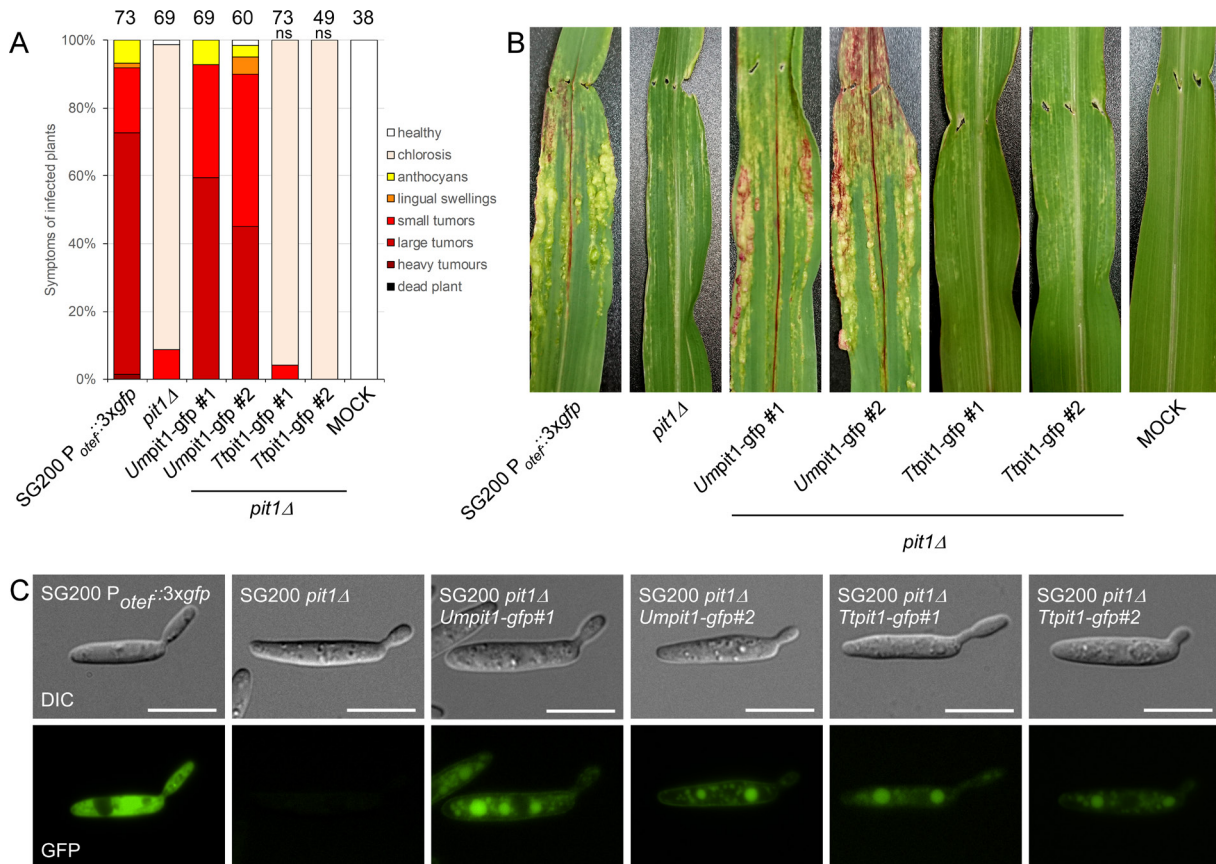


Figure 3-12 *T. thlaspeos pit1* does not complement the *pit1Δ* phenotype in *U. maydis* if expressed under the constitutive *P_{oter}* promoter.

A: Disease rating of Amadeo maize plants 12 dpi with *U. maydis* strains as indicated below. The numbers above the bars indicate the total number of plants infected in three independent experiments. Both *Ttpit1*-gfp complementation strains #1 and #2 do not complement the *pit1Δ* phenotype in *U. maydis*. The strains with #1 harbour single insertions of the respective *pit1* gene while strains with #2 contain multiple copies. In contrast to expression of the construct under the native promoter, both *Ttpit1*-gfp strains do not differ significantly from *pit1Δ* (Mann-Whitney U test).

B: Representative images of maize leaves harvested at 12 dpi with the *U. maydis* strains indicated below. Plants infected with SG200 or *Umpit1*-gfp show chlorosis, anthocyanin formation and tumour formation while the strains *pit1Δ* as well as *Ttpit1*-gfp #1 and #2 show predominantly chlorosis.

C: Microscopy images of *U. maydis* sporidia expressing *pit1*-gfp constructs. *Umpit1*-gfp accumulates in vesicular structures and at the plasma membrane as described in Doehlemann et al (2011). In comparison *Ttpit1*-gfp #1 and #2 also accumulate in vesicular structures, but a membrane localization is not visible. The scale bar equals 10 μ m. Microscopy was performed once. Signal intensities of the GFP channel are comparable between the single insertion strains *Umpit1*-gfp #1 and *Ttpit1*-gfp #1 and *pit1Δ* as well as the multiple insertion strains *Umpit1*-gfp #2 and *Ttpit1*-gfp #2.

Localization of the Pit1-Gfp fusion proteins was verified microscopically in sporidia. Confirming previous observations (Doehlemann et al., 2011), *U. maydis* Pit1-Gfp was found at the fungal plasma membrane as well as vesicular structures (Figure 3-12 C). *TtPit1*-Gfp also localizes to vesicular structures, similar to *UmPit1*-Gfp, but

localization at the plasma membrane was not observed (Figure 3-12 C). In comparison, the *TtPit1*-Gfp signal seems slightly lower than that of the corresponding *UmPit1*-Gfp. Under the artificial P_{otef} promoter *Ttpit1* is definitely expressed in sporidia. While the localization pattern looks partially similar to *UmPit1*, it's unclear if the protein also localizes to plasma membrane.

Another maize cultivar that became available at our institute later in this thesis is Golden Bantam. In comparison to Amadeo and Early Golden Bantam it appears to be even more sensitive towards *U. maydis* infection (general lab observation). With this cultivar there is the advantage that minor differences of avirulent strains might be reflected in the infection symptoms. A single infection experiment was additionally performed with the cultivar Golden Bantam (Figure 3-13). As expected, increased severity of disease symptoms was observed for all strains, but the differences of virulence between the strains remained the same. In this experiment protein expression was also analysed via confocal microscopy. In comparison to expression under the native promoter *TtPit1*-Gfp expression was also verified *in planta* but again localization to the plasma membrane was not observed. In the single insertion strain, *Ttpit1*-gfp #1 accumulated in vesicular structures while for the multiple insertion strain *Ttpit1*-gfp#2 a diffuse Gfp signal was observed. In the *UmPit1*-Gfp#2 strain also only a diffuse GFP signal was observed. To date there is no quantitative data about expression levels *in planta* with the P_{otef} promoter available. Based on microscopy, *Pit1*-Gfp expression under the P_{otef} promoter seems lower compared to the native promoter.

In summary, *Ttpit1*-gfp did not complement the *pit1* Δ phenotype, although the protein is expressed under an artificial promoter *in planta*. Whether this is because *TtPit1* does not functionally complement *UmPit1* or localizes falsely in *U. maydis* could not be determined with the applied methods. Either way the results indicate that *U. maydis* is not a suitable surrogate to investigate *TtPit1* contribution to virulence. In the future a putative virulence function of *TtPit1* needs to be studied in *T. thlaspeos* directly. To do so two techniques will be essential. First, a transformation method to modify genes and their expression in *T. thlaspeos* and second, a culture infection system to study the effects of the genetic manipulation *in planta*. As part of this thesis a transformation system was developed for *T. thlaspeos*.

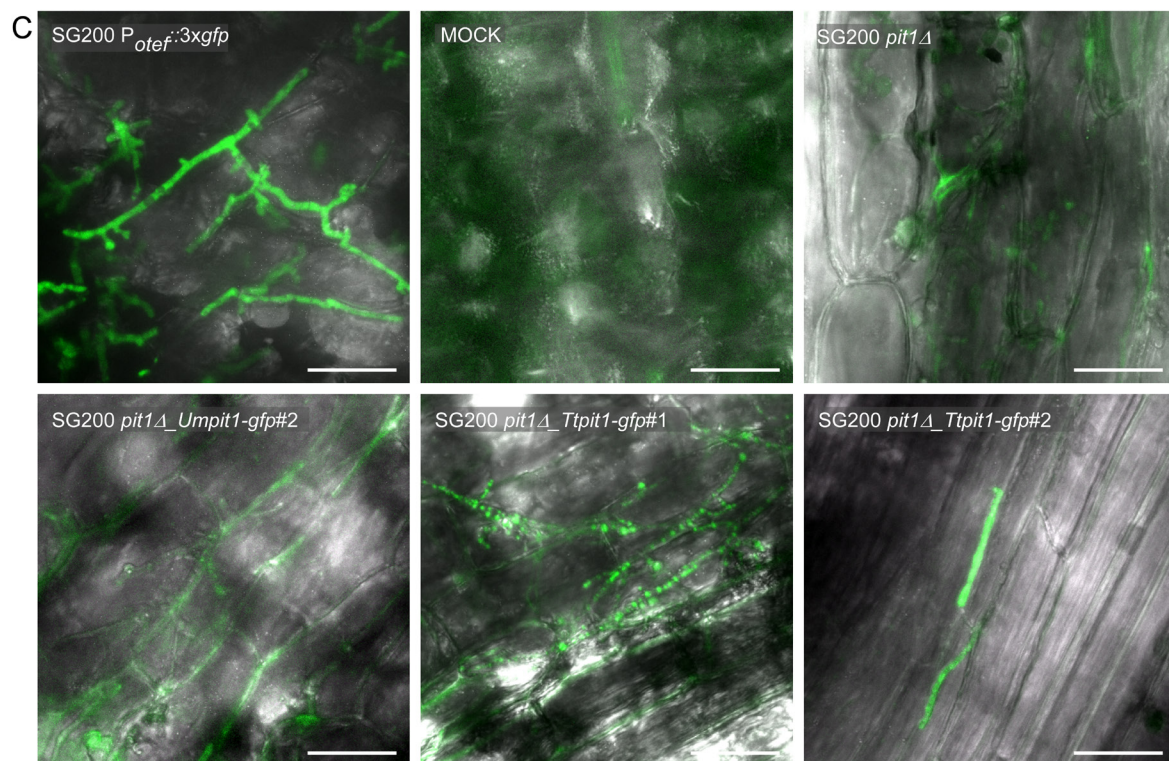
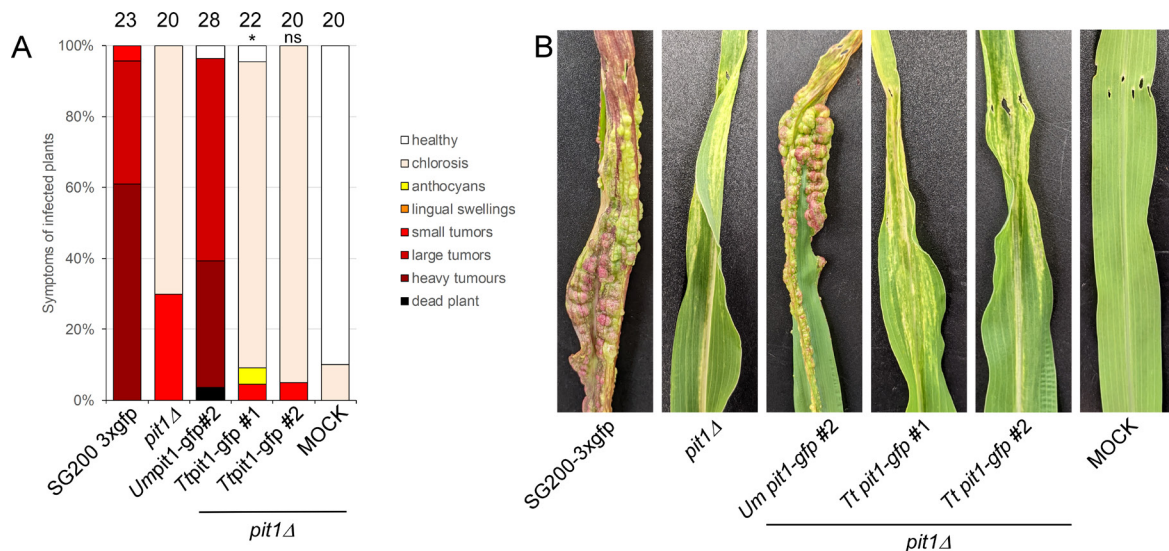


Figure 3-13 *T. thlaspeos pit1* does not complement the *pit1Δ* phenotype in *U. maydis* independent of the maize cultivar.

A: Disease rating of Golden Bantam maize plants 12 dpi with *U. maydis* strains as indicated below. The numbers above the bars indicate the total number of plants infected in one experiment. Both *Ttpit1-gfp* complementation strains #1 and #2 did not complement the *pit1Δ* phenotype in *U. maydis*. The strain #1 harbours a single insertion of the *Ttpit1* gene while the strains with #2 contain multiple copies respective *U. maydis* or *T. thlaspeos pit1* gene. Interestingly, in the Golden Bantam cultivar the single insertion *Ttpit1-gfp* strain differed significantly from *pit1Δ*, while the multiple insertion strain did not (Mann-Whitney U test).

B: Representative images of maize leaves harvested at 12 dpi with the *U. maydis* strains indicated below. Plants infected with SG200 or *Umpit1-gfp #2* show chlorosis, anthocyanin formation and massive tumour formation while the strains *pit1Δ* as well as *Ttpit1-gfp #1* and #2 show predominantly chlorosis.

C: Confocal images of *U. maydis* infected maize leaves 4 dpi. *Umpit1-gfp #2* and *Ttpit1-gfp #2* show a diffuse Gfp signal that is even lower for *Umpit1-gfp #2* than expression under the native promoter. In the strain *Ttpit1-gfp #1* *T. thlaspeos* Pit1-Gfp accumulates in vesicular structures. Membrane localization is not visible under these conditions. The scale bar equals 25 μ m. Microscopy was performed once. The signal intensity of the GFP channel is comparable for the Gfp fusion strains and otherwise adjusted to the individual sample.

3.2.2.4 Establishment of a transformation protocol for *T. thlaspeos*


The article “Genetic Manipulation of the Brassicaceae Smut Fungus *Thecaphora thlaspeos*” published in Journal of fungi (<https://doi.org/10.3390/jof7010038>) is reprinted here with permission according to the open access Creative Commons CC BY 4.0 license of MDPI.

3.2.2.4.1 Summary

Genetic transformation of an organism is an essential technique in research. Gene studies, genetic engineering in biotechnology, in vivo imaging or even basic cloning would be unthinkable without it. For *T. thlaspeos* to become a successful model system this and a culture infection system are the two essential techniques that need to be established. The case of *TtPit1* nicely illustrates that heterologous systems, although they are a very valuable tool to study organisms where a transformation protocol either is not or cannot be established, have their limits. To allow to investigate *T. thlaspeos* infection biology by genetic approaches in the future, for example a putative contribution of Pit1 to virulence, study Mg²⁺ transport or to generate reporter lines, a transformation method was established and published in Journal of Fungi in 2021 as part of this thesis. The established transformation method for *T. thlaspeos* relies on protoplast-mediated transformation, a method that is most common (D. Li *et al.*, 2017) and works well in smut fungi. As a proof-of-principle, fluorescent marker strains were generated (Figure 6) that allowed to visualize cytoplasmic fusion after putative mating events (Figure 7) as well as the deletion of the pheromone receptor *pra1*, that is essential for mating in *T. thlaspeos* to shed light on the conserved molecular mechanisms underlying the mating process. These two examples nicely illustrate the potential of this technique for the *T. thlaspeos* research, which will be essential to address current and future yet unanswered questions of the *T. thlaspeos* infection biology and its life cycle. Two aspects of *T. thlaspeos* research, in which the established transformation method is currently applied include the nutrition of *T. thlaspeos* during biotrophic growth (Natascha Heßler, PhD thesis) and the contribution of RNAi to virulence (Trusha Adeshara, PhD thesis). In the future the generation of a *pit1Δ* mutant in *T. thlaspeos* will establish the basis to study the virulence function of Pit1 directly in *T. thlaspeos*.

Article

Genetic Manipulation of the Brassicaceae Smut Fungus *Thecaphora thlaspeos*

Lesley Plücker [†], Kristin Bösch [†], Lea Geißl, Philipp Hoffmann and Vera Göhre ^{*†} 

Institute of Microbiology, Cluster of Excellence in Plant Sciences, Heinrich-Heine University, Building 26.24.01, Universitätsstr.1, 40205 Düsseldorf, Germany; lesley.pluecker@hhu.de (L.P.); kristin.boesch@hhu.de (K.B.); lea.geissl@hhu.de (L.G.); Philipp.Hoffmann.15@uni-duesseldorf.de (P.H.)

* Correspondence: vera.goehre@hhu.de; Tel.: +49-211-811-1529

† These authors contribute equally to this work.

Abstract: Investigation of plant–microbe interactions greatly benefit from genetically tractable partners to address, molecularly, the virulence and defense mechanisms. The smut fungus *Ustilago maydis* is a model pathogen in that sense: efficient homologous recombination and a small genome allow targeted modification. On the host side, maize is limiting with regard to rapid genetic alterations. By contrast, the model plant *Arabidopsis thaliana* is an excellent model with a vast amount of information and techniques as well as genetic resources. Here, we present a transformation protocol for the Brassicaceae smut fungus *Thecaphora thlaspeos*. Using the well-established methodology of protoplast transformation, we generated the first reporter strains expressing fluorescent proteins to follow mating. As a proof-of-principle for homologous recombination, we deleted the pheromone receptor *pra1*. As expected, this mutant cannot mate. Further analysis will contribute to our understanding of the role of mating for infection biology in this novel model fungus. From now on, the genetic manipulation of *T. thlaspeos*, which is able to colonize the model plant *A. thaliana*, provides us with a pathosystem in which both partners are genetically amenable to study smut infection biology.

Keywords: mating; pheromone receptor; homologous recombination; infection; smut; transformation; protoplast



Citation: Plücker, L.; Bösch, K.; Geißl, L.; Hoffmann, P.; Göhre, V. Genetic Manipulation of the Brassicaceae Smut Fungus *Thecaphora thlaspeos*. *J. Fungi* **2021**, *7*, 38. <https://doi.org/10.3390/jof7010038>

Received: 16 November 2020

Accepted: 7 January 2021

Published: 9 January 2021

Publisher's Note: MDPI stays neutral with regard to jurisdictional claims in published maps and institutional affiliations.



Copyright: © 2021 by the authors. Licensee MDPI, Basel, Switzerland. This article is an open access article distributed under the terms and conditions of the Creative Commons Attribution (CC BY) license (<https://creativecommons.org/licenses/by/4.0/>).

1. Introduction

Smut fungi are important pathogens causing economic losses in crops such as barley, wheat, maize, and potato [1]. The dimorphic lifecycle of grass smut fungi is comprised of a yeast form [2] that, in contrast to many other biotrophic fungi, can be cultured, and is amenable to genetic manipulation [3]. In combination with the efficient homologous recombination, this has turned *Ustilago maydis*, the maize smut fungus [4], into an important model organism for fungal and infection biology [5,6].

U. maydis starts the infection by mating, resulting in the morphological switch to the infectious filamentous form. Mating in smut fungi is controlled by two mating loci. The *a* locus encodes for pheromones (*mfa*) and pheromone receptors (*pra*) that mediate recognition of compatible mating partners and trigger cell fusion [7]. The *b* locus contains two genes (*bW*, *bE*) encoding for subunits of a heterodimeric, homeodomain transcription factor. When an active transcription factor is assembled from different alleles in the common cytosol after plasmogamy, filamentous growth is initiated and thereby the fungus switches from saprophytic to pathogenic growth [8]. Notably, the infectious filaments are arrested in the cell cycle until successful penetration of the host plant [9]. This mating system is widely conserved in grass smut fungi and allows for genetic exchange between the mating partners [10].

In contrast to the well-characterized grass smut fungi infecting important monocot crop plants with *U. maydis* at the forefront, little is known about smut fungi infecting dicot plants. A reemerging example is *Microbotryum* that is regaining attention today [11].

By contrast, the *Thecaphora*-clade [12], with agronomically relevant members such as *T. solani* [13] or *T. frezii* [14] infecting potato and peanut, respectively, remains largely elusive. One member, the Brassicaceae smut fungus *T. thlaspeos*, infects several *Arabidopsis* species [12] and can colonize *Arabidopsis thaliana* [15], making it a good system to study smut infection in model plants. Interestingly, germinating teliospores of *T. thlaspeos* directly give rise to an infectious filament, and no saprophytic phase is known. However, prolonged cultivation leads to fungal proliferation as filamentous, haploid cultures. From such cultures, two filamentous haploid *T. thlaspeos* strains of compatible mating types, LF1 and LF2, could be isolated [15]. The unique germination pattern and the emergence of haploid filaments in culture raise questions about mating and meiosis in *T. thlaspeos*.

The genome of *T. thlaspeos* was recently sequenced and annotated. With 20.5 Mb, 6239 gene models, and a low repeat content, it is a typical smut fungal genome [16]. Notably, we could identify the mating loci *a* and *b* in this genome. In comparison to the grass smut fungi, the *a* locus of *T. thlaspeos* is strongly rearranged, and aligns well to the biocontrol yeast *Anthracozygia flocculosa* (formerly *Pseudozyma flocculosa*). It still contains one copy of the pheromone receptor *pra1* and pheromone *mfa1*, or *pra2* and *mfa2* in *T. thlaspeos* LF1 and LF2, respectively [16]. The *b* locus is conserved with a bi-directional promoter in between the two genes, and we have previously shown that the heterodimer formation of bE and bW is conserved in *T. thlaspeos* [15]. Conservation of the mating genes throughout evolution suggests that *T. thlaspeos* still uses mating, e.g., for exchange of genetic material. However, the infectious lifecycle so far has not revealed a stage where mating is required. Therefore, we aimed for a more detailed understanding of the role of the *T. thlaspeos* mating genes.

To study the mating process in *T. thlaspeos*, genetic manipulation is essential. For example, reporter lines enable life-cell imaging, and deletion mutants can give insight into mutant phenotypes. Several transformation methods have been developed for smut fungi. Protoplast-mediated transformation is used for the grass smuts *U. maydis* [17], *Sporisorium reilianum* [18], *U. hordei* [19], *U. esculenta* [20], and *U. bromivora* [21], as well as the filamentous Basidiomycete *Serendipita indica* (formerly *Piriformospora indica*) [22], and the biocontrol yeast *An. flocculosa* [23]. Agrobacterium-mediated transformation is used for *S. scitamineum* in combination with a CRISPR-Cas9 system [24], and also for bringing larger fragments into *U. hordei* [25] and for gene tagging in *U. maydis* [26].

Here, we have established a protoplast-based PEG-mediated transformation system and generated targeted deletion mutants to investigate the mating process in *T. thlaspeos*.

2. Materials and Methods

2.1. Fungal Culture Conditions

T. thlaspeos LF1 and LF2 haploid strains [15] from our own collection were used in this study. Both were grown in YEPS light liquid medium (1% yeast extract *w/v*, 0.4% *w/v* Bacto TM-Peptone, and 0.4% *w/v* sucrose) or YEPS light solid medium with 0.6% *w/v* plant agar or 1% *w/v* phytagel at 18 °C. Cryostocks of *T. thlaspeos* were generated by mixing exponentially growing cultures with 30% glycerol in growth medium followed by immediate freezing at −80 °C. Filamentous cultures were started by resuspending the glycerol stock in growth medium or plating the cells on solid medium as described above.

2.2. Plasmid Construction

All plasmids used in this study were generated with the Golden Gate Cloning technique (Protocol S1) as described [27]. The *hpt-egfp* and *hpt-mcherry* sequences were codon-optimized for *U. maydis*. Promoter and terminator sequences from *T. thlaspeos* or *U. maydis* were amplified via PCR from genomic DNA.

2.3. Protoplasting

T. thlaspeos cultures were grown in YEPS light medium to an OD₆₀₀ of 0.5–0.8 for 3 to 4 days. Fungal mycelium was collected using cell strainers with 40 µm mesh size (VWR TM Darmstadt, Germany) and washed with protoplasting buffer (0.1 M sodium citrate, 0.01 M

EDTA 1.2 M MgSO₄, and pH 5.8) to remove residual culture medium. *T. thlaspeos* tissue was resuspended in 9 mL protoplasting buffer, supplemented with 10 mg/mL Yatalase (Takara Bio, Kusatsu, Japan) and 20 mg/mL Glucanex (Sigma-Aldrich, St. Louis, MI, USA) per 100 mL cell culture, and incubated for 30–60 min at room temperature. Protoplast formation was controlled microscopically. When protoplasting was finished, protoplasting buffer was added to a total volume of 24 mL. Aliquots of 6 mL crude protoplast solution were overlaid with 5 mL trapping buffer (0.6 M sorbitol, 0.1 M Tris/HCl pH 7.0) and centrifuged at 4863× *g* (5000 rpm) in a swing out rotor at 4 °C for 15 min. The interphase was collected from all tubes and diluted with 2 volumes of ice-cold STC buffer (0.01 M Tris/HCl pH 7.5, 0.1 M CaCl₂, and 1.0 M sorbitol). Protoplasts were pelleted at 4863× *g* (5000 rpm) in a swing out rotor at 4 °C for 10 min and resuspended in 500 µL ice-cold STC buffer. 100 µL protoplast aliquots were used for transformation immediately. A bullet point version of the protocol is available with the supplementary files (Protocol S1).

2.4. Transformation

Transformation of *T. thlaspeos* protoplasts were carried out as described for *U. maydis* [28] with slight modifications. Transformation reactions were spread on YMPG-Reg (0.3% *w/v* Yeast extract, 0.3% *w/v* malt extract, 0.5% *w/v* Bacto-Peptone, 1% *w/v* glucose, 1 M sucrose, 0.6% *w/v* plant agar, Duchefa Biochemie, Haarlem, Netherlands) medium and incubated at 18 °C until colonies appeared (1–2 months). Selection was carried out on 10 µg/mL Hygromycin B (Roth, Karlsruhe Germany) following the layered-plate strategy used for *U. maydis* [28]. In this setup, hygromycin was provided in the bottom layer so that it took time to diffuse to the top before the selection took place. This gave protoplasts time to regenerate and express the resistance gene [28]. Colonies were singled-out on YEPS light solid medium supplemented with 10 µg/mL hygromycin. Single colonies were then used to inoculate YEPS light liquid cultures for molecular analysis.

2.5. Molecular Analysis of Transformants

Successful integration of the constructs were determined by PCR and Southern Blot analysis [28], and eGfp or mCherry fluorescence was used as a rapid indicator for expression of the constructs. Genomic DNA of *T. thlaspeos* was extracted using the NEB Monarch Genomic DNA Purification Kit (New England Biolabs, Frankfurt, Germany).

2.6. Mating Assay

For confrontation assays, liquid cultures of *T. thlaspeos* strains were spotted on YEPS light solid medium in close proximity and allowed to grow towards each other. When the hyphae of both strains were close enough to appear in the display window of the microscope, a time lapse experiment was conducted to monitor mating for 24–72 h.

For liquid mating assays, strains of compatible mating types were mixed in YEPS light liquid medium in equal amounts and incubated at 18 °C and 200 rpm. Medium was exchanged twice a week. After 8–14 days, plasmogamy was observed microscopically via eGfp and mCherry fluorescence.

2.7. Microscopy

Fluorescence microscopy as well time lapse experiments were performed on a Zeiss Axio Immager M1 according to [29]. Microscope control, image acquisition, and processing were done with the software package Meta-Morph (version 7; Molecular Devices).

3. Results

3.1. Protoplast—Generation from Filamentous *T. thlaspeos* Cultures

Protoplast-mediated transformation is well-established for fungi [30]. The protocol for *U. maydis* [17] was successfully adapted for other smut fungi and therefore was also the starting point for *T. thlaspeos* protoplast generation. Critical factors besides cultivation conditions are the enzyme mixture, the buffer composition, and the osmotic stabilizer.

First, we compared different enzyme mixtures. Glucanex, a mix of lysing enzymes from *Trichoderma harzianum* including beta-1,3-glucanase activity, works well for *U. maydis* and the filamentous Basidiomycete *S. indica* [22]. Yatalase comprises of a mix of lysing enzymes from *Corynebacterium*, including chitinase-, chitobiase-, and beta-1,3-glucanase activity, for cell wall lysis of filamentous fungi. In combination with Glucanex, it is used for *U. bromivora* [21] and *Agrocybe aegerita* [31], or supplemented with chitinase for *Aspergillus niger* [32]. Novozyme 234, which worked very well for *U. maydis* [28], is no longer commercially available, so we did not include it in our study. In pilot studies, we compared enzyme and buffer combinations of published protoplasting protocols and found that the combination of Glucanex and Yatalase efficiently protoplasts the *T. thlaspeos* filaments (Table S1).

Therefore, to first optimize the osmotic stabilizer, we used this enzyme mix in the *U. maydis* protoplasting buffer. Typical osmotic stabilizers are inorganic salts, sugars, or sugar alcohols [33]. For example, sorbitol is used for *U. maydis*, and sucrose for *U. esculenta*. Thus, we tested sorbitol and sucrose, as well as $MgSO_4$, which is used frequently in combination with Yatalase. Most protoplasts were obtained using $MgSO_4$ (Figure 1). Notably, sorbitol and sucrose inhibited cell wall lysis, confirming early observations [34,35]. Subsequently, we tested various commonly used protoplasting buffers, in combination with $MgSO_4$ as the osmotic stabilizer. There were no significant differences between the four tested buffers (Table 1), but we observed tendencies that citrate buffers work better for fast growing cultures that were sub-cultured bi-weekly (Figure S1). Ultimately, we decided on the 0.1 M citrate buffer and 0.01 M EDTA, which is also the buffer used for *An. flocculosa*, the closest homolog of *T. thlaspeos*, and a bi-weekly splitting rhythm.



Figure 1. Identification of an osmotic stabilizer. *Thecaphora thlaspeos* LF1 culture was grown to an $OD_{600} = 0.4–0.8$. To optimize protoplasting of *T. thlaspeos* hyphae by Yatalase and Glucanex, the osmotic stabilizers $MgSO_4$, sorbitol, and sucrose were tested. With $MgSO_4$ as osmotic stabilizer, all filaments were digested; while in sorbitol and sucrose, no protoplasts were obtained. Black arrowheads: filaments; white arrowheads: protoplast; scale bar: 50 μm .

An advantage of $MgSO_4$ as osmotic stabilizer is that the majority of intact protoplasts in the presence of $MgSO_4$ have large vacuoles [38], which enables collection and purification, and floating in a trapping buffer [36]. Intact protoplasts accumulate in a sharp band at the interphase, and debris pellet at the bottom (Figure 2). After washing with STC buffer, up to 10^8 protoplasts/g fresh weight can be recovered.

Upon determination of the optimal buffer and osmotic stabilizer, we reevaluated the composition and concentration of the enzyme mix (Figure 3). As the pilot study had indicated, for efficient degradation of the *T. thlaspeos* cell wall, the combined activity of Yatalase and Glucanex is necessary. As expected, individually the enzymes are poorly active, leaving filaments behind (Figure 3A). This emphasizes the importance of testing various lysing enzymes, alone and in combination, in different buffers to find a mix suitable for the organism of choice and its individual cell wall composition [30].

Finally, we aimed to decrease the enzyme concentrations to save costs. However, lowering the concentration to half resulted in incomplete digestion of the fungal cell wall after 30 min (Figure 3B). Since it was described earlier that a shorter incubation time is

preferable, compared to a low enzyme concentration, regarding protoplast viability [39,40], we did not reduce the enzyme concentrations.

Table 1. Optimizing the protoplasting buffer. To identify the optimal osmotic stabilizer, fungal hyphae were filtered and incubated in 0.02 M citrate buffer, supplemented with different osmotic stabilizers and 10 mg/mL Yatalase + 20 mg/mL Glucanex, for 60 min at RT. Protoplasting worked only if MgSO₄ was used as osmotic stabilizer. To optimize the buffer for the use of MgSO₄, hyphae were filtered and incubated in different buffers, supplemented with 1.2 M MgSO₄ and 10 mg/mL Yatalase + 20 mg/mL Glucanex, for 60 min at RT. There was no significant difference between the indicated buffers, but a tendency towards higher yields with citrate buffers.

Buffer	Osmotic Stabilizer	Protoplast Yield/g FW × 10 ⁷
Optimizing the Osmotic Stabilizer		
0.02 M citrate, pH 5.8 [28]	0.4 M sucrose [20]	no protoplasts
	1.2 M MgSO ₄ [36]	5.52 ± 1.22
	1.0 M sorbitol [28]	no protoplasts
Optimizing the buffer composition		
0.1 M citrate, 0.01 M EDTA, pH 5.8 [23]	1.2 M MgSO ₄ [36]	7.46 ± 2.02
0.02 M citrate, pH 5.8 [28]		7.49 ± 1.51
0.02 M MES, pH 5.8 [21]		5.28 ± 0.66
0.01 M phosphate, pH 5.8 [37]		5.01 ± 0.51

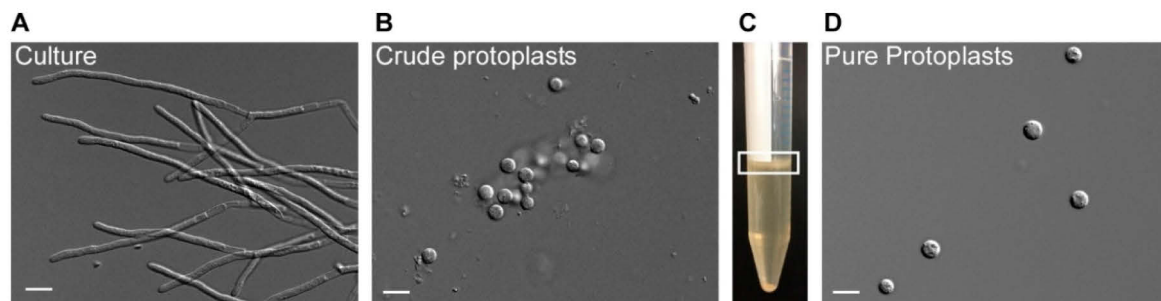


Figure 2. Protoplasting filamentous *T. thlaspeos* cultures. 1–2 g fresh weight of an exponentially growing culture (A) was harvested by filtration and protoplasted with Glucanex and Yatalase for 30–60 min. To purify the crude protoplasts (B), they are floated in a gradient (C). Filaments and debris are found in the pellet, the protoplasts can be collected from the interphase (marked with a white box). (D) An efficient protoplasting reaction results in up to 10⁸ protoplasts/g fresh weight. Scale bar: 10 µm.

In contrast to other applications of protoplasts, for genetic manipulation, the protoplasts have to be viable and able to regenerate their cell wall. Thus, we next investigated the influence of the osmotic stabilizer on regeneration of the protoplasts after transformation. This allowed us to separate optimization of both steps. Using protoplasts generated in the presence of MgSO₄, we assessed regeneration media containing different osmotic stabilizers such as sucrose, glucose, sorbitol, and KCl (Figure 4). MgSO₄ was excluded due to incompatibility with the gelling agent. Maximal regeneration was obtained with 1 M sucrose as osmotic stabilizer, followed by sorbitol and glucose, while 1 M KCl completely inhibited regeneration and fungal growth (Figure 4A). In support, *T. thlaspeos* LF1 cell cultures do not grow on 1 M KCl, indicating that it is toxic at this concentration, while sucrose, glucose, and sorbitol only reduce the growth rate (Figure 4B). Without an osmotic stabilizer, cells were not able to regenerate, indicating that any residual filaments were efficiently removed during purification of the protoplasts (Figure 4A). *U. maydis* protoplasts regenerate into yeast cells and form colonies within three days [17,41]. For *T. thlaspeos*, we expected filaments to emerge from the protoplast, since we had never observed yeast-cells for this fungus. Furthermore, the slow growth rate of *T. thlaspeos* cultures suggests a longer

regeneration time. To confirm our expectation, we described the regeneration process and its timing for *T. thlaspeos* protoplasts on regeneration medium with 1 M sucrose. After one day, protoplasts turned dark, which is indicative of cell wall regeneration. Three to eight days later, a filament emerges from the protoplast that starts branching after 7–13 days, finally resulting in a micro-colony after 11–18 days (Figure 4C). Further proliferation leads to filamentous colonies after four to five weeks, which are indistinguishable from the original culture.

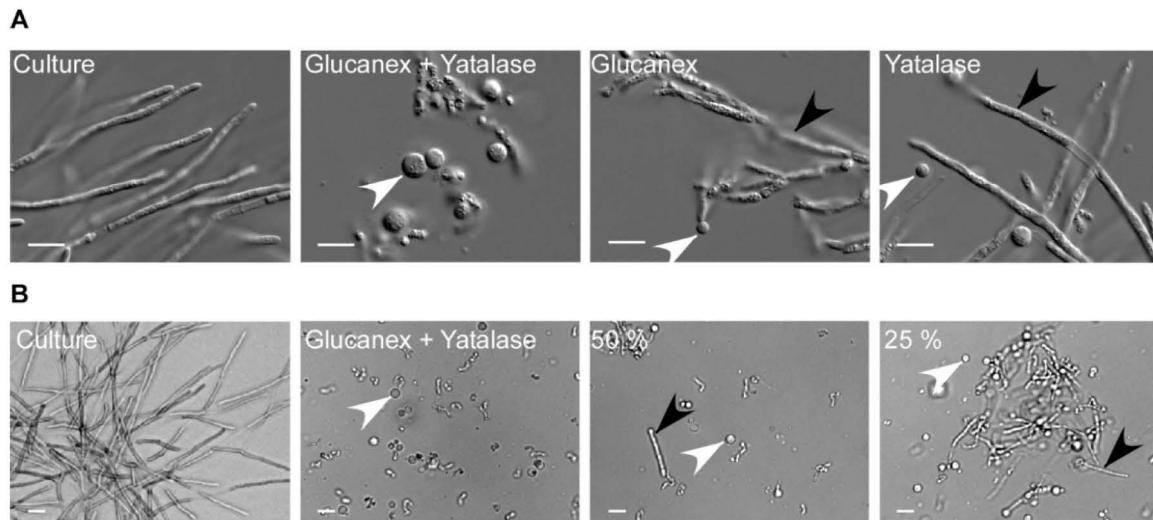


Figure 3. Optimizing the enzyme cocktail for protoplasting. **(A)** Filamentous cultures were harvested and incubated with a combination of 20 mg/mL Glucanex and 10 mg/mL Yatalase, or each enzyme individually, for 30 min. Protoplasting was efficient only when both enzymes were applied. **(B)** The enzymes were diluted to identify the lowest suitable concentration. The frequency of remaining filaments is inversely proportional to the enzyme concentration. The highest efficiency was obtained with 20 mg/mL Glucanex and 10 mg/mL Yatalase. White arrowhead: protoplasts; black arrowhead: residual filaments; scale bar: 10 µm.

3.2. Transformation

Five antibiotic resistance markers directed against phleomycin, hygromycin, nourseothricin, geneticin, and carboxin are routinely used in *U. maydis* [3]. To develop markers for *T. thlaspeos*, we tested culture growth on four of these antibiotics. Phleomycin is a mutagen and therefore was not considered [42]. *T. thlaspeos* cells were efficiently killed by the four antibiotics (Figure S2). Concentration gradients with hygromycin, nourseothricin, and carboxin revealed that *T. thlaspeos* was more sensitive towards these antibiotics than *U. maydis*. 10 µg/ mL hygromycin and 50 µg/ mL nourseothricin efficiently killed *T. thlaspeos* hyphae. This is 20 times and three times less than the standard concentration used for *U. maydis*, respectively. By contrast, cells are less sensitive towards carboxin and remained resistant at 2 µg/ mL, the standard concentration used for *U. maydis*, but were sensitive at 100 µg/ mL. (Figure S2). Carboxin inhibits the mitochondrial succinate dehydrogenase (SDH2), and a point mutation, H253L, leads to a resistant form in *U. maydis* [43]. The *T. thlaspeos* SDH2 was highly conserved, with 82% amino acid similarity, and contained an arginine instead of the histidine at this position (Figure S3). This might explain the reduced sensitivity.

Due to the high hygromycin sensitivity, the bacterial hygromycin-phospho-transferase (*hpt*) [17] was used as the first resistance marker. We expressed it as a fusion protein *hpt-eGfp* [44] under the control of *T. thlaspeos* and *U. maydis* promoters and terminators (Table S2). Promoter activity was verified in *U. maydis*. Both $P_{T_{hsp70}}$ and $P_{T_{trps27}}$ were

active in *U. maydis*, and all five constructs resulted in hygromycin-resistant transformants with eGfp-fluorescence (Figure 5 and Figure S4), suggesting the constructs are functional and can be used to transform *T. thlaspeos*.

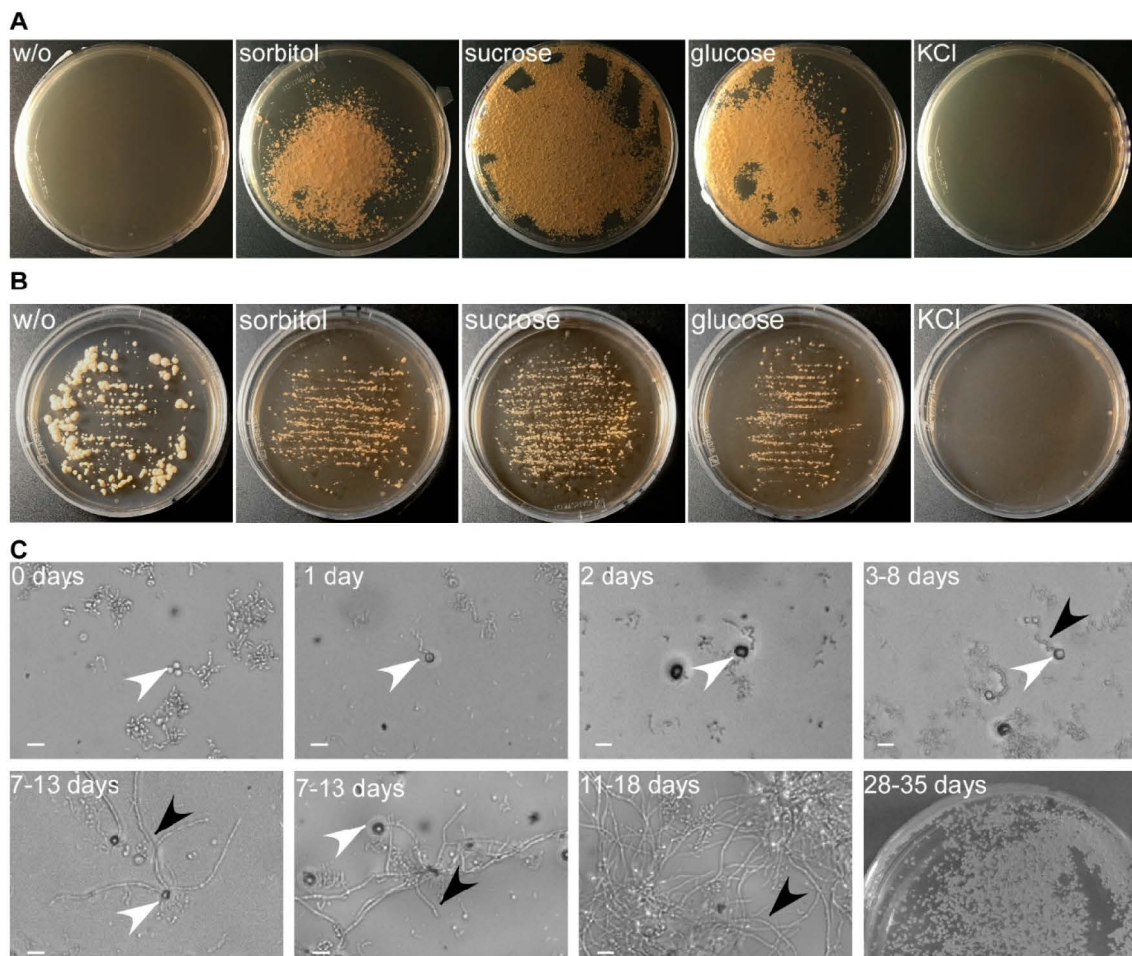


Figure 4. Optimizing protoplast regeneration. (A) Protoplasts regenerated for 39 days on regeneration medium (YMPG) with either 1 M sorbitol, sucrose, glucose, or KCl. No regeneration was observed without osmotic stabilizer. It was most efficient on sucrose, followed by glucose and sorbitol, while KCl inhibited cell growth. (B) *T. thlaspeos* LF1 culture plated on YMPG with sorbitol, sucrose, glucose, KCl, or without osmotic stabilizer. After 21 days, no growth was observed for 1 M KCl. Growth rate is reduced for 1 M sorbitol, glucose, and sucrose compared to absence of osmotic stabilizer. (C) Regeneration of protoplasts on YMPG with 1 M sucrose documented microscopically for 11–18 days. Initially, the protoplasts turned dark (2 days) before new filaments emerged (3–8 days). The filaments proliferated (11–18 days), resulting in macroscopically visible colonies (28–35 days). White arrowhead: protoplasts; black arrowhead: emerging filaments; scale bar: 10 μm.

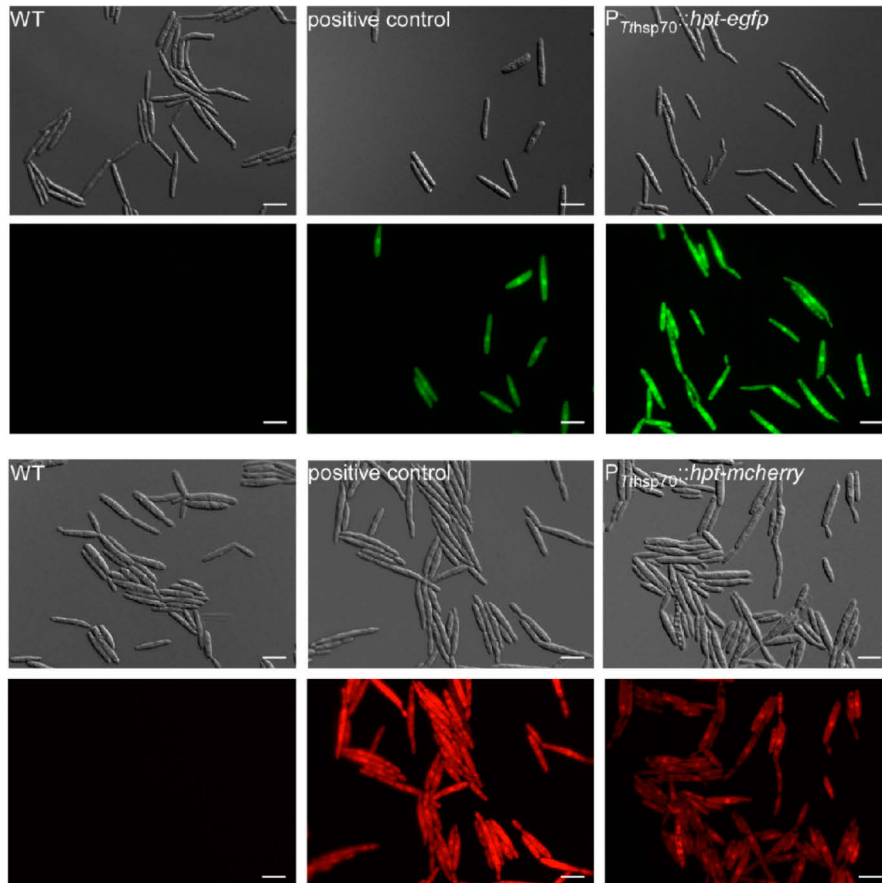


Figure 5. Verification of resistance-reporter constructs in *U. maydis*. Reporter constructs containing a fusion of hygromycin-phospho-transferase gene (*hpt*) and the fluorescent marker (*egfp* or *mcherry*) under the control of *hsp70* promoter and terminator regions derived from the *T. thlaspeos* genome were tested in *U. maydis*. Upon transformation of the linearized construct, it randomly integrates into the genome. Protein accumulation was visualized by the green/red fluorescence. The eGfp expression under the promoter region of *T. thlaspeos* was stronger than compared to the stably integrated construct under the control of a strong, synthetic promoter (*Potef*). This confirms that the fusion protein is active. In comparison, mcherry-fluorescence in the strain carrying the *Tthsp70* promoter was weaker than the stably integrated construct under the control of the *Potef* promoter. Scale bar: 10 μ m.

First, we needed to define which plasmid to use. Therefore, we transformed an equimolar mixture of five *hpt-eGfp* plasmids with different promoters (Table S2) into *T. thlaspeos* LF1 protoplasts generated with the optimized method using the standard *U. maydis* conditions for transformation [28]. This resulted in a single transformant which had stably integrated the $P_{Tthsp70}::hpt-egfp:T_{Tthsp70}$ into the genome (Figure S5, Figure 6). Now, transformations using this plasmid regularly result in fluorescent transformants. Based on this successful transformation, a $P_{Tthsp70}::hpt-mcherry:T_{Tthsp70}$ construct was generated (Table S2), tested in *U. maydis* (Figure 5), and transformed into *T. thlaspeos* LF2 (Figure 6), showing that compatible mating partners of *T. thlaspeos* can be tagged with different reporters to follow the mating process.

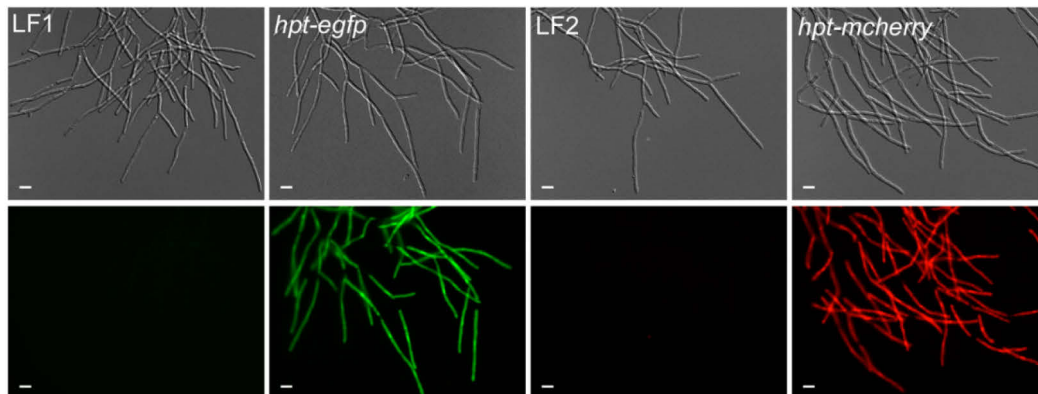


Figure 6. Generation of reporter lines in *T. thlaspeos*. Reporter constructs containing the active fusion of the hygromycin-phospho-transferase gene (*hpt*) and the fluorescent marker (*egfp* or *mcherry*) under the control of the strong *hsp70* promoter from *T. thlaspeos* were transformed into the cultures *T. thlaspeos* LF1 or LF2, respectively. Fluorescent signals accumulate in the cytosol of all cells. Strains: *hpt-egfp*: LF1_ $P_{Thsp70}::hpt-egfp$, and *hpt-mcherry*: LF2_ $P_{Thsp70}::hpt-mcherry$. Scale bar: 10 μ m.

One key aspect for gene targeted manipulations is efficient homologous recombination. To test whether *T. thlaspeos* reaches the same high rates of up to 50% as *U. maydis*, we targeted the pheromone receptor gene *pra1* in the *T. thlaspeos* LF1 background for deletion. The construct design was based on *U. maydis* with 1 kb flanking sequences [27]. Transformation of the construct resulted in 122 candidates on the transformation plates. Reselection of 19 candidates on fresh hygromycin plates led to only nine candidates that remained resistant. The other candidates were either false positives, or they only transiently expressed the resistance protein. These are not interesting for stable integration. In subsequent analysis of the nine candidates, successful deletion of the *pra1* locus was confirmed for two transformants (Figure S5), giving a homologous recombination rate of 22%.

In summary, we have now adapted the protoplast-mediated transformation for the filamentously growing Brassicaceae smut fungus *T. thlaspeos*. Together, with its ability for efficient homologous recombination, this gives us a tool to study plant–microbe interactions of smut fungi in the model plant *A. thaliana* with two genetically tractable partners.

3.3. Mating of Filaments

When *T. thlaspeos* teliospores germinate, they give rise to an infectious filament that can directly penetrate the plant. On the other hand, these filaments also can give rise to haploid culture. Our haploid cultures *T. thlaspeos* LF1 and LF2 have compatible mating types. They can fuse at the tip and form a new filament [15]. To visualize directional growth of compatible LF1 and LF2 hyphae towards each other during mating, we carried out confrontation experiments. In close proximity, LF1 and LF2 hyphae sense each other, and reorient their growth to meet (Figure 7A). In some cases, some hyphae return their growth in direction towards the compatible filament after initial passage. Upon contact, they fuse and result in a new filament (Figure 7A,B, Video S1). To prove that fused hyphae really share a common cytoplasm, mating was also observed in cocultivation experiments of compatible strains expressing eGfp and mCherry (Figure 7C). After hyphal fusion, eGfp and mCherry fluorescence could be observed in one cytoplasmic segment indicative of plasmogamy. On the other hand, if the pheromone receptor *Pra1* is deleted, hyphae of compatible strains grow directly past each other without hyphal fusion (Figure 7A,B and Video S2). These findings confirm that the pheromone-receptor system in *T. thlaspeos* [15] is active and initiates mating. In the future, the generation of nuclei-reporter-strains with

NLS-fusion-constructs will allow tracking of the nuclei and thereby the investigation of karyogamy during mating.

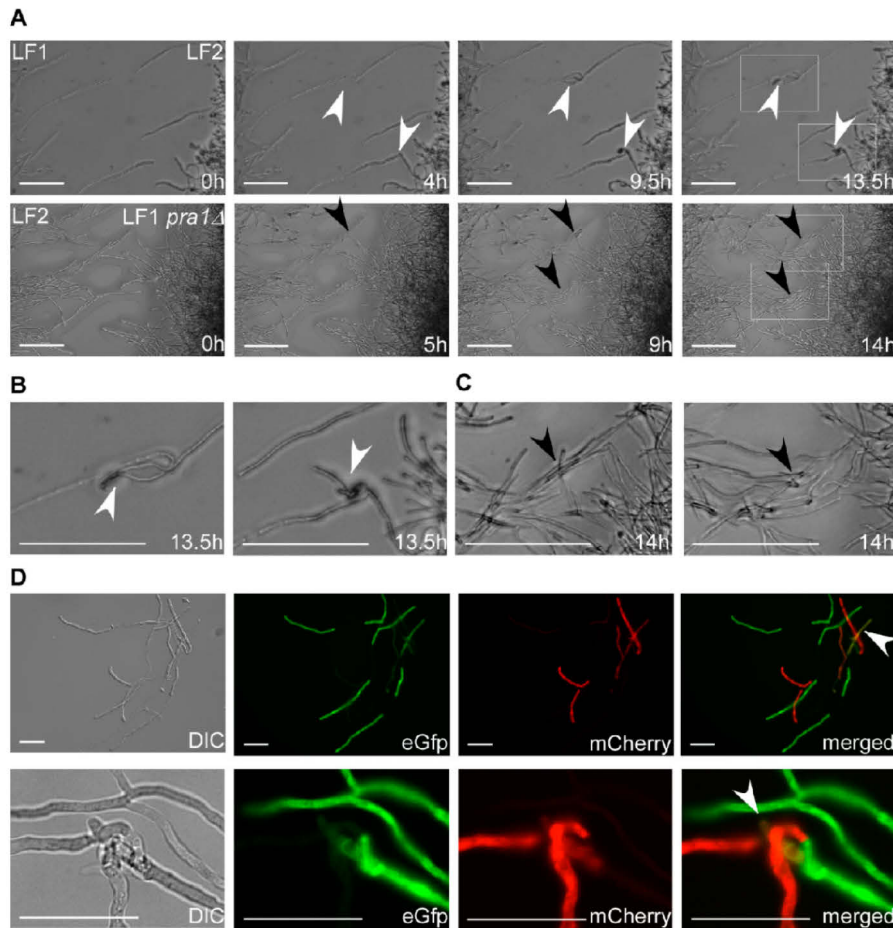


Figure 7. Mating in *T. thlaspeos*. (A) Top: Confrontation assay of mating partners *mfa1/pral* (LF1) or *mfa2/pral* (LF2). Over the course of 13.5 hours, several mating events of LF1 and LF2 were observed. White arrowheads mark the fusion event. Bottom: Confrontation assay of LF1 *pral* Δ and LF2. Over the course of 14 h, hyphae did not mate. Two spots where hyphae could no longer sense each other and cross are marked with black arrow heads. Scale bar: 25 μ m. (B,C) Magnification of the mating and crossing events from the white boxes marked in (A). Scale bar: 100 μ m. (D) Liquid mating assay with mating partners expressing either cytoplasmic eGfp (LF1-eGfp) or mCherry (LF2-mCherry). Fused hyphae express both eGfp and mCherry and appear yellow in the merged picture (white arrowhead). Scale bar: 25 μ m.

4. Discussion

When we first set out to work with *T. thlaspeos*, our aim was to establish a genetically tractable smut fungus in a model host plant such as *A. thaliana* [15]. An important aim for reaching this goal was genetic manipulation. Here, we show that like other smut fungi, *T. thlaspeos* is amenable to protoplast-mediated transformation. We have generated a hygromycin resistance cassette, where expression of the hygromycin-phospho-transferase, *hpt*, is controlled by the *T. thlaspeos hsp70* promoter sequence, similar to the cassettes used in *U. maydis* [3]. Interestingly, promoter sequences seem to be exchangeable between smut fungi, since the *T. thlaspeos* promoters were active in *U. maydis* and several groups have

successfully used *U. maydis* constructs [23,45]. This now enables us to generate reporter strains for a broad range of scientific questions.

Most important to establishing a successful protoplasting protocol is the choice of the lytic enzyme(s). The fungal cell wall is a multilayered, chemically complex structure consisting mainly of polysaccharides and varying amounts of lipids, proteins, and polyphosphates [46]. Its composition is not only variable between species [30], but also highly dependent on the culture conditions [47] and morphology [48]. In our case, the combined activity of Yatalase and Glucanex was necessary for efficient digestion of the *T. thlaspeos* cell wall, although they appear to have overlapping enzymatic properties. Similar additive effects have recently been shown for the ascomycete *Hirsutella sinensis* [49] and *Ag. aegerita* [31]; while in *Cordyceps militaris*, the enzymes mix is less active than Glucanex alone [50]. Hence, during the establishment of conditions for protoplasting, various lytic enzymes and combinations should be tested to reach optimal cell wall degradation [30]. Moreover, commercial manufacturing of enzymes can be stopped, with the broadly used Novozyme 234 being a recent example. Hence, the identification of suitable enzymes can be a reoccurring problem even for established protocols.

The second important factor is the osmotic stabilizer, because it depends on the choice of the protoplasting enzyme. For example, the enzymatic activity of Yatalase is inhibited by sorbitol and sucrose. In the 1970s, similar observations were made for helicase [35] and snail enzyme [34]. Protoplasting protocols with Yatalase use inorganic salts as osmotic stabilizer [21,31,37,40,51] and similar to these old reports, for *T. thlaspeos*, we now use $MgSO_4$ to enable cell wall degradation.

Together with other factors influencing the protoplast formation, such as growth conditions of the culture, buffer composition, pH, temperature, or protoplasting time, establishing new transformation protocols quickly becomes a multi-factorial challenge, and testing full-factorial replicates is time-consuming and costly. For *T. thlaspeos*, we designed pilot studies covering selected combinations in single replicates based on existing transformation protocols, and used the most promising buffer, osmotic stabilizer, and enzyme combination for further optimization. While this approach does not cover all combinations, it allowed us to establish a good transformation protocol with reasonable effort.

As a proof-of-principle for our transformation protocol, we investigated the well-characterized smut fungal mating process in *T. thlaspeos*. In the first step, we generated reporter strains expressing cytosolic eGfp or mCherry to visualize the fusion of hyphae. The resulting filaments express both eGfp and mCherry, indicative of a common cytoplasm, as typical for the dikaryotic smut fungi [52,53]. Next, we looked into dependency on the pheromone receptor. To this end, we generated a deletion mutant of the pheromone receptor *pra1* [15] based on the strategy of *U. maydis* [28]. Notably, homologous recombination also takes place in *T. thlaspeos*, so we can modify genes in the haploid culture background easily.

T. thlaspeos pra1 deletion mutants cannot mate anymore. This finding is especially interesting since it is not yet known whether mating is required for *T. thlaspeos* to fulfil its life cycle. Infectious filaments emerge directly from germinating *T. thlaspeos* teliospores. By contrast, teliospore germination of grass smut fungi gives rise to yeast-like sporidia. Subsequent pathogenic development depends on the morphological switch from yeast to filamentous growth brought about by mating [52]. However, the functional conservation of mating genes in *T. thlaspeos* suggests an evolutionary-conserved, and therefore important, role of mating also in this fungus [15]. This raises several questions. Is mating necessary for the lifecycle of *T. thlaspeos*? Where and when does mating occur? When do *T. thlaspeos* hyphae undergo meiosis? Is the filament emerging from the teliospore diploid or dikaryotic? Is the transition to haploid hyphae also occurring naturally in this state of the lifecycle? With the established transformation protocol, we will be able to further address these questions. This will shed light not only onto the mating process of *T. thlaspeos*, but also on the role of RNA communication in virulence, perennial persistence of the fungus *in planta*, and nutrition of a smut fungus during biotrophic growth.

5. Conclusions

Establishing the genetic manipulation of the Brassicaceae smut fungus *T. thlaspeos* now allows us to generate reporter strains as well as targeted deletions or modifications of fungal genes. Combined with the fungal colonization of the model plant *A. thaliana*, we thereby provide a pathosystem, in which both partners have a small, genetically tractable genome for addressing the current and future questions of plant–microbe interactions.

Supplementary Materials: The following are available online at <https://www.mdpi.com/2309-608X/7/1/38/s1>, Figure S1: buffer_comparison, Figure S2: antibiotics, Figure S3: cbx_alignment, Figure S4: transformation_constructs_in_U_maydis, Figure S5: Molecular confirmation of reporter and mutant strains, Table S1: protoplasting_pilot, Table S2: transformation_constructs, Video S1: LF1+LF2_confrontation_experiment, Video S2: LF2+LF1-pra1Δ_confrontation_experiment, Protocol S1: Plasmid generation, and Protocol S2: Protoplasts and transformation of *Thecaphora thlaspeos*.

Author Contributions: Conceptualization, V.G.; investigation, L.P., K.B., L.G., and P.H.; writing—original draft preparation, L.P. and V.G.; writing—review and editing, V.G.; visualization, L.P.; supervision, V.G.; project administration, V.G.; funding acquisition, V.G. All authors have read and agreed to the published version of the manuscript.

Funding: Research in the laboratory of VG was funded by the Deutsche Forschungsgemeinschaft (DFG, German Research Foundation) under Germany’s Excellence Strategy (EXC-2048/1, project ID 390686111); the International Research Training NEXTplant (DFG, project ID 391465903/GRK 2466); and the Bioeconomy Science Center (BioSC), which is financially supported by the Ministry of Innovation, Science, and Research within the framework of the NRW Strategieprojekt BioSC (No. 313/323-400-00213).

Institutional Review Board Statement: Not applicable.

Informed Consent Statement: Not applicable.

Data Availability Statement: The data presented in this study are available in this manuscript and constructs can be requested from the corresponding author.

Acknowledgments: We are grateful to T. Langner, M. Öztürk, and J. Darenberg for support with cloning of the constructs. R. Kellner helped with discussion and ideas during the development of the transformation protocol. L. Lange provided plates with regenerating protoplasts for microscopy, and K. Vogel supported microscopy. In addition, we would like to thank C. Haag for critically reading the manuscript, M. Feldbrügge for discussions, support, and encouragement throughout the establishment of the method, and P. Künzel for support with preparing the movie files.

Conflicts of Interest: The authors declare no conflict of interest. The funders had no role in the design of the study; in the collection, analyses, or interpretation of data; in the writing of the manuscript, or in the decision to publish the results.

References

1. Kronstad, J.W. Pathogenesis and sexual development of the smut fungi. In *Plant-Microbe Interactions*; Stacey, G.K.N.T., Ed.; Springer: Boston, MA, USA, 1997; Volume 1.
2. Feldbrügge, M.; Kämper, J.; Steinberg, G.; Kahmann, R. Regulation of mating and pathogenic development in *Ustilago maydis*. *Curr. Opin. Microbiol.* **2004**, *7*, 666–672. [[CrossRef](#)] [[PubMed](#)]
3. Brachmann, A.; König, J.; Julius, C.; Feldbrügge, M. A reverse genetic approach for generating gene replacement mutants in *Ustilago maydis*. *Mol. Genet. Genom.* **2004**, *272*, 216–226. [[CrossRef](#)] [[PubMed](#)]
4. Banuett, F. *Ustilago maydis*, the delightful blight. *Trends Genet.* **1992**, *8*, 174–180. [[CrossRef](#)]
5. Vollmeister, E.; Schipper, K.; Baumann, S.; Haag, C.; Pohlmann, T.; Stock, J.; Feldbrügge, M. Fungal development of the plant pathogen *Ustilago maydis*. *Fems. Microbiol. Rev.* **2012**, *36*, 59–77. [[CrossRef](#)] [[PubMed](#)]
6. Lanver, D.; Tollot, M.; Schweizer, G.; Lo Presti, L.; Reissmann, S.; Ma, L.S.; Schuster, M.; Tanaka, S.; Liang, L.; Ludwig, N.; et al. *Ustilago maydis* effectors and their impact on virulence. *Nat. Rev. Microbiol.* **2017**, *15*, 409–421. [[CrossRef](#)] [[PubMed](#)]
7. Böölker, M.; Urban, M.; Kahmann, R. The *a* mating type locus of *U. maydis* specifies cell signaling components. *Cell* **1992**, *68*, 441–450. [[CrossRef](#)]
8. Gillissen, B.; Bergemann, J.; Sandmann, C.; Schroeder, B.; Böölker, M.; Kahmann, R. A 2-component regulatory system for self non-self recognition in *Ustilago maydis*. *Cell* **1992**, *68*, 647–657. [[CrossRef](#)]

9. García-Muse, T.; Steinberg, G.; Pérez-Martín, J. Pheromone-induced G₂ arrest in the phytopathogenic fungus *Ustilago maydis*. *Eukaryot. Cell* **2003**, *2*, 494. [[CrossRef](#)]
10. Kellner, R.; Vollmeister, E.; Feldbrugge, M.; Begerow, D. Interspecific sex in grass smuts and the genetic diversity of their pheromone-receptor system. *PLoS Genet* **2011**, *7*. [[CrossRef](#)]
11. Toh, S.S.; Perlin, M.H. Resurgence of less-studied smut fungi as models of phytopathogenesis in the Omics age. *Phytopathology* **2016**, *106*, 1244–1254. [[CrossRef](#)]
12. Vanky, K.; Lutz, M.; Bauer, R. About the genus Thecaphora (Glomosporiaceae) and its new synonyms. *Mycol. Prog.* **2008**, *7*, 31–39. [[CrossRef](#)]
13. Andrade, O.; Munoz, G.; Galdames, R.; Duran, P.; Honorato, R. Characterization, in vitro culture, and molecular analysis of *Thecaphora solani*, the causal agent of potato smut. *Phytopathology* **2004**, *94*, 875–882. [[CrossRef](#)] [[PubMed](#)]
14. Conforto, C.; Cazón, I.; Fernández, F.D.; Marinelli, A.; Oddino, C.; Rago, A.M. Molecular sequence data of *Thecaphora frezii* affecting peanut crops in Argentina. *Eur. J. Plant Pathol.* **2013**, *137*, 663–666. [[CrossRef](#)]
15. Frantzeskakis, L.; Courville, K.J.; Pluecker, L.; Kellner, R.; Kruse, J.; Brachmann, A.; Feldbrugge, M.; Göhre, V. The plant-dependent life cycle of *Thecaphora thlaspeos*: A smut fungus adapted to Brassicaceae. *Mol. Plant-Microbe Interact.* **2017**, *30*, 271–282. [[CrossRef](#)] [[PubMed](#)]
16. Courville, K.J.; Frantzeskakis, L.; Gul, S.; Haeger, N.; Kellner, R.; Hefler, N.; Day, B.; Usadel, B.; Gupta, Y.K.; van Esse, H.P.; et al. Smut infection of perennial hosts: The genome and the transcriptome of the Brassicaceae smut fungus *Thecaphora thlaspeos* reveal functionally conserved and novel effectors. *New Phytol.* **2019**, *222*, 1474–1492. [[CrossRef](#)] [[PubMed](#)]
17. Wang, J.; Holden, D.W.; Leong, S.A. Gene transfer system for the phytopathogenic fungus *Ustilago maydis*. *Proc. Natl. Acad. Sci. USA* **1988**, *85*, 865–869. [[CrossRef](#)] [[PubMed](#)]
18. Schirawski, J.; Heinze, B.; Wagenknecht, M.; Kahmann, R. Mating type loci of *Sporisorium reilianum*: Novel pattern with three a and multiple b specificities. *Eukaryot. Cell* **2005**, *4*, 1317–1327. [[CrossRef](#)] [[PubMed](#)]
19. Cervantes-Chavez, J.A.; Ali, S.; Bakkeren, G. Response to environmental stresses, cell-wall integrity, and virulence are orchestrated through the calcineurin pathway in *Ustilago hordei*. *Mol. Plant-Microbe Interact.* **2011**, *24*, 219–232. [[CrossRef](#)]
20. Yu, J.; Zhang, Y.; Cui, H.; Hu, P.; Yu, X.; Ye, Z. An efficient genetic manipulation protocol for *Ustilago esculenta*. *FEMS Microbiol. Lett.* **2015**, *362*. [[CrossRef](#)]
21. Rabe, F.; Bosch, J.; Stirnberg, A.; Guse, T.; Bauer, L.; Seitner, D.; Rabanal, F.A.; Czedik-Eysenberg, A.; Uhse, S.; Bindics, J.; et al. A complete toolset for the study of *Ustilago bromivora* and *Brachypodium* sp as a fungal-temperate grass pathosystem. *Elife* **2016**, *5*. [[CrossRef](#)]
22. Zuccaro, A.; Basiewicz, M.; Zurawska, M.; Biedenkopf, D.; Kogel, K.-H. Karyotype analysis, genome organization, and stable genetic transformation of the root colonizing fungus *Piriformospora indica*. *Fungal Genet. Biol.* **2009**, *46*, 543–550. [[CrossRef](#)] [[PubMed](#)]
23. Cheng, Y.; Belzile, F.; Tanguay, P.; Bernier, L.; Bélanger, R. Establishment of a gene transfer system for *Pseudozyma flocculosa*, an antagonistic fungus of powdery mildew fungi. *Mol. Genet. Genom.* **2001**, *266*, 96–102. [[CrossRef](#)] [[PubMed](#)]
24. Lu, S.; Shen, X.; Chen, B. Development of an efficient vector system for gene knock-out and near in-cis gene complementation in the sugarcane smut fungus. *Sci. Rep.* **2017**, *7*, 3113. [[CrossRef](#)] [[PubMed](#)]
25. Ali, S.; Laurie, J.D.; Linning, R.; Cervantes-Chávez, J.A.; Gaudet, D.; Bakkeren, G. An immunity-triggering effector from the barley smut fungus *Ustilago hordei* resides in an ustilaginaceae-specific cluster bearing signs of transposable element-assisted evolution. *PLoS Pathog.* **2014**, *10*, e1004223. [[CrossRef](#)]
26. Ji, L.; Jiang, Z.D.; Liu, Y.; Koh, C.M.; Zhang, L.H. A simplified and efficient method for transformation and gene tagging of *Ustilago maydis* using frozen cells. *Fungal Genet. Biol.* **2010**, *47*, 279–287. [[CrossRef](#)] [[PubMed](#)]
27. Terfrüchte, M.; Joehnk, B.; Fajardo-Somera, R.; Braus, G.H.; Riquelme, M.; Schipper, K.; Feldbrugge, M. Establishing a versatile Golden Gate cloning system for genetic engineering in fungi. *Fungal Genet. Biol.* **2014**, *62*, 1–10. [[CrossRef](#)] [[PubMed](#)]
28. Bösch, K.; Frantzeskakis, L.; Vraneš, M.; Kämper, J.; Schipper, K.; Göhre, V. Genetic manipulation of the plant pathogen *Ustilago maydis* to study fungal biology and plant-microbe interactions. *J. Vis. Exp.* **2016**, *115*. [[CrossRef](#)]
29. Langner, T.; Öztürk, M.; Hartmann, S.; Cord-Landwehr, S.; Moerschbacher, B.; Walton, J.D.; Göhre, V. Chitinases are essential for cell separation in *Ustilago maydis*. *Eukaryot. Cell* **2015**, *14*, 846–857. [[CrossRef](#)]
30. Li, D.; Tang, Y.; Lin, J.; Cai, W. Methods for genetic transformation of filamentous fungi. *Microb. Cell Factories* **2017**, *16*, 168. [[CrossRef](#)]
31. Herzog, R.; Solovyeva, I.; Böcker, M.; Lugones, L.G.; Hennicke, F. Exploring molecular tools for transformation and gene expression in the cultivated edible mushroom *Agrocybe aegerita*. *Mol. Genet. Genom.* **2019**, *294*, 663–677. [[CrossRef](#)]
32. de Bekker, C.; Wiebenga, A.; Aguilar, G.; Wösten, H.A.B. An enzyme cocktail for efficient protoplast formation in *Aspergillus niger*. *J. Microbiol. Methods* **2009**, *76*, 305–306. [[CrossRef](#)]
33. Ruiz-Díez, B. Strategies for the transformation of filamentous fungi. *J. Appl. Microbiol.* **2002**, *92*, 189–195. [[CrossRef](#)]
34. Arnold, W.N.; Garrison, R.G. Isolation and characterization of protoplasts from *Saccharomyces rouxii*. *J. Bacteriol.* **1979**, *137*, 1386–1394. [[CrossRef](#)]
35. Sietsma, J.H.; De Boer, W.R. Formation and regeneration of protoplasts from *Pythium* PRL 2142. *Microbiology* **1973**, *74*, 211–217. [[CrossRef](#)]

36. Tilburn, J.; Scazzocchio, C.; Taylor, G.G.; Zabicky-Zissman, J.H.; Lockington, R.A.; Davies, R.W. Transformation by integration in *Aspergillus nidulans*. *Gene* **1983**, *26*, 205–221. [[CrossRef](#)]
37. Hu, Y.; Dietrich, D.; Xu, W.; Patel, A.; Thuss, J.A.J.; Wang, J.; Yin, W.-B.; Qiao, K.; Houk, K.N.; Vederas, J.C.; et al. A carbonate-forming Baeyer-Villiger monooxygenase. *Nat. Chem. Biol.* **2014**, *10*, 552–554. [[CrossRef](#)]
38. De Vries, O.M.H.; Wessels, J.G.H. Release of protoplasts from *Schizophyllum commune* by a lytic enzyme preparation from *Trichoderma viride*. *Microbiology* **1972**, *73*, 13–22. [[CrossRef](#)]
39. Ferrer, S.; Ramón, D.; Salom, J.; Vicente, E.; Uruburu, F. Protoplasts from *Podospora anserina*: Isolation, purification, and transformation. *Curr. Microbiol.* **1985**, *12*, 301–306. [[CrossRef](#)]
40. Zheng, Y.-M.; Lin, F.-L.; Gao, H.; Zou, G.; Zhang, J.-W.; Wang, G.-Q.; Chen, G.-D.; Zhou, Z.-H.; Yao, X.-S.; Hu, D. Development of a versatile and conventional technique for gene disruption in filamentous fungi based on CRISPR-Cas9 technology. *Sci. Rep.* **2017**, *7*, 9250. [[CrossRef](#)]
41. Eidtmann, A.; Schauz, K. Cryopreservation of protoplasts from sporidia of *Ustilago maydis*. *Mycol. Res.* **1992**, *96*, 318–320. [[CrossRef](#)]
42. van Peer, A.F.; de Bekker, C.; Vinck, A.; Wösten, H.A.B.; Lugones, L.G. Phleomycin increases transformation efficiency and promotes single integrations in *Schizophyllum commune*. *Appl. Environ. Microbiol.* **2009**, *75*, 1243–1247. [[CrossRef](#)]
43. Keon, J.P.R.; Broomfield, P.L.E.; White, G.A.; Hargreaves, J.A. A mutant form of the succinate dehydrogenase iron—sulphur protein subunit confers resistance to carboxin in the maize smut pathogen *Ustilago maydis*. *Biochem. Soc. Trans.* **1994**, *22*, 234–237. [[CrossRef](#)]
44. Lai, J.; Ng, S.K.; Liu, F.F.; Patkar, R.N.; Lu, Y.; Chan, J.R.; Suresh, A.; Naqvi, N.; Jedd, G. Marker fusion tagging, a new method for production of chromosomally encoded fusion proteins. *Eukaryot. Cell* **2010**, *9*, 827–830. [[CrossRef](#)]
45. Ghareeb, H.; Zhao, Y.; Schirawski, J. *Sporisorium reilianum* possesses a pool of effector proteins that modulate virulence on maize. *Mol. Plant Pathol.* **2019**, *20*, 124–136. [[CrossRef](#)]
46. Bartnicki-Garcia, S. Cell wall chemistry, morphogenesis, and taxonomy of fungi. *Annu. Rev. Microbiol.* **1968**, *22*, 87–108. [[CrossRef](#)]
47. Aguilar-Uscanga, B.; François, J.M. A study of the yeast cell wall composition and structure in response to growth conditions and mode of cultivation. *Lett. Appl. Microbiol.* **2003**, *37*, 268–274. [[CrossRef](#)]
48. Gander, J.E. Fungal cell wall glycoproteins and peptido-polysaccharides. *Annu. Rev. Microbiol.* **1974**, *28*, 103–120. [[CrossRef](#)]
49. Jin, L.-Q.; Xu, Z.-W.; Men, X.-H.; Bo, Z.; Liu, Z.-Q.; Zheng, Y.-G. Enhancement of protoplast preparation and regeneration of *Hirsutella sinensis* based on process optimization. *Biotechnol. Lett.* **2020**, *42*, 2357–2366. [[CrossRef](#)]
50. Lou, H.-W.; Ye, Z.-W.; Yu, Y.-H.; Lin, J.-F.; Guo, L.-Q.; Chen, B.-X.; Tang, H.-B.; Wei, T.; Chen, L.-T.; Yun, F. The efficient genetic transformation of *Cordyceps militaris* by using mononuclear protoplasts. *Sci. Hortic.* **2019**, *243*, 307–313. [[CrossRef](#)]
51. Kuwano, T.; Shirataki, C.; Itoh, Y. Comparison between polyethylene glycol- and polyethylenimine-mediated transformation of *Aspergillus nidulans*. *Curr. Genet.* **2008**, *54*, 95–103. [[CrossRef](#)]
52. Casselton, L.; Feldbrügge, M. Mating and sexual morphogenesis in Basidiomycete fungi. In *Cellular and Molecular Biology of Filamentous Fungi*; American Society of Microbiology: Washington, DC, USA, 2010. [[CrossRef](#)]
53. Morrow, C.A.; Fraser, J.A. Sexual reproduction and dimorphism in the pathogenic basidiomycetes. *FEMS Yeast Res.* **2009**, *9*, 161–177. [[CrossRef](#)] [[PubMed](#)]

3.2.2.4.2 Personal contribution to the publication

LP planned, performed and evaluated all experiments for figure 1, 4, 7 a, b, c, S1, S5c, VideoS1, VideoS2 and Table 1. Experiments for the figure 3 were planned and performed in cooperation with KB. The trapping buffer technique depicted in figure 2 was established for *T. thlaspeos* by LP. Strain generation of the strains depicted in figure 6 and 7d was performed for LF1-Gfp and supervised for LF2-mcherry by LP. All figures and tables were designed by LP under supervision of VG. LP drafted the Material & Methods, Results (partially) and Discussion sections of the manuscript including literature research.

3.2.3 Discussion

Over the last years of *T. thlaspeos* research complementation analysis in *U. maydis* were applied several times successfully for *T. thlaspeos* genes like the effector *pep1* (Courville *et al.*, 2019), sucrose transporter *srt1* (Schoen, 2017) or the b mating locus genes *bE* and *bW* (Geißl, 2020). In this work a complementation analysis of *T. thlaspeos* Pit1-Gfp in *U. maydis* showed that *Ttpit1-gfp* does not complement the *pit1Δ* deletion phenotype. Whether this is because *T. thlaspeos* Pit1 does not functionally complement *pit1Δ* or localizes falsely in *U. maydis* could not be determined with the applied methods. Although *U. maydis pit1* is in the top 20 of the genes upregulated compared to axenic culture at 2 dpi, Pit1-Gfp was barely visible at the plasma membrane (Doehlemann *et al.*, 2011). In my observations, the *U. maydis* Pit1-Gfp signal was actually only slightly above background fluorescence making microscopy extremely difficult. The application of the ClearSee technique (Kurihara *et al.*, 2015) to improve signal-to-noise ratio was not successful because the Gfp signal also decreased during the clearing process. The low protein levels of Pit1, despite the high transcript levels and the accumulation in vacuolar structures could indicate a high protein turn-over rate as typical for example for the pheromone receptor Pra1 (Fuchs *et al.*, 2006). Under the native *pit1* promoter *Ttpit1-gfp* was either not expressed or expression levels were so low, that no Gfp signal could be detected *in planta*. The reasons for the reduced expression of the fusion constructs could be versatile. In literature reasons for low expression of heterologous proteins mostly address translational or posttranslational events, like translational pausing due to codon bias (Gustafsson *et al.*, 2012) or a correlation of the transcription rate with the GC content (Jonkers, Kwak and Lis, 2014; Newman *et al.*, 2016). Besides, the GC

content is also important to mark intron exon boundaries and splicing (Amit *et al.*, 2012). Although codon usage in *U. maydis* and *T. thlaspeos* is rather similar, the GC content is in general 7,2 % higher in *T. thlaspeos* than in *U. maydis* (Frantzeskakis, 2016) and the fact that *Ttpit1* contains two introns while *Umpit1* does not contain introns overall could explain the observed differences in expression levels of *Umpit1-gfp* in comparison to *Ttpit1-gfp*. Considering that the *Ttpit1* CDS is expressed under the artificial P_{otef} promoter but still does not complement *pit1* Δ function, further optimization of *TtPit1* expression or additional attempts to show plasma membrane localization seem idle. With the established transformation protocol one of two methods is available to study the virulence function of Pit1 directly in *T. thlaspeos*. The other is a culture infection protocol, that is currently established in our lab (Natascha Heßler PhD thesis). With both being available in the near future, the next step will be to generate a *pit1* Δ mutant and *pit1-gfp* fusion strains expressed under the native and a constitutive promoter in *T. thlaspeos*.

There is a wealth of effector proteins in plant pathogens, while some are unique to the genus or the species (Giraldo and Valent, 2013; Lo Presti *et al.*, 2015), some are conserved or have conserved functional domains (de Jonge *et al.*, 2010; Djamei *et al.*, 2011; Giraldo and Valent, 2013). The conservation of the virulence factor Pit1 on the level of the class *Ustilaginomycetes* suggests also a conserved function. So far there is no specific function known for *UmPit1* besides its importance for tumour formation (Doehlemann *et al.*, 2011). *T. thlaspeos* on the other hand does not form visible infection symptoms like tumours (Frantzeskakis *et al.*, 2017). Therefore, one could assume that Pit1 is needed for efficient proliferation in the host tissue but only indirectly involved in tumour formation. This fits with the fact that *Umpit1* Δ mutants are more restricted to the vasculature and fail to grow in mesophyll layers during infection (Doehlemann *et al.*, 2011).

Interestingly, in maize the transcriptional response in leaves after infection with either *Umpit1* Δ or *Umpit2* Δ was identical, suggesting a link of Pit1 and the cysteine protease inhibitor Pit2 that could not be elucidated so far (Doehlemann *et al.*, 2011). In comparison *pit2* is not present in *T. thlaspeos* as well as *A. flocculosa*. Although overall sequence conservation of Pit2 within the grass smuts is low (Table 3-3) there is a highly conserved amino acid motif crucial for function (Mueller *et al.*, 2013) that could not be identified anywhere in the proteome of *T. thlaspeos*, further supporting

that Pit2 is not present in *T. thlaspeos*. If there is a functional link between Pit1 and Pit2, it is possible to speculate, that Pit2 is a derived trait that evolved in some members of the Ustilaginales along with a neofunctionalization/dualfunctionalization of Pit1. This is further supported by the example of the exobasidiomycete cotton tree smut fungus *Ceraceosorales bombacis*. This fungus is distantly related to *U. maydis* and *T. thlaspeos* (sister taxon of the *Ustilaginomycetes* (Begerow, Stoll and Bauer, 2006)) and thus represents an outgroup in comparison to the other two. In *C. bombacis* *pit1* is conserved, but an orthologue for *pit2* is also missing. To test this hypothesis, first a functional analysis of Pit1 in *T. thlaspeos* is needed. Subsequently, one would expect that the ancestral version of *pit1* (f. ex. *pit1* of *C. bombacis*) is able to complement *pit1* Δ in *T. thlaspeos* but not or only partially in *U. maydis*. In case of a dual function for Pit1 in *U. maydis*, *Umpit1* should complement *pit1* Δ in *T. thlaspeos*, while in case of a neofunctionalization it would not.

Both concepts are known for effectors of *U. maydis*. The effector protein Tin2 is translocated into the host cell to stabilize the protein kinase ZmTTK1 in order to induce anthocyanin biosynthesis (Tanaka *et al.*, 2014). *S. reilianum* possesses in comparison an ancestral version of Tin2 that does not induce anthocyanin biosynthesis and interacts with a paralogue protein kinase, indicating that Tin2 was neofunctionalized in *U. maydis* (Tanaka *et al.*, 2018). An example for a dual function of an effector is Pep1 (Doehlemann *et al.*, 2009). In the apoplast, Pep1 inhibits the maize peroxidase POX12 to suppress an early plant defence oxidative burst (Hemetsberger *et al.*, 2012). In addition to that it was recently shown, that Pep1 is also part of the Stp complex, a complex consisting of five effector proteins and two membrane proteins that protrudes from the fungal plasma membrane into the host cell and is crucial for fungal virulence to suppress host plant defence responses and might be involved in effector translocation (Ludwig *et al.*, 2021). Fitting to the above mentioned experimental strategy, *T. thlaspeos pep1* is able to partially complement the *pep1* Δ phenotype in *U. maydis* (Courville *et al.*, 2019). Taken together, it is possible that *TtPit1* and *UmPit1* still share an ancestral function, but with regard to Pit2 it seems unlikely that *TtPit1* can completely complement *pit1* Δ in *U. maydis*. With a transformation protocol now established for *T. thlaspeos* and a culture infection protocol in progress, it will soon be possible to investigate *TtPit1* function directly in *T. thlaspeos*. These results will contribute to understand the evolution of the virulence

factor Pit1 in comparison to other smut fungi and help to understand its function isolated from a putative link to Pit2.

Currently the function of Pit1 remains elusive, but the Pit1 orthologue in *P. hubeiensis* is annotated as inner membrane magnesium transporter MRS2 in the published genome available at the NCBI database (Konishi, Hatada and Horiuchi, 2015) giving a potential hint on the function of Pit1. The CorA/Mrs2/Alr1 magnesium transporter superfamily is conserved in pro- and eukaryotes (Knoop *et al.*, 2005; Payandeh, Pfoh and Pai, 2013; Sponder *et al.*, 2013). It is essential for magnesium homeostasis of the cell. The conservation of the primary sequence is rather low, but two transmembrane domains at the C-terminus containing a highly conserved G-M-N motif are crucial for magnesium transport (summarized in Sponder *et al.* 2013).

Interestingly an extended Pit1 orthologue alignment including *C. bombacis* Pit1, revealed a G-M-N motif located at the end of a transmembrane domain (Figure 3-14), but in comparison to CorA-type Mg^{2+} transporters Pit1 proteins have 7 predicted TM domains (AlphaFold prediction (Jumper *et al.*, 2021)). In the corresponding positions in *T. thlaspeos* and *A. flocculosa* asparagine (N) is substituted with the functionally conserved amino acid glutamine (Q) (Figure 3-14). In the remaining *Ustilaginales* additionally methionine (M) is substituted with the also hydrophobic leucine (L) (Figure 3-14). This evolution of the G-M-N motif also reflects the phylogenetic relationship of the Pit1 proteins in this alignment (Figure 3-14). While Pit1 does not fit the typical description of CorA-type magnesium transporters it is tempting to speculate that Pit1 belongs to a new type of magnesium transporters that evolved from the family of CorA-type magnesium transporters.

Today there are many different types of Mg^{2+} transporters known (Kolisek *et al.*, 2019) and along with that many exceptions to the rules. For example the maize CorA-type Mg^{2+} transporters ZmMGT4, 6 and 10 have an AMN motif instead of GMN, but ZmMGT6 and ZmMGT10 were tested and found functional in *Salmonella typhimurium* Mg^{2+} transporter complementation analysis (Li *et al.*, 2016; H. Li *et al.*, 2017). There is even evidence that multiple adjacent mutations in the G-M-N motif can result in functional molecules (Sponder *et al.*, 2013). Another example is the SLC11/NRAMP transporters family that specifically transports transition metal ions and not the more abundant magnesium or calcium ions (Ramanadane *et al.*, 2022). Interestingly, a distantly related clade, the NRMTs, was found to transport Mg^{2+} and

Mn²⁺ due to an altered ion binding site (Ramanadane *et al.*, 2022). In this context it would be interesting to examine putative transporter functions of Pit1. One hypothesis Doehlemann *et al.* (2011) suggested why *pit1/2* mutants fail to colonize mesophyll layers during maize infection is that the mutant hyphae fail to acquire essential nutrients. This would fit perfectly with the in this study hypothesized function of Pit1 as a transporter.

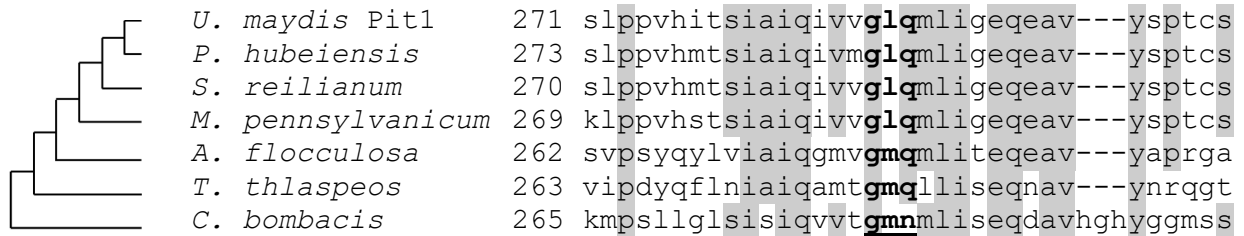


Figure 3-14 Excerpt of Pit1 protein multiway alignment (Scoring matrix: BLOSUM 62): Identical Amino acids are highlighted in grey, bold letters mark the G-M-N motif, the phylogenetic tree is based on the Pit1 sequences.

3.3 Magnesium transport in the smut fungus *Ustilago maydis*

3.3.1 Background

Besides the suggested role of Pit1 in Mg²⁺ homeostasis the impact of Mg²⁺ for plant-microbe interaction is a long known but understudied field. Mg²⁺ as the most abundant divalent cation of the cell is essential for the plant as well as the fungus (Graschopf *et al.*, 2001; Huber and Jones, 2013). Mg²⁺ is involved in a plethora of cellular processes: it functions as a co-factor for hundreds of enzymes and stabilizes proteins, nucleic acids and membranes (Gunther, 1981; Romani and Scarpa, 1992). Thus Mg²⁺ homeostasis is very tightly controlled (Kolisek *et al.*, 2019). Since disturbance of the Mg²⁺ balance affects so many physiological functions its challenging to differentiate individual effects on pathogenicity, virulence or plant defence (Huber and Jones, 2013).

There are a few reports on plant diseases where the Mg²⁺ availability caused either an increase or decrease of disease symptoms (Huber and Jones, 2013). Mg²⁺ deficiency during infection can affect the plant in several ways: Firstly, Mg²⁺ is a structural component of the plant cell wall middle lamella (Marschner, 2012) and if limited, the middle lamella loses structural integrity. For fungi that grow intracellularly this considerably simplifies cell-cell passage. Secondly, as central atom of chlorophyll and enzymatic co-factor, Mg²⁺ is important for energy production via photosynthesis (Strouse, 1974; McSwain, Tsujimoto and Arnon, 1976; Walker and Weinstein, 1991). If limited, this energy is lacking to support plant defence responses (Huber and Jones, 2013). And thirdly, Mg²⁺ is involved in phloem loading of sugars (Hermans *et al.*, 2005). Under deficiency, sugar partitioning between source and sink tissues is impaired and as a result sugar, starch and amino acids accumulate in leaves and photooxidative damage increases (Hermans *et al.*, 2005; Cakmak and Kirkby, 2008).

In *U. maydis* it has been reported that tumours are strong sinks for nitrogen and carbon, thus there is increased phloem flow from systemic source leaves to the infected leaves, combined with delayed senescence in older source leaves (Billett and Burnett, 1978; Horst *et al.*, 2008, 2010). The delay of senescence is typical for biotrophic pathogens, since they depend on living host tissue for their proliferation, while necrotrophs promote senescence to feed of the dead tissue (Häffner, Konietzki and Diederichsen, 2015). Mostly, this delay in senescence is described within the

infected tissue in the formation of so called green islands surrounded by otherwise senescent host tissue (Walters, McRoberts and Fitt, 2008). Although not that frequently observed, a systemic delay of senescence was also described in *Cuscuta reflexa* (parasitic plant) infected *Ricinus communis* (Jeschke and Hilpert, 1997).

Interestingly, it was reported that the Mg^{2+} concentration is significantly reduced in *U. maydis* tumours although Mg^{2+} is a highly phloem mobile ion (Marschner, 2012) and there is increased phloem flow towards the tumours (Horst *et al.*, 2010). In turn, other phloem mobile ions like potassium and phosphorus indeed accumulate in the tumours (Horst *et al.*, 2010). Currently it is unknown why Mg^{2+} does not accumulate in tumours or how this is regulated and if this is actively influenced by the fungus. But it is possible to speculate how this could benefit *U. maydis*. Mg^{2+} deficiency in the infected leaf might ease growth of *U. maydis* between the cells, since the cell walls are weaker. Indeed, the strength of the cell wall has considerable impact on *U. maydis* virulence: The *U. maydis* effector Tin2 is translocated into host plant cells where it induces anthocyanin biosynthesis by stabilizing a protein kinase ZmTTK1 that controls expression of anthocyanin biosynthesis pathway genes (Tanaka *et al.*, 2014). In absence of Tin2 the infected tissue responds with increased lignin biosynthesis that impairs fungal proliferation *in planta* (Tanaka *et al.*, 2014). It seems also possible that *U. maydis* takes up Mg^{2+} of the growing leaf, locally decreasing the Mg^{2+} concentration at points of cell-cell passage to facilitate its proliferation. Additionally, Mg^{2+} deficiency might contribute to turning the tumours into carbon sinks, to ensure sufficient nutrient supply for fungus. Under Mg^{2+} limited conditions the plant and the fungus compete for the available Mg^{2+} . In leaves the amount Mg^{2+} bound to chlorophyll constitutes 6-25 % of the total Mg^{2+} depending on overall Mg^{2+} availability (Marschner, 2012). In *U. maydis*, a reduction up to 90 % of chlorophyll a and b has been reported in tumours (Horst *et al.*, 2008), while the overall Mg concentration is 22 % reduced (Horst *et al.*, 2010). Theoretically, chlorosis could already explain the observed reduction of Mg^{2+} in the tumours if an overall low nutritional Mg^{2+} status is assumed where Mg^{2+} bound to chlorophyll constitutes 25 % of the total Mg. But considering that the experiments were conducted under lab conditions with good nutrient supply and that there is increased phloem flow, and thus Mg^{2+} supply, to the infection side, it seems unlikely that the observed reduction in Mg content can be attributed to chlorosis alone.

To study how *U. maydis* might impact the Mg^{2+} homeostasis during infection it is essential to understand the fungal Mg^{2+} transport. In fungi, Mg^{2+} transport is well studied in *S. cerevisiae*. Until now, two types of Mg^{2+} transporters were identified in *S. cerevisiae*, CorA-type Mg^{2+} transporters and an ACDP/CNNM-type Mg^{2+} transporter (Kolisek *et al.*, 2019; Tang *et al.*, 2022). The CorA-type Mg^{2+} transporters are widely distributed in all domains of life (Maguire, 2006; Groisman *et al.*, 2013). Originally they were characterized together with MgtA and MgtE Mg^{2+} transporters in bacteria, and named CorA since they confer resistance towards cobalt upon deletion (Hmiel *et al.*, 1986, 1989; Smith, Thompson and Maguire, 1995). The first CorA-type Mg^{2+} transporter homologues described in eukaryotic cells were *S. cerevisiae* Mrs2p and Alr1p (Bui *et al.*, 1999; Graschopf *et al.*, 2001; Gregan, Kolisek and Schweyen, 2001). Mrs2p and its homologue Lpe10p, which was identified shortly after Mrs2p, are both required for Mg^{2+} uptake across the inner mitochondrial membrane, while Lpe10p is additionally important to maintain the mitochondrial membrane potential necessary for Mg^{2+} transport (Bui *et al.*, 1999; Gregan *et al.*, 2001; Sponder *et al.*, 2010). Deletion of either one or both results in a petite phenotype (growth defect) on non-fermentable carbon sources since the strains are respiratory deficient (Sponder *et al.*, 2010). Alr1p is the plasma membrane Mg^{2+} transporter of *S. cerevisiae*, essential for Mg^{2+} uptake into the cell and identified in a screen for aluminium resistance, which is conferred by overexpression of Alr1, thus the name (MacDiarmid and Gardner, 1998; Graschopf *et al.*, 2001). If deleted, cells show a severe Mg^{2+} dependent growth defect that can be complemented by application of high external Mg^{2+} concentrations (Graschopf *et al.*, 2001). A second plasma membrane transporter of the CorA-type is Alr2p, which only marginally contributes to Mg^{2+} uptake into the cell, due to a single amino acid exchange in the loop between the TM-domains that results in low transport activity (MacDiarmid and Gardner, 1998; Wachek *et al.*, 2006). In turn, Alr2p can complement the *alr1* deletion only partially if overexpressed (Wachek *et al.*, 2006). The fifth CorA-type Mg^{2+} transporter identified in *S. cerevisiae* is Mnr2p. Mnr2p is the vacuolar Mg^{2+} exporter and upon deletion cells accumulate Mg^{2+} , since they cannot access their intracellular Mg^{2+} store (Pisat, Pandey and MacDiarmid, 2009).

For the bacterial CorA Mg^{2+} transporter of *Thermotoga maritima* (TmCorA) it was shown that the homopentamer forms a cone-shaped channel in the plasma membrane (Eshaghi *et al.*, 2006; Lunin *et al.*, 2006). So far TmCorA is the only CorA-

type Mg^{2+} transporter where the complete crystal structure is solved, but due to the high structural similarity predicted also for other CorA-type Mg^{2+} transporters a pentameric conformation seems also likely. Additionally, CorA-type Mg^{2+} transporters are characterized by two transmembrane domains located at the proteins C-terminus and a highly conserved GMN motif at the end of the first TM domain that acts as a selectivity filter for Mg^{2+} transport (Sponder *et al.*, 2013). Rarely, alterations in the GMN motif are described like AMN, which is still functional (Li *et al.*, 2016; H. Li *et al.*, 2017). This is especially interesting since AMN was tested in a mutational analysis of the GMN motif and found non-functional in *S. typhimurium* CorA (Szegedy and Maguire, 1999). Further deviation of the GMN motif namely GIN and GVN can be found in distant homologues of CorA Mg^{2+} transporters the ZntB type proteins which goes along with a change in substrate specificity to zinc or cadmium (Knoop *et al.*, 2005; Tan *et al.*, 2009). An additional random mutation analysis of the GMN motif of *S. cerevisiae* Mrs2p shows that replacement of two or all amino acids of the motif can result in functional transporters, while single amino acid substitutions were not tolerated (Sponder *et al.*, 2013). The tight regulation of the cellular Mg^{2+} concentration as well as its importance for a wealth of processes likely requires additional Mg^{2+} import and export systems to distribute Mg^{2+} in the cellular compartments. But until recently, no additional Mg^{2+} transporters could be identified in *S. cerevisiae*.

Earlier this year, it was demonstrated, that Mg^{2+} uptake into the vacuole against the concentration gradient is achieved by the ACDP/CNNM-type Mg^{2+} transporter Mam3p (Tang *et al.*, 2022). These Mg^{2+} transporters are characterized by a Cyclin M transmembrane domain (DUF21), which harbours three to four TM-domains and two cytoplasmic cystathionine- β -synthase (CBS) domains (Giménez-Mascarell *et al.*, 2019). Similar to CorA-type Mg^{2+} transporters, they are widely conserved in pro- and eukaryotes (Chen *et al.*, 2021). In bacteria and archaea they export Mg^{2+} from the cell and were identified together with CorA in a screen for cobalt resistance and accordingly named CorB (Hmiel *et al.*, 1986), while in fungi and plants they execute uptake of Mg^{2+} into the vacuole (Tang *et al.*, 2022). Since they transport Mg^{2+} against the concentration gradient, transport energy needs to be raised via primary or secondary active transport but until now there is no consent about the molecular mechanism (Chen *et al.*, 2021). Analysis of the crystal structure of an archaeal CorB/CNNM transporter suggests a rocker-switch mechanism (Chen *et al.*, 2021). In

this transport mechanism the transporter consists of two symmetric bundles with a central substrate-binding site (Drew and Boudker, 2016). During transport, the two bundles move around the substrate (rock) to expose the binding site from one site of the membrane to the other (Drew and Boudker, 2016).

In higher eukaryotes several other Mg^{2+} transporter families are known, but Mg^{2+} transport is independently confirmed only for some and the transport mechanism is identified for even fewer (Kolisek *et al.*, 2019). One well-characterized class is the SLC41 Mg^{2+} transporter family. They are homologues of the bacterial MgtE transporters that arose from gene duplication and fusion (Payandeh, Pfoh and Pai, 2013). Similar to the ACDP/CNNM-type Mg^{2+} transporters they contain CBS domains for Mg^{2+} -ATP binding and export Mg^{2+} either from the cytoplasm or the mitochondria in exchange with Na^+ in *Homo sapiens* (Kolisek *et al.*, 2008, 2012; Mastrototaro *et al.*, 2016).

Last but not least there are the NIPA-type putative Mg^{2+} transporters. Four NIPA-type proteins are described in *Mus musculus* for which Mg^{2+} transport activity was suggested based on transport studies in *X. leavis* oocytes (Goytain *et al.*, 2007; Goytain, Hines and Quamme, 2008; Quamme, 2010), but a confirmation of transport in a homologous system is still missing (Kolisek *et al.*, 2019). Based on expression in oocytes localization of NIPA1 and NIPA2 to the plasma membrane was suggested (Goytain *et al.*, 2007; Goytain, Hines and Quamme, 2008). Besides mouse and human homologues of NIPA transporters were identified also in plants (Heidari *et al.*, 2021), but not in *S. cerevisiae*.

3.3.2 Results

3.3.2.1 Importance of the GLQ motif for Pit1 function

The hypothesis of Pit1 functioning as a Mg^{2+} transporter is based on two findings: First, the identification of an altered GMN motif (GLQ) at the end of a transmembrane domain in Pit1 homologues and second, the annotation of a Pit1 homologue as Mg^{2+} transporter. To test this hypothesis, the importance of the GLQ motif for Pit1 function was investigated in *U. maydis*. To this end, the amino acids G₂₈₇ L₂₈₈ Q₂₈₉ were exchanged with alanine. To ensure that the exchange of the GLQ motif with alanine would likely not affect the protein conformation a secondary structure prediction was performed. Prediction of the secondary structure of the native and mutated Pit1

protein using the Phyre2 algorithm (Kelly *et al.*, 2015) verified that the alanine mutation does not affect the alpha helix conformation at this position (Supplementary Figure 7-2). In the genome the mutated *pit1-gfp* fusion construct was either inserted into the *pit1* locus under the native promoter or the *IP* locus under the P_{otef} promoter via homologous recombination and confirmation via Southern Blot. If expressed under the native *pit1* promoter the alanine-mutated Pit1-Gfp (Pit1_{GLQ3A}-Gfp) was not able to complement the *pit1*Δ phenotype in Amadeo maize infections (Figure 3-15 A and B). The visible infection symptoms on the leaves infected with the Pit1_{GLQ3A}-Gfp strain resembled the *pit1*Δ phenotype (Figure 3-15 B), while quantitatively the Pit1_{GLQ3A}-Gfp strain showed a slightly, but significantly higher small tumour formation rate than *pit1*Δ (Figure 3-15 A). While this could indicate slight residual function of the mutated Pit1 protein, it also supports correct localization. To ensure, that the observed phenotype of Pit1_{GLQ3A} is indeed not a result of abolished protein expression or mislocalization, protein expression was analysed at three dpi *in planta* using confocal microscopy. For Pit1-Gfp the expected accumulation in vesicular structures (Doehlemann *et al.*, 2011) was observed (Figure 3-16 A). In accordance with previous experiments, the localization to the plasma membrane was not visible under the given conditions, probably due to the high turnover rate of Pit1. In contrast, for both Pit1_{GLQ3A}-Gfp strains the protein localized exclusively to the fungal plasma membrane, which argues for reduced protein turnover indicative of impaired function of the mutated protein (Figure 3-16A).

To overcome visualization limitations of the fusion protein *in planta*, *pit1*_{GLQ3A}-*gfp* was expressed under the constitutive P_{otef} promoter to visualize protein localization in sporidia, as this was already shown to work nicely for the WT Pit1 (Doehlemann *et al.*, 2011). In Amadeo maize infections single as well as multiple insertion strains of *pit1-gfp* and *pit1*_{GLQ3A}-*gfp* were tested and showed similar phenotypes than expression of the constructs under the native promoter (Figure 3-15 C and D). In difference to expression under the native promoter, a lower not significant increase of the small tumour formation rate was observed for Pit1_{GLQ3A}-Gfp in comparison to *pit1*Δ, which might correlate with a lower expression level under the P_{otef} promoter compared to the native P_{pit1} promoter. The $P_{otef}::pit1$ _{GLQ3A}-*gfp* strains were also tested in an infection experiment with the more susceptible Golden Bantam cultivar. Similar to previous observations with this cultivar, the phenotypes resembled the

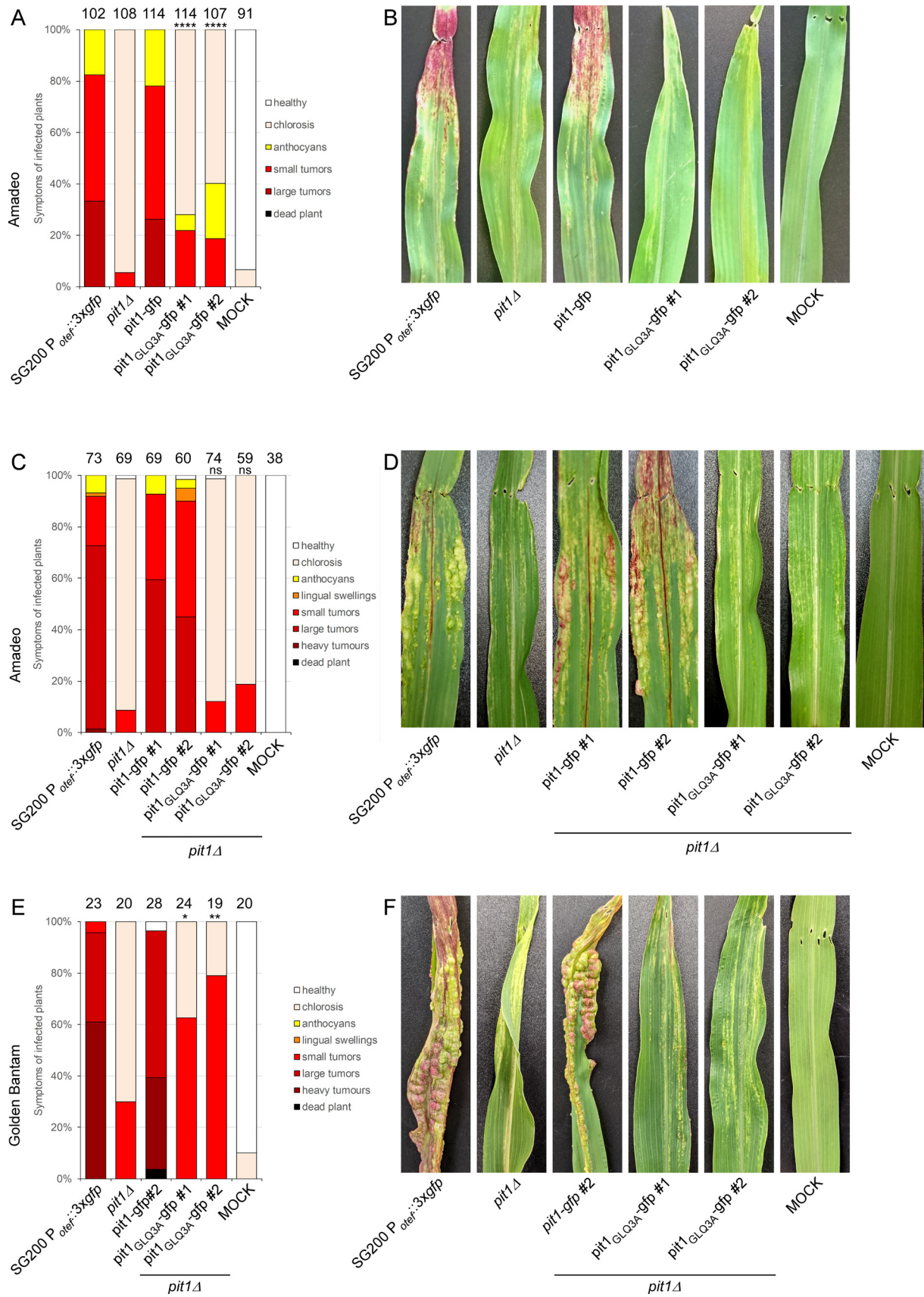


Figure 3-15 The *Pit1_{GLQ3A}-Gfp* mutant does not complement the *pit1Δ* phenotype in *U. maydis* if expressed under the native *U. maydis pit1* promoter or the constitutive *P_{otef}* promoter independent of the maize cultivar.

A: Disease rating of of three independent infections *Zea mays* Amadeo plants 14 dpi with the *U. maydis* strains indicated below. Plants infected with SG200 or *Umpit1-gfp* show chlorosis, anthocyanin formation and tumour formation while the strains *pit1Δ* as well as Pit1_{GLQ3A}-Gfp #1 and #2 show predominantly chlorosis, but Pit1_{GLQ3A}-Gfp shows a higher small tumour formation rate compared to *pit1Δ*. Interestingly, both Pit1_{GLQ3A}-Gfp mutant strains differ significantly in virulence from both SG200 and *pit1Δ* (Mann-Whitney U test).

B: Representative images of maize leaves harvested at 14 dpi with the *U. maydis* strains indicated below. Plants infected with SG200 or *Umpit1-gfp* show chlorosis, anthocyanin formation and tumour formation while the strains *pit1Δ* as well as Pit1_{GLQ3A}-Gfp #1 and #2 show predominantly chlorosis.

C: Disease rating of of three independent infections *Zea mays* Amadeo 12 dpi with the *U. maydis* strains indicated below. Plants infected with SG200 or *Umpit1-gfp* show chlorosis, anthocyanin formation and tumour formation while the strains *pit1Δ* as well as Pit1_{GLQ3A}-Gfp #1 (single insertion) and #2 (multiple insertion) show predominantly chlorosis. In contrast to expression of the construct under the native promoter, both Pit1_{GLQ3A}-Gfp mutant strains do not differ significantly from *pit1Δ* (Mann-Whitney U test).

D: Representative images of Amadeo maize leaves harvested at 12 dpi with the *U. maydis* strains indicated below. Plants infected with SG200 or *Umpit1-gfp* show chlorosis, anthocyanin formation and tumour formation while the strains *pit1Δ* as well as Pit1_{GLQ3A}-Gfp #1 and #2 show predominantly chlorosis.

E: Disease rating of a single infections *Zea mays* Golden Bantam plants 12 dpi with the *U. maydis* strains indicated below. Plants infected with SG200 or *Umpit1-gfp* show chlorosis, anthocyanin formation and tumour formation while the strains *pit1Δ* as well as Pit1_{GLQ3A}-Gfp #1 (single insertion) and #2 (multiple insertion) show predominantly chlorosis, but Pit1_{GLQ3A}-Gfp shows a higher small tumour formation rate compared to *pit1Δ*. Interestingly, both Pit1_{GLQ3A}-Gfp mutant strains differ significantly in virulence from both SG200 and *pit1Δ* (Mann-Whitney U test, only the comparison to *pit1Δ* is indicated in the figure).

F: Representative images of Golden Bantam maize leaves harvested at 12 dpi with the *U. maydis* strains indicated below. Plants infected with SG200 or *Umpit1-gfp* show chlorosis, anthocyanin formation and tumour formation while the strains *pit1Δ* shows mostly chlorosis and Pit1_{GLQ3A}-Gfp #1 and #2 show predominantly small tumour formation.

Note: The data of the control strains SG200 *P_{oter::3xgfp}*, SG200 *pit1Δ* and SG200 *pit1Δ pit1-gfp* #1 and #2 in C-F is from the same dataset as Figure 3-12 and 3-13.

results of the Amadeo infection with an overall increase in symptom severity (Figure 3-15 E and F). Interestingly, similar to the expression under the native promoter, again a significant increase in the small tumour formation rate was observed for the Pit1_{GLQ3A}-Gfp strains in comparison to *pit1Δ* (Figure 3-15 E). Unfortunately, localization of Pit1_{GLQ3A}-Gfp in sporidia was not successful. While the native Pit1-Gfp localized to the plasma membrane and vesicular structures as described before (Doehlemann *et al.*, 2011, see also section 4.2.2), Pit1_{GLQ3A}-Gfp showed a weak and diffuse signal that that could probably be assigned to the ER, indicating the protein might not be processed correctly and is subsequently degraded (Figure 3-16 B). Although the mutated Pit1 was not properly expressed in sporidia, the higher tumour formation rate observed in Golden Bantam infection argues for correct expression and localization *in planta*, similar to the observations for expression under the native promoter. To support this hypothesis and test if the mutated Pit1 protein requires biotrophic growth conditions for correct expression, localization of the fusion proteins was investigated in four dpi infected Golden Bantam leaves via confocal microscopy. As already reported previously, *U. maydis* Pit1-Gfp#2 showed a diffuse signal that

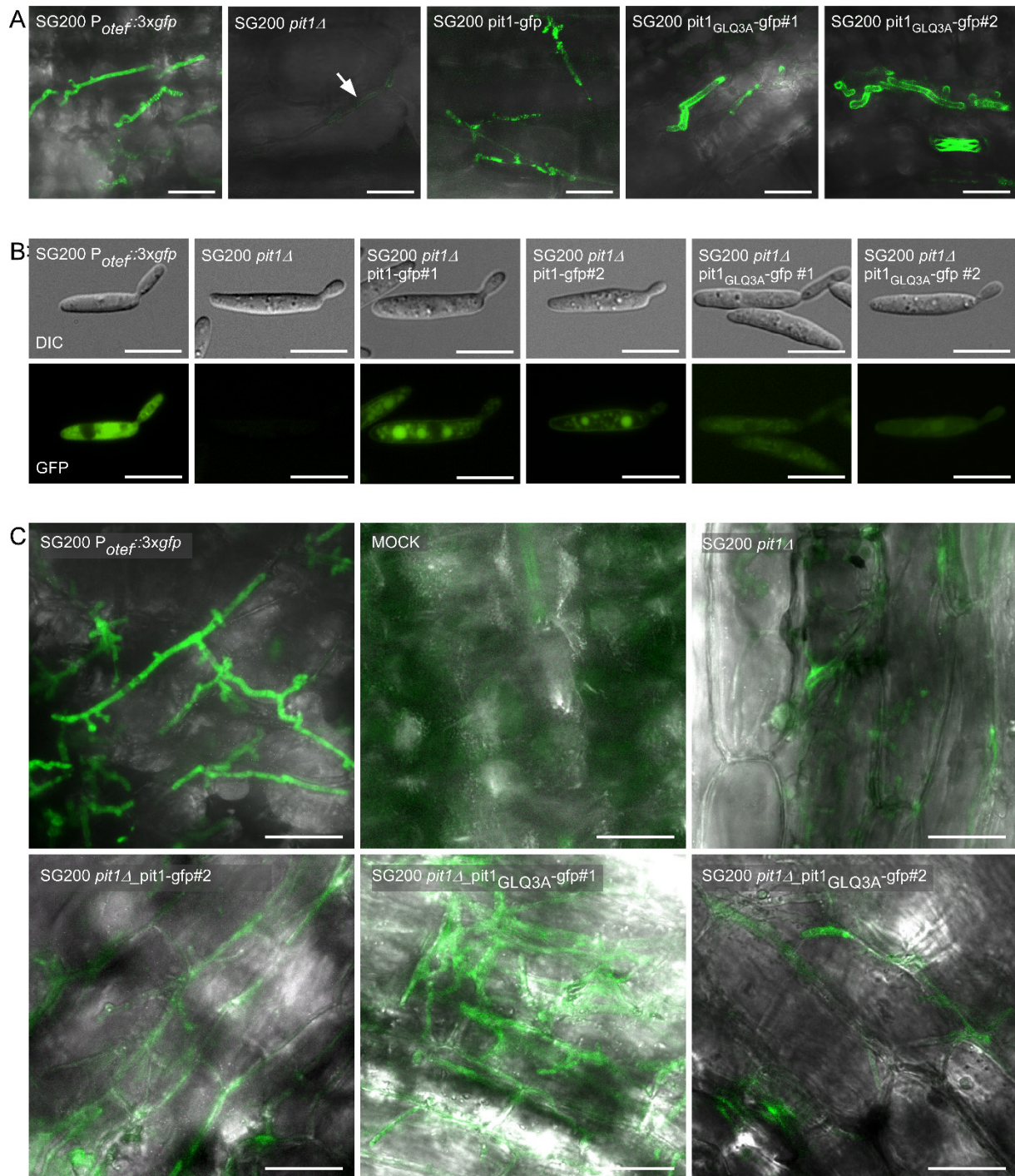


Figure 3-16 Localization Pit1_{GLQ3A}-Gfp if expressed under the native *U. maydis pit1* promoter or the constitutive P_{otef} promoter in sporidia and *in planta*.

A: Confocal images of *U. maydis* infected maize leaves 3 dpi. *UmPit1*-Gfp accumulates in vesicular structures as described in Doehlemann *et al.* (2011). Membrane localization is not visible under these conditions. In comparison Pit1_{GLQ3A}-Gfp #1 and #2 exclusively localize to the plasma membrane. Arrow marks *U. maydis* hyphae. The scale bar equals 25 μm. Microscopy was performed once.

B: Microscopy images of *U. maydis* sporidia expressing *pit1*-gfp constructs. *UmPit1*-Gfp accumulates in vesicular structures and at the plasma membrane as described in Doehlemann *et al.* (2011). In comparison Pit1_{GLQ3A}-Gfp #1 and #2 only show a weak diffuse signal that might indicate that the fusion protein is stuck in the ER. The scale bar equals 10 μm. Microscopy was performed once. Signal intensities of the GFP channel are comparable between the single insertion strains *Umpit1*-gfp #1 and Pit1_{GLQ3A}-Gfp #1 and *pit1*Δ as well as the multiple insertion strains *Umpit1*-gfp #2 and Pit1_{GLQ3A}-Gfp #2.

C: Confocal images of *U. maydis* infected Golden Bantam maize leaves 4 dpi. *Umpit1-gfp* #2 (multiple insertion) and *Pit1_{GLQ3A}-Gfp* #1 and #2 show a diffuse Gfp signal that is even lower than expression under the native promoter. Membrane localization is not visible under these conditions. The scale bar equals 25µm. Microscopy was performed once. The signal intensity of the GFP channel is comparable for the Gfp fusion strains and otherwise adjusted to the individual sample.

Note: The data of the control strains strains SG200 *P_{otef}::3xgfp*, SG200 *pit1Δ* and SG200 *pit1Δ pit1-gfp* #1 and #2 in B and C is from the same dataset as Figure 3-12 and 3-13.

was similarly observed for both *Pit1_{GLQ3A}-Gfp* strains (Figure 3-16 C). The comparison to the MOCK control and the *pit1Δ* strain shows that the detected Gfp signal is barely above background fluorescence of the plant tissue. This additionally supports that expression levels under the *P_{otef}* promoter are lower than under *P_{pit1}* *in planta*, thus live imaging is not possible under these conditions. In summary, the results support importance of the GLQ motif for Pit1 function. Although unambiguous evidence is still missing, the results so far indicate that the alanine substitution of the GLQ motif does not impair localization *in planta*.

3.3.2.2 Can *U. maydis pit1* complement the *alr1Δ* phenotype in *Saccharomyces cerevisiae*?

The importance of the GLQ motif for Pit1 function so far is in line with the hypothesis of Pit1 as a magnesium transporter. Thus, a putative Mg²⁺ transport activity of Pit1 was studied in *S. cerevisiae*. In *S. cerevisiae* magnesium transport is well studied. In difference to higher eukaryotes it possesses only two plasma membrane Mg²⁺ transporters Alr1p and Alr2p. Deletion of *ALR1* results in a clear magnesium dependent growth phenotype (Graschopf *et al.*, 2001), thus this strain is frequently used for complementation analysis. For this purpose, an *ALR1/alr1* *S. cerevisiae* strain was purchased from Euroscarf (Accession number: Y26280) and haploid *alr1* candidates were isolated after random sporulation and confirmed via colony PCR and Mg²⁺ dependent growth tests (Supplementary Figure 7-3).

To determine if *pit1* is able to complement the *alr1* phenotype in *S. cerevisiae*, C-terminally Gfp-tagged fusions of Pit1, *Pit1_{GLQ3A}*, *S. cerevisiae* Alr1p and the closest *U. maydis* homologue UMAG_00361 (Alr1, see subsequent chapter) were expressed from a centromeric plasmid. Analysis of 10 transformants each revealed that only the *S. cerevisiae* Alr1p was able complement the yeast *alr1* phenotype (Supplementary Figure 7-4 A), because all other fusion proteins were either not expressed or did not localize to the plasma membrane (Supplementary Figure 7-4 B). To test if the mislocalization of the proteins is caused by the Gfp-tag, the gfp was mostly (6 amino

acid residue) removed from the constructs. Unfortunately, the constructs still did not complement the *alr1* phenotype (Peter Wegjan, Bachelors thesis 2021). In the end, it was not possible to test if Pit1 is able to complement the *alr1* phenotype in *S. cerevisiae*, because the proteins mislocalized. As *S. cerevisiae* seemed to be a suboptimal host for expression of *U. maydis* membrane proteins, I decided to study magnesium transport and a putative contribution of Pit1 directly in *U. maydis*.

3.3.2.3 An inventory of potential magnesium transporters in *U. maydis*

Until now magnesium transport was not studied in *U. maydis*. To get an overview about all potential magnesium transporters present in *U. maydis*, I searched the proteome for PFAM domains associated with magnesium transport (additionally to the PFAM domains listed in Table 3-4 the initial search also included the domains MgtC (PF02308) and ATPase_gene1 (PF09527)). In difference to *S. cerevisiae*, which possesses only two known types of magnesium transporters (CorA and ancient conserved domain proteins (ACDP)), *U. maydis* harbours magnesium transporters of four different families: tree CorA-type transporters, one MgtE-type transporter, four NIPA-type transporters, and one ACDP-type as well as one ACDP-like transporter (Table 3-4). All potential *U. maydis* Mg²⁺ transporters are constitutively expressed on a low level in sporidia as well as biotrophic hyphae except for ACDP-like transporter UMAG_02682, where expression is upregulated during infection in comparison to axenic culture (Table 3-4; expression data acc. to Lanver et al 2018). Homology of the transporter candidates to characterized representatives of the different magnesium transporter families (*S. cerevisiae* or *Homo sapiens*) as well as conservation within the smut fungi was verified manually via blast search. Based on this the *U. maydis* Mg²⁺ transporter candidates were named according to already characterized homologues (Table 3-4). From the sequence alignments a phylogenetic tree was calculated showing that the magnesium transporter repertoire of *U. maydis* is conserved in smut fungi (Figure 3-17). Additional to sequence similarity, homology was analysed based on structure similarity, supporting the blast search results. Protein structure predictions of all putative transporters (Supplementary Figure 7-5) were generated using the Alphafold2 algorithm (Jumper *et al.*, 2021) and superposed on the structure of the corresponding homologue using Pymol as well as the Tm Align algorithm (Zhang and Skolnick, 2005) (Supplementary Table 7-1).

Table 3-4 Putative Mg²⁺ transporter repertoire of *U. maydis*

Name	Protein ID	Expression acc. Lanver et al. 2018	No. TM domains*	PFAM domain	Interpro domain	Orthologue in <i>S. cerevisiae/ H. sapiens</i>	Description	Reference
MgtE	UMAG_00219	constitutive	13	MgtE PF01769	SLC41A/MgtE IPR006667	<i>H. sapiens</i> SLC41A3	Na ⁺ /Mg ²⁺ ion exchanger; Mg ²⁺ efflux system in the inner mitochondrial membrane	Quamme 2010; Mastrototaro et al. 2016
Mnr2	UMAG_10049	constitutive	2	CorA PF01544	Mg ²⁺ transporter protein, CorA-like/Zinc transport protein ZntB IPR002523	<i>S. cerevisiae</i> YL064W MNR2	CorA-type vacuolar Mg ²⁺ exporter	Pisat et al. 2009
Alr1	UMAG_00361	constitutive	2	CorA PF01544	Mg ²⁺ transporter protein, CorA-like/Zinc transport protein ZntB IPR002523	<i>S. cerevisiae</i> YFL050C ALR2/ YOL130W ALR1	CorA-type Plasma membrane magnesium importer	Graschopf et al. 2001; Wachek et al. 2006
Lpe10	UMAG_10884	constitutive	2	CorA PF01544	Mg ²⁺ transporter protein, CorA-like/Zinc transport protein ZntB IPR002523	<i>S. cerevisiae</i> YPL060W LPE10/ YOR334W MRS2	CorA-type MRS2/LPE10 heterodimer; Mg ²⁺ importer of the inner mitochondrial membrane	Bui et al. 1999; Gregan et al. 2001; Sponder et al. 2010
Nipa1	UMAG_01797	constitutive	9	Mg_trans_NIPA PF05653	Magnesium transporter NIPA IPR008521	<i>H. sapiens</i> NIPA2 isoform a	putative plasma membrane Mg ²⁺ importer with a in general broad substrate specificity; Mg transport not yet confirmed in a homologous system	Goytain et al. 2008; Quamme 2010
Nipa2	UMAG_02316	constitutive	9	Mg_trans_NIPA PF05653	Magnesium transporter NIPA IPR008521	<i>H. sapiens</i> NIPA2 isoform a		
Nipa3	UMAG_02993	constitutive	9	Mg_trans_NIPA PF05653	Magnesium transporter NIPA IPR008521	<i>H. sapiens</i> NIPA2 isoform a		
Nipa4	UMAG_03028	constitutive	9	Mg_trans_NIPA PF05653	Magnesium transporter NIPA IPR008521	-		
	UMAG_12094**	constitutive	2	MMgT PF10270	Membrane magnesium transporter IPR018937	<i>S. cerevisiae</i> YIL027C EMC5	The endoplasmic reticulum-membrane protein complex (EMC); protein complex for biogenesis of integral membrane proteins; promotes insertion and stability of atypical and sub-optimal TM domains	Volkmar and Christianson 2020
Mam3	UMAG_06268	constitutive	3	Cyclin M transmembrane N-terminal domain PF01595 2x CBS domain PF00571	CNNM, transmembrane domain IPR002550 2x CBS domain IPR000644 + IPR044751	<i>S. cerevisiae</i> YOL060C MAM3	Ancient conserved domain proteins-/ cyclin M-type divalent metal cation transport mediators-type vacuolar Mg ²⁺ importer	Tang et al. 2022
Mam3-like	UMAG_02682	constitutive, upregulated during infection	4	Cyclin M transmembrane N-terminal domain PF01595	CNNM, transmembrane domain IPR002550	<i>S. cerevisiae</i> YOL060C MAM3		

*DeepTMHMM prediction; ** UMAG_12094 was excluded as Mg²⁺ transporter due to known function of the homologous yeast ECM complex.

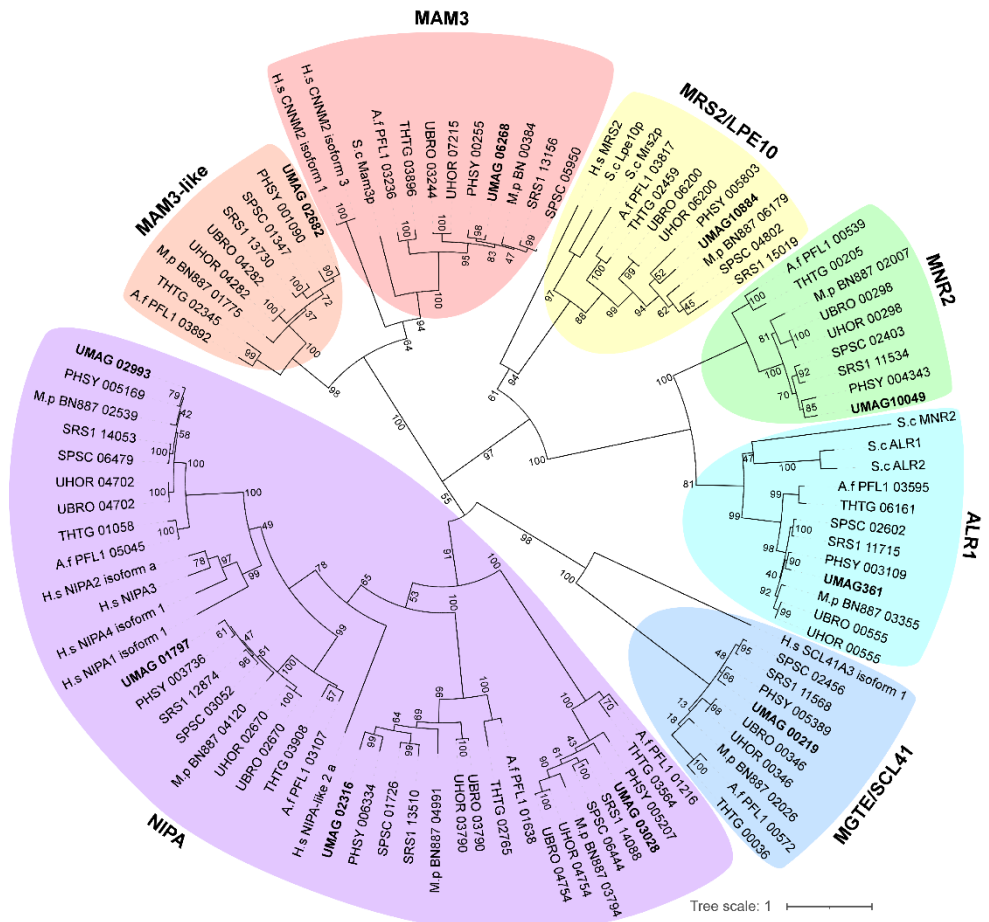
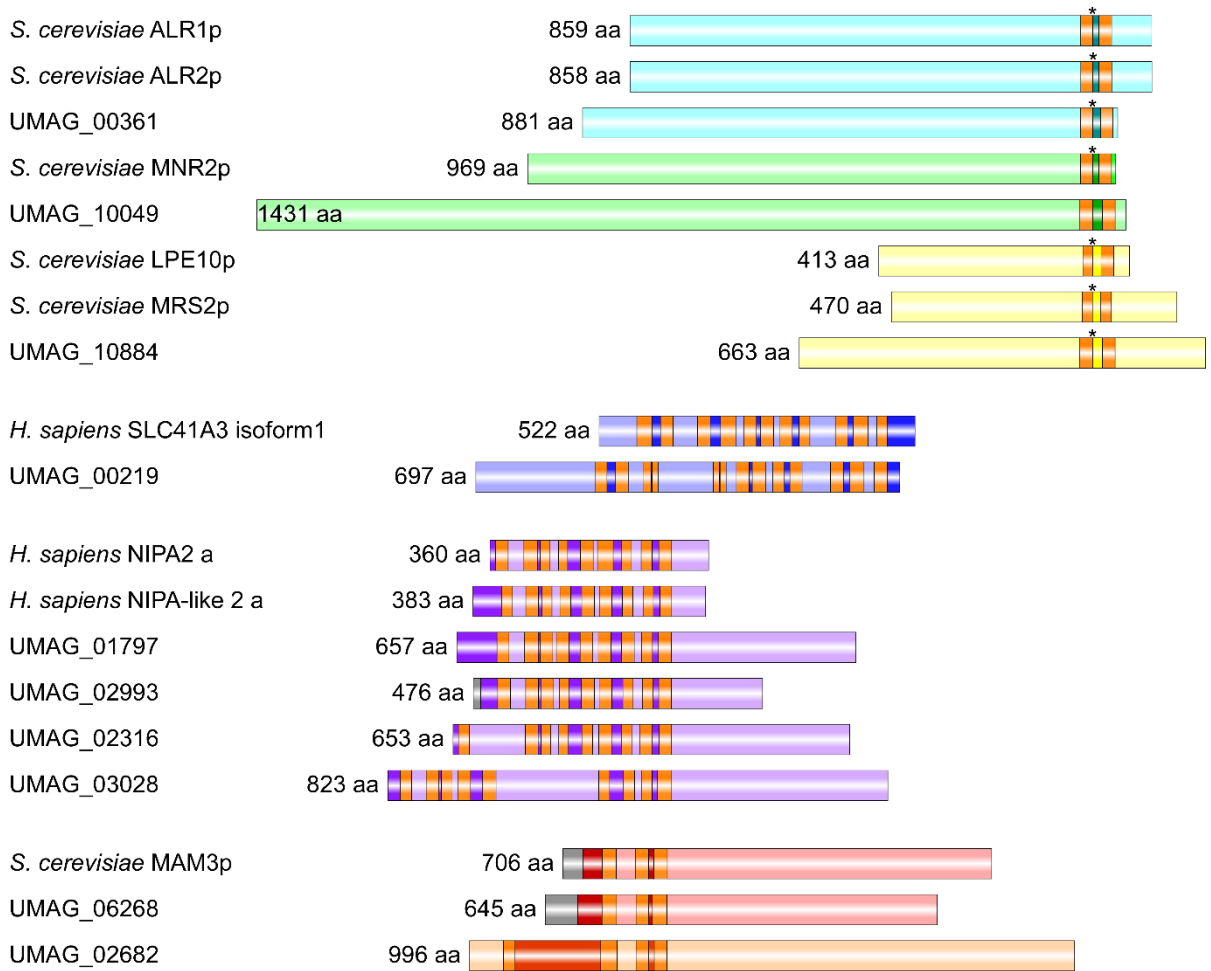


Figure 3-17 Membrane topology models of all putative Mg^{2+} transporters and their closest characterized homologue based on DeepTMHMM algorithm predictions. Orange: TM domain; light color: intracellular; dark color: extracellular; grey: signal peptide; * GMN motif. **Phylogeny of the putative Mg^{2+} transporter families in smut fungi:** The phylogenetic tree was calculated from a CLUSTALW protein sequence alignment based on maximum likelihood algorithm with a bootstrap support of 100 replicates generated with the MEGA11 software.

As the different magnesium transporter families differ strongly in their membrane topology, predictions for all transporter candidates and their reference homologues were generated using the DeepTMHMM algorithm (Figure 3-17). Based on these analyses a schematic representation of the cellular magnesium transport mechanisms was generated (Figure 3-18).

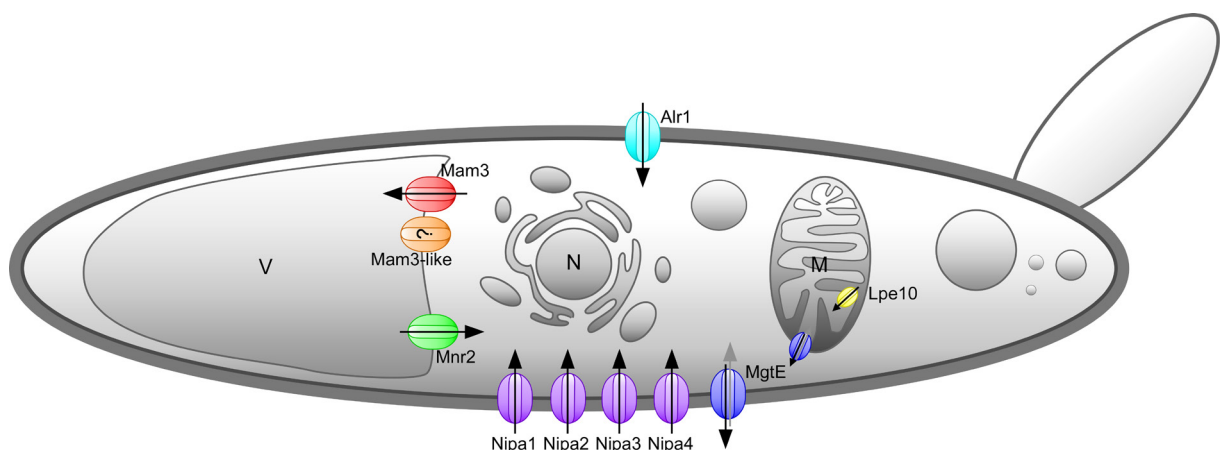


Figure 3-18 Schematic overview of *U. maydis* putative Mg^{2+} transporters and their potential localization. Suggested localization is based on homology to at least partially characterized representatives of the respective transporter family. For MgtE localization to the mitochondria as well as plasma membrane seems possible.

3.3.2.3.1 CorA-type magnesium transporters

U. maydis has three CorA-type magnesium transporters UMAG_10884, UMAG_10049 and UMAG_00361. Based on sequence and structure alignments their closest *S. cerevisiae* homologues are Lpe10p, Mnr2p and Alr2p and this would localize them to the mitochondria, vacuole and plasma membrane, respectively.

For UMAG_10884/Lpe10 a mitochondrial targeting sequence (MTS, Mitofates prediction) can be predicted strengthening the proposed localization to the mitochondria.

UMAG_10049/Mnr2 shows highest structural and sequence similarity with ScMnr2p, but interestingly the whole smut fungal Mnr2 clade differs to an extent from ScMnr2p that ScMnr2p groups with the smut fungal Alr1/Alr2 group instead of the smut Mnr2

group (see phylogenetic tree Figure 3-17). This is further supported by the observation that the whole smut Mnr2 group is on average 472 aa longer than yeast Mnr2p and contains a SxN motif instead of the highly conserved GMN signature motif at the end of the first TM-domain (Figure 3-19).

<i>S. c</i> Mnr2p	LPMNVITGLW GMN VIVPG	936
<i>M. p</i> BN887_02007	-----	1300
<i>U. h</i> UHOR_00298	FIAVFMTSIF SVN VNRPG	1393
<i>U. b</i> UBRO_00298	FIAVFMTSIF SVN VNRPG	1393
<i>P. h</i> PHSY_004343	LIIVFITSVF SLN VKRPG	1440
<i>U. m</i> UMAG_10049	LIIVFITSIF SVN VTRPG	1384
<i>S. r</i> SRS_111534	LIIVFITSIF SLN VNRPG	1350
<i>S. s</i> SPSC_02403	LIIVFITSVF SLN VARPG	1352
<i>T. t</i> THTG_00205	LCMQFTTSLF SIN VKTPH	1477
<i>A. f</i> PFL1_00539	LCMQFTTSLF SIN VKVPH	1481

Figure 3-19 Mnr2 homologues sequence alignment. In smut fungi at the position of the highly conserved GMN motif there is a SxN motif. In *M. pennsylvanicum* the sequence suddenly ends before the first TM-domain, meaning this protein is either no membrane protein or the gene model is wrong.

UMAG_00361/Alr1 is the closest homologue of the yeast plasma membrane magnesium transporter Alr2p. In *S. cerevisiae* two plasma membrane transporters Alr1p and Alr2p as well as two mitochondrial transporters Mrs2p and Lpe10p are present that both form heterooligomers. While Alr2p is dispensable for Mg²⁺ uptake, Mrs2p and Lpe10p are required for Mg²⁺ uptake into the mitochondria. This diversification of CorA-type transporters does not seem to be conserved in smut fungi, thus functionally it can be expected that UMAG_00361 resembles rather Alr1p than Alr2p while UMAG_10884 might combine the functions of Mrs2p and Lpe10p. Which transporter set represents the ancestral trait cannot be distinguished with the present data set.

3.3.2.3.2 MgtE/SLC41-type magnesium transporters

U. maydis possesses one MgtE/SLC41-type transporter UMAG_00219 (named MgtE) Based on the structural and sequence homology the closest homologue is the human SLC41A3 (isoform 1) Mg²⁺/Na⁺ exchanger, which exports Mg²⁺ from the mitochondria while its homologue SLC41A1 is located at the plasma membrane. Neither SLC41A3 nor UMAG_00219 harbour any predicable mitochondrial targeting sequence. Additionally, as *U. maydis* has only one transporter of this family and is phylogenetically very distant to *H. sapiens*, plasma membrane and mitochondria localization seem equally likely. A localization to the mitochondrial membrane or the

plasma membrane is preferentially suggested because of the homology to SLC4A3 but localization to another cellular compartment is of course also possible.

3.3.2.3.3 ACDP/CNNM-type magnesium transporters

U. maydis has two proteins that are homologues to the *S. cerevisiae* Mam3p vacuolar Mg²⁺ importer. Strictly, only UMAG_06268 (named Mam3) contains the CNNM- and two CSB-domains that characterize the ACDP/CNNM group of Mg²⁺ transporters, while UMAG_2682 (named Mam3-like) contains only the CNNM domain. But the close structural resemblance to Mam3p suggests that UMAG_2682 might be a Mam3-like protein. It was shown for *H. sapiens* CNNM proteins that the CBS domain is crucial for Mg²⁺ efflux (Hirata *et al.*, 2014), thus it is questionable if UMAG_2682 is able to transport magnesium.

3.3.2.3.4 NIPA-type magnesium transporters

UMAG_01797 (named Nipa1), UMAG_02316 (named Nipa2), UMAG_02993 (named Nipa3) and UMAG_03028 (named Nipa4) were identified as NIPA-type transporters with *H. sapiens* NIPA2a a putative plasma membrane Mg²⁺ importer as closest homologue based on sequence and structure alignment, except for UMAG_03028. Interestingly, the protein structure of UMAG_03028 aligns very well to the structure of *H. sapiens* NIPA2a, although it is not homologues on the sequence level (Supplementary Table 7-1).

In summary, the Mg²⁺ transporter repertoire of *U. maydis* appears more versatile in comparison to *S. cerevisiae*. In other ascomycetes like *Botrytis cinerea*, *Piriformospora indica*, *Aspergillus nidulans* or *Neurospora crassa* the four NIPA transporters seem to be conserved as well and even the human pathogenic yeast *Candida albicans* has two NIPA homologues (Supplementary Figure 7-6). In contrast, MgtE appears to be conserved only in smut fungi and *P. indica* while Mam3-like proteins are only found in smut fungi (Supplementary Figure 7-6). The three CorA-type Mg²⁺ transporters seem to be conserved in asco- as well as basidiomycetes (Supplementary Figure 7-6).

Overall, *U. maydis* allows to study the fungal Mg²⁺ homeostasis on a more holistic level than currently possible in *S. cerevisiae*, since its Mg²⁺ transporter repertoire is more versatile. This has on the one hand the advantage to study the contribution of the different Mg²⁺ transporter families to Mg²⁺ homeostasis and on the other hand

harbours the potential to identify transporters of other cellular compartments like the nucleus, ER or Golgi. As *U. maydis* is a biotrophic pathogen it also offers the possibility to discover potential links of fungal Mg²⁺ homeostasis and plant disease. For both, testing a potential Mg²⁺ transport function of Pit1 as well as investigating a contribution of fungal Mg²⁺ uptake to infection, understanding Mg²⁺ uptake into the cell is key. In *S. cerevisiae* Mg²⁺ uptake into the cell is facilitated via CorA-type transporters, thus further analysis of the *U. maydis* Mg²⁺ transporter candidates were prioritized for the CorA-type Mg²⁺ transporters.

3.3.2.4 Localization of CorA-type Mg²⁺ transporters in *U. maydis*

Information on the subcellular localization may provide first insights into the function of the transporter candidates, thus all CorA-type Mg²⁺ transporters were over expressed with C-terminal Gfp-tags in the heterologous *IP* locus in SG200 background and analysed microscopically (Peter Wegjan, Bachelors thesis under my supervision). The distribution of the fusion protein observed for two lpe10-gfp strains perfectly co-localized with the mitochondrial dye TMRE, confirming the predicted localization to the mitochondria (Figure 3-20 C). For Alr1 and Mnr2 the C-terminal Gfp-tag resulted in weak expression and a distribution pattern typical for *U. maydis* proteins that reside in the ER and in the case of the multiple insertion strain alr1-gfp #2 the fusion protein also accumulated in speckles in the cytoplasm (Figure 3-20 B). For *S. cerevisiae* it was shown that C-terminal tagging affects Alr1p accumulation, but not localization (Lim *et al.*, 2011). In *U. maydis* Alr1 and Mnr2 the C-terminal tail after the second transmembrane domain is considerably shorter in comparison to Alr1p (6/18 aa vs 66 aa, Figure 3-20). Since the channel likely has a homopentameric conformation like its bacterial homologue, the position of the C-terminus results in the accumulation of five Gfp molecules directly in the centre of the channel pore. Thus the Gfp-tags could easily cause a steric hindrance that impairs insertion of the monomer into the membrane as well as homooligomerization. In case the C-terminal Gfp-tag poses a steric hindrance, Alr1 and Mnr2 were also tagged N-terminally. Unfortunately, both gfp-mnr2 #1 and #2 strains still showed the same weak expression in the ER than the C-terminally tagged version, but Gfp-Alr1 exclusively localized to the membrane of the vacuole, indicated by co-localization with the vacuolar staining CMAC (Figure 3-20 A and B). For Alr1 this was rather unexpected since Alr1p and Alr2p of *S. cerevisiae* both localize to the plasma membrane.

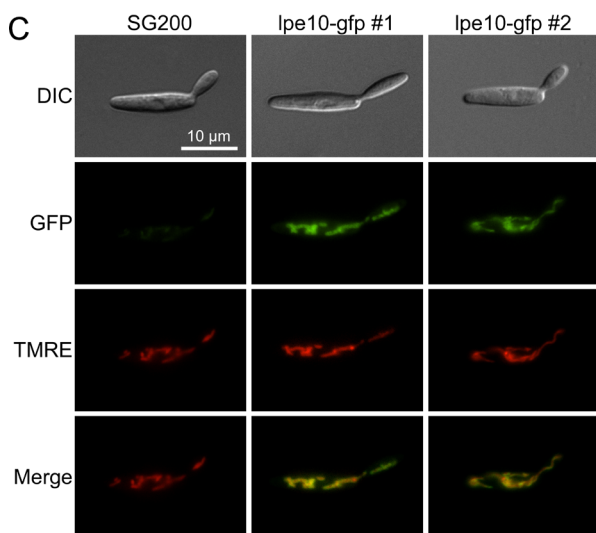
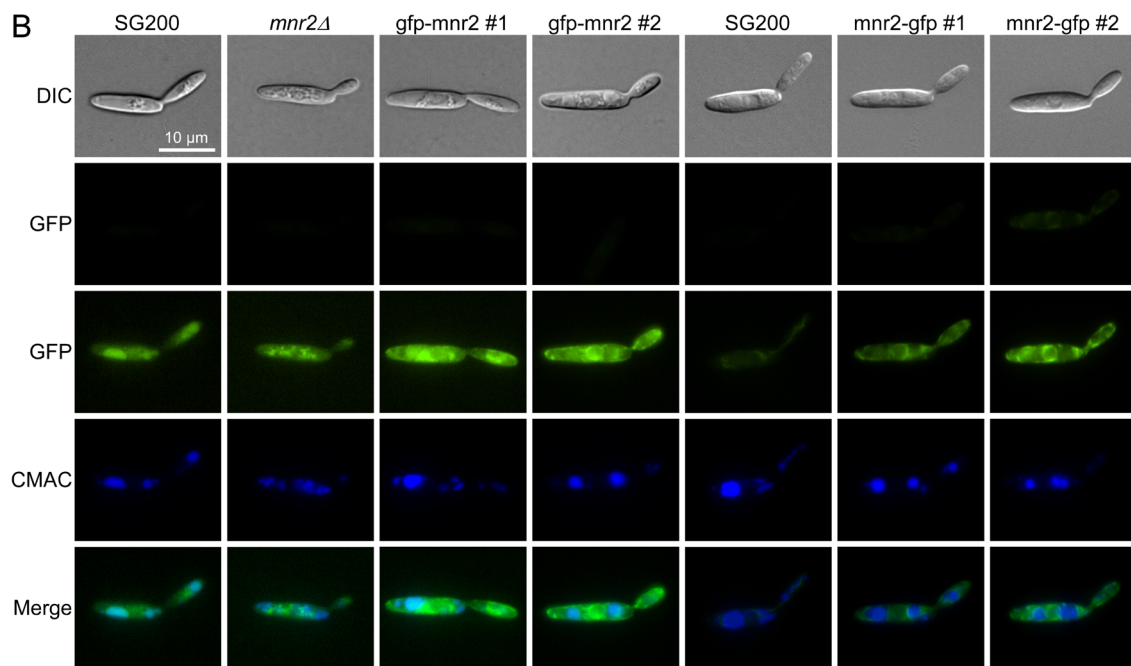
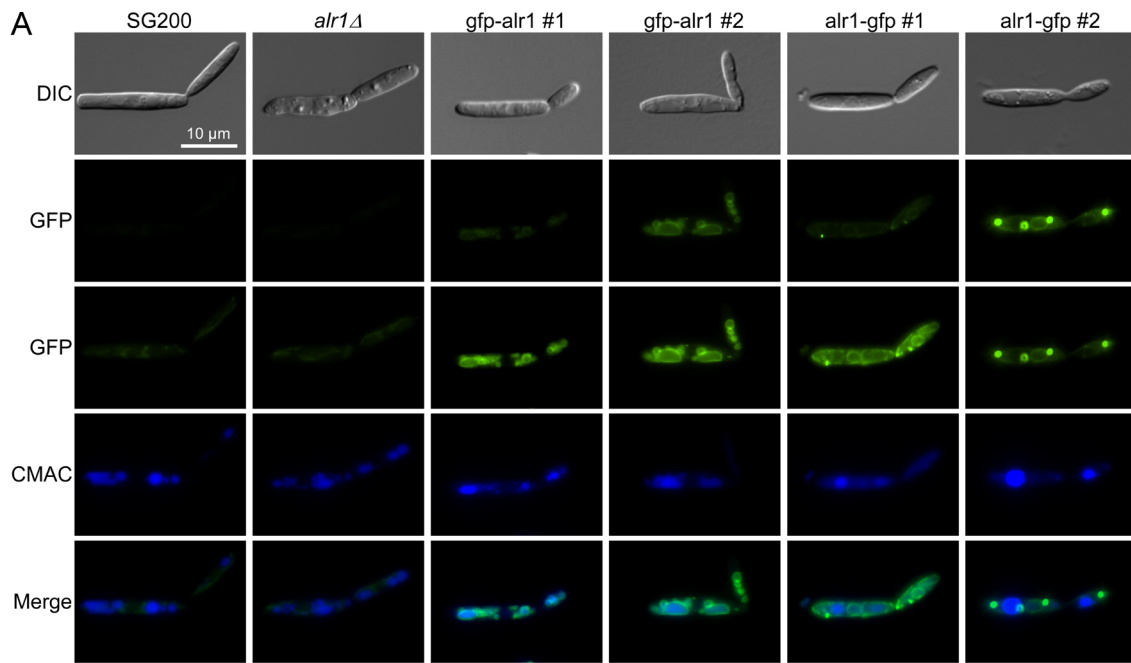


Figure 3-20 Localization of CorA-type Mg²⁺ transporters in *U. maydis*.

A: Gfp-Alr1 localizes to the vacuolar membrane, while Alr1-Gfp localizes to the ER or speckles depending on gene expression. Alr1 was tagged C- and N-terminally with Gfp and localization of the fusion proteins was examined microscopically in three independent replicates in comparison to SG200 WT and *alr1Δ*. Depicted are representative images of sporidia in the DIC channel, GFP (upper) with a set pixel scale to remove background fluorescence to show Gfp signal intensity, GFP (lower) with a pixel scale optimized individually for each Gfp-fusion to show localization (in SG200 and the *alr1Δ* the scale is adjusted to the image with the smallest pixel intensity range showing the maximum portion of background fluorescence in the images under these settings), CMAC channel showing the vacuolar dye 7-amino-4-chloromethylcoumarin and a merged image of the CMAC and GFP channels to show co-localization. Both Gfp fusion constructs are in *alr1Δ* background (#1: single insertion; #2: multiple insertion, similar for N- and C-terminal fusion).

B: Both C- and N-terminal Gfp fusion of Mnr2 are weakly expressed and appear to localize to the ER. Images are taken, processed and depicted similar to A. The Gfp-Mnr2 strains (#1: single insertion; #2: multiple insertion) are in *mnr2Δ* background while the Mnr2-Gfp strains (#1 and #2: multiple insertion) are in SG200 background.

C: Lpe10-Gfp localizes to the mitochondria. Lpe10 was tagged C-terminally with Gfp in SG200 background and localization of the fusion protein was examined microscopically in three independent replicates in comparison to SG200. Depicted are representative images of sporidia in the DIC channel, GFP channel with a pixel scale optimized individually for each Gfp-fusion to show localization (in SG200 the scale is adjusted to the image with the smallest pixel intensity range showing the maximum portion of background fluorescence in the images under these settings), TMRE channel showing the mitochondrial dye tetramethylrhodamine and a merged image of the TMRE and GFP channels to show co-localization.

Note: The strains Alr1-Gfp, Mnr2-Gfp and Lpe10-Gfp were generated by Peter Wegjan during his bachelor's thesis (under my supervision). He also performed the microscopy of the images depicted in C.

Native localization of Mnr2 to the ER cannot be excluded at this point, but the weak Gfp signal although the construct is expressed under a strong promoter (P_{otef}) could indicate that the protein is stuck in the ER.

To test, if rapid protein turnover masks plasma membrane localization of Alr1, cells were treated with latrunculin A, an inhibitor of receptor-mediated endocytosis. Unfortunately, no difference on localization of Gfp-Alr1 or Alr1-GFP was observed, while for the positive control Pit1-Gfp accumulation at the plasma membrane was visible (Figure 3-21).

In summary, the predicted localization of Lpe10 to the mitochondria was confirmed. For Mnr2 the results are inconclusive, while Alr1 seems to localize to the vacuolar membrane, which contradicts the expectations based on structural similarity to the yeast plasma membrane transporter. The localization experiments did not allow to identify a plasma membrane transporter. In the next step both, Alr1 and Mnr2 were deleted to test for Mg²⁺ growth phenotypes.

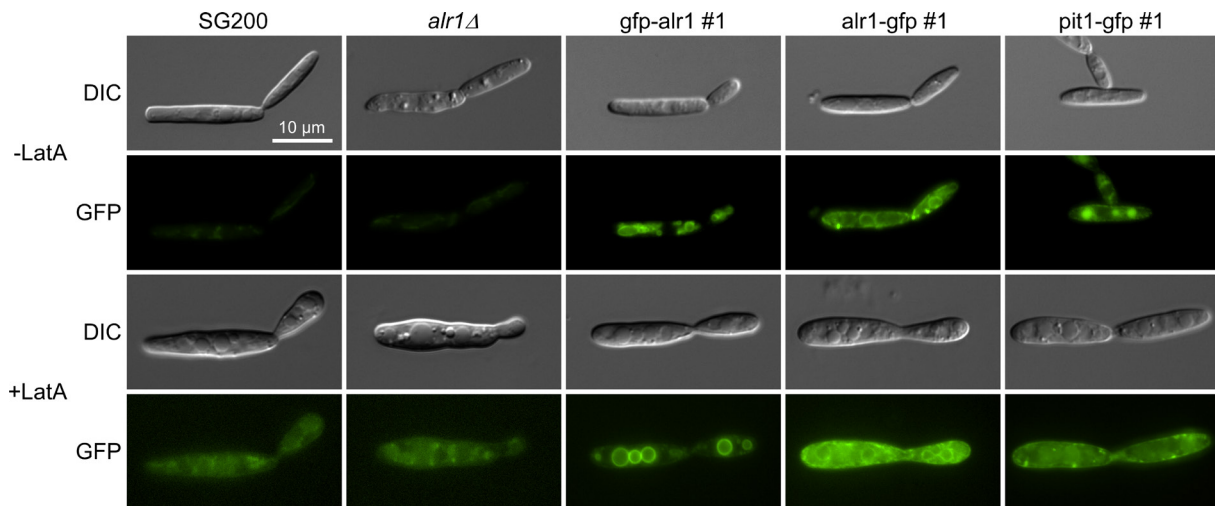


Figure 3-21 Localization of Alr1-Gfp and Gfp-Alr1 does not change after latrunculin A treatment in *U. maydis*. Gfp-Alr1 localizes to the vacuolar membrane, while Alr1-Gfp localizes to the ER also after latrunculin A treatment. The single insertion strains of Alr1, tagged C- and N-terminally with Gfp, as well as SG200, *alr1Δ* and Pit1-Gfp#1 were treated with latrunculin A and localization of the fusion proteins was examined microscopically in two independent replicates. Depicted are representative images of sporidia in the DIC channel and GFP channel with a pixel scale optimized individually for each Gfp-fusion to show localization (in SG200 and the *alr1Δ* the scale is adjusted to the image with the smallest pixel intensity range showing the maximum portion of background fluorescence in the images under these settings. The scale bar equals 10 μm).

3.3.2.5 Deletion of Alr1 and Mnr2 in *U. maydis*

Mg²⁺ dependent growth phenotypes

In *S. cerevisiae* deletion of Alr1p and Mnr2p have clearly distinct phenotypes, fitting to their localization. Upon deletion of *ALR1* *S. cerevisiae* shows a severe Mg²⁺ dependent growth defect (Graschopf *et al.*, 2001). With increasing external Mg²⁺ concentrations growth is restored and reaches WT level in presence of 50 mM MgCl₂ and higher, but also under high Mg²⁺ conditions the intracellular Mg concentrations remains reduced compared to the WT (Graschopf *et al.*, 2001). If Alr1p is overexpressed, *S. cerevisiae* shows increased sensitivity towards other divalent cations like Mn²⁺, Co²⁺, Zn²⁺ or Ni²⁺, which are known low-affinity substrates of Alr1p (Blackwell, Tobin and Avery, 1997; MacDiarmid and Gardner, 1998; Lim *et al.*, 2011). In turn this means increased tolerance towards these ions upon deletion. Deletion of *MNR2* on the other hand, results only in a growth reduction in Mg²⁺ limited conditions below 100 μM , but the internal Mg concentrations are elevated since *S. cerevisiae* cannot access its vacuolar Mg²⁺ storage (Pisat, Pandey and MacDiarmid, 2009). In difference to *ALR1* deletion, upon *MNR2* deletion *S. cerevisiae* shows increased sensitivity towards other divalent cations like Mn²⁺, Co²⁺ or Zn²⁺ which could be

explained by increased Alr1p activity in the *mnr2* mutant (Pisat, Pandey and MacDiarmid, 2009; Lim *et al.*, 2011), similar to the *ALR1* overexpression phenotype.

To test for Mg^{2+} growth phenotypes in *U. maydis* *mnr2* and *alr1* were deleted. In the genome the respective open reading frame of the gene was replaced with a resistance cassette via homologous recombination and correct insertion was confirmed using Southern Blot. To test for Mg^{2+} growth phenotypes *alr1* Δ and *mnr2* Δ strains were dropped on complete medium with increasing Mg^{2+} concentrations. To verify that the N-terminal Gfp fusions of Alr1 and Mnr2 are functional, the fusion constructs were reinserted into the *IP* locus under control of the P_{otef} promoter in the respective deletion strain background (same strains as depicted in chapter 3.3.2.4 Localization of CorA-type Mg^{2+} transporters in *U. maydis*) and included in the Mg^{2+} dependent growth analysis.

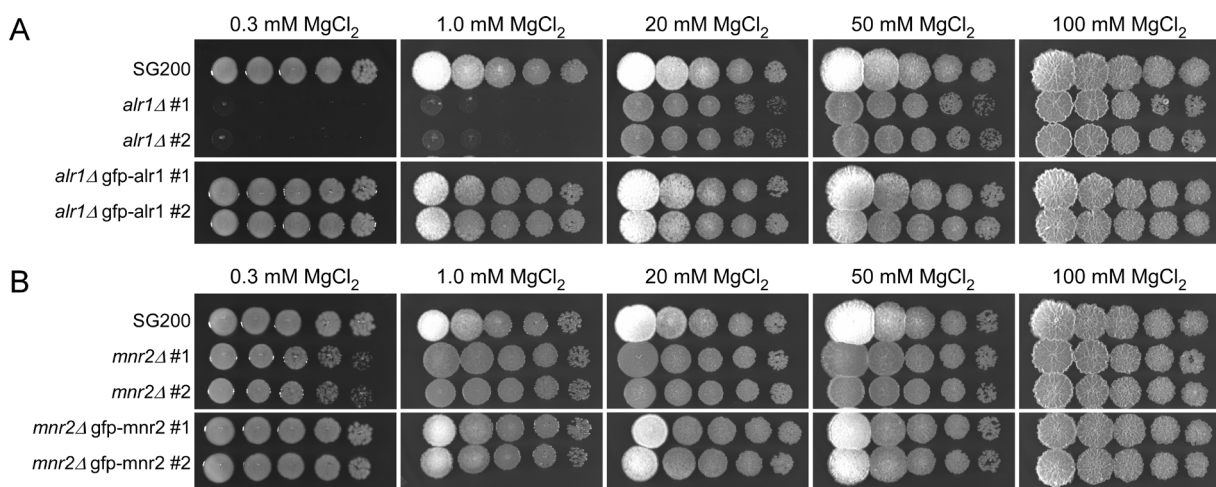


Figure 3-22 Growth of CorA-type Mg^{2+} transporter deletion mutants in presence of different $MgCl_2$ concentrations.

A: *U. maydis alr1* Δ strains show a Mg^{2+} dependent growth phenotype. SG200, *alr1* Δ and egfp-*alr1* complementation strains were grown in serial dilutions on YEPS light complex medium supplemented with $MgCl_2$ in the concentrations indicated above in three independent replicates. *Alr1* Δ does not grow at 0.3 mM and 1 mM $MgCl_2$. Between 20 mM and 100 mM the deletion strains grew like WT, but with a slight reduction in growth rate. Reinsertion of *egfp-alr1* into the deletion strain restored growth to WT at all $MgCl_2$ concentrations.

B: *U. maydis mnr2* Δ strains do not show a Mg^{2+} dependent growth phenotype. SG200, *mnr2* Δ and egfp-*mnr2* complementation strains were grown in serial dilutions on YEPS light complex medium supplemented with $MgCl_2$ in the concentrations indicated above in three independent replicates. *Mnr2* Δ grew like WT at all tested Mg^{2+} concentrations, but with a slight reduction in growth rate at 0.3 mM $MgCl_2$. Reinsertion of *egfp-mnr2* into the deletion strain restored growth speed to WT at 0.3 mM $MgCl_2$.

On medium supplemented with 0.3 mM and 1.0 mM $MgCl_2$ *alr1* Δ strains failed to grow. Between 20 mM and 100 mM $MgCl_2$ WT-like growth was restored, but compared to the WT the strains showed a slight reduction in growth rate indicated by

the smaller colony size (Figure 3-22 A). In contrast *mnr2Δ* only showed a slight reduction in growth at 0.3 mM MgCl₂ recognizable by the smaller colony size compared to the WT, but otherwise grew like WT (Figure 3-22 B). The complementation strains *gfp-alr1* #1 and #2 and *gfp-mnr2* #1 and #2 restored growth on all MgCl₂ concentrations to WT level, which argues for functional fusion proteins (Figure 3-22).

Deletion of *alr1* and *mnr2* in *U. maydis* showed that only *alr1Δ* results in a Mg²⁺ growth phenotype similar to *ALR1* deletion in *S. cerevisiae* (Graschopf *et al.*, 2001). This is in line with the structural similarity to Alr1p but contradicts the localization to the vacuole. For *mnr2Δ* the slight reduction in growth rate shows similarities to *MNR2* deletion in *S. cerevisiae* as there also a reduction in growth speed is reported but only below 100 μM Mg²⁺ (Pisat, Pandey and MacDiarmid, 2009).

Sensitivity towards heavy metals and Co(III)Hex

Besides Mg²⁺ growth phenotypes *ALR1* and *MNR2* deletions also differ in their tolerance towards other cations. Assuming this is similar in *U. maydis*, this knowledge can be utilized to indirectly differentiate between transport across the plasma membrane or the vacuolar membrane. Thus growth of all strains described above was tested on complete medium supplemented with 20 mM MgCl₂ and different heavy metals (MnSO₄, Co(NO₃)₂, ZnSO₄ and NiSO₄).

Comparing the results of the different strains there are several interesting aspects to note:

The *alr1Δ* strains showed increased sensitivity towards Mn²⁺, that was restored to WT-level if Gfp-Alr1 is overexpressed (Figure 3-23 A). In contrast, the *mnr2Δ* did not show increased sensitivity towards Mn²⁺ (Figure 3-23 B).

In presence of Co²⁺ Gfp-Alr1 overexpression strains showed increased sensitivity, while the *alr1Δ* grew like WT (Figure 3-23 A). Similarly, also the *gfp-mnr2* #2 overexpression strain (multiple insertion) showed increased sensitivity, while the deletion strain was unaffected (Figure 3-23 B).

In presence of Zn²⁺ or Ni²⁺ all strains grew WT-like.

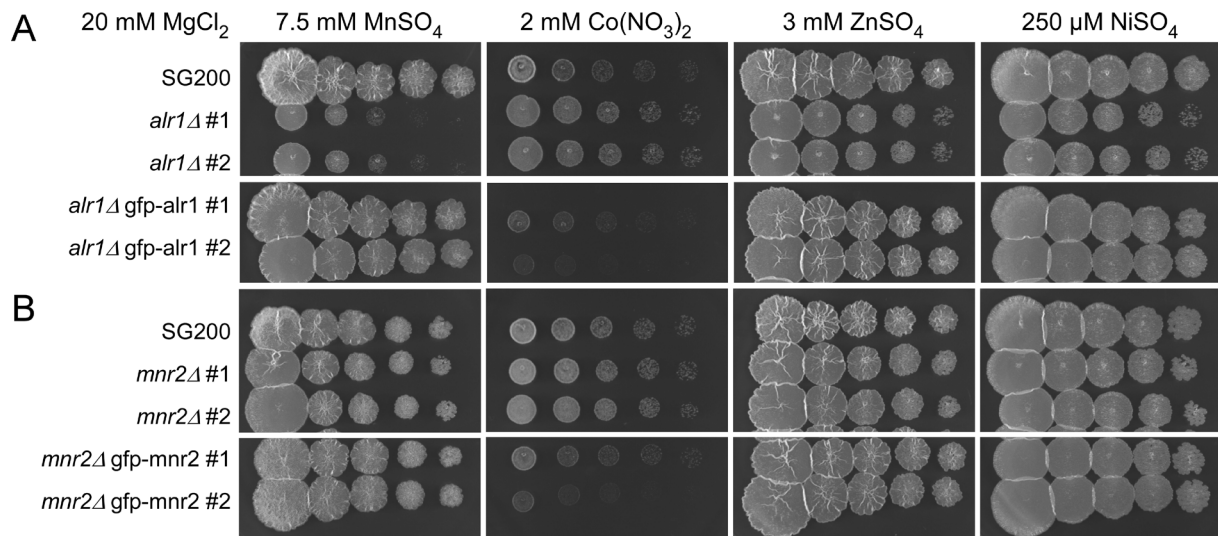


Figure 3-23 Growth of CorA-type Mg^{2+} transporter deletion mutants and complementation strains in presence of heavy metals.

A: *U. maydis alr1* deletion strains show increased sensitivity towards manganese, while *alr1Δ gfp-alr1* overexpression strains show increased sensitivity towards cobalt. SG200, *alr1Δ* and *egfp-alr1* complementation strains were grown in serial dilutions on YEPS light complex medium supplemented with 20 mM $MgCl_2$ and $MnSO_4$, $Co(NO_3)_2$, $ZnSO_4$ and $NiSO_4$ in the indicated concentrations in four independent replicates except for the Gfp-Alr1 complementation strains that were included only once. *Alr1Δ* showed reduced growth in the presence of 7.5 mM $MnSO_4$, while the Gfp-Alr1 complementation strains show strong growth reduction in the presence of 2 mM Co. This effect seems stronger in the multiple insertion strain Gfp-Alr1 #2 compared to single insertion strain #1. $ZnSO_4$ and $NiSO_4$ did not impact growth of the strains in the tested concentrations.

B: *U. maydis mnr2Δ gfp-mnr2* overexpression strains show increased sensitivity towards cobalt. SG200, *mnr2Δ* and *egfp-mnr2* complementation strains were grown in serial dilutions on YEPS light complex medium supplemented with 20 mM $MgCl_2$ and $MnSO_4$, $Co(NO_3)_2$, $ZnSO_4$ and $NiSO_4$ in the indicated concentrations in four independent replicates except for the Gfp-Mnr2 complementation strains that were included only once. *Mnr2Δ* grew like WT, while the Gfp-Mnr2 complementation strains showed growth reduction in the presence of 2 mM Co. This effect seems stronger in the multiple insertion strain Gfp-Mnr2 #2 compared to single insertion strain #1. $MnSO_4$, $ZnSO_4$ and $NiSO_4$ did not impact growth of the strains in the tested concentrations.

Note: For growth of the strains at 20 mM $MgCl_2$ alone see Figure 3-22 (images are from the same experiment).

Again these results do not match the expectations for only either plasma membrane or vacuolar localization. Assuming that the CorA-type Mg^{2+} transporter-regulated Mg^{2+} homeostasis is similar in *U. maydis* and *S. cerevisiae*, the increased manganese sensitivity of the *alr1Δ* strains was expected for vacuolar localization (Pisat, Pandey and MacDiarmid, 2009). In contrast, the increased sensitivity towards cobalt of both the *gfp-alr1* and *gfp-mnr2* overexpression strains argues for plasma membrane localization (MacDiarmid and Gardner, 1998).

As an additional attempt to distinguish between plasma membrane and vacuolar localization of the *U. maydis* CorA-type Mg^{2+} transporters, all strains were dropped in serial dilutions on complete medium supplemented with 20 mM $MgCl_2$ to support

growth of the *alr1Δ* strains and either 300 μM or 400 μM Co(III)Hex, since these concentrations were successfully applied in the hemibiotrophic ascomycete *Magnaporthe oryzae* (Reza *et al.*, 2016). Cobalt(III)hexaammine (Co(III)Hex) can be used as a selective inhibitor of CorA-type Mg^{2+} transporters since the size of the molecule is similar to the hydration shell of Mg^{2+} (Kucharski, Lubbe and Maguire, 2000). Co(III)Hex outcompetes hydrated Mg^{2+} and binds to the channel pore, blocking it (Lerche *et al.*, 2017). Since it appears not to be taken up into the cell (Kucharski, Lubbe and Maguire, 2000), it can be used to specifically inhibit plasma membrane CorA-type Mg^{2+} transporters.

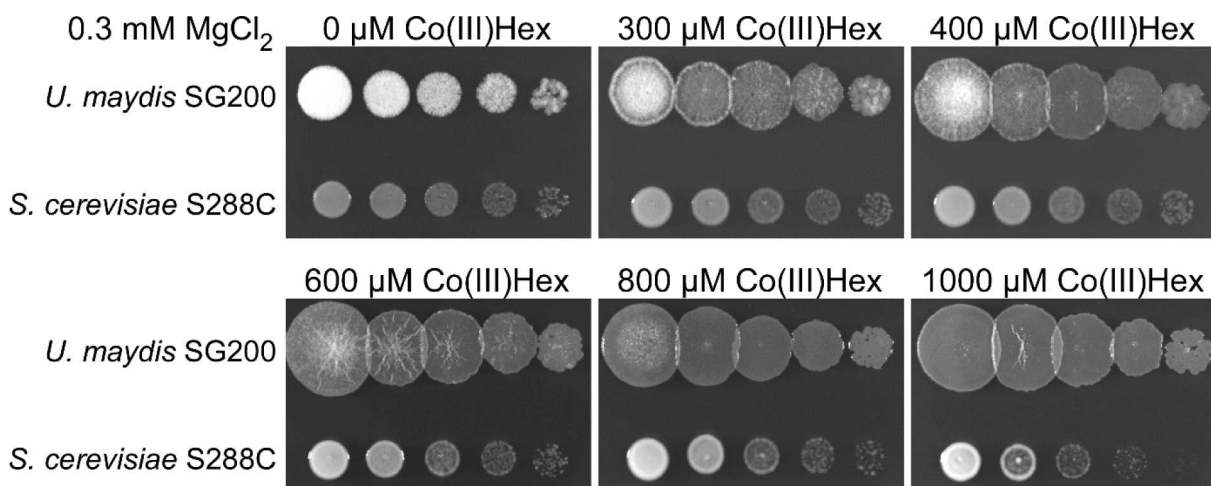


Figure 3-24 Growth of *U. maydis* SG200 is not affected by the CorA-type Mg^{2+} transporter inhibitor Co(III)Hex in the tested concentrations. *U. maydis* SG200 and *S. cerevisiae* S288C were grown in serial dilutions on YEPS light complex medium supplemented with hexaammin-cobalt(III)-chloride (Co(III)Hex) in the indicated concentrations. While *S. cerevisiae* showed a slight growth defect at 1000 μM Co(III)Hex, no effect was observed for SG200.

Unexpectedly, none of the strains showed a growth response to the inhibitor (Supplementary Figure 7-7). In case 20 mM MgCl_2 outcompete Co(III)Hex, *U. maydis* SG200 and *S. cerevisiae* S288C were grown on complete medium without additional Mg^{2+} supplementation with increasing Co(III)Hex concentrations. An inhibitory effect that was shown for *S. cerevisiae* liquid culture already at 100 μM Co(III)Hex could not be confirmed (Lim *et al.*, 2011). Instead, *S. cerevisiae* showed a slight growth defect at 1000 μM Co(III)Hex (Figure 3-24). In comparison, *U. maydis* was not inhibited at any tested concentration (Figure 3-24). Testing of higher Co(III)Hex concentrations was not possible due to incompatibilities with medium preparation. In summary, the results argue either for a higher resistance of *U. maydis* towards Co(III)Hex in comparison to *S. cerevisiae* or for the presence of an additional CorA-type Mg^{2+} transporter independent Mg^{2+} uptake system.

The element composition of *alr1Δ* and *mnr2Δ*

In a final attempt to clarify plasma membrane and vacuolar localization of Mnr2 and Alr1 the element composition of the deletion strains was analysed using Inductively Coupled Plasma- Mass Spectrometry (ICP-MS). If the plasma membrane transporter is deleted, a decrease of the intracellular Mg concentration can be expected (Graschopf *et al.*, 2001), while an increase is reported for deletion of the vacuolar exporter (Pisat, Pandey and MacDiarmid, 2009). The dataset revealed that both *alr1Δ* and *mnr2Δ* caused a 75 % reduction of the cellular Mg content on average in comparison to the WT, if the cells were pre-grown in complete medium supplemented with 50 mM MgCl₂ and subsequently shifted to medium without additional MgCl₂ supplementation for 8 h (Figure 3-25 A). Growth of the strains for 8 h in medium supplemented with 50 mM MgCl₂ resulted in an overall increase of the Mg concentration (20 % in WT) in all strains, but Mg concentration in the deletion strains was still 40-50 % lower than in the WT (Figure 3-25 A). Altering the element composition of a cell either through element depletion or extracellular excess can affect the uptake of other ions (Graschopf *et al.*, 2001). In the case of *mnr2Δ* and *alr1Δ*, depletion of Mg caused a strong increase of the intracellular Ca and Mn concentrations (*alr1Δ*: Ca ~250 %, Mn ~300 %; *mnr2Δ*: Ca ~100 % Mn ~200 %) under standard growth conditions (Figure 3-25 B). This effect seems less severe in *mnr2Δ* than *alr1Δ*. In the presence of 50 mM external Mg²⁺ the Ca content of the cells dropped below the detection limit in all strains, while all other elements were not significantly affected (Figure 3-25 B).

In summary the results of the deletion strains are still contradictory. Some aspects support vacuolar localization of Alr1, while others strongly support plasma membrane localization. The results for Mnr2 on the other hand support plasma membrane localization while the key characteristic, the Mg²⁺ dependent growth defect, of the mutant is missing. Interestingly, some striking similarities between Alr1 and Mnr2 were observed although the proteins are obviously not redundant.

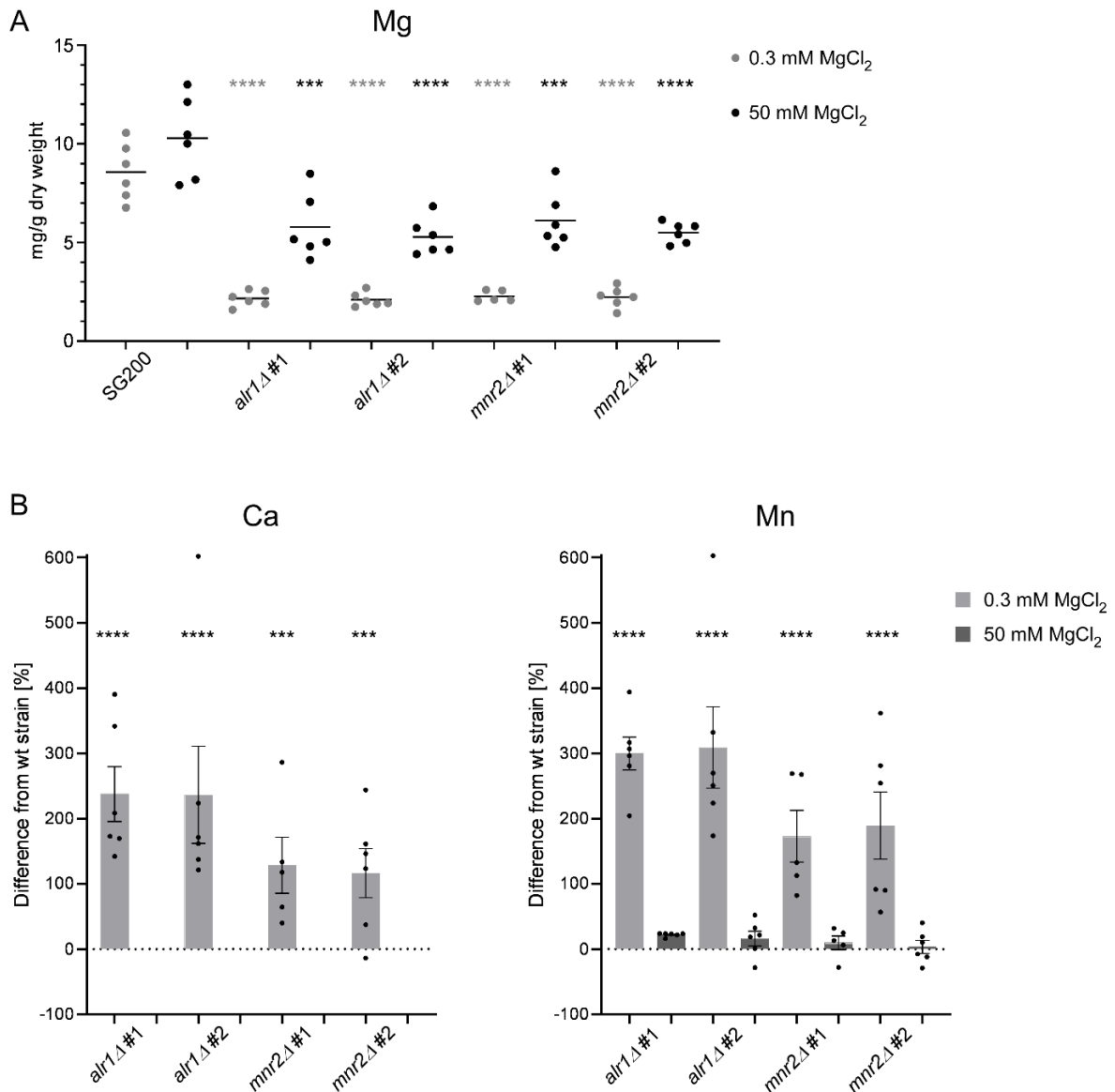


Figure 3-25 Analysis of the element composition of Mg²⁺ transporter deletion strains in *U. maydis*.

A: Cellular Mg content is 75 % reduced in *alr1Δ* and *mnr2Δ* under standard growth conditions (0.3 mM MgCl₂). SG200, *alr1Δ* and *mnr2Δ* strains were pregrown in YEPS light supplemented with 50 mM MgCl₂ and subsequently shifted to standard YEPS light complex medium for 8 h. The element composition of the cells was analysed using ICP-MS. The deletion strains *alr1Δ* and *mnr2Δ* showed a significant 75 % reduction of the intracellular Mg concentration in comparison to the WT SG200 (multiple unpaired t test comparisons calculated with Prism8 software). Graphs for the other evaluated elements can be found in Supplementary Figure 7-8 and Figure 7-9.

Under high Mg²⁺ growth conditions (50 mM MgCl₂) the reduction of the intracellular Mg concentration in *alr1Δ* and *mnr2Δ* is partially complemented. SG200, *alr1Δ* and *mnr2Δ* strains were pregrown in YEPS light supplemented with 50 mM MgCl₂ and subsequently shifted to standard YEPS light complex medium for 8 h. All strains show elevated Mg concentrations in comparison to growth in 0.3 mM MgCl₂. *Alr1Δ* and *mnr2Δ* show compared to WT only 40-50 % reduction of the cellular Mg²⁺ concentration. Graphs for the other evaluated elements can be found in Supplementary Figure 7-8 and Figure 7-9.

B: Mg²⁺ deficiency results in accumulation of Ca and Mn in the cell. The divergence of the Ca and Mn composition from the WT is plotted for *alr1Δ* and *mnr2Δ* deletion strains, grown under standard and high Mg²⁺ conditions (0.3 mM + 50 mM MgCl₂). The whole dataset with all analysed elements can be found in Supplementary Figure 7-10. Mg²⁺ deficiency in either *alr1Δ* or *mnr2Δ* results in strong accumulation of Ca and Mn in the cells. The effect is similar in *alr1Δ* and *mnr2Δ*, but appears more pronounced in *alr1Δ* (multiple unpaired t test comparisons calculated with Prism8 software). This effect was not detected under high Mg²⁺ conditions. To the contrary high Mg²⁺ reduced Ca concentration below the detection limit of the ICP data set.

3.3.2.6 Can Pit1 complement a Mg²⁺ dependent growth defect in *U. maydis*?

Although the plasma membrane Mg²⁺ transporter was not yet clearly identified, *alr1Δ* showed a Mg²⁺ growth phenotype typical for deletion of the plasma membrane Mg²⁺ uptake system. Thus I tested if Pit1 is able to complement the phenotype. To this end *alr1* was deleted in the *pit1Δ* strain background and subsequently a *pit1-gfp* construct constitutively expressed under the P_{otef} promoter was inserted into the *IP* locus of the *alr1Δ pit1Δ* deletion strain.

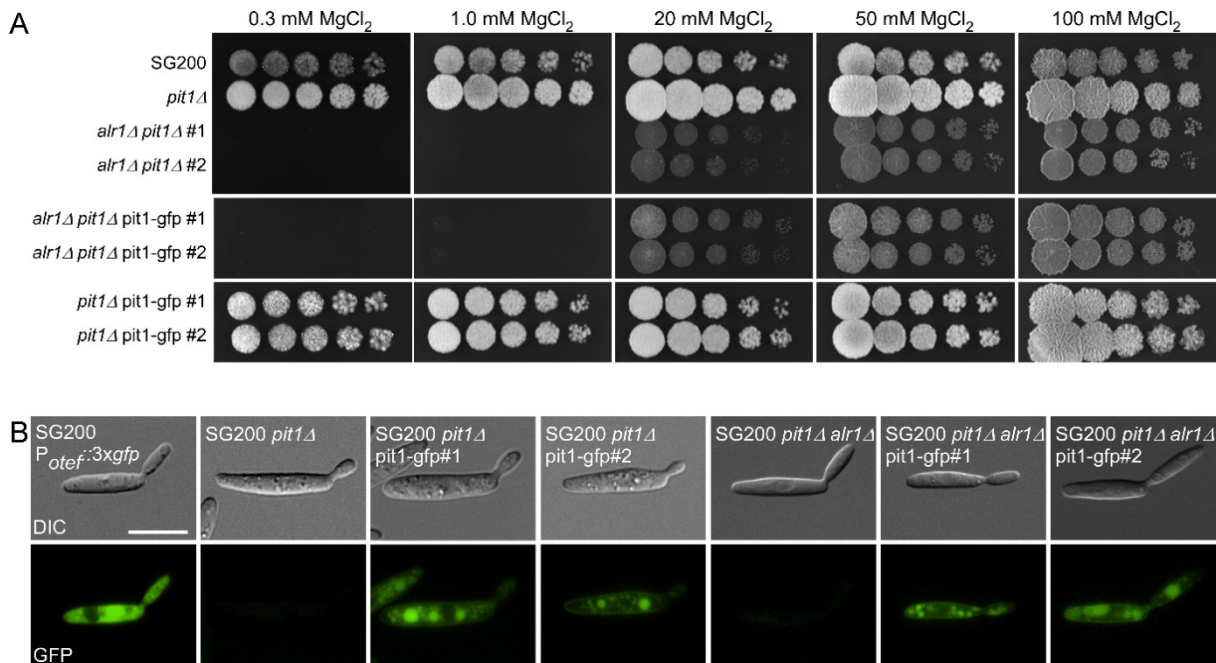


Figure 3-26 Pit1-Gfp is not able to complement the Mg²⁺ dependent growth defect of *alr1Δ*.

A: *U. maydis alr1Δ pit1Δ* double knockout strains show a Mg²⁺ dependent growth phenotype identical to *alr1Δ*. SG200, *pit1Δ*, *alr1Δ pit1Δ*, *pit1-gfp* over expression strains and *alr1Δ pit1Δ pit1-gfp* complementation strains were grown in serial dilutions on YEPS light complex medium supplemented with MgCl₂ in the concentrations indicated above in two independent replicates (on different medium, but with identical results). *Alr1Δ pit1Δ* as well does not grow at 0.3 mM and 1 mM MgCl₂. Between 20 mM and 100 mM the deletion strains grew like WT, but with a slight reduction in growth rate. Insertion of *pit1-gfp* into the double knockout strain (#1: single insertion, #2: multiple insertion) was not able to restore growth.

B: *U. maydis* Pit1-Gfp is expressed and localizes to the plasma membrane in *alr1Δ pit1Δ* background. *UmPit1-Gfp* accumulates in vesicular structures and at the plasma membrane in the *alr1Δ pit1Δ* double knockout background similar to the Pit1-Gfp overexpression strain. The scale bar equals 10 μm. Microscopy was performed once. The images of SG200, *pit1Δ* and Pit1-Gfp #1 and #2 were not generated in this experiment but taken from Figure 3-12 and are depicted for better comparison. Signal intensities of the GFP channel are optimized for each image to show localization. The scale range of the respective deletion strain is adjusted to the smallest range of the Pit1-Gfp strain from the corresponding experiment.

Contradictory to the hypothesis of a Mg²⁺ transport function, drop plates on different Mg²⁺ concentrations showed, that Pit1 is not able to complement the *alr1Δ* phenotype, while microscopic analysis confirmed expression and localization to the plasma membrane and vesicular structures of Pit1-Gfp (Figure 3-26 A and B). Due to

the contradicting results of the Alr1 localization and the Mg^{2+} phenotype of the *alr1* deletion it is actually not possible to exclude that Pit1 is nonetheless a Mg^{2+} transporter. Until Mg^{2+} uptake across the plasma membrane is not fully understood it will not be possible to test this hypothesis in *U. maydis*.

To find indications for a transport activity of Pit1 the strains from above were also grown in the presence of heavy metals. Interestingly, Pit1-Gfp overexpression in the *alr1Δ pit1Δ* background was able to slightly improve Mn^{2+} tolerance compared to the double knockout (Figure 3-27). In the presence of Co^{2+} , the Pit1-Gfp overexpression strain (multiple insertion strain #2) showed reduced growth in the *pit1Δ* background, but not in the *pit1Δ alr1Δ* double knockout (Figure 3-27).

In presence of Zn^{2+} or Ni^{2+} it can be noted, that Pit1-Gfp overexpression in the *pit1Δ alr1Δ* background slightly increased the growth rate compared to the *pit1Δ alr1Δ* double knockout (Figure 3-27). In comparison no difference in growth between the strains was observed at 20 mM $MgCl_2$ alone (compare Figure 3-26).

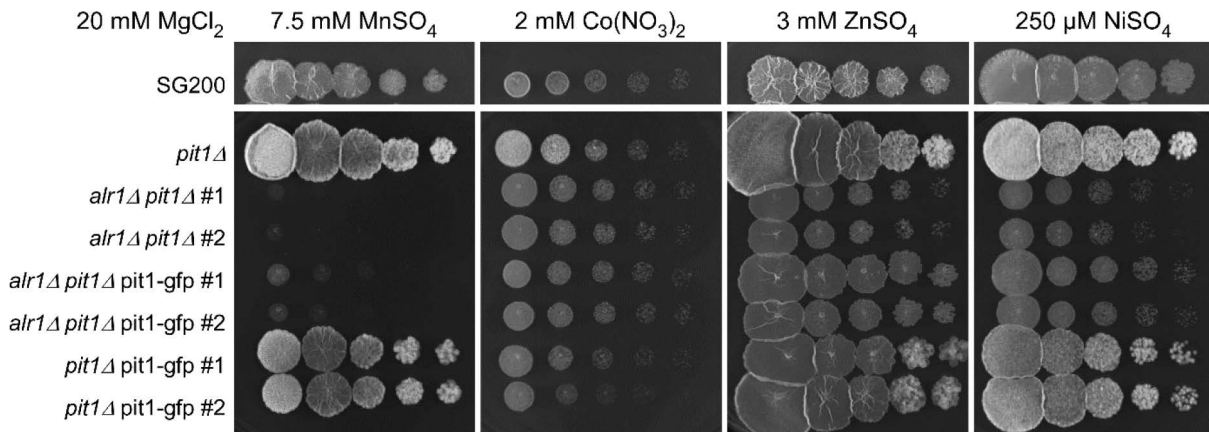


Figure 3-27 Growth of *alr1* Mg^{2+} transporter deletion mutants and *pit1* complementation strains in presence of heavy metals.

U. maydis alr1Δ pit1Δ pit1-egfp complementation strains show slightly improve growth in presence of heavy metals in comparison to the double knockout. *Pit1Δ*, *alr1Δ pit1Δ*, *pit1-egfp* over expression strains and *alr1Δ pit1Δ pit1-egfp* complementation strains were grown in serial dilutions on YEPS light complex medium supplemented with 20 mM $MgCl_2$ and $MnSO_4$, $Co(NO_3)_2$, $ZnSO_4$ and $NiSO_4$ in the indicated concentrations in a single replicate except for *pit1Δ pit1-egfp #2* which was tested in three replicates. The *alr1Δ pit1Δ pit1-egfp* complementation strains slightly improved growth in comparison to the double knockout in the presence of and $MnSO_4$, $ZnSO_4$ and $NiSO_4$. No difference was observed for $Co(NO_3)_2$. Interestingly, the multiple insertion *pit1-egfp #2* over expression strain showed a slight growth reduction in the presence of $Co(NO_3)_2$ in comparison to the other strains.

Note: For growth of the strains at 20 mM $MgCl_2$ alone see Figure 3-26 (images are from the same experiment). The data of the control strain SG200 is from the same dataset as Figure 3-23.

To test if the Pit1-Gfp overexpression has an impact on the intracellular element

composition, which could indicate transport activity, the *pit1Δ* *pit1-gfp* over expression strains were included in the Inductively Coupled Plasma- Mass Spectrometry (ICP-MS) analysis. But the Pit1-Gfp overexpression strains did not differ significantly from the WT for any of the tested elements (Supplementary Figure 7-8 and Figure 7-9). Interestingly there was a slight not significant increase of Mn and Fe in the *pit1-gfp* overexpression strain that seemed to be dependent on the expression level, since this trend was observed in the multiple insertion strain but not in the single insertion strain.

In summary, Pit1 was not able to complement the Mg^{2+} dependent growth defect caused by *alr1Δ* in *U. maydis*, but due to the contradicting localization of Alr1 to the vacuole this currently not possible reject the hypothesis of Pit1 functioning as a transporter. On the other hand, the slight growth improvement of the Pit1-Gfp overexpression strains in the *pit1Δ alr1Δ* background in comparison to the double knockout in the presence of Mn^{2+} , Zn^{2+} and Ni^{2+} was well as the increased sensitivity of the Pit1-Gfp overexpression strain in the *pit1Δ* background towards Co^{2+} might indicate minor transport activity of divalent cations, which is typical for transporters like Alr1 (Lim *et al.*, 2011).

3.3.2.7 The role of Mg^{2+} transporters for virulence in *U. maydis*

A connection between Mg^{2+} homeostasis of *U. maydis* and the host plant with regard to virulence was suggested earlier. In the next step, the virulence of Mg^{2+} transporter mutants was tested in maize infections. Magnesium is one of the essential macro nutrients for both, plant and fungus (Tang *et al.*, 2022). During infection, alteration of the Mg^{2+} homeostasis of the host or the pathogen thus can have tremendous effects on plant susceptibility or fungal virulence respectively. To get a better understanding of this relationship, Mg^{2+} transporter mutants, which affect the fungal Mg^{2+} homeostasis, were tested in *Zea mays* Golden Bantam infections. The plasma membrane Mg^{2+} uptake system would have the biggest impact on the fungal Mg^{2+} homeostasis, but since this was not clearly identified both *alr1Δ* and *mnr2Δ* were analysed. Additionally, *mgtEΔ* and *lpe10Δ* strains were generated and included in the analysis. Maize infection with *alr1Δ* strains resulted in a complete loss of virulence. The strains *alr1Δ* #1 and #2 induced predominantly chlorosis and appeared clearly less virulent than the already strongly impaired *pit1Δ* strain

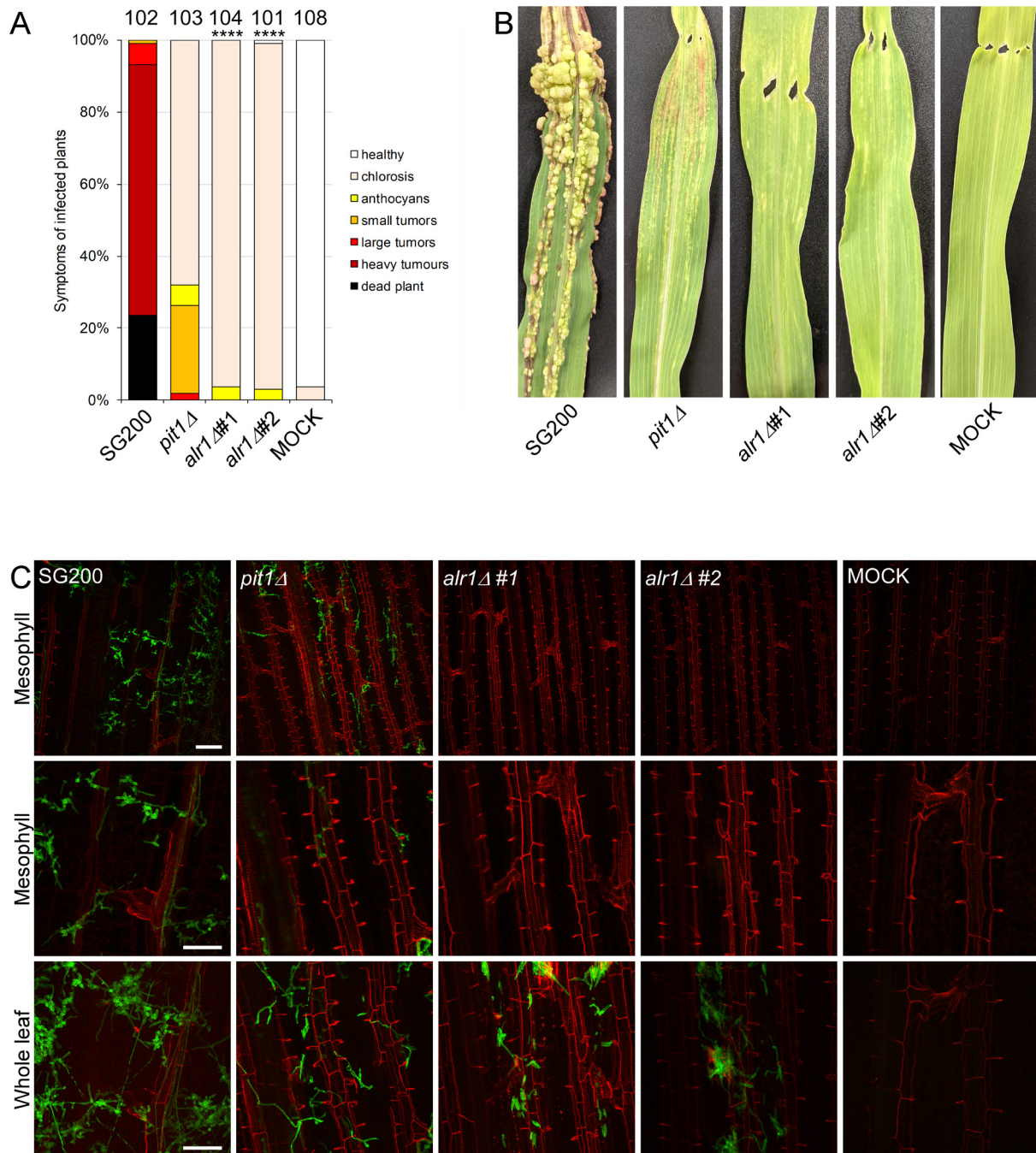


Figure 3-28 *U. maydis alr1Δ* mutant completely lost virulence in *Zea mays* Golden Bantam infection.

A: Disease rating of four independent infections of *Zea mays* Golden Bantam plants 12 dpi with the *U. maydis* strains indicated below. Plants infected with SG200 show chlorosis, anthocyanin formation and tumour formation. In comparison to *pit1Δ* disease symptoms are even weaker in both *alr1Δ* strains. Thus *alr1Δ* differs significantly from both SG200 and *pit1Δ* (Mann-Whitney U test).

B: Representative images of maize leaves harvested at 12 dpi with the *U. maydis* strains indicated below. Plants infected with SG200 shows chlorosis, anthocyanin formation and tumour formation while the strains *pit1Δ* and *alr1Δ* show mostly chlorosis.

C: Confocal images of *U. maydis* infected maize leaves 5 dpi. SG200 colonized the whole leaf section at 5 dpi. In comparison *pit1Δ* shows strongly limited growth in the mesophyll layers and appeared mostly restricted to the vasculature tissue, while for *alr1Δ* no hyphae were found in planta (mesophyll projections) but instead sporidia were detected on the leaf surface (Whole leaf projections). The scale bar equals 100 μ m (upper row) or 50 μ m (middle and lower row). Microscopy was performed three times. Plant tissue was stained with WGA (fungus, green) and PI (plant, red).

(Figure 3-28 A and B). Microscopy of the plant tissue below the injection side at five dpi showed, that the loss of virulence in *alr1Δ* was caused by failure to induce filamentous growth (Figure 3-28 C). While SG200 completely colonized the maize leaf tissue, *pit1Δ* was mostly restricted to vasculature tissue, but for *alr1Δ* no hyphae were found inside the leaf (Figure 3-28 C Mesophyll projections). Instead, mostly sporidia were found on the leaf surface (Figure 3-28 C whole leaf projections).

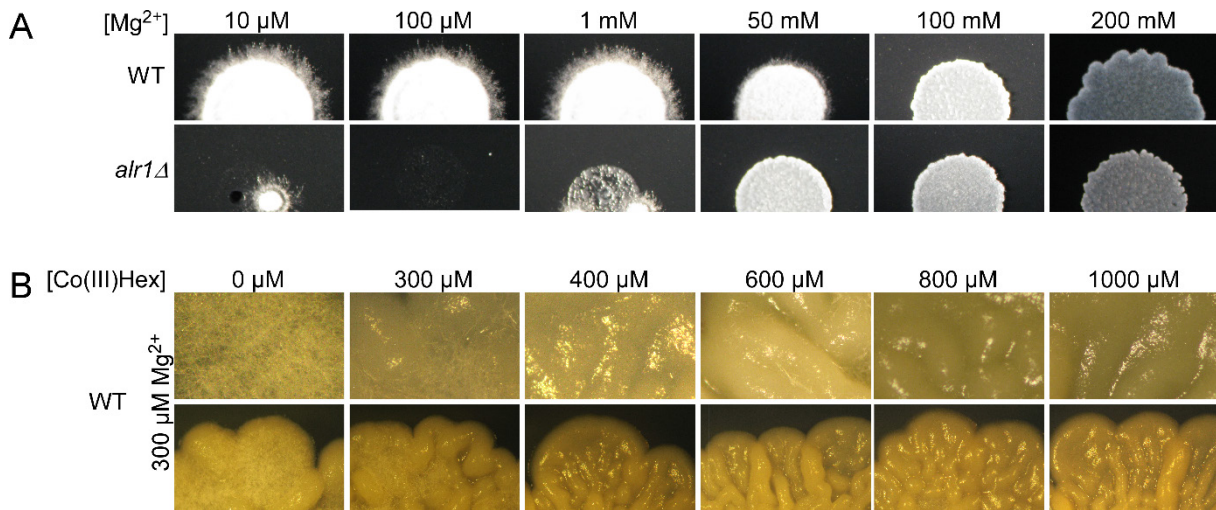


Figure 3-29 *U. maydis alr1Δ* does not grow filamentously on charcoal containing medium.

A: *U. maydis* WT and *alr1Δ* #1 strains were grown in serial dilutions on SD medium supplemented with the indicated Mg^{2+} concentration and 1 % charcoal to induce filamentous growth. The experiment was performed once. While *alr1Δ* did not grow filamentously at all, the WT showed a decrease in filamentous growth with increasing Mg^{2+} concentration.

B: *U. maydis* was grown in serial dilutions on YEPS light complex medium supplemented with hexaamminocobalt(III)-chloride (Co(III)Hex) in the indicated concentrations. The lower images depict the colony morphology of *U. maydis* in dependence of the Co(III)Hex concentration. The upper images show a section of the respective images below in higher magnification to show filament formation of the colony. Similar to increasing Mg^{2+} concentrations, a decrease in filamentous growth was observed with increasing Co(III)Hex concentrations.

To confirm loss of filament induction, *alr1Δ* was grown on filament inducing charcoal medium supplemented with different Mg^{2+} concentrations.

Indeed, *alr1Δ* did not grow filamentously independent of the Mg^{2+} concentration (Figure 3-29 A). In comparison, the WT showed typical filamentous growth (fuzzy white colony morphology) at 10 μ M -1 mM $MgCl_2$. Interestingly, at 50 mM $MgCl_2$ filamentous growth was reduced and abolished at 100 - 200 mM $MgCl_2$ (Figure 3-29 A). Fitting to this observation, increasing concentrations of the CorA-type Mg^{2+} transporter inhibitor Co(III)Hex also correlated with a decrease in filamentous growth in SG200 (Figure 3-29 B).

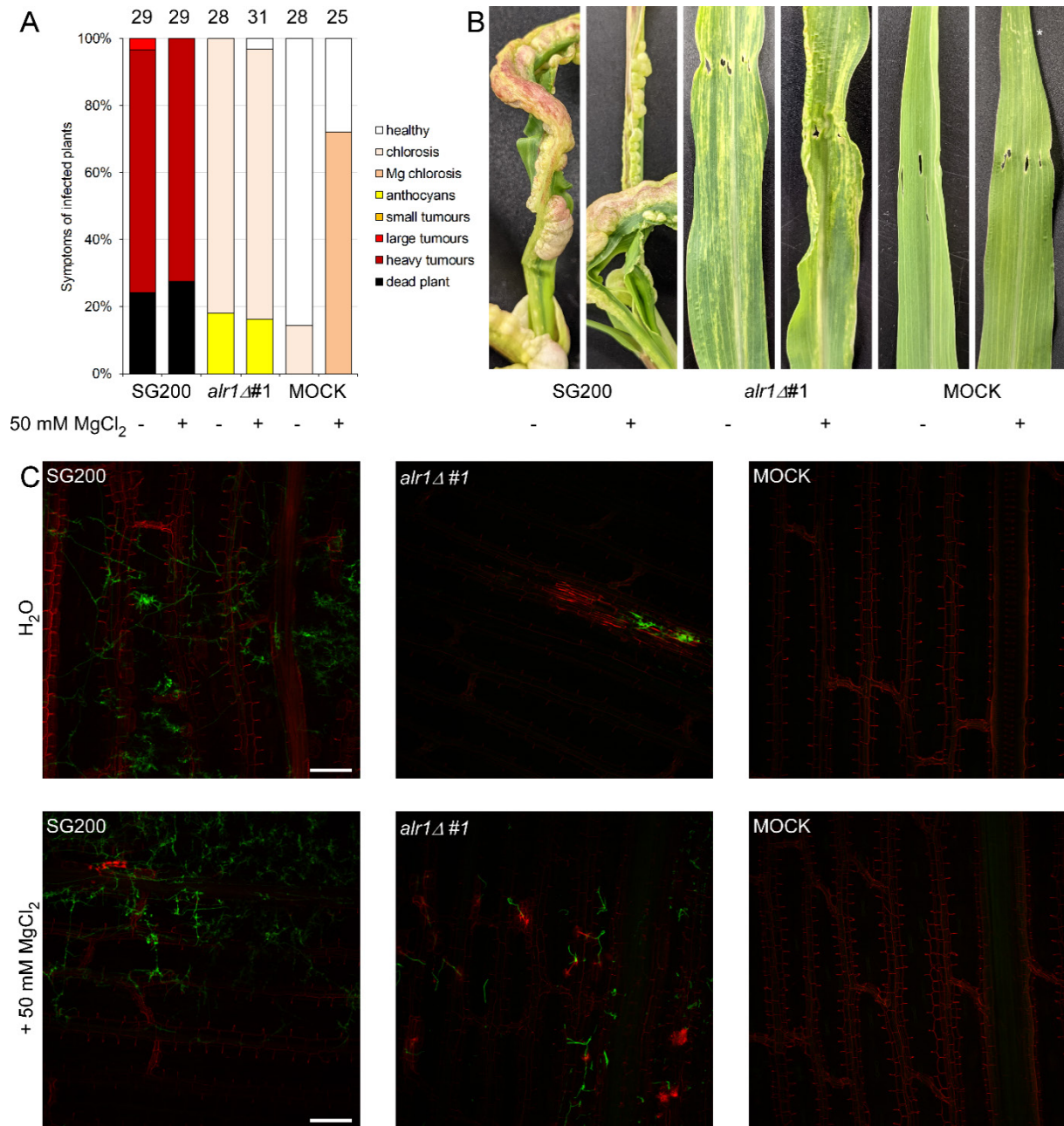


Figure 3-30 *U. maydis* *alr1Δ* mutant loss of virulence cannot be complemented by initial Mg²⁺ application during *Zea mays* Golden Bantam infection.

A: Disease rating of one infections of *Zea mays* Golden Bantam plants 12 dpi with the *U. maydis* strains indicated below. The strains were either resuspended in water or 50 mM MgCl₂ for injection into the plant. The injection of 50 mM MgCl₂ caused chlorosis above the injection site (marked with * in B), clearly distinct from chlorosis caused by *U. maydis* infection. Besides, no differences in disease symptoms between water and MgCl₂ injected strains were observed. Plants infected with SG200 showed chlorosis, anthocyanin formation and tumour formation, while *alr1Δ* remained avirulent.

B: Representative images of maize leaves harvested at 12 dpi with the *U. maydis* strains indicated below. Plants infected with SG200 showed chlorosis, anthocyanin formation and tumour formation while the *alr1Δ* showed mostly chlorosis. Chlorosis induced by MgCl₂ infection is indicated with (*).

C: Confocal images of *U. maydis* infected maize leaves 5 dpi. SG200 colonized the whole leaf section at 5 dpi. In comparison, no *alr1Δ* hyphae were found *in planta* but instead sporidia were detected on the leaf surface (Whole leaf projections). Injection of the strains resuspended in 50 mM MgCl₂ made no difference. The scale bar equals 100 μm. Microscopy was performed once. Plant tissue was stained with WGA (fungus, green) and PI (plant, red).

To test, if the loss of filament induction on the plant surface can at least be partially complemented, *U. maydis* strains were resuspended in 50 mM MgCl₂ solution for injection into the maize plants to ensure increased Mg²⁺ availability during the early infection phase. A pilot study with SG200 and *alr1Δ* #1 showed that resuspension of the cells in 50 mM MgCl₂ does not alter virulence of *alr1Δ* (Figure 3-30 A and B). Instead, microscopy of the leaves showed no difference compared to standard infection conditions (Figure 3-30 C).

In summary, the *alr1Δ* strains are apathogenic due to loss of filament induction on the plant surface. Loss of filament induction can also be artificially induced by high Mg²⁺ concentrations or the Mg²⁺ transporter inhibitor Co(III)Hex. As Mg²⁺ is an essential macronutrient and the deletion of *alr1* causes a severe drop in the intracellular Mg²⁺ concentration, which subsequently causes additional pleiotropic effects, it is impossible to test effects of the *alr1Δ* deletion for virulence.

In difference to *alr1Δ*, the deletion strains of *mnr2*, *mgtE* or *lpe10* were all still virulent (Figure 3-31). While *mgtEΔ* and *mnr2Δ* looked visually indistinguishable from the WT, symptoms in *lpe10Δ* appeared slightly less severe. Quantitatively, both *mnr2Δ* and *lpe10Δ* showed significantly lighter disease symptoms compared to WT, indicating that alterations of the fungal Mg²⁺ homeostasis, as long as they do not cause severe growth defects, lead to reduced fitness that is reflected in slightly reduced virulence.

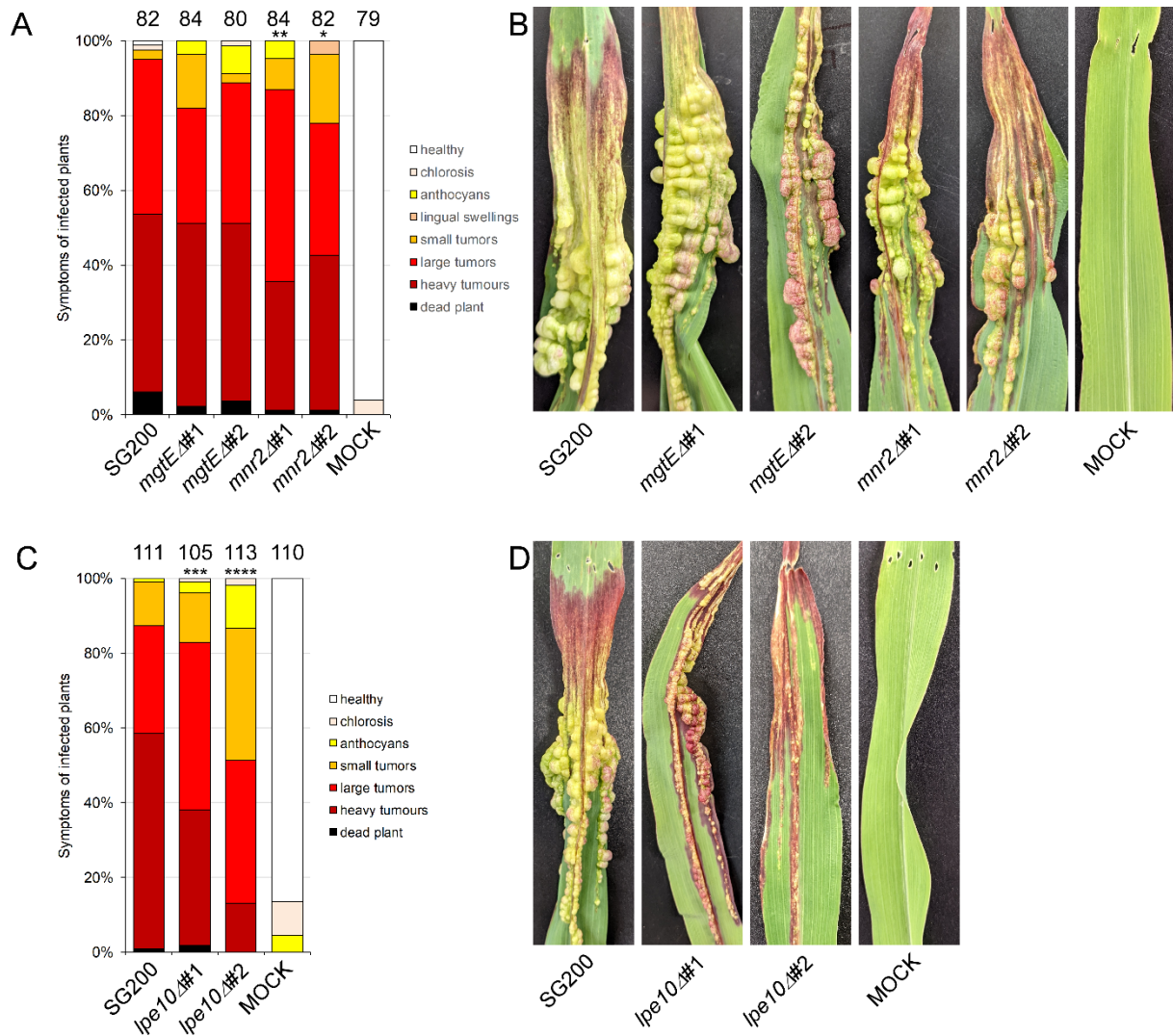


Figure 3-31 Figure Virulence of *U. maydis mnr2*Δ, *mgtE*Δ and *lpe10*Δ mutants was analysed in *Zea mays* Golden Bantam infection.

A: Disease rating of three independent infections of *Zea mays* Golden Bantam plants 12 dpi with the *U. maydis* strains indicated below. *MgtE*Δ showed similar virulence to SG200 while virulence of *mnr2*Δ was significantly reduced compared to SG200, but not to *mgtE*Δ (Mann-Whitney U test).

B: Representative images of maize leaves harvested at 12 dpi with the *U. maydis* strains indicated below. Plants infected with SG200 as well as *mnr2*Δ, *mgtE*Δ showed chlorosis, anthocyanin formation and tumour formation.

C: Disease rating of three independent infections of *Zea mays* Golden Bantam plants 12 dpi with the *U. maydis* strains indicated below. *Lpe10*Δ showed significantly reduced virulence compared to SG200 (Mann-Whitney U test).

D: Representative images of maize leaves harvested at 12 dpi with the *U. maydis* strains indicated below. Plants infected with SG200 as well as *lpe10*Δ, *mgtE*Δ showed chlorosis, anthocyanin formation and tumour formation.

3.3.2.8 The impact of the fungal Mg²⁺ homeostasis on Mg²⁺ distribution in the host plant during infection

To test, if alteration of the fungal Mg²⁺ uptake could also cause differences on Mg²⁺ distribution of the infected plant, infected leaf material from infection with SG200,

mnr2Δ, or *mgtEΔ* deletion was harvested at 12 dpi and analysed using ICP-MS. Since the *alr1Δ* deletion is avirulent it was not included in the analysis.

Initially a pilot study was conducted where all leaves (L2-L5) of an SG200 infected, a water infected (MOCK), and an untreated plant were sampled to test several aspects: First, to test if the injection itself affects the element composition of the leaf. Second, to look at the developmental element distribution in the plant leaves. Third, to confirm published data on the element composition of *U. maydis* infected maize leaves (Horst *et al.*, 2010). And fourth, to obtain first insights into putative systemic effects of the *U. maydis* infection.

At 12 dpi the plants are 20 days old. At this stage they are mostly developing the 6th leaf. Leaf 1 is already dead at this time point and was thus not sampled. L2-3 show leaf yellowing starting from the tip indicating the onset of leaf senescence (Lim, Kim and Nam, 2007). In the MOCK treated plants, leaf yellowing of L2 seemed further progressed than in the untreated plant, while the SG200 infected plants did not show any signs of leaf senescence, not even in L1.

As expected, the injection of the plant did not cause significant differences in the element composition of the leaves, indicated by the high correlation of the element composition in MOCK treated plants if plotted against the untreated sample (Figure 3-32 A).

An overview of the element composition in MOCK treated plants per leaf allowed to show how the amount of an element in a leaf changes with leaf age (Figure 3-32 B). Of the analysed elements, Mg, K, Ca, Mn and Mo increase with leaf age, while P, Zn and Cu decrease. In comparison, Fe remained stable. Overall this is in line with observations made for soybean leaves (Liu *et al.*, 2019).

Next it was analysed how the element composition of SG200 infected plants differs from MOCK treated plants. In my hands SG200 infected plants developed infection symptoms from L3 onwards. Puncture holes from the injection were visible in L3 and L4 but until 12 dpi also the subsequent leaves developed infection symptoms. At this stage L5 is not as far developed in SG200 infected plants than in MOCK treated and untreated plants and was therefore not considered for the comparison of MOCK treatment and SG200 infection (for the whole data set also see Supplementary

Figure 7-11, Figure 7-12 and Figure 7-13). Thus L4 showed the most infection symptoms.

With regard to magnesium, SG200 infected plants showed 68 % (L3) and 53 % (L4) lower Mg concentration than the MOCK treated plant (Figure 3-32 C). In absolute numbers this amount of Mg is similar to the L5 leaf in MOCK plants, indicating the infected leaves maintain the Mg nutritional status of a juvenile leaf (Supplementary Figure 7-11). Considering the high phloem mobility of Mg^{2+} and the increased phloem flow towards the infected tissue, this result was counter intuitive but expected based on the previous study by Horst *et al.* (Horst *et al.*, 2010).

A similar pattern, reduced concentration in infected leaves (L3 and L4) in comparison to MOCK, which resembles the concentration of a juvenile MOCK leaf (L5), was observed for Ca, Mn and Mo ((Figure 3-32 C and Supplementary Figure 7-11 and Figure 7-12). For Ca this was reported before (Horst *et al.*, 2010). Ca^{2+} is known to be almost exclusively transported in the xylem (Marschner, 2012), while Mn^{2+} and Mo^{2+} are considered moderately phloem mobile (Kadereit *et al.*, 2014). Since Mn and Mo showed the same developmental distribution pattern in the leaves as Ca it could be argued that in maize under these experimental conditions phloem mobility of Mn^{2+} and Mo^{2+} was low.

In contrast, P, K, Cu and Zn concentrations were elevated in the infected tissue in comparison to the MOCK plant (Figure 3-32 C). For P and K this fits to previous observations (Horst *et al.*, 2010). P and K are highly phloem mobile elements (Marschner, 2012) thus their accumulation can be expected at the infection site due to increased phloem flow towards this tissue. Cu and Zn are also considered moderately phloem mobile (Kadereit *et al.*, 2014). Based on the accumulation in the infected tissue their phloem mobility is probably higher than for Mn and Mo.

Although a reduction of Fe at the infection site was reported before (Horst *et al.*, 2010), no significant difference was found in comparison to the MOCK treatment in this study (Figure 3-32 B). Like Mn and Mo, Cu and Zn and iron is also considered moderately phloem mobile (Kadereit *et al.*, 2014). Since iron remains constant in infected and MOCK treated leaves, the phloem mobility is probably between Cu + Zn and Mo +Mn.

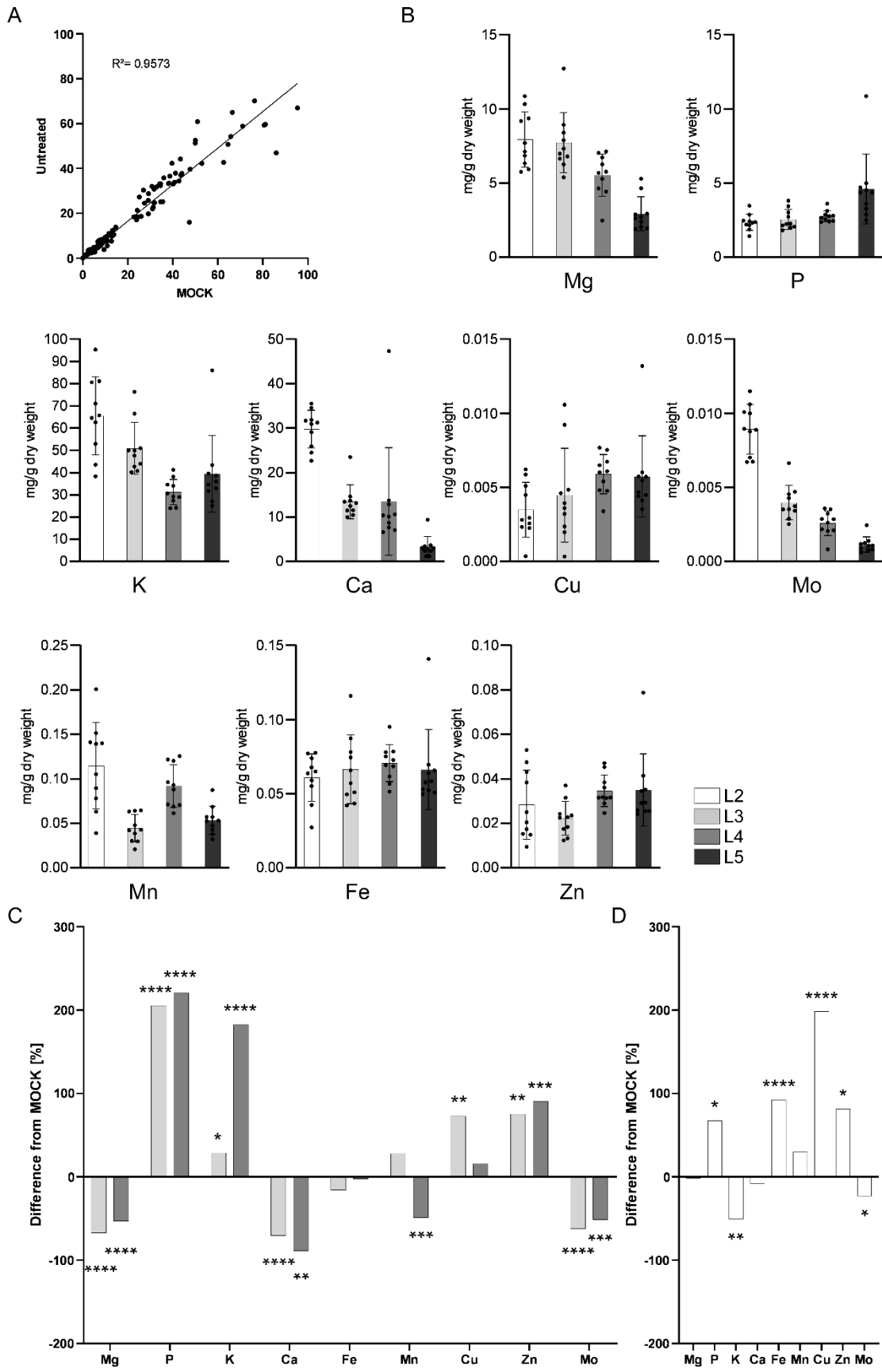


Figure 3-32 Element composition of *Zea mays* Golden Bantam leaves after SG200 infection and MOCK treatment in comparison to untreated plants from one infection experiment.

A: MOCK treatment of maize plants does not significantly alter the plants element composition. Data from all analysed elements of untreated or MOCK treated plants is plotted against each other and shows high correlation.

B: The concentration of the element indicated below in dependence of the leaf number (L2-L5) of MOCK treated maize plants.

C: Differences in element composition in % of SG200 infected L3 and L4 leaves in comparison to MOCK treated leaves. The level of significance is indicated by (*) above or below the respective bar (unpaired t test).

D: Differences in element composition in % of SG200 infected but symptomless L2 leaves in comparison to MOCK treated leaves. The level of significance is indicated by (*) above or below the respective bar (unpaired t test).

Overall the accumulation or depletion of an element at the infection side can be explained with its phloem mobility. In general, nutrients are imported into the plant tissue via xylem and exported and redistributed via phloem with the exception of Ca, and in this dataset maybe also Mn and Mo, which are negligibly phloem mobile. Due to the increased phloem flow towards the infected tissue the accumulation of phloem mobile elements can thus be expected. The only exception here is Mg^{2+} which is 59 % reduced although it is highly phloem mobile. Partially this might be explained by the strongly reduced amount of chlorophyll in the tumour tissue that reduced the total amount of Mg needed.

First insights in potential systemic effects on element composition caused by *U. maydis* infection could be gained from the corresponding dataset of the L2 leaves (Figure 3-32 D). Mg, Ca and Mn do not differ significantly from healthy leaves. In comparison P, Fe, Cu and Zn are strongly increased, while K and Mo are decreased. In the case of P, Cu, Zn and Mo this is similar to the tumour tissue. In contrast, K is decreased in L2 while its increased in the tumour tissue. The main difference between L2 in the MOCK treated and the infected leaf is, that the MOCK leaf is already senescent while the onset of this process is delayed in the infected plant. During senescence there is increased export of nutrients from the leaf and especially the highly phloem mobile elements P, K as well as Zn are remobilized, while Ca, Mg, Mn and Fe accumulate (Marschner, 2012). For the infected L2 leaf it could thus be expected that Mg, Ca, Mn, Fe concentrations are lower while the P, K and Zn concentrations should be higher than in the senescent leaf. But these expectations, were only observed for P and Zn and not for the other elements (Figure 3-32 D),

indicating that the *U. maydis* infection has systemic effects on the element composition.

In the case of magnesium there is more Mg in the infected L2 than expected (Supplementary Figure 7-11). This might be because much less Mg²⁺ is incorporated into chlorophyll in L3-L5 leaving more Mg²⁺ to circulate in the plant. In L2 there is on the other hand increased photosynthetic activity (Horst *et al.*, 2010) which could lead to an accumulation of Mg²⁺ in comparison to L3, L4 and L5 that is by chance as high as the Mg²⁺ accumulation in the senescent MOCK L2 leaf.

In summary the results confirm, that *U. maydis* infections alters the element composition of the leaf in symptomatic tissue but for some elements there are also systemic effects.

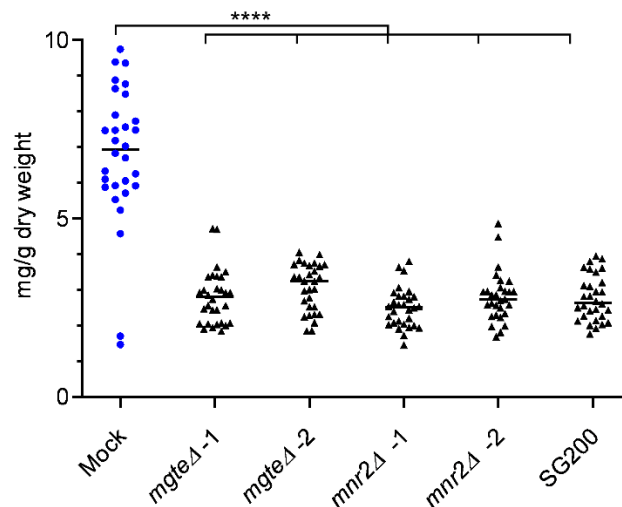


Figure 3-33 The Mg concentration in *Zea mays* Golden Bantam leaves infected with SG200, *mgteΔ* or *mnr2Δ* is significantly reduced in comparison to MOCK treated leaves. Scatter plot of three independent infection experiments with 10 biological replicates per experiment. All strains cause a significant reduction of the Mg content in comparison to the MOCK control, but no difference was observed between the mutant strains and SG200 (unpaired t tests, only the comparison to MOCK treatment is depicted in the figure for clarity). Plots of the other evaluated elements can be found in Supplementary Figure 7-14 and Figure 7-15.

Specifically, in the case of Mg it was tested if the Mg²⁺ household of the fungus contributes to the observed decrease of the Mg content in the tumours by comparing infection with *mnr2/mgtE* deletion strains. Unfortunately, Mg decrease is identical in all strains (Figure 3-33), but also for the other elements no differences between the strains were observed (Supplementary Figure 7-14 and Figure 7-15).

In closing, it was proposed that Pit1 is a magnesium transporter. To support the hypothesis, it was shown that the GLQ motif is indeed important for Pit1 function, but

there is no evidence yet that allows to reject or accept the initial hypothesis. Still, growth in presence of several heavy metals might indicate limited transport activity of Pit1 for divalent cations. To shed light on Mg²⁺ homeostasis in *U. maydis* a repertoire of potential Mg²⁺ transporters was identified. Of these the CorA-type Mg²⁺ transporters were investigated in more detail. Alr1 and Mnr2 both share features typical for plasma membrane localized CorA-type Mg²⁺ transporters, while other findings fit rather to a vacuolar localization. Thus it is not yet clear which transporter(s) *U. maydis* utilizes for Mg²⁺ uptake into the cell. Although deletion of *alr1* or *mnr2* results in a strong decrease of the cellular Mg content, only *alr1*Δ is also avirulent due to loss of filament induction. During *U. maydis* infection it could be confirmed that the infection alters the element composition of the plant locally and systemically. With the applied method, no influence of the tested Mg²⁺ transporter candidates Mnr2 or MgtE on these alterations of the element composition *in planta* could be detected. As an alternative, it would be interesting to include the NIPA-type Mg²⁺ transporter candidates into the analysis in the future.

3.3.3 Discussion

3.3.3.1 Pit1 a Mg²⁺ transporter?

In order to test if Pit1 functions as a magnesium transporter it was shown that the GLQ motif at the end of the seventh transmembrane domain is important for Pit1 function. If replaced with alanine the mutant strain showed strongly reduced virulence in maize infections similar to the *pit1*Δ strain. At the same time live imaging showed that the mutated Pit1 (Pit1_{GLQ3A}-Gfp) accumulates at the fungal plasma membrane *in planta*. Unfortunately, all attempts to confirm this observation were so far unsuccessful, probably due to the unfavourable signal-to-noise ratio of the Gfp signal *in planta* as already discussed in the previous chapter.

Assuming the accumulation of Pit1_{GLQ3A}-Gfp at the plasma membrane is correct, this would support a transport function of Pit1. Ion uptake is often regulated by substrate (ion) availability, for example via transcriptional activation in substrate deficient conditions or via posttranslational degradation under replete conditions (Eide, 1998). For example, iron availability regulates gene expression of FET3 a copper-dependent oxidase and FRE1 a ferric reductase, both required iron uptake in *S. cerevisiae* (Dancis *et al.*, 1992; Yamaguchi-Iwai *et al.*, 1996). This regulation is mediated by the

iron responsive transcription factors Aft1/Aft2. Under iron replete conditions the mitochondrial iron-sulfur cluster mediates homodimerization of Aft1/Aft2 which reduces their DNA binding affinity and induces export from the nucleus to the cytosol (Ramos-Alonso *et al.*, 2020). On the other hand Zrt1, a high affinity zinc transporter is ubiquitinated, endocytosed and degraded under zinc replete conditions (Gitan *et al.*, 1998; Gitan and Eide, 2000). In *S. cerevisiae*, Alr1p protein activity increases about nine-fold under Mg^{2+} -deficient conditions, but this can be only partially explained by a slight accumulation of Alr1p at the plasma membrane and is majorly caused by other yet unidentified mechanisms independent of gene expression and protein stability (Lim *et al.*, 2011). Thus I hypothesize, that under substrate replete conditions, Pit1 is subjected to a constant and fast turnover, which is why it is not visible at the plasma membrane *in planta*. In the mutated Pit1^{GLQ3A}-Gfp protein the loss of transport function results in an artificial substrate deficiency that causes a reduced turnover rate. As a consequence, Pit1^{GLQ3A}-Gfp accumulates at the plasma membrane and becomes visible *in planta*.

The significantly higher small tumour formation rate observed for Pit1^{GLQ3A}-Gfp under the native promoter in *Zea mays* Amadeo infection as well as for expression under the P_{otef} promoter in *Zea mays* Golden Bantam infection in comparison to the deletion strain *pit1* Δ also support correct localization of the mutated protein and could indicate minimal residual function. Unfortunately, confirmation of the plasma membrane accumulation of Pit1^{GLQ3A}-Gfp in sporidia was not successful because the protein was hardly expressed and did not localize to the plasma membrane. Although predictions did not show alterations of the secondary structure by replacing the GLQ motif with alanine, at least in sporidia the mutation seems to impair protein folding and processing in the ER. While localization of native Pit1 seems not impaired by a C-terminal Gfp-tag (Doehlemann *et al.*, 2011), it is still possible that the Gfp-tag impairs protein folding additionally. As demonstrated in *S. cerevisiae* Alr1p, complementation of the deletion phenotype by the N- or C-terminally tagged protein does not mean that the tag does not influence protein function or behaviour (Lim *et al.*, 2011). If the plasma membrane localization of Pit1^{GLQ3A}-Gfp *in planta* is true, the question is why the protein is not properly expressed in sporidia. In difference to sporidia, unfolded protein response (UPR) is constantly active in all stages of pathogenic development probably to allow efficient secretion of the high amounts of effector proteins (Heimel, Freitag, Hampel and Ast, 2013). Furthermore, the shared promoter region of *pit1* and

pit2 contains a Cib1 (homologue of Hac1: a transcription factor that induces UPR target gene expression) binding site directly linking *pit1/2* expression with UPR (Hampel *et al.*, 2016). While *pit1/2* are also expressed without the Cib1 binding site the connection to UPR seems to be important for efficient secretion of Pit2 and virulence (Hampel *et al.*, 2016). It is possible that Pit1_{GLQ3A}-Gfp can be properly expressed under UPR conditions while in absence of UPR in sporidia folding is impaired and results in degradation. To test this hypothesis, ER stress assays could be performed to induce UPR in sporidia and compare if expression and localization of Pit1_{GLQ3A}-Gfp changes.

The importance of the GLQ motif for Pit1 function and localization *in planta* supports a transport activity of Pit1. Regrettably, all attempts to test Mg²⁺ transport activity of Pit1 so far failed. First because *S. cerevisiae* did not properly express the tested *U. maydis* or *T. thlaspeos* proteins and second because until now the Mg²⁺ uptake system of *U. maydis* could not be clearly identified. Thus a complementation analysis could not be executed appropriately. Nevertheless, additional results support a transport activity of Pit1. The slight growth improvement in presence of manganese, zinc and nickel if Pit1-Gfp is expressed in *alr1Δ* and *pit1Δ* background together with the increased sensitivity towards cobalt of the Pit1-Gfp overexpression strain might indicate minor transport activity of these ions. The *S. cerevisiae* Mg²⁺ transporter Alr1p for examples also shows low affinity uptake of other divalent cations like Mn²⁺, Ni²⁺, Co²⁺ and Zn²⁺ (MacDiarmid and Gardner, 1998). Uptake studies of several human Mg²⁺ transporters also show limited uptake of other divalent cations (Quamme, 2010). The transporter of the low affinity iron uptake system in *S. cerevisiae* Fet4p also transports other metal ions like Mn²⁺, Co²⁺ and Zn²⁺ and Cu²⁺. Increased activity of Fet4p which can be induced by defects in the Fet3p high affinity uptake system, result in increased sensitivity towards these other metal ions (Li and Kaplan, 1998). While the element composition of the Pit1-Gfp overexpression strains did not differ significantly from the WT, the multiple insertion strain showed a slight increase of the cellular Mn and Fe concentrations in comparison to the WT that appears to depend on the expression level since it was not observed in the single insertion strain. Although this is only a slight trend it might supports limited transport of ions. If we assume there is also limited transport of other divalent cations like cobalt this could explain the higher sensitivity of the multiple insertion strain Pit1-Gfp towards Co²⁺. Potential transport of other metal ions is no indicator for Mg²⁺

transport, but it at least supports Pit1 being a transporter. Against expectations, the Mg^{2+} levels in the Pit1-Gfp overexpression strain were not increased in comparison to the WT. This implies either that Pit1 does not transport Mg^{2+} or that Mg^{2+} homeostasis is so tightly regulated, that additional import via Pit1 is equalized by the other import and export systems, since Pit1 is usually not expressed in sporidia (Doehlemann *et al.*, 2011).

Based on structural similarity, Pit1 clearly differs from CorA-type Mg^{2+} transporters, still there is great versatility between the different Mg^{2+} transporter families. The SLC41 Mg^{2+} transporters for example evolved through gene duplication and fusion from their *mgtE* ancestor (Payandeh, Pfoh and Pai, 2013). Gene duplication and fusion appears to be a common driver of evolution also for other transporters like the oligopeptide transporter family or the UPF0016 family (Gomolplitinant and Saier, 2011; Demaegd *et al.*, 2014). The evolutionary ancestry of Pit1 remains to be elucidated. Based on the protein sequence no homologues of Pit1 outside the smut fungi could be identified, but an extended analysis of the protein structure might provide further clues on Pit1 function.

The data presented here provides first experimental clues on a transport function of Pit1 as well as the identification of a motif important for Pit1 function. Both justify additional analysis in the future to elucidate the function of Pit1. In my opinion the most sensible and simple approach to test a Mg^{2+} transport function of Pit1 would be to optimize Pit1 expression in *S. cerevisiae* *alr1*. If used as an expression host, signal sequences like the *S. cerevisiae* α -mating factor signal sequence can be used to target recombinant proteins to the membrane (Routledge *et al.*, 2015). For example, commercial expression plasmids thus contain the *S. cerevisiae* α -mating factor signal sequence (pPICZ, Invitrogen™; Thermo Fisher Scientific). Incorporation of the α -mating factor signal sequence might be a fast, cost effective and easy approach to express Pit1-Gfp at the plasma membrane in *S. cerevisiae* and test complementation of the *alr1* phenotype. Should Pit1 still mislocalize, switching to bacteria for the complementation analysis like *Salmonella typhimurium* (H. Li *et al.*, 2017; Tong *et al.*, 2020) or performing ion uptake assays in *Xenopus laevis* oocytes could be considered.

As mentioned earlier, recent progress in structure predictions opens up another approach to gain insights into Pit1 function. The new AlphaFold2 algorithm that

predicts protein structures with high atomic accuracy without the need of a known homologous structure (Jumper *et al.*, 2021) now provides a new structure prediction of Pit1. Based on structural alignment, the arrangement of the seven transmembrane domains of Pit1 shows great similarity to G-protein coupled receptors (GPCR). The hypothesis of Pit1 acting as GPCR represents an interesting alternative. The family of GPCRs is probably the largest group of membrane proteins and transduces cellular responses to environmental signals (Rosenbaum, Rasmussen and Kobilka, 2009). In fungi they are involved in the regulation of versatile processes including pathogenic development, cell growth and division and mating (El-Defrawy and Hesham, 2020). In humans the direct and indirect interaction of GPCRs with ion channels is well studied (Inanobe and Kurachi, 2014). G-protein-gated potassium channels in neurons for example are inhibited by direct interaction with the G-protein $\beta\gamma$ complex (De Waard *et al.*, 1997), while cyclic-nucleotide-gated nonselective ion channels (CNGCs) are indirectly modulated by G-proteins via cAMP/cGMP signalling, for example important for the sympathetic stimulation of the heart (Inanobe and Kurachi, 2014). In plants, CNGCs are involved in various signalling pathways during development and growth and in response to abiotic and biotic stresses (Duszyn *et al.*, 2019). In *A. thaliana* it was shown that CNCG2 is essential for Ca^{2+} influx in innate immunity during infection of *A. thaliana* with *Pseudomonas syringae* and subsequent nitric oxide production and hypersensitive response (Ali *et al.*, 2007). In this context, Pit1 being a GPCR might also explain the observed growth effects of the Pit1-Gfp overexpression strain in presence of heavy metals, although ion channel activation might be mediated indirectly by other GPCR downstream signalling pathways since, both G-protein-gated ion channels and CNGCs seem not present in fungi (Zelman *et al.*, 2012).

Although the function of Pit1 could not be elucidated in the frame of this thesis, there now is additional experimental data to support the hypothesis of Pit1 functioning as transporter as well as new structural information on Pit1 that sets the foundation for further studies to elucidate its function.

3.3.3.2 Mg^{2+} homeostasis in *U. maydis*

An initial characterization of Mg^{2+} transport in *U. maydis* is presented in this thesis. Within this project this was of interest for two reasons. First, knowledge on the Mg^{2+} transport of *U. maydis* was necessary to explore a potential Mg^{2+} transport activity of Pit1. Second, Mg^{2+} transport was investigated with its significance for pathogenicity.

In the proteome of *U. maydis* four different families of Mg²⁺ transporters were identified. Namely CorA-type, MgtE/SLC41-type, NIPA-type, and ACDP/CNNM-type Mg²⁺ transporters. In comparison, in *S. cerevisiae* only CorA-type and ACDP/CNNM-type Mg²⁺ transporters could be identified so far (MacDiarmid and Gardner, 1998; Bui *et al.*, 1999; Graschopf *et al.*, 2001; Gregan *et al.*, 2001; Pisat, Pandey and MacDiarmid, 2009; Sponder *et al.*, 2010; Tang *et al.*, 2022), although Mg²⁺ transport is studied in yeast for many years. In comparison to other ascomycetes the Mg²⁺ transporter repertoire of *S. cerevisiae* appears to be the most limited, while smut fungi show the highest versatility in their Mg²⁺ transporter repertoire as far as analysed in this study (Supplementary Figure 7-6). Thus *U. maydis* might represent a more comprehensive fungal model system to study Mg²⁺ transport and homeostasis, especially since *U. maydis* has yeast-like as well as filamentous growth and therefore could represent both, filamentous fungi and yeasts.

In the frame of this thesis the CorA-type Mg²⁺ transporter candidates of *U. maydis* were studied in further detail. While in *S. cerevisiae* the CorA-type Mg²⁺ transporters can be clearly associated with the cellular compartments mitochondria, plasma membrane and vacuole, the analysis of the corresponding *U. maydis* homologues did not support a clear assignment to a certain compartment, except for Lpe10 which localizes to the mitochondria similar to *S. cerevisiae* (Gregan *et al.*, 2001). To further support the function of Lpe10 as inner membrane magnesium importer the next step would be to analyse if a *lpe10*Δ strain also shows strongly reduced growth on a non-fermentable carbon source, similar to *S. cerevisiae* (Gregan *et al.*, 2001).

My data from the *U. maydis* CorA-type transporter candidates Alr1 and Mnr2 suggest a different regulation than in *S. cerevisiae*. The Mg²⁺ dependent growth defect of *alr1*Δ as well as the reduced intracellular Mg²⁺ concentration support plasma membrane localization of Alr1. The microscopy of the Gfp-fusion protein and the increased sensitivity of *alr1*Δ towards Mn²⁺ on the other hand support vacuolar localization. The deletion of *mnr2* does not show a Mg²⁺ dependent growth phenotype, which is the strongest indicator for plasma membrane localization, yet the intracellular Mg²⁺ concentration is reduced to the level of the *alr1*Δ strain. There is no increased sensitivity towards other divalent cations which argues against vacuolar localization. Finally, the increased sensitivity towards cobalt of both Alr1-Gfp and Mnr2-Gfp overexpression strains fits to plasma membrane localization. A hypothesis

to explain the observations, is that Alr1 and Mnr2 form heteropentamers (Figure 3-34 middle): In *S. cerevisiae* there are two plasma membrane transporters Alr1p and Alr2p but Alr2p only slightly contributes to Mg^{2+} uptake due to a single amino acid exchange in the extracellular loop connecting the two TM-domains (Wachek *et al.*, 2006). While no specific reason or purpose for this was found, it was shown that Alr1p and Alr2p can form homo- as well as heterooligomers (Wachek *et al.*, 2006). To the contrary, overexpression of Alr2p results in a dominant-negative effect on Mg^{2+} uptake by Alr1p, likely due to increased heterooligomer formation (Wachek *et al.*, 2006).

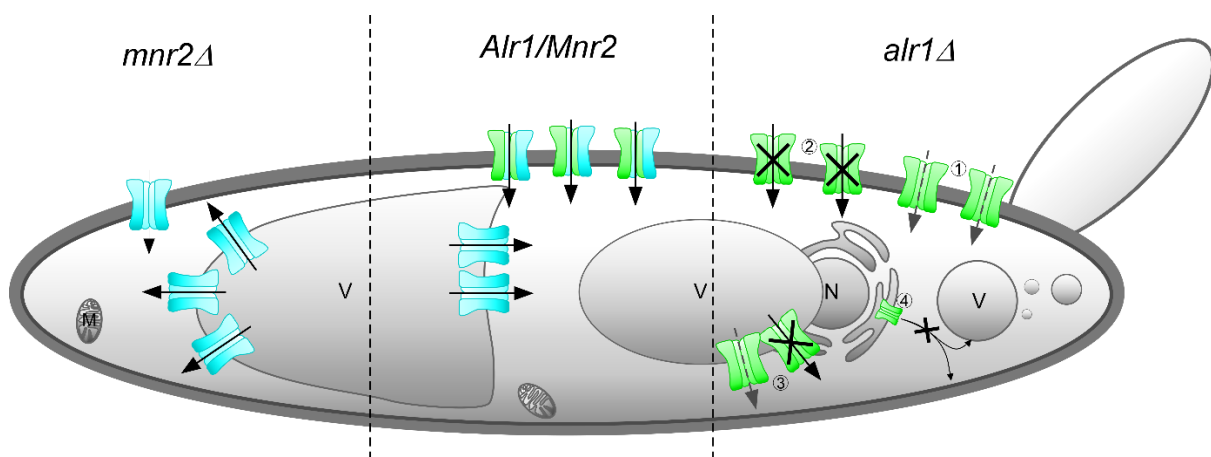


Figure 3-34 Model for Alr1/Mnr2 regulated Mg^{2+} transport in *U. maydis*. The model shows localization of the transporters in case of *mnr2* deletion (left), WT (middle) and *alr1* deletion.

***Mnr2*Δ:** Alr1 (blue) forms homooligomers that localize mostly to the vacuole and transport Mg^{2+} from the vacuole into the cytoplasm while a small portion also reaches the plasma membrane to allow limited Mg^{2+} influx into the cell.

***Alr1/Mnr2*:** If Alr1 and Mnr2 are present and the heterooligomer localizes to the plasma membrane, while the Alr1 homooligomer localizes to the vacuole. The composition of the oligomer determines localization and ensures sufficient distribution between the two compartments.

***Alr1*Δ:** 1) Mnr2 (green) forms homooligomers that localize to the plasma membrane and allow low-affinity transport of divalent cations due to the alteration of the GMN motif to SxN, but this is not sufficient to compensate the Mg^{2+} dependent growth defect. 2) The homooligomer localizes to the plasma membrane but cannot transport ions due to the altered GMN motif. 3) A small portion of Mnr2 reached the vacuole and there either transports divalent cations with low affinity or is non-functional. 4) Localization of Mnr2 depends on heterooligomerization with Alr1, thus Mnr2 accumulates in the ER and is eventually degraded.

In *U. maydis* my data suggest that heterooligomerisation might be instead required. This is supported by the observation that *alr1*Δ and *mnr2*Δ both show a strong decrease in the cellular Mg^{2+} concentration (Figure 3-25), that is so far only associated with impaired or abolished Mg^{2+} uptake into the cell for CorA-type Mg^{2+} transporters (Graschopf *et al.*, 2001; Reza *et al.*, 2016). Overexpression of Alr1 or Mnr2 also resulted in increased sensitivity towards Co^{2+} , also typical for plasma membrane localized CorA-type Mg^{2+} transporters (MacDiarmid and Gardner, 1998). I

propose that Alr1 and Mnr2 can form homo- and heterooligomers (Figure 3-34 middle) similar to *S. cerevisiae* and likely pentamers similar to the bacterial CorA Mg²⁺ transporter (Eshaghi *et al.*, 2006; Wachek *et al.*, 2006).

In contrast to yeast, the Alr1 homooligomer would localize to the vacuole (Figure 3-34 middle). This is supported by the observation that Gfp-Alr1 was found only at the vacuole (Figure 3-20). The N-terminal Gfp-tag might promote the homooligomerization of Alr1 since it itself is able to oligomerize (Wachek *et al.*, 2006) and the long N-terminus of Alr1 provides sufficient flexibility. Additionally, the *alr1Δ* strain, but not *mnr2Δ*, showed increased sensitivity towards Mn²⁺, which is described for vacuolar Mg²⁺ transporters (Pisat, Pandey and MacDiarmid, 2009).

The Alr1/Mnr2 heterooligomerization then shifts localization to the plasma membrane. An overexpression of any of the two would then result in an increased amount of the transporter at the plasma membrane. Typically, CorA-type Mg²⁺ transporters also transport other divalent cations like Ni²⁺, Co²⁺, Mn²⁺ or Zn²⁺ with lower affinity and thus plasma membrane transporters show increased sensitivity towards these ions if overexpressed (MacDiarmid and Gardner, 1998). In *U. maydis* this was indeed observed for Co²⁺ but not for the other tested ions (Figure 3-23). Indeed, this could simply mean, that an effect for Mn²⁺, Ni²⁺ and Zn²⁺ would be visible at different concentrations. The tested concentrations were chosen based on experience from *S. cerevisiae* (MacDiarmid and Gardner, 1998; Pisat, Pandey and MacDiarmid, 2009), but not optimized for *U. maydis*. Instead of a clear differentiation between homo- and heterooligomer it is also thinkable that the portion of Alr1 and Mnr2 in the heterodimer determines its localization. A majority of Alr1 protein in the heterooligomer could localize to the vacuole while a majority of Mnr2 could localize to the plasma membrane. If this hypothesis is true what would happen if *alr1* or *mnr2* is deleted?

Scenario 1: *mnr2Δ* (Figure 3-34 left)

If *mnr2* is deleted, Alr1 can only homooligomerize. The homooligomer would then predominantly localize to the vacuole. Between plasma membrane and vacuolar membrane there is some crosstalk via retrograde signalling that could result in a small portion of Alr1 being retrieved from the vacuolar membrane via the retromer and redistributed to the plasma membrane (Ma and Burd, 2020). In *S. cerevisiae* it

was for example shown that the transmembrane receptor Vps10 can be recycled from the vacuole via the retromer (Arlt, Reggiori and Ungermann, 2015). In case of Alr1 this redistributed portion would be too small to allow sufficient uptake of Mg^{2+} into the cell, explaining the reduced Mg concentration measured for *mnr2Δ*, but sufficient to allow growth with a slightly reduced growth rate at low external Mg^{2+} concentrations, explaining why no phenotype was observed on drop plates (Figure 3-22). In *S. cerevisiae* it was for example shown that a portion of Mnr2 is redirected from the vacuole to the plasma membrane if overexpressed. Accumulation of Alr1 at the vacuolar membrane would also mean increased efflux activity, which is not detectable due to the overall reduced cellular Mg concentrations.

Scenario 2: *alr1Δ* (Figure 3-34 right)

If *alr1* is deleted, Mnr2 can only homooligomerize. Mnr2 differs from most CorA-type transporters as the GMN motif is replaced with an SxN motif in smut fungi. This could have two possible effects. First, similar to Alr2p in *S. cerevisiae* the Mnr2 homooligomer could still transport divalent cations with low affinity. This would not be sufficient to complement the severe growth defect of *alr1Δ* under low Mg^{2+} conditions but would explain how Mn^{2+} is taken up into the cell to cause the increased sensitivity phenotype observed for *alr1Δ* (Figure 3-23), although there is apparently no noteworthy Mg^{2+} uptake into the cell. Second, the Mnr2 homooligomer might be completely non-functional due to the altered motif. If this were true, Mn^{2+} uptake must occur via other transport systems. In the ICP-MS dataset the Mg concentrations measured for *alr1Δ* and *mnr2Δ* were similar (Figure 3-25), but I would expect, that if the cells were kept under low Mg^{2+} conditions for longer that the concentration for *alr1Δ* would drop further until they cease to grow and eventually die, while the concentrations for *mnr2Δ* would stabilize at a low level that still allows growth. Opposite to Alr1, a small portion of the Mnr2 homooligomer would also reach the vacuolar membrane but would also only allow low affinity transport or no transport at all. Through absence of Mg^{2+} uptake into the cell any effect of this would not be detectable. Another possibility, that seems less likely in my opinion, would be, that localization of Mnr2 depends on the heterooligomerization with Alr1. Thus, Mnr2 would accumulate in the ER and eventually be degraded.

How do the results of the Gfp-tagged transporters fit into the picture?

Gfp-Alr1 was observed at the vacuolar membrane and a hypothesis for the localization and an effect of the tag was already explained above. In difference C-terminally tagged Alr1 but also Mnr2 showed a weak signal in the ER that likely indicates that the proteins are stuck and frequently degraded (Figure 3-20). A likely explanation for this is that the Gfp prevents correct insertion into the ER membrane. In *S. cerevisiae* Alr1p C-terminal truncations, which are additionally tagged with Gfp at the C-terminus, show impaired localization and the authors propose that the truncations impair the anchoring in the plasma membrane (Wachek *et al.*, 2006). In comparison to *S. cerevisiae* the C-terminus of *U. maydis* Alr1 and Mnr2 is already much shorter, which makes it likely that the tag per se causes a sterical problem. Unexpectedly, the N-terminal Gfp tag of Mnr2 also resulted in the weak ER signal observed for the C-terminal tag (Figure 3-20). A potential explanation is, that the Gfp tag masks an N-terminal unconserved localization signal sequence or a domain important for heterooligomerization and as a result Gfp-Mnr2 remains in the ER and is eventually degraded. With all problems the Gfp-tag might cause, it should be noted that both the N- and C-terminal tagged Alr1 fusion proteins as well as the Gfp-Mnr2 were able to complement their respective deletion phenotypes (Figure 3-22; Alr1-Gfp: Peter Wegjan Bachelors thesis). Considering the native expression levels of the transporters and the estimated expression level of the P_{otef} promoter, it can likely be assumed that gene expression under the P_{otef} is several fold higher than in the WT. Thus it is likely that the small portions of the proteins that do reach their destined localization are sufficient to complement their deletion phenotypes.

In summary, I propose that in *U. maydis* the two CorA-type Mg^{2+} transporters Alr1 and Mnr2 are not functionally redundant. Both are necessary for sufficient transport across the plasma membrane and at least Alr1 if not both also transport Mg^{2+} across the vacuolar membrane. To this end, heterodimerization of Alr1 and Mnr2 is essential to achieve sufficient distribution to and between the two compartments.

To test this hypothesis, the first step would be to show heterooligomerization and homooligomerization of Alr1 and Mnr2 ideally with localization at the plasma membrane and the vacuole. There are several techniques that could be applied, including crosslinking, Co-Immunoprecipitation, Split-Ubiquitin and imaging techniques like FRET (Wachek *et al.*, 2006; Avila, Lee and Toriia, 2015; Škerle *et al.*, 2020). All of them require tagging of the proteins of interest. As tagging of the *U.*

maydis CorA-type Mg^{2+} transporters already proved to be problematic, tags and controls need to be chosen very carefully. So far, Alr1 was only tested alone in *S. cerevisiae* complementation analysis, but based on the hypothesis present here it might need Mnr2 in order to complement. Thus the easiest approach would be to express both proteins in the *S. cerevisiae alr1* deletion strain. To avoid interference with the bulky fluorescent tags small N-terminal tags like HA or Myc could be used to track the proteins instead. Subsequently hetero- and homooligomerization should be shown directly in *U. maydis*. In my opinion, the FRET technique is here the most promising approach as it allows to show localization as well. To reduce interference of the tag with oligomerization and insertion into the plasma membrane the tags could be integrated into flexible loops of the transporters. Since the cytosolic N-terminal part of Alr1 and Mnr2 comprises most of the proteins, several suitable positions could be identified. This approach has been tried successfully before for proteins where C- and N-terminal tags failed, also in a FRET-based application (Bendezú *et al.*, 2015; Mastop *et al.*, 2018). Additionally, there are versions of fluorescent proteins like mGFP that do not self-dimerize which should be used to avoid promotion of homooligomerization of Alr1 and possibly also Mnr2 (Zacharias *et al.*, 2002).

3.3.3.3 The Role of Mg^{2+} -nutrition during plant infection

To investigate the significance of Mg^{2+} transport in *U. maydis* for pathogenicity several transporter mutants were tested in maize infection as well as analysis of the element composition of the infected leaf.

The *alr1Δ* strain was completely avirulent. Sporidia on the leaf surface were found unable to induce filamentous growth. The loss of filament induction itself could already explain the avirulence of *alr1Δ*, since the yeast-like form of *U. maydis* is not infectious (Brefort *et al.*, 2009). But even if this were not the case the deletion of a Mg^{2+} transporter, that is essential for Mg^{2+} uptake into the cell, would result in loss of virulence, since Mg^{2+} is one of the essential macro nutrients (Kadereit *et al.*, 2014), thus no uptake simply means eventually cell death. Since the effects of Mg^{2+} deficiency are pleiotropic it is currently not possible assign the avirulence to a specific effect of *alr1* deletion. The injection of *U. maydis* into the maize seedling in presence of 50 mM $MgCl_2$, a concentration that was sufficient to restore growth of *alr1Δ* in axenic culture (Figure 3-22), was not able to complement the Mg^{2+} deficiency caused

by *alr1Δ* on the leaf surface. It is possible that this initial supply of additional Mg^{2+} is not sufficient to support initial growth on the leaf surface. It could be tested if daily foliar applications of Mg^{2+} are sufficient to elevate the Mg^{2+} concentrations to a level that keeps the sporidia alive and allows limited growth. If under these conditions still no initial infection occurs, the cause of the avirulence could be assigned to the loss of filament induction.

The loss of filament induction of the *alr1Δ* strains was also observed on filament induction medium. In this context it was additionally found, that filament induction appears to be inversely proportional to the extracellular Mg^{2+} and Co(III)Hex concentration. For the Mg^{2+} concentration this might be a calcium signalling based effect. In presence of high concentrations of a certain ion, this can impair the uptake of other ions. In case of high Mg^{2+} concentrations the Ca^{2+} uptake is strongly impaired (Figure 3-25, (Graschopf *et al.*, 2001)). But Ca^{2+} signalling relies on Ca^{2+} influx into the cell (Park *et al.*, 2019; Roy *et al.*, 2020), if this is impaired a plethora of processes are affected. In *U. maydis* filament induction signalling involves among other pathways Ucn1, a homologue of a calcineurin subunit, that is activated during calcium signalling (Kijpornyongpan and Aime, 2020). Fittingly, deletion of *ucn1* results in loss of pathogenicity and a filament defect (Egan *et al.*, 2009). The filamentation defect of *alr1Δ* and in presence of Co(III)Hex on the other hand suggest induction of filamentous growth to depend either on the intracellular Mg^{2+} concentration or Mg^{2+} uptake via CorA-type Mg^{2+} transporters. At 50 mM $MgCl_2$ filament induction of the SG200 is reduced but still visible, while it is absent in *alr1Δ*. At the same time Mg^{2+} levels of *alr1Δ* under high Mg^{2+} conditions reach roughly 2/3 of the WT level under normal Mg^{2+} conditions (Supplementary Figure 7-8).

A lot of enzymes rely on Mg^{2+} as a co-factor including small GTPases (Zhang *et al.*, 2000). In *U. maydis* filament induction is prompted by the cyclic-AMP/ protein kinase A (PKA) pathway, the mitogen-activated protein kinase pathway and GTPase mediated signalling (Kijpornyongpan and Aime, 2020). The small GTPase Ras2 acts upstream of the MAPK cascade and is important for response to mating, filamentous growth, and pathogenicity of the dikaryon (Lee and Kronstad, 2002). Thus *ras2Δ* strains grow yeast-like on charcoal containing filament induction medium and are avirulent in maize infection (Lee and Kronstad, 2002). Overall the phenotype of *ras2Δ* strongly resembled the *alr1Δ* phenotype. Thus I hypothesise, that the cellular

Mg²⁺ deficiency caused by *alr1Δ* deletion impairs Ras2 activity to an extent that *alr1Δ* mimics the *ras2Δ* phenotype. Under high Mg²⁺ conditions Ras2 activity should be restored in *alr1Δ* but then Ca²⁺ depletion likely impairs filamentous growth via the cAMP/PKA pathway.

In contrast, deletion of *mnr2* or *lpe10* only resulted in a slight decrease in virulence, while *mgtEΔ* had no detectable effect at all. Lpe10 is most likely the mitochondrial Mg²⁺ importer while Mnr2 is important to reach WT Mg²⁺ levels in the cell, although uptake into the cell is still possible without Mnr2. If any of the two is deleted this will alter Mg²⁺ homeostasis which results in an overall fitness decrease. The generally worse performance of the deletion strains will also be reflected in decreased virulence during infection but does not necessarily mean a direct impact on pathogenicity. However, the deletion strains did not affect the decrease of the Mg concentration in the infected leaf.

The interesting questions are: How does *U. maydis* achieve this low Mg-levels in infected leaves considering Mg²⁺ is a highly phloem mobile ion (Marschner, 2012) and there is increased phloem flow into the tumour tissue (Horst *et al.*, 2010)? Is this an active process to facilitate infection or just a (beneficial) side effect? The data presented here shows that alteration of the fungal Mg²⁺ homeostasis at least does not have effects that could be detected on the tissue level. Still, it is possible that *U. maydis* induces micro Mg²⁺ deficiencies for example at points of cell-cell passage to facilitate growth through the plant tissue. To show this it would be necessary to measure Mg²⁺ fluxes with spatial resolution at the cell level. Possible approaches could be Mg²⁺ biosensors, laser-ablation ICP-MS or X-ray fluorescence microscopy (Becker *et al.*, 2009; Lindenburg *et al.*, 2013; Naim *et al.*, 2021).

If the Mg²⁺ homeostasis of the fungus is likely not involved in the overall Mg deficiency of the infected leaf, how is it induced? ICP-MS data of the infected leaves show, that the Mg content of the infected leaf is very similar to the Mg content of the next younger leaf of both MOCK control and SG200 infected (Supplementary Figure 7-11). So it could be possible, that *U. maydis* affects maturation of the plant leaves that results in the case of Mg²⁺, in an adult leaf having the Mg content of a juvenile leaf. Fitting to this idea, no senescence of the older leaves was observed for *U. maydis* infected plants until 12 dpi, while MOCK control - and untreated plants show

signs of leaf senescence in L2 and partly also in L3. This is in line with previous observations of delayed host cell senescence upon *U. maydis* infection (Horst *et al.*, 2010; Gao *et al.*, 2013) In plant leaves 6-25 % of the Mg^{2+} content is bound to chlorophyll, depending on the nutritional status of Mg^{2+} in the plant (Marschner, 2012). In *U. maydis*, a reduction up to 90 % of chlorophyll a and b has been reported in tumours (Horst *et al.*, 2008), while the overall Mg concentration is 59 % reduced in all tested *U. maydis* strains at 12 dpi. The Mg^{2+} reduction in the leaf is much higher than the 22 % reported by Horst *et al.* (2010). This difference might be a result of the sampling time point. In the study by Horst *et al.* the leaves were sampled at 8 dpi while in this study the leaves were sampled at 12 dpi where the plants are much bigger. But based on the data presented here, it becomes clear, that chlorosis in the tumours of *U. maydis* infected plants cannot solely explain the lower Mg concentrations. Actually, the cytoplasmic and apoplastic Mg^{2+} concentrations might even be higher than in the healthy plant, due to the increased phloem flow to the infected tissue, combined with less Mg^{2+} being incorporated into chlorophyll. Thus, there might be a higher amount of Mg^{2+} available to circulate in the plant. If this is true, this would not be detectable with the applied method. The Mg concentration in L2 of the infected plant is as high as the concentration in the senescent L2 of the MOCK plant which supports a higher apoplastic Mg^{2+} concentration in the infected plant, since Mg normally further accumulates in the senescent leaf in comparison to a mature leaf (Marschner, 2012). Thus higher amounts of Mg^{2+} circulating through the plant, combined with increased photosynthetic activity in the L2 leaf of the infected plant and thus a higher demand of Mg^{2+} , might explain the higher Mg^{2+} concentration found in this leaf.

4 Conclusions and Outlook

Smut fungi are a group of plant pathogenic fungi that infect mostly grasses, including essential crop plants. An important representative is *Ustilago maydis*, a fungus that served the last decades as a scientific model for DNA recombination and repair, signalling pathways, translational and posttranslational regulation, cell cycle regulation as well as mating, morphogenesis and pathogenicity. *T. thlaspeos* on the other hand, is a smut fungus of the order *Urocystiales*, related to *U. maydis*. Unlike *U. maydis* and closely related smut fungi, *T. thlaspeos* infects *Brassicaceae* plants like *Arabis hirsuta* and colonizes under lab conditions also the model plant *A. thaliana*. With the possibility to combine the knowledge from smut fungi and *A. thaliana* there is much potential for *T. thlaspeos* to be part of a new model pathosystem genetically accessible from both sites. Although the life cycle was described by our group recently there are aspects that are not completely understood.

The aim of this thesis was to further characterize the infection biology of *T. thlaspeos* and characterize Mg^{2+} transport and its potential contribution to virulence in *U. maydis*. To this end this thesis addresses three aspects:

Chapter 1 comprises a detailed microscopic description of the initial infection phase which revealed that *T. thlaspeos* penetrates the plant via appressoria-like structures on roots and shoots similarly in the two host plants *Ar. hirsuta* and *Ar. alpina* as well as *A. thaliana*. On leaves *T. thlaspeos* forms appressoria on guard cells, epidermal cells or grows directly through the stoma to then grow intracellularly directly after penetration. If penetration occurs via stomata the guard cells are also colonized, which is so far not reported for any other fungus. If we assume that this infection strategy observed under lab conditions also reflects natural plant infection, it suggests that *T. thlaspeos* forms a tight biotrophic interaction with its host very early on. While in some fungi appressoria formation is induced by very specific surface cues, *T. thlaspeos* seems to be less restricted in the position where an appressorium is formed. I suggest to focus initially on appressoria formation on the guard cells to investigate the early molecular response of *T. thlaspeos* and the plant towards infection via RNAseq and gain for example temporal insights into the effectorome of *T. thlaspeos* in the future because available stomata mutants might simplify structure isolation. Conservation of these structures between the hosts and *A. thaliana*

suggests also conservation on a molecular level to some extent. Thus, the combination of *T. thlaspeos* and the *A. thaliana* present a useful surrogate system which allows to methodically isolate the penetration structures for subsequent analysis and simplifies analysis of the plant response since the genome data is available. For example, the huge mutant collection of *A. thaliana* offers the possibility to manipulate stomata conductance and number with the *A. thaliana* mutant *speechless* (spch-3; T-DNA insertion line SAIL_36_B06; MacAlister, Ohashi-Ito and Bergmann, 2007) that does not form stomata or *too many mouth* (*tmm-1*; EMS mutant; Nadeau and Sack, 2002) where stomata appear in clusters, which is especially interesting to increase appressoria formation. Additionally, the *A. thaliana* reporter line COLORFUL-PR1pro offers the possibility to identify and specifically isolate plant cells responding to *T. thlaspeos* infection, which will considerably ease the analysis of the plant response. Since *speechless* does not form stomata this mutant forces *T. thlaspeos* to form appressoria on epidermal cells which might allow to distinguish and compare appressoria formation on the two cell types to test if pathogen and host responses differ depending on the cell type.

With regard to the open questions about the *T. thlaspeos* infection biology, the data presented here shows that appressoria formation of *T. thlaspeos* on the leaf surface is more versatile than initially thought and likely results in systemic infection of the plant. Although it remains to be elucidated if this infection strategy is relevant under natural conditions. With regard to feeding structures, no haustoria were so far observed for *T. thlaspeos* but here I showed for the first time, that *T. thlaspeos* hyphae in leaves grow intracellularly, creating a biotrophic interphase for interaction with the host plant. With regard to nutrient uptake and exchange with the host during systemic infection, where *T. thlaspeos* grows along the vasculature, it will be interesting to show where the fungus exactly grows in the vasculature tissue and if it is also growing intracellularly in this infection stage.

The comparison of the hosts *Ar. hirsuta* and *Ar. alpina* as well as different *Ar. hirsuta* ecotypes during *T. thlaspeos* soil infection indicates different isolates of *T. thlaspeos* adapted to the host species might exist. If true, collection of additional compatible *T. thlaspeos* host plant combinations provides the possibility to study host adaptation.

In my opinion the *T. thlaspeos* pathosystem is currently at a crossroad. With the establishment of a transformation protocol one of the essential techniques is

available that is required for *T. thlaspeos* to gain importance as a model system in the plant-microbe community. The other is the development of a culture infection protocol that allows to investigate genetically modified strains *in planta*. Considering the advantages of smut fungi, like the possibility to cultivate them under axenic conditions and genetic amenability, which warrant their potential as surrogate system for less accessible pathogens like rust fungi (Jaswal, Rajarammohan, *et al.*, 2020), the *T. thlaspeos* pathosystem in combination with *A. thaliana* is of particular importance. The following years will show if it will be possible to make full use of this potential.

Chapter 2 aimed to characterize a potential virulence factor of *T. thlaspeos* THTG_00998 that is a homologue of the *U. maydis* virulence factor Pit1. The complementation analysis showed, that *T. thlaspeos pit1* is not able to complement the *pit1Δ* phenotype in *U. maydis*, although it is expressed under an artificial promoter *in planta*, indicating *U. maydis* is not a suitable surrogate system to study the virulence function of *T. thlaspeos* Pit1. To study the virulence contribution of Pit1 and allow the analysis of other interesting genetic targets directly in *T. thlaspeos* in the future, a transformation protocol was established and published in Journal of Fungi. With that and a culture infection protocol currently being established in our group, the next steps will be to generate a *pit1Δ* mutant as well as a *pit1-gfp* fusion strain directly in *T. thlaspeos* to test if Pit1 has a similarly important role for virulence as Pit1 in *U. maydis* and show the localization of Pit1 in *T. thlaspeos* hyphae. Considering that *T. thlaspeos* does not cause any symptoms in its host plants I would expect less fungal proliferation *in planta*, loss of spore formation and maybe even loss of the infection itself in a *T. thlaspeos pit1Δ* mutant if Pit1 is of equal importance for *T. thlaspeos* than *Um* Pit1 for *U. maydis*.

Although the function of neither *T. thlaspeos* nor *U. maydis* Pit1 could not be elucidated in the frame of this thesis, I suggest two potential functions for Pit1 either as a Mg²⁺ transporter or G-protein coupled receptor. With regard to the Mg²⁺ transporter hypothesis I showed in *U. maydis* that a GLQ motif at the end of a transmembrane domain in Pit1 is important for Pit1 function, but there is no evidence yet that allows to reject or accept the initial hypothesis. Still, growth in presence of several heavy metals might indicate limited transport activity of Pit1 for divalent cations. On the other hand, new structural information on Pit1 supports a role as

GPCR. In my opinion the most sensible and simple approach to test a Mg^{2+} transport function of Pit1 would be to optimize Pit1 expression in *S. cerevisiae* *alr1*. If used as an expression host, signal sequences like the *S. cerevisiae* α -mating factor signal sequence can be used to target recombinant proteins to the membrane (Routledge *et al.*, 2015). Incorporation of the α -mating factor signal sequence might be a fast, cost effective and easy approach to express Pit1-Gfp at the plasma membrane in *S. cerevisiae* and test complementation of the Mg^{2+} dependent growth defect in the *alr1* mutant. In parallel the GPCR hypothesis represents an interesting alternative that should be investigated. If Pit1 is a GPCR, G-protein interaction could be tested using a split-ubiquitin assay in *S. cerevisiae* similar to an approach for a *Fusarium graminearum* GPCR by Dilks *et al* (2019), while its activating ligand could be identified using the open source resource PRESTO-Tango (**parallel receptorome expression and screening via transcriptional output - Tango**). This assays, originally established for human GPCRs, works with a β -arrestin recruitment based approach that translates agonist binding into a luminescence output signal (Kroeze *et al.*, 2015) and could be adapted for *U. maydis*. Either way, elucidating the function of Pit1 will deliver another piece of information to understand the versatile interactions of smut fungi with their host plants during infection but also provides the basis for drug development. Both, transporters as well as GPCRs represent important drug targets (Georgiev, 2000; El-Defrawy and Hesham, 2020; Masaryk and Sychrová, 2022). Since Pit1 is conserved in smut fungi and plays an essential role for virulence it represents an interesting target for drug development in plant protection once its function is elucidated.

Chapter 3 dealt with Mg^{2+} homeostasis in *U. maydis*. A previous study showed, that *U. maydis* infection results in decreased Mg content in the tumours, although there is increased phloem flow towards the infected leaf and Mg^{2+} is highly phloem mobile (Horst *et al.*, 2010; Marschner, 2012). While there is currently no explanation for this observation the possibility that *U. maydis* manipulates the plants Mg^{2+} homeostasis on purpose to facilitate infection is highly interesting. Mg^{2+} availability to the plant also impacts the plants susceptibility towards infection (Huber and Jones, 2013). If we understand the role of Mg^{2+} for infection better, it might be possible to develop new approaches for crop protection, for example, the right fertilizers to strengthen the plant against infection or identify common traits of the pathogens Mg^{2+} homeostasis

to develop new broad spectrum fungicides. A summary of studies that examined the effect of Mg^{2+} application on a certain plant disease shows that most studies were conducted in the second half of the last century (Huber and Jones, 2013). The majority of these studies is not publicly available anymore, but they demonstrate the value of well-balanced nutrition for crop protection. In line, a recent study showed that Mg application improves yield in most production systems (Wang *et al.*, 2020). Reviving this field could thus provide a valuable contribution to sustainable agriculture in the future. In order to develop new powerful fungicides targeting the fungal Mg^{2+} homeostasis, detailed understanding is essential.

In this thesis an initial characterization of the Mg^{2+} transport is described in *U. maydis*. In comparison to *S. cerevisiae* additional families of Mg^{2+} transporter candidates were identified. At least in smut fungi this Mg^{2+} transporter repertoire seems to be conserved and appears more versatile in comparison to *S. cerevisiae*. Further analysis of the CorA-type Mg^{2+} transporters identified in *U. maydis*, Alr1 and Mnr2 indicate a different regulation of Mg^{2+} import into the cell and export from the vacuole than known from *S. cerevisiae*. I show that both CorA-type Mg^{2+} transporter candidates share features typical for plasma membrane and well as vacuole localized Mg^{2+} transporters. While Alr1 appeared indispensable for Mg^{2+} uptake into the cell, both Alr1 and Mnr2 seem equally important to maintain WT-like intracellular Mg^{2+} levels. Based on my data I propose that Alr1 and Mnr2 operate as heterooligomers, while the composition of the heterooligomer determines localization either to the vacuole or the plasma membrane. To test this hypothesis, the first step would be to show heterooligomerization of Alr1 and Mnr2 ideally with localization at the plasma membrane and the vacuole. There are several techniques that could be applied, including crosslinking, Co-Immunoprecipitation, Split-Ubiquitin and imaging techniques like FRET (Wachek *et al.*, 2006; Avila, Lee and Toriia, 2015; Škerle *et al.*, 2020). Further investigation of all identified transporter candidates provides the possibility to understand Mg^{2+} homeostasis in fungi on a much more holistic level than possible in *S. cerevisiae*.

Furthermore, deletion of *alr1* in *U. maydis* results in a filamentation defect which blocks infection on the plant surface. In contrast, deletion of *mnr2* resulted only in a very slight decrease in virulence, that did not affect the overall Mg reduction in the infected leaf in comparison to the WT. While it is not clear if *U. maydis* interferes with

its host Mg^{2+} homeostasis, I hypothesize that Mg^{2+} transporters could contribute to *U. maydis* virulence by taking up Mg^{2+} at the points of cell-cell passage to weaken the plant cell wall and at the infection site to redirect sugar partitioning. To show this, it would be necessary to measure Mg^{2+} fluxes with spatial resolution at the cell level. Possible approaches could be Mg^{2+} biosensors, laser-ablation ICP-MS or X-ray fluorescence microscopy (Becker *et al.*, 2009; Lindenburg *et al.*, 2013; Naim *et al.*, 2021).

Taken together, the results presented in this thesis greatly contribute to our knowledge on the *T. thlaspeos* infection biology set the foundation to gain further insights on the molecular level of the interaction with the host in the future. The technical advances in the transformation protocol have biggest impact on *T. thlaspeos* research to establish it as a model system in the field. Additionally, the extensive knowledge about *U. maydis* is expanded with an initial characterization of Mg^{2+} homeostasis, a field not yet investigated in this fungus.

5 Material and Methods

5.1 Material

5.1.1 Solutions, media, enzymes, kits and chemicals

5.1.1.1 Buffer and solutions

All standard buffer and solutions used in this work were prepared according to Ausubel (1987) and Sambrook (1989) if not indicated otherwise.

5.1.1.2 Media

E. coli:

E. coli was cultivated in dYT medium (liquid) or YT medium (solid):

YT-Medium (Sambrook, 1989)	dYT-Medium (Sambrook, 1989)
0,8 % (w/v) Tryptone	1,6 % (w/v) Tryptone
0,5 % (w/v) Yeast extract	1,0 % (w/v) Yeast extract
0,5 % (w/v) NaCl	0,5 % (w/v) NaCl
1 % (w/v) Bacto Agar (for solid medium)	In H_2O_{bid} .

In H₂O_{bid.}

Sterilization: autoclaved for 5 min at
121°C

Antibiotics were added if needed in the following concentrations:

Ampicillin: 100 µg/ml

Kanamycin: 50 µg/ml

Gentamycin: 50 µg/ml

S. cerevisiae:

S. cerevisiae was cultivated in Synthetic Dropout (SD) or YPD medium. To induce sporulation GNA pre-sporulation medium and SPOR medium was used.

solution	composition
YPD medium	2.5 % (w/v) Bacto peptone 1,25 % (w/v) Bacto Yeast extract 2.0 % (v/v) glucose (added after autoclaving) 1.3 % (w/v) Bacto Agar (for solid medium) In H ₂ O _{bid.} Sterilization: autoclaved for 5 min at 121°C
Synthetic Dropout medium	0.5 % (w/v) amino acid mix 1.7 % (w/v) Yeast nitrogen base w/o amino acids 2.0 % (v/v) glucose (added after autoclaving) 1.3 % (w/v) Bacto Agar (for solid medium) in H ₂ O _{bid.} adjust pH to 5.8 Sterilization: autoclaved for 5 min at 121°C
Synthetic Dropout medium w/o Mg	0.5 % (w/v) amino acid mix 1.7 % (w/v) Yeast nitrogen base w/o amino acids and magnesium 2.0 % (v/v) glucose (added after autoclaving) 1.3 % (w/v) Bacto Agar (for solid medium)

	in H ₂ Obid. adjust pH to 5.8
	Sterilization: autoclaved for 5 min at 121°C
Amino acid mix for SD medium,	4.2 % (w/w) Alanine
	4.2 % (w/w) Lysine
Amino acids used for selection	4.2 % (w/w) Arginine
were not added to the mix.	4.2 % (w/w) Phenylalanine
	4.2 % (w/w) Asparagine
	4.2 % (w/w) Proline
	4.2 % (w/w) Aspartate
	4.2 % (w/w) Serine
	4.2 % (w/w) Cysteine
	4.2 % (w/w) Threonine
	4.2 % (w/w) Glutamine
	4.2 % (w/w) Tyrosine
	4.2 % (w/w) Glutamate
	4.2 % (w/w) Uracile
	4.2 % (w/w) Glycine
	4.2 % (w/w) Valine
	4.2 % (w/w) (myo)-inositol
	4.2 % (w/w) Isoleucine
	4.2 % (w/v) Histidine
	8.5 % (w/v) Leucine
	4.2 % (w/v) Methionine
	4.2 % (w/v) Tryptophane
	1.1 % (w/v) Adenine
	0.42 % (w/w) 4-Aminobenzoic acid
	The powder was mixed overnight on a wheel at 4 °C and stored at 4 °C.
GNA pre sporulation medium	1.0 % (w/v) Yeast-Extract (Difco)
	3.0 % (w/v) Nutrient broth (Difco)
	5.0 % (w/v) Glucose
	2.0 % Bacto agar
	in H ₂ Obid.
	Sterilisation: autoclaved for 5 min at 121°C

SPOR medium	1.0 % (w/v) Potassium acetate 0.005 % (w/v) Zinc acetate 0.2 % (v/v) Uracil 0.2 % (v/v) Histidine 0.3 % (v/v) Leucine in H ₂ Obid. Sterilisation: autoclaved for 5 min at 121°C add amino acids after autoclaving
-------------	---

***T. thlaspeos*:**

T. thlaspeos was cultivated in YL- or YMPG liquid or solid medium:

solution	composition
CM (complete medium)	0.25 % (w/v) Casein-hydrolysate 0.1 % (w/v) yeast extract 1.0 % (v/v) Vitamin-solution (Holliday et al., 1974) 6.25 % (v/v) salt-solution (Holliday et al., 1974) 0.05 % (w/v) herring testis DNA 0.15 % (w/v) NH ₄ NO ₃ 1.0 % (v/v) glucose solution (added after autoclaving) in H ₂ Obid. For solid medium: 0.6 % plant agar / 2.0 % bacto agar / 1.5 % phytigel Sterilisation: autoclaved for 5 min at 121°C
Vitamin solution (Holiday 1974)	0.1 ‰ (w/v) Thiamine 0.2 ‰ (w/v) Calcium pantothenate 0.05 ‰ (w/v) p-Amino benzoate 0.2 ‰ (w/v) Nicotinic acid 0.2 ‰ (w/v) Choline chloride

	<p>1.0 ‰ (w/v) myo-Inositol 0.05 ‰ (w/v) Riboflavin 0.05 ‰ (w/v) Pyridoxine in H₂O bid.</p> <p>Sterilisation: sterile filtration</p>
Salt solution (Holiday 1974)	<p>1.6 ‰ (w/v) KH₂PO₄ 0.4 ‰ (w/v) Na₂SO₄ 0.8 ‰ (w/v) KCl 0.4 ‰ (w/v) MgSO₄ x 7 H₂O 0.132 ‰ (w/v) CaCl₂ x 2 H₂O 0.8 ‰ (v/v) trace elements solution in H₂O bid.</p> <p>Sterilisation: autoclaved for 5 min at 121°C</p>
Trace element solution	<p>0.06 ‰ H₃BO₃ 0.14 ‰ (w/v) MnCl₂ · 4 H₂O 0.4 ‰ (w/v) ZnCl₂ 0.4 ‰ (w/v) Na₂MoO₄ · 2 H₂O 0.1 ‰ (w/v) FeCl₃ · 6 H₂O 0.04 ‰ (w/v) CuSO₄ · 5 H₂O in H₂O bid.</p> <p>Sterilisation: sterile filtration</p>
YL medium (YEPSlight)	<p>1.0 ‰ (w/v) Yeast-Extract (Difco) 0.4 ‰ (w/v) Bacto™-Peptone (Dico) 0.4 ‰ (w/v) Sucrose in H₂O bid.</p> <p>For solid medium: 0.6 ‰ plant agar / 2.0 ‰ bacto agar / 1.5 ‰ phytigel</p> <p>Sterilisation: autoclaved for 5 min at 121°C</p>
YMPG REG medium	<p>0.3 ‰ (w/v) Yeast-Extract (Difco) 0.3 ‰ (w/v) malt extract 0.5 ‰ (w/v) Bacto-Peptone (Difco) 1.0 ‰ glucose</p>

1 M sucrose

0.6 % plant agar (Duchefa)

in H₂O bid.

Sterilisation: autoclaved for 5 min at 121°C

Antibiotics were added if needed:

Hygromycin: 10 µg/ml

Nourseothricin: 50 µg/ml

Carboxin: 100 µg/ml

G418: 500 µg/ml

***U. maydis*:**

U. maydis was cultivated in CM-, YL- liquid or solid medium (see composition in *T. thlaspeos*) or Regeneration medium light (REGlight).

solution	composition
REGlight (Schulz et al. 1990)	1,5 % (w/v) Bacto Agar 1 M Sorbitol In YL medium Sterilisation: autoclaved for 5 min at 121°C

Antibiotics were added if needed in the following concentrations:

Hygromycin: 200 µg/ml

Nourseothricin: 150 µg/ml

Carboxin: 2 µg/ml

Plants:

A. thaliana, *Ar. hirsuta* or *Ar. alpina* was cultivated on soil or in liquid ½ MSN medium.

solution	composition
½ MSN medium	2.2 g/l Murashig & Skoog medium (Duchefa) 1 % (w/v) sucrose adjust pH to 5.7 Sterilisation: autoclaved for 5 min at 121°C

5.1.1.3 Enzymes

Enzymes used in this work are listed in Tab 5.1.

Table 5-1 Enzymes used in this work.

Enzyme	supplier
Lysozyme	Thermo Fisher Scientific
Phusion polymerase	New England Biolabs
Restriction enzymes	New England Biolabs
Rnase A	Boehringer Ingelheim
Taq-DNA-Polymerase	In house preparation
T4-DNA-Ligase	New England Biolabs
Quick T4 DNA-Ligase	New England Biolabs
Yatalase	Takara
Glucanex	Sigma

5.1.1.4 DNA ladders

λPstI: genomic λ phage DNA (purchased from Thermo Scientific) restricted with PstI.

2-Log DNA Ladder (0.1 – 10.0 kb): purchased from New England Biolabs.

GeneRuler 1 kb DNA Ladder: purchased from Thermo Fisher Scientific.

GeneRuler 50 bp DNA Ladder: purchased from Thermo Fisher Scientific.

5.1.1.5 Kits

NucleoSpin Plasmid (NoLid) (Macherey-Nagel; Düren, Germany)
 Monarch® DNA Gel Extraction Kit (New England Biolabs; Ipswich, UK)
 Monarch® PCR & DNA Cleanup Kit (New England Biolabs; Ipswich, UK)
 TOPO-TA cloning Kit with pCRII Vector (Thermo Fisher Scientific)
 Zero Blunt TOPO-PCR cloning Kit with pCR Blunt II vector (Thermo Fisher Scientific)
 GeneArt™ Gibson Assembly HiFi Master mix (Thermo Fisher Scientific)
 PCR DIG Labeling Mix (Roche)
 CDP Star® (Roche)
 QIAGEN Plasmid Midi Kit (Qiagen; Hilden, Germany)

5.1.2 Oligonucleotides

The oligonucleotides used or generated in this work are listed in Table 5-2. Oligonucleotides used for sequencing are not included. The oligonucleotides were purchased from Metabion (Martinsried), Integrated DNA Technologies Inc. (Coralville) or Merck (Darmstadt).

Table 5-2 Designation and sequence details of oligonucleotides used in this work.

Number	Name	Sequence
AB490	Um pit1 BamHI F	CGCGGATCCGCGATGGAGCGTCACGATGGTG
AB491	Um pit1 Sall R	ACGCGTCGACGTCTGAACATGTATGGGGCCGGAAG
AB493	Sc alr1 BamHI F	CGCGGATCCC GCGATGTCATCATCCTCAAG
AB494	Sc alr1 Sall R	ACGCGTCGACGTCTGTCGTAGCGGCTATATC
AB495	Tt pit1 SmaI F	TCCCCCGGGGGAACCTTCTGCCCTGAGCGAG
AB496	Tt pit1 XbaI-R	CTAGTCTAGACTAGATGGTCCGACACGACGGC
AB497	UMAG00361 Sall R	ACGCGTCGACGTCTGAAATGCGAACGCTCCAGATAC
AB498	UMAG00361 XbaI F	CTAGTCTAGACTAGATGTCGTCTGCCACAGCAG
CD112	UMAG00361 alr1-P1	CGCACCGAAATCCGACATTG
CD113	UMAG00361 alr1-P2	ATGCGAACGCTCCAGATACC
CD276	kanMX4 F	ACTGTCTGCGCCGTACATTTAG
CD277	kanMX4 R	ATGCTTGATGGTCCGGAAGAG
CD278	promoter Sc alr1 F	TGCCGTAATACATGGGACTC
CD391	Um egfp-HYGR Gibson F	CGCATGCCAACGCGGCCACCATGGTGAGCAAGGG
CD392	Um eGFP-HygR Gibson R	CTTCGCAATCACGCAAGGCCACTCAGGCCTATTAATG
CD393	Um Alr1 Gibson F	TCAAGCAACCGGCCTAGAATGTCGTCTGCCACAGCAG
CD394	Um Alr1-Gibson R	TGGCCGCGTTGGCATGCGAACGCTCCAGATACCTCGTAG
CD56	UmAlr1 U2	GGTCTCGCCTGCAATATTCGATTCACATGGCCGAG
CD57	UmAlr1 U3	GGTCTCCAGGCCGTTGCTTGACAAAAGATCTCG
CD58	UmAlr1 D1	GGTCTCCGGCCTTGCGTGATTGCGAAGC

CD582	MgtE-XbaI F	CGCTCTAGAATGGTCAACGCGTCACCTCC
CD583	MgtE-EcoRI R	ATAGAATTCAAGACCCCGTGACCAG
CD584	UMAG01797-XbaI F	CGCTCTAGAATGTCTCGACAGTTGCAACAATC
CD585	UMAG01797-XmaI R	CAGCCCGGGTCGACGGCTGTAGCCCAATCTTGAC
CD586	UMAG02316-XbaI F	CGCTCTAGAATGGAGATGCTCTCGTCCAGTC
CD587	UMAG02316-XmaI R	CAGCCCGGGTGTGTGTGAGTCCGATTGCGATCGAGAATCAG
CD588	UMAG02993-XbaI-F	CGCTCTAGAATGCTGCTATGGACACTGGTAAC
CD589	UMAG02993-XmaI-R	ATACCCGGGCTTGCCGGTCTCGTAATGTG
CD59	UmAlr1 D2	GGTCTCGCTGCAATATTCAGCCCCAGTGAATGG
CD590	UMAG03028-XbaI F	CGCTCTAGAATGTGACCGTAAGCATTGATGG
CD591	UMAG03028-XmaI R	ATTCCCGGGTCTCCCGTCCGCATCTG
CD592	UMAG00219 UF U2	GCGGCTCTCCGTGAATATTTGATTACAGCGGAGCGGACAAAC
CD593	UMAG00219 UF U3	ATAGCTCTCCGGCGGATCGCTGGCAAGATATTGG
CD594	UMAG00219 DF D1	CGCGCTCTTACCTTACACAACGTTCTGTTCCATTC
CD595	UMAG00219 DF D2	TCAGCTCTCCGACAATATTCGGAATGGCATGAGGCGTCCGATAC
CD598	Umalr1-NotI R	ATTGCGGCCGCTCAATGCGAACGCTCCAGATACC
CD599	Umalr1-Ascl F	ATAGGCGCGCCTCGTCGCCACAGCAGTACCATC
CD600	UmMNR2-NotI R	ATTGCGGCCGCTACCTTGC GGCACTCCTGTG
CD601	mnr2-Ascl F	ATAGGCGCGCCTCTGACTTAGCTCCTCTGCACATG
CD678	mnr2 UF U2 F	GGTCTCGCCTGCAATATTTGCCGTGATTTTTCCAAGAGG
CD679	mnr2 UF U3 R	GGTCTCCAGGCCATTGGTTGCGCTTCCCTCGACTG
CD680	mnr2 DF D1 F	GGTCTCCGGCCAGTACAACGCCCATGTCTCG
CD681	mnr2 DF D2 R	GGTCTCGCTGCAATATTCACATAGCGTGTGCAGCTTG
CD682	mgte NotI R	ATTGCGGCCGCTCAAAGACCCCGTGACCAGCACCAG
CD683	mgte Ascl F	ATAGGCGCGCCGTCAACGCGTCACCTCCAAC
CD761	lpe10 UF U2 F	GCGGCTCTCCGTGAATATTCATGGCTCTGGCAGCGTACTC
CD762	lpe10 UF U3 R	ATAGCTCTCCGGCCCCCGTCTTGATCTCGAGTTCTG
CD763	lpe10 DF D1 F	CGCGCTCTTACCTTCCGCGCCGTGCCATCCGCCATGTTG
CD764	lpe10 DF D2 R	TCAGCTCTCCGACAATATTCAGCTCGACTTTAGCG
CD820	UMAG 10049 XbaI F	CGCTCTAGAATGTCTGACTTAGCTCCTCTGCAC
CD821	UMAG 10049 EcoRI R	ATAGAATCCCTTGCGGCACTCCTGTGCG
DD870	Bra264 F	ACATGGTGCTGGATGTTTGA
DD871	Bra264 R	CGATGTCTCTGAGTGTACCAT
MB167	Tt GAPDH tt02826 1 FRW	GCATCGCCCTCAACGAGAAC
MB168	Tt GAPDH tt02826 1 REV	GTCCTTCTGGGCCATGAAGC
MB813	U2-UM-Pit1-F	GGTCTCGCCTGCAATATTGCACGGGAGCAGCTACTGTG
MB814	U3-UM-Pit1-R	GGTCTCCTCCGCCTTGACCAACTTGCTACGATGG
MB815	G1-TT-Pit1-F	GGTCTCCCGGAATGGTCCGACACGACGGCAG
MB821	D1-UM-Pit1-F	GGTCTCCGGCCTCAATCCGTGTAGTCGTGCCTGTG
MB822	D2-UM-Pit1-R	GGTCTCGCTGCAATATTCCTCTTTGACGTGGGCTCATG
MB865	G1-UM-Pit1-F	GGTCTCCCGGAATGGAGCGTCACGATGGTGAAG
UM210	Um pit1 NcoI rev	TGAACCTGTGGCCGTTTACGTC
UM211	Um pit1 XmaI for	GTCACCCGGGATGGAGCGTCACGATGGTGAAGAG
UM212	Tt pit1 XmaI for	GACTCCCGGGATGGTCCGACACGACGGCAGCGAGCTCATA
UM213	G1-Tt-pit1 wo introns-R	GGTCTCGCAGCTGCACGATGATGGTGAC
UM214	G2-Tt-pit1-wo introns-F	GGTCTCGGCTGACGGGGTCCCGAATAGCAG
UM215	G2-Tt-pit1-wo introns-R	GGTCTCGTCTATAGTAGTTGTTGACTGCCAGCCGGTCAG

UM252	G2-TT-Pit1-R new	GGTCTCGACAGACCGTTGGGGAGGAGGAC
UM253	G3-TT-Pit1-F new	GGTCTCGCTGTGCGCCGCGATCGACG
	G3-Tt-pit1-wo introns-F	
UM254	new	GGTCTCGTAGAACGCCCGTCCTCCTCCCAACGGTCTGTG
UP272	G3-TT-Pit1-R new	GGTCTCCTGGCACTTCTGCCCTGAGCGAGTCGAGTTTC
UP301	Tt Pit1 900 cDNA	CCGCCTACGATGTGGACAAC
UP303	Tt Pit1 cDNA 4296 R	GGTTGCGCATCTAACTTCTG
UP43	G2-UM-Pit1-R new	GGTCTCGTGGCCATGTATGGGGCCGGAAGGG
UP772	G2F Umpit1 GLQ to AAA	GGTCTCGCAGATCGTGGTTCGCGGCCGCTATGTTGATCGGCGAGCAGG
UP773	G1R UmPit1 GLQ to AAA	GGTCTCGTCTGGATCGCGATCGAAGTAATGTG

5.1.3 Plasmids

Table 5-3 Designation and description of plasmids used or generated in this work.

Plasmid	Number	Purpose	<i>E. coli</i> resistance	<i>U. maydis</i> resistance	<i>U. maydis</i> insertion locus	Referenz
pCR®II-Topo	-	Storage vector for TOPO TA cloning of PCR products with help of the type I Topoisomerase; possibility of blue-white selection for correct insertion.	AmpR KanR	-	-	
pDestI	pUMa1467	destination vector for Bsal Golden Gate cloning	AmpR	-	-	Terfrüchte <i>et al.</i> , 2013
pStorI	pUMa1507	storage vector for HygR cassette with Bsal and SfiI sites	GentR	HygR	-	Terfrüchte <i>et al.</i> , 2013
PStorII	pUMa1546	storage vector for egfp-HygR cassette for C-terminal fusion with Bsal and SfiI sites	GentR	HygR	-	Terfrüchte <i>et al.</i> , 2013
PStorIII	pUMa1694	storage vector for egfp-NatR cassette for C-terminal fusions with Bsal sites	GentR	NatR	-	Carl Haag
pDestII	pUMa2074	destination vector for SapI Golden Gate cloning	AmpR	-	-	Kira Müntjes
PStorIV	pUMa2242	storage vector for HygR cassette with SapI and SfiI sites	GentR	HygR	-	Kira Müntjes
p123-Potef-Exg1G	pUMa3115	backbone was used for C-terminal Gfp-fusions constructs in pUMa3879, 3881 and 3882	AmpR	CbxR	<i>IPS</i>	Philipp Rink
Potef-egfp-idi1-Tnos_cbxR	pUMa4121	backbone was used for N-terminal Gfp-fusions constructs in pQL57,	AmpR	CbxR	<i>IPS</i>	Jungho Lee

		58, 63				
UmPit1-GLQ to AAA-GFP_NatR_Bsal_destination	pUMa3624	expression of <i>Umpit1-gfp</i> with mutated GLQ motif in the native locus	AmpR	NatR	<i>pit1</i>	this study
Potef_Ttpit1_wo introns_egfp_Tnos_Cbx	pUMa3879	expression of <i>Ttpit1-gfp</i> in the <i>IP^S</i> locus under control of the constitutive P _{otef} promoter	AmpR	CbxR	<i>IP^S</i>	this study
Potef_Umpit1_GLQ to AAA_egfp_Tnos_Cbx	pUMa3880	expression of <i>Umpit1-gfp</i> with mutated GLQ motif in the <i>IP^S</i> locus under control of the constitutive P _{otef} promoter	AmpR	CbxR	<i>IP^S</i>	this study
Potef_Umpit1-egfp_Tnos_Cbx	pUMa3881	expression of <i>Umpit1-gfp</i> in the <i>IP^S</i> locus under control of the constitutive P _{otef} promoter	AmpR	CbxR	<i>IP^S</i>	this study
TtPit1-wo_introns-GFP_NatR_Bsal_destination	pUMa3882	expression of <i>Ttpit1-gfp</i> without introns in the native <i>Umpit1</i> locus;	AmpR	NatR	<i>IP^S</i>	this study
TtPit1-new-GFP_NatR_Basl_destination_new	pUMa3894	expression of <i>Ttpit1-gfp</i> with introns in the native <i>Umpit1</i> locus;	AmpR	NatR	<i>pit1</i>	this study
Um_alr1D_NatR_pDest	pUMa4758	Knockout of the UMAG_00361 ORF with a NatR cassette via homologues recombination	AmpR	NatR	<i>alr1</i> UMAG_00361	this study
Um_alr1D_HygR_pDest	pUMa4773	Knockout of the UMAG_00361 ORF with a HygR cassette via homologues recombination	AmpR	HygR	<i>alr1</i> UMAG_00361	this study
Alr1D UmAlr1-GFP_HygR_Bsal_destination	pUMa4785	Knockin of <i>alr1-gfp</i> (UMAG_00361) with a HygR cassette via homologues recombination (counter selection)	AmpR	HygR	<i>alr1</i> UMAG_00361	this study
UMAG_00219D_HygR_pDest	pQL56	Knockout of the UMAG_00219 ORF with a HygR cassette via homologues recombination	AmpR	HygR	<i>mgtE</i> UMAG_00219	this study
potef_egfp-alr1_Cbx	pQL57	expression of <i>Umegfp-alr1</i>	AmpR	CbxR	<i>IP^S</i>	this study

		(UMAG_00361) in the <i>IP^S</i> locus under control of the constitutive P _{otef} promoter				
potef_egfp-mnr2_Cbx	pQL58	expression of <i>Umegfp-mnr2</i> (UMAG_10049) in the <i>IP^S</i> locus under control of the constitutive P _{otef} promoter	AmpR	CbxR	<i>IP^S</i>	this study
mnr2-TOPO	pQL60	storage of the mnr2 ORF (UMAG_10049) in pCR®II-Topo	AmpR; KanR	-	-	this study
Ummnr2D_hygR_pDest	pQL62	Knockout of the UMAG_10049 ORF with a HygR cassette via homologues recombination	AmpR	HygR	<i>mnr2</i> UMAG_10049	this study
potef_egfp-mgte_Cbx	pQL63	expression of <i>Umegfp-mgtE</i> (UMAG_10049) in the <i>IP^S</i> locus under control of the constitutive P _{otef} promoter	AmpR	CbxR	<i>IP^S</i>	this study
UM_lpe10D_hygR_pDest	pQL64	Knockout of the UMAG_10884 ORF with a HygR cassette via homologues recombination	AmpR	HygR	<i>lpe10</i> UMAG_10884	this study
Ummnr2D_NatR_pDest	pQL65	Knockout of the UMAG_10049 ORF with a NatR cassette via homologues recombination	AmpR	NatR	<i>mnr2</i> UMAG_10049	this study
Plasmid	Number	Purpose	<i>E. coli</i> resistance	<i>S. cerevisiae</i> auxotrophy marker		Reference
pUG23_UMAG_01797-egfp	pQL51	transient expression of UMAG_01797-egfp under the constitutive P _{MET25} promoter in <i>S. cerevisiae</i>	AmpR	HIS		this study
pUG23_UMAG_02316-egfp	pQL52	transient expression of UMAG_02316-egfp under the constitutive P _{MET25} promoter in <i>S.</i>	AmpR	HIS		this study

		<i>cerevisiae</i>			
pUG23_UMAG_02993-egfp	pQL53	transient expression of UMAG_02993-egfp under the constitutive P _{MET25} promoter in <i>S. cerevisiae</i>	AmpR	HIS	this study
pUG23_UMAG_03028-egfp	pQL54	transient expression of UMAG_03028-egfp under the constitutive P _{MET25} promoter in <i>S. cerevisiae</i>	AmpR	HIS	this study
pUG23_UMAG_00219-egfp	pQL55	transient expression of UMAG_00219-egfp under the constitutive P _{MET25} promoter in <i>S. cerevisiae</i>	AmpR	HIS	this study
pUG23_Um_pit1_gfp	pUMa4486	transient expression of Um pit1-egfp (UMAG_2222) under the constitutive P _{MET25} promoter in <i>S. cerevisiae</i>	AmpR	HIS	this study
pUG23_Um_pit1_GLQ_gfp	pUMa4487	transient expression of mutated Um pit1-egfp (UMAG_2222) under the constitutive P _{MET25} promoter in <i>S. cerevisiae</i>	AmpR	HIS	this study
pUG23_Tt_pit1_gfp	pUMa4488	transient expression of Tt pit1-egfp under the constitutive P _{MET25} promoter in <i>S. cerevisiae</i>	AmpR	HIS	this study
pUG23_Um_alr1_gfp	pUMa4489	transient expression of UMAG_00361-egfp (alr1) under the constitutive P _{MET25} promoter in <i>S. cerevisiae</i>	AmpR	HIS	this study
pUG23_Sc_alr1_gfp	pUMa4512	transient expression of Sc alr1-egfp (YOL130w) under the constitutive P _{MET25} promoter in <i>S. cerevisiae</i>	AmpR	HIS	this study

pUG23	pUMa4780	transient expression C-terminal egfp fusions under the constitutive P _{MET25} promoter in <i>S. cerevisiae</i>	AmpR	HIS	AG Hegemann, HHU
-------	----------	---	------	-----	------------------

5.1.4 Strains/Lines

E. coli:

For all transformations the strain *E. coli* TOP10 (Life Technologies) was used. This strain is a derivative of *E. coli* K12 with the following genotype: F⁻, *mcrA*, (*mrr-hsdRMSmcrBC*), *80lacZM15*, *lacX74*, *deoR*, *recA1*, *araD139*, (*ara-leu*) 7697, *galU*, *galK*, *rpsL* (St_R), *endA1*, *nupG*.

S. cerevisiae:

A heterozygous *ALR1/alr1Δ* strain in BY4743 background was purchased from Euroscarf and a haploid *alr1Δ* strain was generated using random sporulation.

Table 5-4 Designation and description of *S. cerevisiae* strains used or generated in this work.

Strain	Genotype	Number	Locus	Progenitor strain	integrated plasmid pUMa	Reference
BY4743 <i>alr1/ALR1</i>	<i>MATa/MATa; ura3Δ0/ura3Δ0;</i> <i>leu2Δ0/leu2Δ0;</i> <i>his3Δ1/his3Δ1;</i> <i>met15Δ0/MET15;</i> <i>LYS2/lys2Δ0;</i> <i>YOL130w/YOL130w::kanMX4</i>	UMa3404	-	-	-	Euroscarf
BY4743 <i>alr1Δ</i>	<i>MAT α; ura3Δ0; leu2Δ0;</i> <i>his3Δ1; met15Δ0/MET15?;</i> <i>LYS2/lys2Δ0?;</i> <i>YOL130w::kanMX4</i>	UMa3436	-	UMa3404	-	this study
CEN.PK2-1C	<i>MATa ura3-52 HIS3-Δ1 leu2-3, 112 trp1-89, MAL2-8c SUC2</i>	-	-	-	-	Euroscarf (Van Dijken <i>et al.</i> , 2000)

T. thlaspeos:

In liquid culture the strains LF1 and LF2 were used. For infections spore material from Lab infected *Arabis hirsuta* plants was used (RK2018 spores [Ronny Kellner harvested 1.18 and 08/18]).

Table 5-5 Designation and description of *T. thlaspeos* strains used or generated in this work.

Strain	Genotype	Number	Locus	Progenitor strain	integrated plasmid pUMa	Reference
<i>Thecaphora thlaspeos</i> LF1 (a1b1)	wt	UMa2019	-	-	-	Frantzeskakis <i>et al.</i> , 2017
<i>Thecaphora thlaspeos</i> LF2	wt	UMa2020	-	-	-	Frantzeskakis <i>et al.</i>

(a2b2)						<i>al.</i> , 2017
Tt LF1_Δpra1_hpt	<i>pra1Δ</i>	UMa3155	<i>pra1</i>	UMa2019	3866	Plücker <i>et al.</i> , 2021
LF2_hpt-mcherry	<i>mcherry</i>	UMa2750	ectopic	UMa2020	3576	Plücker <i>et al.</i> , 2021
<i>T. thlaspeos</i> LF1_hpt-gfp - greenT	<i>egfp</i>	UMa2478	ectopic	UMa2019	2790	Plücker <i>et al.</i> , 2021

U. maydis:

All strains used in this work are listed below. Recombination into the intended locus was confirmed for all strains generated in this work by Southern blot analysis.

Table 5-6 Designation and description of *U. maydis* strains used or generated in this work.

Strain	Genotype	Number	Locus	Progenitor strain	integrated plasmid	Reference
SG200_alr1D_Potef: Umalr1-egfp_Tnos	<i>alr1Δ alr1-gfp</i>	QL0001	UMAG_0036 1	UMa3434	pQL0032	Peter Wegjan
SG200_mgteD_Phsp70 HygR_Thsp70	<i>mgtED</i>	QL0015	UMAG_0021 9	SG200	pQL56	this study
UMa3434_potef_egfp-alr1_Cbx	<i>alr1D egfp-alr1</i>	QL0016	UMAG_0036 1	UMa3434	pQL57	this study
SG200_potef_egfp-mn Cbx	<i>egfp-mnr2</i>	QL0017	UMAG_1004 9	SG200	pQL58	this study
SG200_mnr2D	<i>mnr2D</i>	QL0019	UMAG_1004 9	SG200	pQL62	this study
SG200_mgetD_potef_egfp-mgte_Cbx	<i>mgtED egfp-mgte</i>	QL0020	UMAG_0021 9	QL0015	pQL63	this study
SG200_lpe10D	<i>lpe10D</i>	QL0021	UMAG_1088	SG200	pQL64	this study
SG200_mnr2D_potef_egfp-mnr2_Cbx	<i>mnr2D egfp-mnr2</i>	QL0022	UMAG_1004 9	QL19	pQL58	this study
SG200Δpit1	<i>pit1Δ</i>	UMa222 2	UMAG_0137 4	-	-	(Doehlema nn <i>et al.</i> , 2011)
SG200pit1-GFP_NatR	<i>pit1-egfp</i>	UMa222 5	UMAG_0137 4	UMa2222	pUMa3274	Lesley Plücker

SG200	pit1-GLQ-AAA- GFP_NatR	<i>pit1^{GLQ3A}-egfp</i>	UMa255 6	UMAG_0137 4	UMa2222	pUMa3624	this study
SG200	Potef_Tpit1_w/ introns_egfp_Tnos_Ct	<i>pit1DTt pit1-egfp</i>	UMa293 0	<i>IP^S</i>	UMa2222	pUMa3879	this study
SG200	Potef_Umpit1_ GLQ to AAA_egfp_Tnc	<i>pit1D pit1^{GLQ3A}- egfp</i>	UMa293 1	<i>IP^S</i>	UMa2222	pUMa3881	this study
SG200	Potef_Umpit1- egfp_Tnos_Cbx	<i>pit1D pit1-egfp</i>	UMa293 2	<i>IP^S</i>	UMa2222	pUMa3881	this study
SG200	TtPit1-wo_intron -GFP_NatR	<i>Tt pit1-egfp</i>	UMa293 3	UMAG_0137 4	UMa2222	-	this study
SG200	alr1D_hygR	<i>alr1Δ</i>	UMa340 7	UMAG_0036 1	UMa67	pUMa4773	this study
SG200	alr1D_NatR	<i>alr1Δ</i>	UMa343 4	UMAG_0036 1	UMa67	pUMa4758	this study
UMa2222	alr1D_NatR	<i>alr1Δ pit1Δ</i>	UMa343 5	UMAG_0036 1	UMa2222	pUMa4758	this study
SG200	alr1D-gfp_hygF	<i>alr1-gfp</i>	UMa344 1	UMAG_0036 1	UMa3434	pUMa4785	this study
SG200	alr1D_NatR_pit	<i>alr1Δ pit1Δ pit1- egfp</i>	UMa344 2	<i>IP^S</i>	UMa3435	pUMa3881	this study
SG300	3xGFP	<i>egfp</i>	UMa587	<i>IP^S</i>	-	-	Stephan Genin
SG200		<i>a1 mfa2 bWe bE1</i>	UMa67	-	-	-	(Kämper <i>et al.</i> , 2006)

Plants:

In this work the seeds of *A. thaliana*, *Ar. hirsuta*, *Ar. alpina* and *Z. mays* were used for infection experiments with *T. thlaspeos* spores or *U. maydis*.

Table 5-7 Seeds used in this work.

Plant ID	Species	Name	Ecotype	Source
At0001	<i>A. thaliana</i>	Col-0	Col-0	AG Weber HHU 2010

At0019	<i>A. thaliana</i>	COLORFUL-PR1pro	Col-0	Ghareeb <i>et al.</i> , 2020
Ah0005	<i>Ar. hirsuta</i>	Ah Slovenia 2012	Slovenia	Collection 2012
Ah0004	<i>Ar. hirsuta</i>	Ah Hohe Leite 2015	Hohe Leite	Collection 2015
Ah0003	<i>Ar. hirsuta</i>	Ah Bad Berneck 2015	Bad Berneck	Collection 2015
Ah0002	<i>Ar. hirsuta</i>	Ah Ronheim 2015	Ronheim	Collection 2015
Aa0001	<i>Ar. alpina</i>	<i>Arabis alpina</i> Pajares	Pajares	MPIPZ Köln George Coupland
Zm0001	<i>Z. mays</i>	Golden Bantham	Golden Bantham	Bingenheimer Saatgut, April 2021
Zm0007	<i>Z. mays</i>	Amadeo	Amadeo	KWS 2017

5.2 Microbiologic, cell biologic and genetic methods

5.2.1 *Escherichia coli*

5.2.1.1 Culture conditions

E. coli was cultivated in the media mentioned above at 37°C under aerobic conditions. Liquid cultures were incubated in Erlenmeyer flasks at 110 rpm or in test tubes on a rotating wheel.

5.2.1.2 Measuring optical density of cell cultures

The optical density of cell cultures was obtained by measuring absorption at 600 nm. Therefor cultures were diluted within a range 0.1 -1.0. An OD₆₀₀ = 1.0 equals roughly 10⁹ cells/ml.

5.2.1.3 Transformation of competent *E. coli* cells

Competent *E. coli* TOP10 cell were readily available in the lab. Those were prepared according to a modified protocol from Cohen *et al.* (1972). For transformation 50 µl aliquots stored at -80°C were thawed on ice for 10 min. Depending on the purpose of the transformation the competent cells were mixed with DNA according to the following ratios:

Retransformation	TOPO Cloning	Ligation	Golden-Gate Cloning
------------------	--------------	----------	---------------------

V DNA (μ l)	0.5	5	10	2
V <i>E. coli</i> (μ l)	15-50	50	50	50

Afterwards the cells were incubated for 30 min on ice, followed by heat shock for 45 sec at 42°C and 2 min on ice. 250 μ l dYT were added before the cells were incubated at 37°C and 1000 rpm for 30 – 60 min, depending on the antibiotic used for selection. If ampicillin was used 30 min were sufficient, while for Kanamycin or Gentamycin 60 min were necessary. Later on the mixture was plated on YT selection plated containing the corresponding antibiotic. If a blue/white selection was done 60 μ l X-Gal (2 % in DMSO) were spread on the plates before. In the end the plates were incubated at 37°C overnight.

5.2.2 *Saccharomyces cerevisiae*

5.2.2.1 Culture conditions

S. cerevisiae cultures were cultivated in liquid or on solid media at 28 °C - 30 °C under aerobic conditions. Liquid cultures were incubated in baffled flasks at 200 rpm or in test tubes on a rotating wheel. Colonies on plates were kept up to six weeks at 4°C and used to inoculate liquid cultures.

5.2.2.2 Measuring optical cell density

The optical cell density of liquid cultures was obtained by measuring absorption at 600 nm. Cultures were diluted to obtain values between 0.1-1.0. An OD₆₀₀ of 1.0 equals roughly 2x10⁷ cells/ml.

5.2.2.3 Random sporulation assay

S. cerevisiae was grown on YPD. Cell material from fresh plates were patched on GNA pre-sporulation plates for one day at 30°C. The next day, cell material was repatched on a fresh GNA pre-sporulation plate for 1 day at 30°C. A small amount of cells was resuspended in 2 ml freshly prepared sporulation medium. The culture was incubated shaking for 5 days at 25°C followed by 3 days at 30°C. Afterwards the cultures may be stored up to 1 week at 4°C. To release the ascospores, the sporulation culture was centrifuged for 5 min at 5000 rpm. The pellet was resuspended in 1 mg/ml Zymolase in 1 M sorbitol and incubated for 20-30 min at 37°C. Then 500 μ l sterile MilliQ water was added and vortexed vigorously to break

up the tetrads. 10-fold serial dilutions were plated on YDP + 200 mM MgCl₂ and incubated for 2 days at 28°C. To select for *alr1D* strains, colonies were patched on SD medium supplemented with either 100 mM or 10 µM MgCl₂. Candidates growing at 100 mM MgCl₂ but not 10 µM were selected for further analysis.

5.2.2.4 Preparation of competent cells

S. cerevisiae was grown YPD plates. A preculture of 10 ml YPD + 200 mM MgCl₂ was inoculated with the respective strain and incubated O/N at 28°C on a rotating wheel. The next morning 100 ml YPD + 200 mM MgCl₂ were inoculated with the preculture to an OD₆₀₀ of 0.1 and grown until they reach an OD₆₀₀ between 0.5 and 0.7. The cells were collected by centrifugation for 5min at 500 x g. The pellet was washed with 20 ml water and centrifuged again. Then the pellet was washed with 10 ml HefeSORB, centrifuged and resuspended in 360 µl HefeSORB. 50 µl aliquots in 2 ml reaction tubes were stored at -80°C until transformation.

HefeSORB	TE-buffer	Salmon testis-DNA
10 mM Tris-HCl (pH 8,0)	10 mM Tris-HCl, pH 8,0	10 mg/ml Salmon testis-DNA (Sigma-Aldrich, D1626)
1 M Sorbitol	1 mM EDTA	In TE-Puffer, pH 8,0
100 mM LiOAc	In H ₂ O _{bid.} , autoclave	denaturated for 5 min at 95 °C and kept on ice for at least 5 min
1 mM EDTA (pH8,0)		
In H ₂ O _{bid.} ,		
adjust to pH 8.0 with acetic acid; sterile filter		

5.2.2.5 Transformation of competent cells

S. cerevisiae competent cells were thawed for 10 min on ice. Per 50 µl competent cells 1 µg plasmid DNA, 5 µl salmon testis DNA and 300 µl PEG in LiT were added. After 30 min incubation on a rotating wheel at RT, the cells were heat shocked for 15 min at 42°C and 700 rpm. Subsequently, the cells were kept for 2 min on ice and 600 µl YPD was added. The cells were pelleted for 5 min at 400 x g, washed with 1 ml YPD, centrifuged and again resuspended in 1 ml YPD. The cells were incubated for 1-4 h at 28°C on a rotating wheel before they centrifuged again, resuspended in 150

µl YPD and plated on SD-His + 100 mM MgCl₂. The plates were incubated for 2-4 days at 28°C until colonies appear.

LiT	PEG in LiT
100 mM Lithiumacetat	40 % (w/v) PEG 3350
10 mM Tris-HCl (pH 8,0)	100 mM Lithiumacetat
In H ₂ O _{bid.} , autoclave	10 mM Tris-HCl (pH 8,0)
	1 mM EDTA (pH 8,0)
	In H ₂ O _{bid.} , sterile filter

5.2.3 *T. thlaspeos*

5.2.3.1 Culture conditions

T. thlaspeos LF1 or LF2 cultures were incubated at 20°C under aerobic or anaerobic conditions in YL or YMPG medium. Liquid cultures were incubated in baffled flasks at 200 rpm. Culture on plates was incubated 4 to 6 weeks and stored at 4°C afterwards.

5.2.3.2 Measuring optical cell density

The optical density of cell cultures was obtained by measuring absorption at 600 nm. Therefor cultures were diluted within a range 0.1 -1.0.

5.2.3.3 Generation of transformable protoplasts

100 ml of YMPG or YL medium were inoculated with exponentially growing LF1 to an OD₆₀₀ of 0.075 in a 500 ml baffled flask and incubated 3-4 days at 20°C and 200 rpm until an OD₆₀₀ of 0.6 -0.8 was reached. Filaments were harvested by filtering through a 40µm pore size cell strainer and washed with citrate buffer and finally resuspended in 9 ml citrate buffer supplemented with 20 mg/ml Glucanex (Sigma) and 10 mg/ml Yatalase (Takara) and incubated for 30-60 min. Protoplast formation was controlled microscopically. The enzymatic reaction was stopped adding 15 ml of citrate buffer. Afterwards the protoplast solution was distributed in 6 ml aliquots in 15 ml centrifuge tubes. The protoplast solutions were overlaid with 5 ml trapping buffer each and centrifuged at 4863 x g and 4°C for 15 min in a swing out rotor. The interphase was collected from all tubes and diluted with 1-2 volumes of STC buffer. The protoplasts were pelleted for 10 min at 4863 x g and 4°C in a swing out rotor and resuspended in 500 µl of STC buffer. 100 µl aliquots were used for transformation directly.

solution	composition
citrate buffer	0.1 M trisodium citrate 2x H ₂ O 0.01 M EDTA 1.2 M MgSO ₄ In H ₂ O bidest. pH was adjusted to 5.8 with Citric acid solution Sterilisation: autoclaved for 5 min at 121°C
Citric acid solution	0.1 M citric acid 1.2 M MgSO ₄
Trapping buffer	0.6 M sorbitol 0.1 M Tris/HCl, pH 7.0
STC buffer	0.01 M Tris/HCl, pH 7.5 0.1 M CaCl ₂ 1 M sorbitol In H ₂ O bidest. Sterilisation: sterile filtration

5.2.3.4 Transformation of *T. thlaspeos*

Transformation of *T. thlaspeos* protoplasts was carried out exactly like *U. maydis* protoplast transformation (see 5.2.4.4). But instead of REGlight, the transformants were plated on YMPG Reg medium (30 ml/ plate) and the plates were grown at RT for several weeks until colonies appear.

5.2.3.5 Generation of *T. thlaspeos* spore batches

An *Arabidopsis hirsuta* silique from a plant infected with *T. thlaspeos* was opened inside a 1.5 ml reaction tube. Tweezers were used to release spore material from the silique, thus a brown powder was sticking to the tube surface. The spores were resuspended in 100 µl sterile water and diluted with the same volume of 3 % CuSO₄. The tube was incubated at RT for 15 min. After centrifugation (14.800 rpm, 2 min) the supernatant was removed and the spores were washed three times with sterile water (centrifugation 14.800 rpm, 2 min). Finally, the spores were resuspended in 200 ml water or ½ MSN medium. The concentration of the spores was determined using haemocytometer. The spores loose viability within a week and were thus always prepared freshly.

5.2.3.6 *T. thlaspeos* teliospores germination assay

To determine the germination rate of *T. thlaspeos* teliospores, 300 spores were mixed with 300 μ l *A. thaliana* Col-0 exudate in 24 well plates in triplicates and incubated for 7 days in the light chamber (settings according to *A. thaliana*: 21°C with 100 μ E for 12 h). $\frac{1}{2}$ MSN was used as instead of exudate as a negative control. To calculate the germination rate, pictures of the (germinating) spores on the bottom of the wells were taken with an inverse microscope (4x objectives). Germination was counted on a yes no basis for at least 100 spores and out of it a percentage germination rate was calculated.

5.2.4 *U. maydis*

5.2.4.1 Culture conditions

U. maydis strains were incubated at 28°C under aerobic conditions in the media indicated above. Liquid cultures were incubated in baffled flasks at 200 rpm or in test tubes on a rotating wheel. Cultures on plate were kept 4 weeks at 4°C at a maximum. To inoculate liquid cultures from plate, max. 2 week old colonies were used.

5.2.4.2 Measuring optical cell density

The optical density of cell cultures was obtained by measuring absorption at 600 nm. Therefor cultures were diluted within a range 0.1 -1.0. An OD₆₀₀ = 1.0 equals roughly 1x10⁷-5x10⁷ cells/ml.

5.2.4.3 Generation of transformable protoplasts

This protocol is a modified version from Schulz et al. (1990) and Gillissen et al. (1992). An *U. maydis* preculture in 3 ml CM was incubated for 24 h. Afterwards, 25 μ l preculture were used to inoculate 50 ml YL and incubated until an OD₆₀₀ of 0.6 -0.8 was reached. *U. maydis* cells were pelleted by centrifugation at 3000 rpm for 5 min. Then the cells were washed in 25 ml SCS and centrifuged again. To gain protoplasts the cells were resuspended in 4 ml SCS supplemented with 12 mg/ml Glucanex and incubated up to 15 min at RT. Protoplast formation was controlled microscopically. Subsequent steps were performed at 4°C. The enzymatic reaction was stopped using 10 ml cold SCS. Subsequently the protoplasts were pelleted for 5 min at 2400 rpm 4°C and washed two times with 10 ml SCS. The third wash was in 10 ml STC and finally the cells were resuspended in 1 ml STC. 100 μ l aliquots were stored at -

80°C or used directly for transformation. The quality of the protoplasts was controlled in a test transformation using a self-replicating plasmid.

solution	composition
SCS buffer	0.2 M trisodium citrate 2x H ₂ O 1.0 M sorbitol In H ₂ O bidest. pH was adjusted to 5.8 with Citric acid solution Sterilisation: sterile filtration
Citric acid solution	0.1 M citric acid 1.0 M sorbitol
STC buffer	0.01 M Tris/HCl, pH 7.5 0.1 M CaCl ₂ 1 M sorbitol In H ₂ O bidest. Sterilisation: sterile filtration

5.2.4.4 Transformation of *U. maydis* protoplasts

U. maydis protoplast aliquots were thawed on ice for up to 10 min. 1 µl heparin and 1-5 µg linearized plasmid DNA were added and incubated for 10 min on ice. Afterwards 500 µl STC/PEG were added and incubated for another 15 min on ice. Finally, the mix was spread on two top- bottom layer REGlight plates. The bottom layer consisted of REGlight supplemented with the corresponding double concentrated antibiotic and the top layer consisted only of REGlight. The plates were incubated for 5-9 days at 28°C until colonies appeared. Those colonies were singled out on CM plates supplemented with the corresponding antibiotic.

solution	composition
Heparin solution	15 mg/ml heparin In H ₂ O bidest. Sterilisation: sterile filtration
STC/PEG	15 ml STC 10 g PEG 4000

5.2.4.5 Analysis of growth on different media

For analysis of growth under different conditions precultures in YL supplemented with 50 mM MgCl₂ were inoculated with colony material of the respective *U. maydis* strains and incubated O/N at 28°C on a rotating wheel. The next morning, 20 ml of

YL + 50 mM MgCl₂ were adjusted to an OD₆₀₀ of 0.25 with the preculture and incubated until the cultures reach an OD₆₀₀ of 1. 1 ml of each culture was transferred into 2 ml reaction tubes and centrifuged at 3500 rpm for 5 min. The pellet was washed three times with YL and finally resuspended to an OD₆₀₀ of 0.5 in 200 µl. Serial dilution of 1 to 5 were prepared in a 96 well plate. 4 µl of each dilution were dropped on YL plates supplemented with different MgCl₂ concentrations. Depending on the experiment, heavy metals (MnSO₄, Co(NO₃)₂, ZnSO₄ or NiSO₄) in different concentrations according to MacDiarmid and Gardner (1998) and Pisat, Pandey and MacDiarmid (2009) or Hexaammino-cobalt(III)-trichloride (300, 400, 600, 800, 1000 µM) was additionally added. For analysis for filamentous growth the strains were dropped on SD medium supplemented with different MgCl₂ concentrations and 1 % charcoal. All plates were incubated at RT or 28°C until the drops were sufficiently grown. The growth morphology was documented using the ImageQuant LAS 4000 (GE Healthcare) for whole plate images and with a stereomicroscope Zeiss Stemi 2000C equipped with the light source Zeiss KL1500 LCD (Zeiss) for close up images of the colonies. Images from the stereomicroscope were taken using a Canon PowerShot A650 IS-camera (Canon GmbH, Krefeld).

5.2.4.6 Infection of *Zea mays* with *U. maydis* SG200 derivatives

A pre- and main culture of *U. maydis* strains were made as described earlier. When the cells reached an OD₆₀₀ of 1.0 the cells were harvested by spinning down with 3500 rpm for 5 min. Afterwards the cell pellet was washed three times with sterile H₂O. After the final centrifugation step the pellet was resuspended in sterile H₂O to an OD₆₀₀ of 3.0. The cells were kept on a horizontal rotator until used for infection. For each infection 8-day old maize cv. Amadeo or Golden Bantam seedlings were used. For each strain at least 20-50 plants were infected by injecting 250-500 µl cell suspension into the stem of the seedling roughly 1 cm above ground. The injection was successful if liquid emerged between the leaves arising from the stem. For MOCK controls water was injected into the maize stem. After 7 and 12 days of incubation the plants were scored for the infection symptoms (healthy plants, chlorosis, anthocyanins, lingual swellings, small tumours, large tumours, heavy tumours or dead plants).

5.2.5 *Zea mays*

5.2.5.1 Culture conditions

Zea mays cv. Amadeo plants were grown in standard soil in a phyto chamber with a night phase of 8 h, 60 % relative humidity and 20°C and a day phase for 16 h, 40 % relative humidity, 28°C and 600 μ E. *Zea mays* cv. Golden Bantam seeds were surface sterilized in 1 % bleach for 5 min, washed with water and then soaked in MilliQ water O/N. Subsequently the seeds were planted in standard soil and grown for 8 days under the same conditions as Amadeo plants.

5.2.5.2 Microscopy of *U. maydis* infected leaves

Maize leaves were harvested three to five days post infection. Leaf pieces 2 cm below the injection spots were examined using a confocal microscope (Zeiss LSM 780 or Leica SP8) using the DIC and GFP channel respectively. Editing of the pictures was done using the program ZEN 2012 (black version) or Leica LAS X.

5.2.5.3 WGA + PI staining

WGA/PI staining of maize leaves was performed according to Redkar, Jaeger and Doehlemann, 2018.

5.2.6 *Arabidopsis thaliana*/ *Ar. hirsuta* / *Ar. alpina*

5.2.6.1 Culture conditions

A. thaliana or *Arabis spec.* were cultivated either in 1/2 MSN medium supplemented with 1 % sucrose in well plates (96, 24, 6), solid 1/2 MSN medium supplemented with 1 % sucrose and 0.6 % plant agar or on soil. *A. thaliana* plants on soil were grown in a phyto chamber ambient humidity, 21°C and 120 μ E for 12 h (long day) or 8 h (short day) and 18°C during the night period. *Arabis* plants on soil were grown in a phyto chamber with ambient humidity, 22°C and 160 μ E for 16 h and 8 h at 18°C without light. *A. thaliana* and *Arabis* plants in liquid culture were grown in a light chamber at 21°C with 100 μ E for 12 h (18°C for 12 h without light). To induce germination *A. thaliana* seeds were vernalized for 2-7 days and *Arabis* seeds for 3-7 days at 4°C right after planting. *Arabis* plants on soil were grown for 12 weeks, then vernalized for 12 weeks at 4 °C and 8 h light from 60W standard light bulbs. Afterwards the plants were shifted back to *Arabis* growth conditions until plants set seeds. The plants were

fertilized once a week with Wuxal® fertilizer (NPK 8-8-6 and with trace elements, 0.2 % in tap water).

5.2.6.2 Liquid infection with *T. thlaspeos* spores

A. thaliana or *Arabidopsis* seeds were surface sterilized 2 times for 5 min with 1 ml 70 % (v/v) ethanol and 1x for 5 min with 1 ml 100 % ethanol in 1.5 ml reaction tubes. The sterile seeds were kept in ½ MSN medium. For infection 1 seed was mixed with 500 *T. thlaspeos* teliospores in a total volume of 200 µl for each well. As a MOCK control seeds were incubated only in ½ MSN medium. 96 well plates were sealed with parafilm vernalized at 4°C for 2-7 days and incubated in the light chamber for 3 weeks afterwards. To examine infection, seedlings were stained with WGA + PI and examined under a fluorescence microscope (10x objective) using the DIC, GFP and mCherry channel, respectively. WGA stained fungal material was detected in the GFP channel, PI stained plant tissue was visible in the mCherry channel.

5.2.6.3 Plate infection with *T. thlaspeos* spores

A. thaliana or *Arabidopsis* seeds were surface sterilized 2 times for 5 min with 1 ml 70 % (v/v) ethanol and 1x for 5 min with 1 ml 100 % ethanol in 1.5 ml reaction tubes. The seeds were washed with water to remove residual ethanol and directly vernalized in the tubes. The sterile seeds were then placed on ½ MSN plates supplemented with 1 % sucrose and 0.6 % plant agar or 1 % phytigel. The plates were incubated for 10 days in the light chamber. For infection *T. thlaspeos* teliospores were adjusted to a concentration of 1000 spores/µl in water and 0.0375 % silwet. 1 µl of spore solution was pipetted on two leaves per seedling and allowed to dry. The plates were sealed with Leucopor (BSN medical GmbH) and the lid was replaced with another bottom plate of a petri dish to provide more height for growth of the plants. Like that the plates were incubated for another 10-14 days. For microscopic analysis the inoculated leaves were cut off and stained for 1 min in 1 µg/ml Calcofluor White. Spore germination and formation of appressoria was observed under a fluorescent microscope (Zeiss Axiostar M1) using the DIC and DAPI channel. Frequently the leaves were afterwards placed in ethanol and stained with WGA/PI to examine potential infection of the leaf.

5.2.6.4 WGA + PI staining

Plant tissue was bleached in 100 % ethanol until completely white. Afterwards the ethanol was removed and the samples were boiled in 10 % KOH up to 60 min at

95°C until sufficient clearing of the tissue was achieved. Then the samples were washed in PBS and stained in PBS + 10 µg/ml PI and 5 µg/ml WGA for 30 min. Vacuum pressure was applied 2-3 times for 2 min during staining. Finally, the samples were washed again with PBS and then stored in PBS in the dark until microscopy imaging was done.

5.3 Molecular biologic methods

5.3.1 Isolation of nucleic acids

5.3.1.1 Isolation of plasmid DNA from *E. coli*

This protocol was done according to a modified version from Sambrook (1989). An *E. coli* colony was used to inoculate 1.75 ml dYT medium supplemented with the corresponding antibiotic in a 2 ml reaction tube and incubated at 37°C, 1000 rpm overnight. Cells were centrifuged at 8000 rpm for 2 min to harvest the cells. The supernatant was discarded and the pellets were resuspended in 200 µl STET buffer and 20 µl lysozyme. Afterwards the suspension was boiled for 60 sec at 95°C and then centrifuged for 10 min at 13.000 rpm. The pellet was subsequently removed with a tooth pick. To precipitate the DNA 20 µl Mini III (3 M sodium acetate pH 5.3) solution and 500 µl isopropanol were added to the remaining liquid. To mix the tube was inverted 6-10 times. Afterwards the DNA was pelleted by centrifugation for 10 min at 13.000 rpm. Then the DNA pelleted was washed with 300 µl 70 % ethanol and centrifuged again for 3 min at 13.000 rpm. Finally, the pellet was dried at 50°C for 3 min and resuspended in 100 µl TE/RNase at 50°C and 1000 rpm for 10 min.

STET	Lysozyme solution	TE/RNase A
50 mM Tris-HCl, pH 8.0	10 mg/ml lysozyme	10 mM Tris/HCl, pH 7.9
50 mM Na ₂ -EDTA	10 mM Tris-HCl, pH 8,0	1 mM Na ₂ -EDTA
8 % (w/v) sucrose	In H ₂ O _{bid} .	20 µg/ml RNase A
5 % (w/v) Triton x-100		In H ₂ O _{bid} .
In H ₂ O _{bid} .		

5.3.1.2 Isolation of genomic DNA from *U. maydis*

This method is based on a protocol by Bösch et al (2016). 5 ml CM or YL medium were inoculated with an *U. maydis* colony and incubated overnight at 28°C on a rotating wheel. When the culture was dense 4 ml of culture were centrifuged (13,000 rpm, 5 min). The pellet was resuspended in 200 µl Ustilago lysis buffer 2 and 200 µl glass beads were added. The samples were incubated for 15 min on a vibrax with 1500 rpm, followed by 20 min incubation at 65°C. The samples were kept 5 min on ice. Afterwards, 100 µl 8 M potassium acetate were added and mixed by inverting 8-10 times. Then the samples were centrifuged (13,000 rpm 15 min) and 500 µl supernatant were transferred into a new 1.5 ml reaction tube. 400 µl isopropanol were added mixed by inverting 8-10 times. Subsequently the DNA was pelleted by centrifugation (13,000 rpm 15 min). The supernatant was discarded and the pellet was washed with 500 µl 70 % ethanol. After another centrifugation step (13,000 rpm 5 min) the supernatant was removed and the pellet was dried for 3-5 min at RT. Finally, 50 µl TE/RNase were added and incubated for 15 min and 400 rpm at 50°C. Successful extraction was verified by running an aliquot of the samples on a gel. The samples were stored at – 20 °C.

5.3.1.3 Isolation of genomic DNA from *T. thlaspeos*

5-10 ml *T. thlaspeos* YL or YMPG liquid culture were used for extraction. Filaments were collected repeated centrifugation for 5 min at 13,000 rpm. The supernatant was discarded and 2 metal beads were added to the pellet. The samples were snap frozen in liquid nitrogen and smashed to a fine powder using a Retsch mill (30 beads/sec 5min). 200 µl Ustilago lysis buffer 2 and 200 µl glass beads were added and then treated according to the gDNA extraction described for *U. maydis* (5.3.1.2).

5.3.2 Working with nucleic acids

5.3.2.1 Measure the concentration

The concentration of nucleic acids was determined photometrically using a NanoDrop ND-2000c spectra photometer (Thermo Scientific). Absorption was measured at 260 nm. An OD₂₆₀ of 1.0 equals a concentration of 50 µg/ml for double stranded DNA and 40 µg/ml for RNA. For pure DNA a value of 1.8 was expected for the OD₂₆₀/OD₂₈₀ ration, while a value of 2.0 was expected for pure RNA.

5.3.2.2 Restriction digest

Each restriction digest was done using enzymes supplied from New England Biolabs. Reaction volume and DNA amount varied depending on the purpose. A standard mix for restrictions was:

Table 5-8 Standard reaction mix for restriction digests.

Component	volume (μ l)
Cutsmart Buffer NEB	2
DNA	1
Enzyme	0,2
H ₂ O	16,8
Σ	20

Table 5-9 Standard mix for digestion of DNA molecules for ligation.

Component	Volume (μ l)
Cutsmart Buffer NEB	2 or 3
DNA	PCR product or min. 1 μ g
Enzyme	1
H ₂ O	ad 20 or 30 μ l
Σ	20 or 30

The incubation of each reaction was carried out depending on the temperature optimum of each enzyme for at least 1 h for analytic reaction and 3 h – overnight for preparative reactions.

5.3.2.3 Gel electrophoresis of DNA fragments

DNA fragments were separated by size using gel electrophoresis. Gels were prepared in TAE buffer using agarose in concentrations between 0.8 – 2.0 % depending on the fragment size. Agarose was boiled in a corresponding volume of TAE buffer until completely dissolved and then stored at 60°C. Ethidium bromide or MIDORI Green (NIPPON Genetics EUROPE, Düren) was added to a final concentration of 1 μ g/ml or 5 % (v/v) respectively. Gels were made by pouring gel into

a gel tray and letting it solidify for 20 min. The gel was then placed into a gel chamber filled with TAE buffer. The sample were loaded into the pockets and were separated at 80-120V for 20 min – 2.5 h.

TAE (50x)	DNA loading dye
2 M Tris acetate	30 % (v/v) glycerol
100 mM Na ₂ -EDTA	0,4 % (w/v) bromophenol blue
In H ₂ O _{bid.}	In H ₂ O _{bid.}

5.3.2.4 Gel extraction of DNA fragments

Isolation of DNA fragments from agarose gels was done using the Monarch Gel extraction Kit (NEB) according to the user manual of the manufacturer.

5.3.2.5 Ligation

DNA-Fragments were ligated using T4 DNA ligase (NEB). The reaction mix of a total volume of 10 µl was done in 1:3 molecular ratio of vector backbone to insert. The reaction incubated at 16°C overnight or at RT for 10 min for sticky overhangs or 2 h for blunt ends.

Table 5-10 Standard mix for ligations.

Component	Volume (µl)
T4 ligase buffer (10x)	1
DNA insert	3x
DNA vector backbone	x
T4 ligase	0,5
H ₂ O	ad 10 µl

5.3.2.6 Ligation with Quick T4 DNA Ligase

Ligations using the Quick Ligation Kit (NEB) were done according to manufacturer instructions.

5.3.2.7 Golden-Gate cloning

The golden gate cloning strategy combines restriction and ligation into a single one pot reaction step as described in Terfrüchte et al. (2013). A typical one pot reaction mix included these components:

Table 5-11 Standard mix for Golden-Gate Cloning.

Component	Volume (µl) / mass (ng)
T4 ligase buffer (10x, Roche)	1.5 µl
Destination vector	75 ng
Storage vector	75 ng
Inserts/ flanks	40 ng/kb
T4 DNA ligase (Roche)	0.75 µl
<i>Bsa</i> I-HF	0.5 µl
H ₂ O	ad 15 µl

The reaction was carried out in a thermo cycler using the following program:

(37°C 2 min → 16°C 5 min)x50 cycles

37°C 5 min

50°C 5 min

80°C 5 min

16°C ∞

The final mix was stored at –20°C until used for transformation into *E. coli*.

5.3.2.8 Gibson Cloning

If suitable restriction sites for classical and Golden Gate based cloning were lacking, plasmids were assembled using Gibson cloning (Gibson *et al.*, 2009). For this purpose, PCR fragments were amplified with 15 to 25 nucleotide overlap between the fragments supposed to be fused together. The backbone vector was linearized with suitable restriction enzymes and purified. 0.02 up to 0.5 pmol of all fragments were mixed with 5 µl GeneArt™ Gibson Assembly HiFi Master Mix (Thermo Fisher Scientific) in a total volume of 20 µl. The Gibson assembly mix was incubated at 50

°C for 1 h. Subsequently, competent *E. coli* cells were transformed with 5 µl of the Gibson assembly mix.

5.3.3 Southern Blot analysis

Verification of DNA fragments was done using a Southern blot with a modified protocol according to Southern (1975). Genomic DNA of the *U. maydis* strains that should be verified was digested with a restriction enzyme (depending on the strain) overnight. Afterwards loading dye was added and the DNA fragments were separated in 0.8 % agarose gel. Proper separation and digestion of the DNA was confirmed under UV light. Then the gel was incubated in 0.25 M HCl, DENAT and REANT solution for 20 min each. Between each incubation step the gel was rinsed quickly with water. Transfer of nucleic acids onto a membrane was achieved by flowing blotting setup (top to bottom):

Weight

Paper towels

2 layers of Whatman paper 3mm (pre-wetted in 20xSSC)

Hybond-N⁺-Nylon membrane

Agarose gel

Whatman paper salt bridge (pre-wetted in 20xSCS)

20xSCS buffer reservoir

The blotting procedure was done overnight. Subsequently DNA on the membrane was cross-linked with the membrane using a UV-Stratalinker 1800 (Stratagene) at 120 mJ. Afterwards the membrane incubated in hybridising buffer for 30 min at 65°C. In between the probe (upstream flank and downstream flank PCR products of the transformed plasmid generated with DIG labelled dNTPs) was diluted in 15 ml hybridising buffer and denaturised for 5 min at 95°C. The probe then incubated with the membrane at least overnight at 65°C. The probe was stored subsequently at – 20°C and reused up to 5 times. The membrane was washed three times in Southern wash buffer I, II and III for 15 min at 65°C each. Afterwards the membrane was washed for 5 min at 25°C in DIG wash buffer and incubated 30 min at 25°C in DIG2. Then the membrane was incubated for at least 1 h with anti-dioxygenin antibody (Roche) in DIG2. Finally, the membrane was washed two times for 15 min with DIG

wash buffer and 5 min with DIG3 buffer before the membrane was incubated in 8 ml CPD-Star solution for 5 min in the dark. Chemiluminescent was detected using an ImageQuant LAS 4000 (GE Healthcare).

solution	composition
0.25 M HCl DENAT	3.26 % (v/v) HCl in H ₂ O _{bid.} 1.5 M NaCl 0.4 M NaOH in H ₂ O _{bid.}
RENAT	1.5 M NaCl 282 mM Tris-HCl 218 mM Tris-Base in H ₂ O _{bid.}
20xSCS	3 M NaCl 0.3 M tri-sodium citrate *2H ₂ O in H ₂ O _{bid.} pH 7
Hybridisation buffer	26 % (v/v) SSPE (20x) 5 % (v/v) Denhardt solution 5 % (v/v) SDS (10 %) in H ₂ O _{bid.}
20xSSPE	0.02 M EDTA 2.98 M NaCl in 0.2 M phosphate buffer pH 7.4
Denhardt solution	2 % (w/v) BSA fraction V 2 % (w/v) ficoll 2 % (w/v) polyvinylpyrrolidon in H ₂ O _{bid.}
Southern wash I	10 % (v/v) SSPE (20x) 1 % (v/v) SDS (10 %) in H ₂ O _{bid.}
Southern wash II	5 % (v/v) SSPE (20x) 1 % (v/v) SDS (10 %) in H ₂ O _{bid.}
Southern wash III	0.5 % (v/v) SSPE (20x) 1 % (v/v) SDS (10 %) in H ₂ O _{bid.}
DIG1	100 mM maleic acid 150 mM NaCl in H ₂ O _{bid.} pH 7.5 (adjust with NaOH)

DIG wash	0.3 % Tween-20 in DIG1
DIG2	1 % (w/v) skim milk powder in DIG1
DIG3	0.1 M Tris-HCl 0.1 M NaCl in H ₂ O _{bid.} pH 9.5 (adjust with NaOH)
CPD-Star solution	1 % CDP-Star in DIG3

5.3.3.1 PCR

Polymerase chain reactions (PCR) were carried out according to a modified protocol from Innis (1990). A typical reaction mix consisted of 1-50 ng template, two sequence specific oligonucleotide primers (10 μ M), dNTPs (25 μ M), PCR buffer and NEB Phusion polymerase:

Table 5-12 Standard mix for PCR reactions.

Component	Volume (μ l)
NEB Phusion Buffer (5x)	5
dNTPs	0.25
NEB Phusion-Polymerase	0.25
Forward-Primer (10 μ M)	1.25
Reverse-Primer (10 μ M)	1.25
DNA-Template (1-50 ng)	1-2
optional: DMSO	0.75
H ₂ O	ad 25 μ l

Exemplary PCR program:	98 °C	2 min	
	98 °C	20 s	34 cycles
	50-70 °C	20 s	
	72 °C	10 s up to 3 min	
	72 °C	8 min	
	4 °C	∞	

The extension time was adjusted for the expected PCR product with 30 s per 1 kb.

5.3.4 DNA sequence analysis

5.3.4.1 Sequencing of DNA

DNA sequencing reactions were carried out by Eurofins Genomics GmbH in Cologne or by the sequencing service of the Biozentrum LMU Munich (using the BigDye v3.1 method).

5.3.4.2 Sequence and structure analysis

Sequencing files were analysed with sequence assemblies using the program CloneManager (version 9; scientific and educational software).

5.4 Microscopy and image processing

5.4.1 Microscopes

Microscopy imaging of this study was performed at a Zeiss Axio Imager.M1 provided with a Spot Pursuit CCD camera (Diagnostic Instruments, Sterling Heights, MI, USA) and objective lenses Plan Neofluar (40x and 100x, NA 1.3; 63x, NA 1.25) were used. Excitation of fluorescently-labeled proteins was carried out using an HXP metal halide lamp (LEJ, Jena, Germany) in combination with filter sets for Gfp (ET470/40BP, ET495LP, ET525/50BP), Rfp/mCherry (ET560/40BP, ET585LP, ET630/75BP) and for DAPI (AT350/50BP, ET400LP, ET460/50BP; Chroma, Bellow Falls, VT, USA). The microscope system was controlled with the software package MetaMorph (Molecular Devices, version 7). Image processing was also done with the MetaMorph software.

Confocal microscopy was performed using three microscopes accessible in the Center for Advanced Imaging at HHU:

Zeiss LSM 780 equipped with an GaAsP, PMT and T-PMT detectors and laser excitation at 405, 458, 488, 515, 561, 594 and 633 nm with corresponding emission filters. Images were processed using the Zen software (black edition).

Zeiss LSM 880 Airyscan equipped with an Airyscan detector, GaAsP, PMT and T-PMT detectors and laser excitation at 405, 458, 488, 514, 561 and 633 nm with corresponding Airyscan emission filters at 420-480 + 495-550 nm, 420-480 +495-620 nm, 465-535 + >555 nm, 495-550 + 570-620 nm and 570-620 + >645 nm. Images were taken with a 10x objective. Images were processed using the Zen software (black edition).

Leica SP8 equipped with HyD and PMT and transmitted light detectors, White Light laser 470-670 nm, diode 405 nm, Argon laser 458, 476, 488, 496 and 514 nm and STED-depletion at 592, 660 and 775 nm. 20x multi (NA 0.75) or 40 x water (NA 1.10) objectives were used. Images were processed using the Leica LAS X software.

5.4.2 Cell TrackerTM blue (CMAC) staining

To visualize vacuoles in *U. maydis* sporidia, 1 ml of cell culture was incubated for 20 min at 28°C and 1000 rpm with CMAC dye (10 µM final concentration in PBS). Subsequently the cells were pelleted at 3500 rpm for 5 min and washed with PBS twice prior to microscopy.

5.4.3 Latrunculin A

To stop endocytosis via impaired actin polymerization, *U. maydis* sporidia were treated with Latrunculin A (Sigma-Aldrich, St. Louis USA). 100 µl cell solution were mixed with 1 µl Latrunculin A (stock: 1 mM in DMSO) and incubated at 28°C for 30 min prior to microscopy.

5.5 Inductively coupled plasma mass spectrometry

The elemental composition of cell pellets or leaf material was analysed using Inductively coupled plasma mass spectrometry (ICP-MS) at the Biocenter-MS-

Plattform of the University Cologne. The preparation of the samples for the measurement was carried out as follows:

Cell pellets

Precultures of 6 ml YL + 50 mM MgCl₂ were inoculated with colony material and incubated O/N. The next morning the OD₆₀₀ was measured and two main cultures per strain were prepared, one in YL the other in YL+50mM MgCl₂. To this end the amount of preculture needed to inoculate 25 ml main culture was pelleted at 3500 rpm for 5 min at RT and washed three times with YL or YL + 50 mM MgCl₂. Finally, the pellet was resuspended in 1 ml YL or YL + 50 mM MgCl₂ and transferred into a baffled flask prefilled with 24 ml YL or YL + 50 mM MgCl₂, respectively. The main cultures were incubated for 8 h at 28°C and 200 rpm. The OD₆₀₀ was measured and the amount of culture that equals 15 ml of an OD₆₀₀=1 pelleted at 3500 rpm and 4°C in a swing out rotor for 5 min. The pellets were washed three times with 10 ml sterile MilliQ water. After the first washing step the cell suspension was transferred into pre-weighted 15 reaction tubes. After the final centrifugation step the water was removed by pouring and the tubes were stored at -80°C in between. For further preparation, the tubes were weighted again to obtain the fresh weight. Afterwards the lids were loosened and the tubes placed at 65°C until the cell pellets were completely dry (several days). Once dry the lids of the tubes were screwed tight and the tubes weighted again to obtain the dry weight of the cell pellets. Once dry, the pellets were stored at RT until wet digestion.

Leaf samples

12 days post infection 100-200 mg leaf tissue was harvested 2 cm below the infection holes for the MOCK control, while tumour tissue was isolated from *U. maydis* infected plants. Always the last infected leaf and the next younger leaf without symptoms was sampled. This corresponds to leaf L4 and L5. The tissue was collected in pre-weighted 15 ml reaction tubes and the tubes were weighted again to obtain the fresh weight of the leaf sample. Then the tubes were placed with partly unscrewed caps at 65°C until the leaf material was dry (1-2 days). Subsequently the tubes were weighted again to obtain the dry weight of the leaf tissue. Once dry, the samples were stored at RT until wet digestion.

Wet digestion

Dry cell pellets or leaf samples were mixed with 0.5 or 1.0 ml 65 % nitric acid (analytical grade) using a 25 ml combitip to add the acid under the fume hood. The samples were incubated for 4 h at 65 °C. Using 50 ml Combitips (Eppendorf) 4.5 ml (cell pellets) or 9 ml (leaf samples) sterile MilliQ water was added into the tubes under the fume hood (nitrous gases evaporate). Afterwards the tubes were weighted again to obtain the weight of the digested samples. The samples were centrifuged for 20 min at 4 °C and 4863 x g in a swing out rotor to pellet undigested residual plant material. After centrifugation the cell pellet samples were poured into fresh 15 ml tubes and stored at 4 °C until transport of the samples to the Biocenter-MS-Plattform in Cologne. 5-6 ml of the supernatant from the leaf samples were filtered through 0.25 µm syringe filters into fresh 15 ml reaction tubes to remove visible remaining particles. Afterwards, the samples were stored at 4 °C until transport of the samples to the Biocenter-MS-Plattform in Cologne for measurement.

Data Analysis

For analysis, the ICP-MS data was normalized: The average blank values were subtracted from the sample values. Afterwards a dilution factor was calculated for each sample and multiplied with each corresponding element concentration. The dilution factor was calculated by dividing the weight of the digested sample with the weight of the dried sample. Element concentrations below or at the detection limit were excluded from the analysis. Further evaluation and statistical analysis of the normalized data was done using Microsoft Excel 2016 and GraphPad Prism 8.

5.6 Computer programs and bioinformatics

5.6.1 Analysis of DNA and amino acid sequences

CloneManager 9 (Scientific and Educational Central Software; Cary, USA)

PEDANT (<http://pedant.helmholtz-muenchen.de/>)

Ensemble Fungi (<https://fungi.ensembl.org/index.html>)

Blastn /Blastp (<http://blast.ncbi.nlm.nih.gov/Blast.cgi>)

Clustal Omega (<https://www.ebi.ac.uk/Tools/msa/clustalo/>)

Pfam database (<http://pfam.xfam.org/search/sequence>)

InterPro database (<https://www.ebi.ac.uk/interpro/>)

SMART Database (<http://smart.embl-heidelberg.de/>)

Phyre2 (<http://www.sbg.bio.ic.ac.uk/~phyre2/html/page.cgi?id=index>)

CCTOP (<http://cctop.ttk.hu/>)

DeepTMHMM prediction server (<https://dtu.biolib.com/DeepTMHMM/>)

PDB (<https://www.rcsb.org/search/advanced/sequence>)

Pymol (<https://pymol.org/2/>)

Uniprot (<https://www.uniprot.org/>)

MEGA11 software (Molecular Evolutionary Genetics Analysis)
(<https://www.megasoftware.net/>)

5.6.2 *Data analysis, writing and graphical design*

Microsoft Office 2016 (Microsoft Corporation)

Canvas 12 (ACDSee Systems)

GraphPad Prism 8 (GraphPad Software Inc.)

6 References

- Ali, R. *et al.* (2007) 'Death don't have no mercy and neither does calcium: Arabidopsis CYCLIC NUCLEOTIDE GATED CHANNEL2 and innate immunity', *Plant Cell*, 19(3), pp. 1081–1095. doi: 10.1105/tpc.106.045096.
- Allen, E. A. *et al.* (1991) 'Appressorium formation in response to topographical signals by 27 rust species', *Phytopathology*, 81(3), pp. 323–331. doi: 10.1094/Phyto-81-323.
- Amit, M. *et al.* (2012) 'Differential GC Content between Exons and Introns Establishes Distinct Strategies of Splice-Site Recognition', *Cell Reports*. The Authors, 1(5), pp. 543–556. doi: 10.1016/j.celrep.2012.03.013.
- Andargie, M. and Li, J. (2016) 'Arabidopsis thaliana: A Model Host Plant to Study Plant–Pathogen Interaction Using Rice False Smut Isolates of *Ustilaginoidea virens*', *Frontiers in Plant Science*, 7(February), pp. 1–10. doi: 10.3389/fpls.2016.00192.
- Andrade, O. *et al.* (2004) 'Characterization, In Vitro Culture, and Molecular Analysis of *Thecaphora solani*, the Causal Agent of Potato Smut.', *Phytopathology*, 94(8), pp. 875–882. doi: 10.1094/PHYTO.2004.94.8.875.
- Arias, S. L. *et al.* (2021) 'Where does the peanut smut pathogen, *Thecaphora frezii*, fit in the spectrum of smut diseases?', *Plant Disease*, 105(9), pp. 2268–2280. doi: 10.1094/PDIS-11-20-2438-FE.
- Arlt, H., Reggiori, F. and Ungermann, C. (2015) 'Retromer and the dynamin Vps1 cooperate in the retrieval of transmembrane proteins from vacuoles', *Journal of Cell Science*, 128(4), pp. 645–655. doi: 10.1242/jcs.132720.
- Asai, S. and Shirasu, K. (2015) 'Plant cells under siege: Plant immune system versus pathogen effectors', *Current Opinion in Plant Biology*. Elsevier Ltd, 28, pp. 1–8. doi: 10.1016/j.pbi.2015.08.008.
- Ausubel, F. M. *et al.* (1987) *Current protocols in molecular biology*. USA: John Wiley & Sons, Inc. doi: 10.1002/0471142727.mb0302s1.
- Avila, J. R., Lee, J. S. and Toriia, K. U. (2015) 'Co-Immunoprecipitation of Membrane-Bound Receptors', *The Arabidopsis Book*, 13, p. e0180. doi:

10.1199/tab.0180.

Bakkeren, G., Kämper, J. and Schirawski, J. (2008) 'Sex in smut fungi: Structure, function and evolution of mating-type complexes', *Fungal Genetics and Biology*, 45(SUPPL. 1). doi: 10.1016/j.fgb.2008.04.005.

Becker, J Sabine *et al.* (2009) 'Bioimaging of metals by laser ablation inductively coupled plasma mass spectrometry (LA-ICP-MS)', *Mass Spectrometry Reviews*, 29(1), pp. 156–175. doi: 10.1002/mas.20239.

Begerow, D., Stoll, M. and Bauer, R. (2006) 'A phylogenetic hypothesis of Ustilaginomycotina based on multiple gene analyses and morphological data', *Mycologia*, 98(6), pp. 906–916. doi: 10.1080/15572536.2006.11832620.

Bendezú, F. O. *et al.* (2015) 'Spontaneous Cdc42 Polarization Independent of GDI-Mediated Extraction and Actin-Based Trafficking', *PLoS Biology*, 13(4), pp. 1–30. doi: 10.1371/journal.pbio.1002097.

Benevenuto, J. *et al.* (2018) 'Comparative genomics of smut pathogens: Insights from orphans and positively selected genes into host specialization', *Frontiers in Microbiology*, 9(APR), pp. 1–17. doi: 10.3389/fmicb.2018.00660.

Bentham, A. R. *et al.* (2020) 'A molecular roadmap to the plant immune system', *Journal of Biological Chemistry*, 295(44), pp. 14916–14935. doi: 10.1074/jbc.REV120.010852.

Berhin, A. *et al.* (2019) 'The Root Cap Cuticle: A Cell Wall Structure for Seedling Establishment and Lateral Root Formation', *Cell*. Elsevier Inc., 176(6), pp. 1367–1378.e8. doi: 10.1016/j.cell.2019.01.005.

Billett, E. E. and Burnett, J. H. (1978) 'The host-parasite physiology of the maize smut fungus, *Ustilago maydis* I. The effect of smut infection on maize growth', *Physiological Plant Pathology*, 12(1), pp. 93–102. doi: 10.1016/0048-4059(78)90022-X.

Blackwell, K. J., Tobin, J. M. and Avery, S. V. (1997) 'Manganese uptake and toxicity in magnesium supplemented and unsupplemented *Saccharomyces cerevisiae*', *Applied Microbiology and Biotechnology*, 47(2), pp. 180–184. doi: 10.1007/s002530050909.

- Bölker, M. (2001) 'Ustilago maydis - A valuable model system for the study of fungal dimorphism and virulence', *Microbiology*, 147(6), pp. 1395–1401.
- Bösch, K. *et al.* (2016) 'Genetic Manipulation of the Plant Pathogen *Ustilago maydis* to Study Fungal Biology and Plant Microbe Interactions', *Journal of Visualized Experiments*, 115(September), pp. e54522, doi:10.3791/54522. doi: 10.3791/54522.
- Brefort, T. *et al.* (2009) 'Ustilago maydis as a pathogen', *Annual Review of Phytopathology*, 47, pp. 423–445. doi: 10.1146/annurev-phyto-080508-081923.
- Bui, D. M. *et al.* (1999) 'The bacterial magnesium transporter CorA can functionally substitute for its putative homologue Mrs2p in the yeast inner mitochondrial membrane', *Journal of Biological Chemistry*. © 1999 ASBMB. Currently published by Elsevier Inc; originally published by American Society for Biochemistry and Molecular Biology., 274(29), pp. 20438–20443. doi: 10.1074/jbc.274.29.20438.
- Cakmak, I. and Kirkby, E. A. (2008) 'Role of magnesium in carbon partitioning and alleviating photooxidative damage', *Physiologia Plantarum*, 133(4), pp. 692–704. doi: 10.1111/j.1399-3054.2007.01042.x.
- Chen, Y. S. *et al.* (2021) 'Crystal structure of an archaeal CorB magnesium transporter', *Nature Communications*. Springer US, 12(1), pp. 1–14. doi: 10.1038/s41467-021-24282-7.
- Coates, M. E. and Beynon, J. L. (2010) 'Hyaloperonospora arabidopsidis as a pathogen model', *Annual Review of Phytopathology*, 48, pp. 329–345. doi: 10.1146/annurev-phyto-080508-094422.
- Cohen, S. N., Chang, a C. and Hsu, L. (1972) 'Nonchromosomal antibiotic resistance in bacteria: genetic transformation of Escherichia coli by R-factor DNA.', *Proceedings of the National Academy of Sciences of the United States of America*, 69(8), pp. 2110–2114. doi: 10.1073/pnas.69.8.2110.
- Courville, K. J. *et al.* (2019) 'Smut infection of perennial hosts: the genome and the transcriptome of the Brassicaceae smut fungus Thecaphora thlaspeos reveal functionally conserved and novel effectors', *New Phytologist*, 222(3), pp. 1474–1492. doi: 10.1111/nph.15692.
- Dancis, A. *et al.* (1992) 'Ferric reductase of Saccharomyces cerevisiae: Molecular

- characterization, role in iron uptake, and transcriptional control by iron', *Proceedings of the National Academy of Sciences of the United States of America*, 89(9), pp. 3869–3873. doi: 10.1073/pnas.89.9.3869.
- Dean, R. *et al.* (2012) 'The Top 10 fungal pathogens in molecular plant pathology', *Molecular Plant Pathology*, 13(4), pp. 414–430. doi: 10.1111/j.1364-3703.2011.00783.x.
- Demaegd, D. *et al.* (2014) 'Molecular evolution of a novel family of putative calcium transporters', *PLoS ONE*, 9(6). doi: 10.1371/journal.pone.0100851.
- Denchev, T. T. and Denchev, C. M. (2019) 'Contributions to the smut fungi of Africa. 5. First record of *Thecaphora thlaspeos*', *Mycobiota*, 9, pp. 1–6. doi: 10.12664/mycobiota.2019.09.01.
- Van Dijken, J. P. *et al.* (2000) 'An interlaboratory comparison of physiological and genetic properties of four *Saccharomyces cerevisiae* strains', *Enzyme and Microbial Technology*, 26(9–10), pp. 706–714. doi: 10.1016/S0141-0229(00)00162-9.
- Dilks, T. *et al.* (2019) 'Non-canonical fungal G-protein coupled receptors promote *Fusarium* head blight on wheat', *PLoS Pathogens*, 15(4), pp. 1–26. doi: 10.1371/journal.ppat.1007666.
- Djamei, A. *et al.* (2011) 'Metabolic priming by a secreted fungal effector', *Nature*, 478(7369), pp. 395–398. doi: 10.1038/nature10454.
- Dobson, L., Reményi, I. and Tusnády, G. E. (2015) 'CCTOP: A Consensus Constrained TOPology prediction web server', *Nucleic Acids Research*, 43(W1), pp. W408–W412. doi: 10.1093/nar/gkv451.
- Dodds, P. N. and Rathjen, J. P. (2010) 'Plant immunity: towards an integrated view of plant–pathogen interactions', *Nature Reviews Genetics*. Nature Publishing Group, 11(8), pp. 539–548. doi: 10.1038/nrg2812.
- Doehlemann, G. *et al.* (2009) 'Pep1, a secreted effector protein of *Ustilago maydis*, is required for successful invasion of plant cells', *PLoS Pathogens*, 5(2). doi: 10.1371/journal.ppat.1000290.
- Doehlemann, G. *et al.* (2011) 'Two linked genes encoding a secreted effector and a

- membrane protein are essential for *Ustilago maydis*-induced tumour formation', *Molecular Microbiology*, 81(3), pp. 751–766. doi: 10.1111/j.1365-2958.2011.07728.x.
- Doehlemann, G. *et al.* (2017) 'Plant pathogenic fungi', *Microbiology S*, 5(1), pp. 703–726. doi: 10.1128/9781555819583.ch34.
- Dolatabadian, A. (2021) 'Plant–microbe interaction', *Biology*, 10(1), pp. 1–3. doi: 10.3390/biology10010015.
- Donaldson, M. E. and Saville, B. J. (2008) 'Bioinformatic identification of *Ustilago maydis* meiosis genes', *Fungal Genetics and Biology*, 45(SUPPL. 1). doi: 10.1016/j.fgb.2008.04.012.
- Drew, D. and Boudker, O. (2016) 'Shared Molecular Mechanisms of Membrane Transporters', *Annual Review of Biochemistry*, 85, pp. 543–572. doi: 10.1146/annurev-biochem-060815-014520.
- Duszyn, M. *et al.* (2019) 'Cyclic nucleotide gated channels (CNGCs) in plant signalling—Current knowledge and perspectives', *Journal of Plant Physiology*, 241. doi: 10.1016/j.jplph.2019.153035.
- Egan, J. D. *et al.* (2009) 'Calcineurin is an antagonist to PKA protein phosphorylation required for postmating filamentation and virulence, while PP2A is required for viability in *ustilago maydis*', *Molecular Plant-Microbe Interactions*, 22(10), pp. 1293–1301. doi: 10.1094/MPMI-22-10-1293.
- Eide, D. J. (1998) 'The molecular biology of metal ion transport in *Saccharomyces cerevisiae*', *Annual Review of Nutrition*, 18, pp. 441–469. doi: 10.1146/annurev.nutr.18.1.441.
- El-Defrawy, M. M. H. and Hesham, A. E.-L. (2020) *G-protein-coupled Receptors in Fungi*. doi: 10.1007/978-3-030-41870-0_3.
- Emmett, R. W. and Parbery, D. G. (1975) 'R. W Emmett', (85).
- Eshaghi, S. *et al.* (2006) 'Crystal Structure of a Divalent Metal Ion Transporter CorA at 2.9 Angstrom Resolution', *Science*, 313(2006), pp. 354–357. doi: 10.1126/science.1127121.
- Feldbrügge, M. *et al.* (2004) 'Regulation of mating and pathogenic development in

- Ustilago maydis', *Current Opinion in Microbiology*, 7(6), pp. 666–672. doi: 10.1016/j.mib.2004.10.006.
- Feldbrügge, M. *et al.* (2008) 'The posttranscriptional machinery of Ustilago maydis', *Fungal Genetics and Biology*, 45(SUPPL. 1), pp. 40–46. doi: 10.1016/j.fgb.2008.03.013.
- Feliciano, A. J. and Gubler, W. D. (2001) 'Histological investigations on infection of grape roots and shoots by Phaeoacremonium spp.', *Phytopathologia Mediterranea*, 40(3), pp. 387–393.
- Fernández-Álvarez, A. *et al.* (2012) 'Identification of O-mannosylated virulence factors in Ustilago maydis.', *PLoS pathogens*, 8(3). doi: 10.1371/journal.ppat.1002563.
- Feys, B. J. *et al.* (2001) 'Direct interaction between the Arabidopsis disease resistance signaling proteins, EDS1 and PAD4.', *The EMBO Journal*, 20(19), pp. 5400–11. doi: 10.1093/emboj/20.19.5400.
- Frantzeskakis, L. (2016) 'The genome of the fungal plant pathogen Thecaphora thlaspeos'.
- Frantzeskakis, L. *et al.* (2017) 'The plant-dependent life cycle of Thecaphora thlaspeos: a smut fungus adapted to Brassicaceae', *Mpmi*, 30(4), pp. 271–282. doi: 10.1094/MPMI-08-16-0164-R.
- Fuchs, U. *et al.* (2006) 'Endocytosis is essential for pathogenic development in the corn smut fungus Ustilago maydis', *Plant Cell*, 18(8), pp. 2066–2081. doi: 10.1105/tpc.105.039388.
- Gao, L. *et al.* (2013) 'Ustilago maydis reprograms cell proliferation in maize anthers', *Plant Journal*, 75(6), pp. 903–914. doi: 10.1111/tpj.12270.
- Garg, H. *et al.* (2010) 'The infection processes of Sclerotinia sclerotiorum in cotyledon tissue of a resistant and a susceptible genotype of Brassica napus', *Annals of Botany*, 106(6), pp. 897–908. doi: 10.1093/aob/mcq196.
- Garnica, D. P. *et al.* (2014) 'The Ins and Outs of Rust Haustoria', *PLoS Pathogens*, 10(9), pp. 10–13. doi: 10.1371/journal.ppat.1004329.

- Geißl, L. (2020) *Charakterisierung des Paarungsprozesses und seine Rolle für die Pflanzeninfektion in dem Brassicaceenbrandpilz Thecaphora thlaspeos* . *Characterizing the mating process and its role for plant infection in the Brassicaceae smut fungus Thecaphora thlaspeos* . Heinrich-Heine-Universität.
- Georgiev, V. (2000) 'Membrane Transporters and Antifungal Drug Resistance', *Current Drug Targets*, 1(3), pp. 261–284. doi: 10.2174/1389450003349209.
- Ghareeb, H. et al. (2020) 'Quantitative Hormone Signaling Output Analyses of Arabidopsis thaliana Interactions With Virulent and Avirulent Hyaloperonospora arabidopsidis Isolates at Single-Cell Resolution', *Frontiers in Plant Science*, 11(November), pp. 1–15. doi: 10.3389/fpls.2020.603693.
- Ghareeb, H., Laukamm, S. and Lipka, V. (2016) 'COLORFUL-circuit: A platform for rapid multigene assembly, delivery, and expression in plants', *Frontiers in Plant Science*, 7(MAR2016), pp. 1–15. doi: 10.3389/fpls.2016.00246.
- Gibson, D. G. et al. (2009) 'Enzymatic assembly of DNA molecules up to several hundred kilobases', *Nature Methods*, 6(5), pp. 343–345. doi: 10.1038/nmeth.1318.
- Gillissen, B. et al. (1992) 'A two-component regulatory system for self/non-self recognition in Ustilago maydis.', *Cell*, 68(4), pp. 647–657. doi: 10.1016/0092-8674(92)90141-X.
- Giménez-Mascarell, P. et al. (2019) 'Current structural knowledge on the CNNM family of magnesium transport mediators', *International Journal of Molecular Sciences*, 20(5). doi: 10.3390/ijms20051135.
- Giraldo, M. C. and Valent, B. (2013) 'Filamentous plant pathogen effectors in action', *Nature Reviews Microbiology*. Nature Publishing Group, 11(11), pp. 800–814. doi: 10.1038/nrmicro3119.
- Gitan, R. S. et al. (1998) 'Zinc-induced inactivation of the yeast ZRT1 zinc transporter occurs through endocytosis and vacuolar degradation', *Journal of Biological Chemistry*. © 1998 ASBMB. Currently published by Elsevier Inc; originally published by American Society for Biochemistry and Molecular Biology., 273(44), pp. 28617–28624. doi: 10.1074/jbc.273.44.28617.
- Gitan, R. S. and Eide, D. J. (2000) 'Zinc-regulated ubiquitin conjugation signals

endocytosis of the yeast ZRT1 zinc transporter', *Biochemical Journal*, 346(2), pp. 329–336. doi: 10.1042/0264-6021:3460329.

Gomolplitinant, K. M. and Saier, M. H. (2011) 'Evolution of the oligopeptide transporter family', *Journal of Membrane Biology*, 240(2), pp. 89–110. doi: 10.1007/s00232-011-9347-9.

Goytain, A. *et al.* (2007) 'NIPA1(SPG6), the basis for autosomal dominant form of hereditary spastic paraplegia, encodes a functional Mg²⁺ transporter', *Journal of Biological Chemistry*. © 2007 ASBMB. Currently published by Elsevier Inc; originally published by American Society for Biochemistry and Molecular Biology., 282(11), pp. 8060–8068. doi: 10.1074/jbc.M610314200.

Goytain, A., Hines, R. M. and Quamme, G. A. (2008) 'Functional characterization of NIPA2, a selective Mg²⁺ transporter', *American Journal of Physiology - Cell Physiology*, 295(4), pp. 944–953. doi: 10.1152/ajpcell.00091.2008.

Graschopf, A. *et al.* (2001) 'The Yeast Plasma Membrane Protein Alr1 Controls Mg²⁺ Homeostasis and is Subject to Mg²⁺-dependent Control of Its Synthesis and Degradation', *Journal of Biological Chemistry*, 276(19), pp. 16216–16222. doi: 10.1074/jbc.M101504200.

Gregan, J. *et al.* (2001) 'The mitochondrial inner membrane protein Lpe10p, a homologue of Mrs2p, is essential for magnesium homeostasis and group II intron splicing in yeast', *Molecular and General Genetics*, 264(6), pp. 773–781. doi: 10.1007/s004380000366.

Gregan, J., Kolisek, M. and Schweyen, R. J. (2001) 'Mitochondrial Mg²⁺ homeostasis is critical for group II intron splicing in vivo', *Genes and Development*, 15(17), pp. 2229–2237. doi: 10.1101/gad.201301.

Groisman, E. A. *et al.* (2013) 'Bacterial Mg²⁺ homeostasis, transport, and virulence', *Annual Review of Genetics*, 47, pp. 625–646. doi: 10.1146/annurev-genet-051313-051025.

Gunther, T. (1981) 'Biochemistry and pathobiochemistry of magnesium', *Artery*, 9(3), pp. 167–181.

Gustafsson, C. *et al.* (2012) 'Engineering genes for predictable protein expression',

- Protein Expression and Purification*. Elsevier Inc., 83(1), pp. 37–46. doi: 10.1016/j.pep.2012.02.013.
- Gutjahr, C. and Parniske, M. (2013) 'Cell and developmental biology of arbuscular mycorrhiza symbiosis', *Annual Review of Cell and Developmental Biology*, 29, pp. 593–617. doi: 10.1146/annurev-cellbio-101512-122413.
- Guzman-Plazola, R. A., Davis, R. M. and Marois, J. J. (2003) 'Effects of relative humidity and high temperature on spore germination and development of tomato powdery mildew (*Leveillula taurica*)', *Crop Protection*, 22(10), pp. 1157–1168. doi: 10.1016/S0261-2194(03)00157-1.
- Häffner, E., Konietzki, S. and Diederichsen, E. (2015) *Keeping control: The role of senescence and development in plant pathogenesis and defense*, *Plants*. doi: 10.3390/plants4030449.
- Hampel, M. *et al.* (2016) 'Unfolded Protein Response (UPR) Regulator Cib1 Controls Expression of Genes Encoding Secreted Virulence Factors in *Ustilago maydis*', pp. 1–16. doi: 10.1371/journal.pone.0153861.
- Hansjakob, A. *et al.* (2010) 'Very-long-chain aldehydes promote in vitro prepenetration processes of *Blumeria graminis* in a dose- and chain length-dependent manner', *New Phytologist*, 188(4), pp. 1039–1054. doi: 10.1111/j.1469-8137.2010.03419.x.
- Harris, J. M. *et al.* (2020) 'What are the top 10 unanswered questions in molecular plant-microbe interactions?', *Molecular Plant-Microbe Interactions*, 33(12), pp. 1354–1365. doi: 10.1094/MPMI-08-20-0229-CR.
- Hassani, M. A., Durán, P. and Hacquard, S. (2018) 'Microbial interactions within the plant holobiont', *Microbiome*. *Microbiome*, 6(1), p. 58. doi: 10.1186/s40168-018-0445-0.
- He, D. C., Zhan, J. S. and Xie, L. H. (2016) 'Problems, challenges and future of plant disease management: From an ecological point of view', *Journal of Integrative Agriculture*. Chinese Academy of Agricultural Sciences, 15(4), pp. 705–715. doi: 10.1016/S2095-3119(15)61300-4.
- Heidari, P. *et al.* (2021) 'Magnesium transporter gene family: Genome-wide

- identification and characterization in theobroma cacao, corchorus capsularis, and gossypium hirsutum of family malvaceae', *Agronomy*, 11(8). doi: 10.3390/agronomy11081651.
- Heimel, K., Freitag, J., Hampel, M., Ast, J., *et al.* (2013) 'Crosstalk between the unfolded protein response and pathways that regulate pathogenic development in Ustilago maydis.', *The Plant cell*, 25(10), pp. 4262–77. doi: 10.1105/tpc.113.115899.
- Heimel, K., Freitag, J., Hampel, M. and Ast, J. (2013) 'Crosstalk between the Unfolded Protein Response and Pathways That Regulate Pathogenic Development in Ustilago maydis', 25(October), pp. 4262–4277. doi: 10.1105/tpc.113.115899.
- Hemetsberger, C. *et al.* (2012) 'The Ustilago maydis effector Pep1 suppresses plant immunity by inhibition of host peroxidase activity', *PLoS Pathogens*, 8(5). doi: 10.1371/journal.ppat.1002684.
- Hermans, C. *et al.* (2005) 'Magnesium deficiency in sugar beets alters sugar partitioning and phloem loading in young mature leaves', *Planta*, 220(4), pp. 541–549. doi: 10.1007/s00425-004-1376-5.
- Hirata, Y. *et al.* (2014) 'Mg²⁺-dependent interactions of ATP with the cystathionine- β -synthase (CBS) domains of a magnesium transporter', *Journal of Biological Chemistry*. © 2014 ASBMB. Currently published by Elsevier Inc; originally published by American Society for Biochemistry and Molecular Biology., 289(21), pp. 14731–14739. doi: 10.1074/jbc.M114.551176.
- Hmiel, S. P. *et al.* (1986) 'Magnesium transport in Salmonella typhimurium: Characterization of Magnesium Influx and Cloning of a Transport Gene', *Journal of Bacteriology*, 168(3), pp. 1444–1450. doi: 10.1128/jb.168.3.1444-1450.1986.
- Hmiel, S. P. *et al.* (1989) 'Magnesium transport in Salmonella typhimurium: Genetic characterization and cloning of three magnesium transport loci', *Journal of Bacteriology*, 171(9), pp. 4742–4751. doi: 10.1128/jb.171.9.4742-4751.1989.
- Hoch, H. C. *et al.* (1987) 'Signaling for growth orientation and cell differentiation by surface topography in Uromyces', *Science*, 235(4796), pp. 1659–1662. doi: 10.1126/science.235.4796.1659.
- Horst, R. J. *et al.* (2008) 'Infection of maize leaves with Ustilago maydis prevents

establishment of C4 photosynthesis', *Journal of Plant Physiology*, 165(1), pp. 19–28. doi: 10.1016/j.jplph.2007.05.008.

Horst, R. J. *et al.* (2010) 'Ustilago maydis Infection Strongly Alters Organic Nitrogen Allocation in Maize and Stimulates Productivity of Systemic Source Leaves', *Plant Physiology*, 152(1), pp. 293–308. doi: 10.1104/pp.109.147702.

Huber, D. M. and Jones, J. B. (2013) 'The role of magnesium in plant disease', 368(1), pp. 73–85.

Inanobe, A. and Kurachi, Y. (2014) 'Membrane channels as integrators of G-protein-mediated signaling', *Biochimica et Biophysica Acta*. The Authors, 1838(2), pp. 521–531. doi: 10.1016/j.bbamem.2013.08.018.

Innis, M. A., Gelfand, D. H. and Sninsky, J. J. (1990) *PCR Protocols: A guide to methods and applications, Stochastic Local Search*. San Diego, USA: Academic press. doi: <http://dx.doi.org/10.1016/B978-1-55860-872-6.50033-0>.

Jambunathan, N., Siani, J. M. and McNellis, T. W. (2001) 'A humidity-sensitive Arabidopsis copine mutant exhibits precocious cell death and increased disease resistance.', *The Plant Cell*, 13(October), pp. 2225–2240. doi: 10.1105/tpc.010226.

Jaswal, R., Kiran, K., *et al.* (2020) 'Effector Biology of Biotrophic Plant Fungal Pathogens: Current Advances and Future Prospects', *Microbiological Research*. Elsevier, 241(July), p. 126567. doi: 10.1016/j.micres.2020.126567.

Jaswal, R., Rajarammohan, S., *et al.* (2020) 'Smut fungi as a stratagem to characterize rust effectors: opportunities and challenges', *World Journal of Microbiology and Biotechnology*. Springer Netherlands, 36(10), pp. 1–10. doi: 10.1007/s11274-020-02927-x.

Jeger, M. *et al.* (2021) 'Global challenges facing plant pathology: multidisciplinary approaches to meet the food security and environmental challenges in the mid-twenty-first century', *CABI Agriculture and Bioscience*. BioMed Central, 2(1), pp. 1–18. doi: 10.1186/s43170-021-00042-x.

Jeschke, W. D. and Hilpert, A. (1997) 'Sink-stimulated photosynthesis and sink-dependent increase in nitrate uptake: Nitrogen and carbon relations of the parasitic association *Cuscuta reflexa*-*Ricinus communis*', *Plant, Cell and Environment*, 20(1),

pp. 47–56. doi: 10.1046/j.1365-3040.1997.d01-2.x.

Jones, J. D. G. and Dangl, J. L. (2006) 'The plant immune system', *Nature*, 444(7117), pp. 323–329. doi: 10.1038/nature05286.

de Jonge, R. *et al.* (2010) 'Conserved fungal LysM effector Ecp6 prevents chitin-triggered immunity in plants.', *Science (New York, N.Y.)*, 329(5994), pp. 953–5. doi: 10.1126/science.1190859.

Jonkers, I., Kwak, H. and Lis, J. T. (2014) 'Genome-wide dynamics of Pol II elongation and its interplay with promoter proximal pausing, chromatin, and exons', *eLife*, 2014(3), pp. 1–25. doi: 10.7554/eLife.02407.

Jumper, J. *et al.* (2021) 'Highly accurate protein structure prediction with AlphaFold', *Nature*. Springer US, 596(7873), pp. 583–589. doi: 10.1038/s41586-021-03819-2.

Kadereit, J. W. *et al.* (2014) *Strasburger Lehrbuch der Pflanzenwissenschaften*. 37th edn. Berlin Heidelberg: Springer Spektrum. doi: 10.1007/978-3-642-54435-4.

Kahmann, R. and Kämper, J. (2004) 'Ustilago maydis: How its biology relates to pathogenic development', *New Phytologist*, 164(1), pp. 31–42. doi: 10.1111/j.1469-8137.2004.01156.x.

Kämper, J. *et al.* (2006) 'Insights from the genome of the biotrophic fungal plant pathogen *Ustilago maydis*.', *Nature*, 444(7115), pp. 97–101. doi: 10.1038/nature05248.

Kelly, L. A. *et al.* (2015) 'The Phyre2 web portal for protein modelling, prediction, and analysis', *Nature Protocols*. Nature Publishing Group, 10(6), pp. 845–858. doi: 10.1038/nprot.2015-053.

Kijpornyongpan, T. and Aime, M. C. (2020) 'Investigating the smuts: Common cues, signaling pathways, and the role of mat in dimorphic switching and pathogenesis', *Journal of Fungi*, 6(4), pp. 1–26. doi: 10.3390/jof6040368.

Knoop, V. *et al.* (2005) 'Transport of magnesium and other divalent cations: Evolution of the 2-TM-GxN proteins in the MIT superfamily', *Molecular Genetics and Genomics*, 274(3), pp. 205–216. doi: 10.1007/s00438-005-0011-x.

Koeck, M., Hardham, A. R. and Dodds, P. N. (2011) 'The role of effectors of

- biotrophic and hemibiotrophic fungi in infection', *Cellular Microbiology*, 13(12), pp. 1849–1857. doi: 10.1111/j.1462-5822.2011.01665.x.
- Kolisek, M. *et al.* (2008) 'SLC41A1 is a novel mammalian Mg²⁺ carrier', *Journal of Biological Chemistry*, 283(23), pp. 16235–16247. doi: 10.1074/jbc.M707276200.
- Kolisek, M. *et al.* (2012) 'Human gene SLC41A1 encodes for the Na⁺/Mg²⁺ exchanger', *American Journal of Physiology - Cell Physiology*, 302(1), pp. 318–326. doi: 10.1152/ajpcell.00289.2011.
- Kolisek, M. *et al.* (2019) 'Magnesium extravaganza: A critical compendium of current research into cellular Mg²⁺ transporters other than TRPM6/7', *Reviews of Physiology, Biochemistry and Pharmacology*, 176, pp. 65–105. doi: 10.1007/112_2018_15.
- Konishi, M., Hatada, Y. and Horiuchi, J. (2015) *inner membrane magnesium transporter MRS2, mitochondrial precursor [Ps - Protein - NCBI*. Available at: [https://www.ncbi.nlm.nih.gov/protein/808370479?report=genbank&log\\$=protop&blast_rank=10&RID=00BMNNU3015](https://www.ncbi.nlm.nih.gov/protein/808370479?report=genbank&log$=protop&blast_rank=10&RID=00BMNNU3015) (Accessed: 20 July 2022).
- Koornneef, M. and Meinke, D. (2010) 'The development of Arabidopsis as a model plant', *Plant Journal*, 61(6), pp. 909–921. doi: 10.1111/j.1365-313X.2009.04086.x.
- Kroeze, W. K. *et al.* (2015) 'PRESTO-Tango as an open-source resource for interrogation of the druggable human GPCRome', *Nature Structural and Molecular Biology*. Nature Publishing Group, 22(5), pp. 362–369. doi: 10.1038/nsmb.3014.
- Kruse, J. *et al.* (2018) 'The first smut fungus, *Thecaphora anthemidis* sp. nov. (Glomosporiaceae), described from *Anthemis* (Asteraceae)', *MycKeys*, 41, pp. 39–50. doi: 10.3897/mycokeys.41.28454.
- Kucharski, L. M., Lubbe, W. J. and Maguire, M. E. (2000) 'Cation hexaammines are selective and potent inhibitors of the CorA magnesium transport system', *Journal of Biological Chemistry*. © 2000 ASBMB. Currently published by Elsevier Inc; originally published by American Society for Biochemistry and Molecular Biology., 275(22), pp. 16767–16773. doi: 10.1074/jbc.M001507200.
- Kurihara, D. *et al.* (2015) 'ClearSee: A rapid optical clearing reagent for whole-plant fluorescence imaging', *Development (Cambridge)*, 142(23), pp. 4168–4179. doi:

10.1242/dev.127613.

Lanver, D. *et al.* (2014) 'Plant Surface Cues Prime *Ustilago maydis* for Biotrophic Development', *PLoS Pathogens*, 10(7). doi: 10.1371/journal.ppat.1004272.

Lanver, D. *et al.* (2017) 'Ustilago maydis effectors and their impact on virulence', *Nature Reviews Microbiology*. Nature Publishing Group, 15(7), pp. 409–421. doi: 10.1038/nrmicro.2017.33.

Lanver, D. *et al.* (2018) 'The biotrophic development of *Ustilago maydis* studied by RNAseq analysis', *The Plant Cell*, p. tpc.00764.2017. doi: 10.1105/tpc.17.00764.

Lee, N. and Kronstad, J. W. (2002) 'ras2 controls morphogenesis, pheromone response, and pathogenicity in the fungal pathogen *Ustilago maydis*', *Eukaryotic Cell*, 1(6), pp. 954–966. doi: 10.1128/EC.1.6.954-966.2002.

Lerche, M. *et al.* (2017) 'Structure and Cooperativity of the Cytosolic Domain of the CorA Mg²⁺ Channel from *Escherichia coli*', *Structure*, 25(8), pp. 1175-1186.e4. doi: 10.1016/j.str.2017.05.024.

Li, D. *et al.* (2017) 'Methods for genetic transformation of filamentous fungi', *Microbial Cell Factories*. BioMed Central, pp. 1–13. doi: 10.1186/s12934-017-0785-7.

Li, H. *et al.* (2016) 'Identification, and Functional and Expression Analyses of the CorA/MRS2/MGT-Type Magnesium Transporter Family in Maize', *Plant and Cell Physiology*, 57(6), pp. 1153–1168. doi: 10.1093/pcp/pcw064.

Li, H. *et al.* (2017) 'The maize CorA/MRS2/MGT-type Mg transporter, ZmMGT10, responses to magnesium deficiency and confers low magnesium tolerance in transgenic *Arabidopsis*', *Plant Molecular Biology*. Springer Netherlands, 95(3), pp. 269–278. doi: 10.1007/s11103-017-0645-1.

Li, L. and Kaplan, J. (1998) 'Defects in the yeast high affinity iron transport system result in increased metal sensitivity because of the increased expression of transporters with a broad transition metal specificity', *Journal of Biological Chemistry*. © 1998 ASBMB. Currently published by Elsevier Inc; originally published by American Society for Biochemistry and Molecular Biology., 273(35), pp. 22181–22187. doi: 10.1074/jbc.273.35.22181.

- Lim, P. H. *et al.* (2011) 'Regulation of *alr1* mg transporter activity by intracellular magnesium', *PLoS ONE*, 6(6). doi: 10.1371/journal.pone.0020896.
- Lim, P. O., Kim, H. J. and Nam, H. G. (2007) 'Leaf senescence', *Annual Review of Plant Biology*, 58, pp. 115–136. doi: 10.1146/annurev.arplant.57.032905.105316.
- van der Linde, K. and Göhre, V. (2021) 'How do smut fungi use plant signals to spatiotemporally orientate on and in planta?', *Journal of Fungi*, 7(2), pp. 1–13. doi: 10.3390/jof7020107.
- Lindenburg, L. H. *et al.* (2013) 'MagFRET: The first genetically encoded fluorescent Mg²⁺ sensor', *PLoS ONE*, 8(12). doi: 10.1371/journal.pone.0082009.
- Liu, Y. *et al.* (2019) 'Physiological and metabolomics analyses of young and old leaves from wild and cultivated soybean seedlings under low-nitrogen conditions', *BMC Plant Biology*. *BMC Plant Biology*, 19(1), pp. 1–15. doi: 10.1186/s12870-019-2005-6.
- Ludwig, N. *et al.* (2021) 'A cell surface-exposed protein complex with an essential virulence function in *Ustilago maydis*', *Nature Microbiology*. Springer US. doi: 10.1038/s41564-021-00896-x.
- Lunin, V. V. *et al.* (2006) 'Crystal structure of the CorA Mg²⁺ transporter', *Nature*, 440(7085), pp. 833–837. doi: 10.1038/nature04642.
- Ma, M. and Burd, C. G. (2020) 'Retrograde trafficking and plasma membrane recycling pathways of the budding yeast *Saccharomyces cerevisiae*', *Traffic*, 21(1), pp. 45–59. doi: 10.1111/tra.12693.
- MacAlister, C. A., Ohashi-Ito, K. and Bergmann, D. C. (2007) 'Transcription factor control of asymmetric cell divisions that establish the stomatal lineage', *Nature*, 445(7127), pp. 537–540. doi: 10.1038/nature05491.
- MacDiarmid, C. W. and Gardner, R. C. (1998) 'Overexpression of the *Saccharomyces cerevisiae* magnesium transport system confers resistance to aluminum ion', *Journal of Biological Chemistry*. © 1998 ASBMB. Currently published by Elsevier Inc; originally published by American Society for Biochemistry and Molecular Biology., 273(3), pp. 1727–1732. doi: 10.1074/jbc.273.3.1727.

- Maguire, M. E. (2006) 'Magnesium Transporters: Properties, Regulation and Structure Michael', *Frontiers in Bioscience*, 11(3), pp. 3149–3163. doi: 10.2741/2039.
- Mansfield, J. *et al.* (2012) 'Top 10 plant pathogenic bacteria in molecular plant pathology', *Molecular Plant Pathology*, 13(6), pp. 614–629. doi: 10.1111/j.1364-3703.2012.00804.x.
- Marschner, P. (2012) *Marschner's mineral nutrition of higher plants*. 3rd Editio, *Mineral nutrition of higher plants*. 3rd Editio. Edited by H. Marschner. London: Academic press.
- Martínez-Espinoza, A. D., García-Pedrajas, M. D. and Gold, S. E. (2002) 'The Ustilaginales as plant pests and model systems.', *Fungal genetics and biology: FG & B*, 35(1), pp. 1–20. doi: 10.1006/fgbi.2001.1301.
- Martinez, C. *et al.* (2000) 'Early infection of maize roots by *Sporisorium reilianum* f. sp. *zeae*', *Protoplasma*, 213(1–2), pp. 83–92. doi: 10.1007/BF01280508.
- Martinez, C. *et al.* (2002) 'The biological cycle of *Sporisorium reilianum* f.sp. *zeae*: An overview using microscopy', *Mycologia*, 94(3), pp. 505–514. doi: 10.1080/15572536.2003.11833215.
- Masaryk, J. and Sychrová, H. (2022) 'Yeast Trk1 Potassium Transporter Gradually Changes Its Affinity in Response to Both External and Internal Signals', *Journal of Fungi*, 8(5), pp. 1–22. doi: 10.3390/jof8050432.
- Mastop, M. *et al.* (2018) 'A FRET-based biosensor for measuring Gα13 activation in single cells', *PLoS ONE*, 13(3), pp. 1–19. doi: 10.1371/journal.pone.0193705.
- Mastrototaro, L. *et al.* (2016) 'Solute carrier 41A3 encodes for a mitochondrial Mg²⁺ efflux system', *Scientific Reports*. Nature Publishing Group, 6(June), pp. 1–14. doi: 10.1038/srep27999.
- Max Planck Society (2021) *On the trail of an expert plant intruder | Max Planck Institute for Terrestrial Microbiology*. Available at: <https://www.mpi-marburg.mpg.de/1099801/2021-05-a> (Accessed: 18 July 2022).
- McSwain, B. D., Tsujimoto, H. Y. and Arnon, D. I. (1976) 'EFFECTS OF MAGNESIUM AND CHLORIDE IONS ON LIGHT-INDUCED ELECTRON

- TRANSPORT IN MEMBRANE FRAGMENTS FROM A BLUE- GREEN ALGA*', *Biochimica et Biophysica Acta BBA47038*, 423, pp. 313–322. doi: 10.1016/0005-2728(76)90188-2.
- Mendgen, K. and Hahn, M. (2002) 'Plant infection and the establishment of fungal biotrophy', *Trends in Plant Science*, 7(8), pp. 352–356. doi: 10.1016/S1360-1385(02)02297-5.
- Mendoza-Mendoza, A. *et al.* (2009) 'Physical-chemical plant-derived signals induce differentiation in *Ustilago maydis*', *Molecular Microbiology*, 71(4), pp. 895–911. doi: 10.1111/j.1365-2958.2008.06567.x.
- Meng, S. *et al.* (2009) 'Common processes in pathogenesis by fungal and oomycete plant pathogens, described with Gene Ontology terms', *BMC Microbiology*, 9(SUPPL. 1), pp. 1–11. doi: 10.1186/1471-2180-9-S1-S7.
- Mueller, A. N. *et al.* (2013) 'Compatibility in the *Ustilago maydis*-Maize Interaction Requires Inhibition of Host Cysteine Proteases by the Fungal Effector Pit2', *PLoS Pathogens*, 9(2). doi: 10.1371/journal.ppat.1003177.
- Murray, J. D. *et al.* (2013) 'Signaling at the root surface: The role of cutin monomers in mycorrhization', *Molecular Plant*, 6(5), pp. 1381–1383. doi: 10.1093/mp/sst090.
- Nadeau, J. A. and Sack, F. D. (2002) 'Control of stomatal distribution on the *Arabidopsis* leaf surface', *Science*, 296(5573), pp. 1697–1700. doi: 10.1126/science.1069596.
- Naim, F. *et al.* (2021) 'Synchrotron X-ray fluorescence microscopy-enabled elemental mapping illuminates the "battle for nutrients" between plant and pathogen', *Journal of Experimental Botany*, 72(7), pp. 2757–2768. doi: 10.1093/jxb/erab005.
- Newman, Z. R. *et al.* (2016) 'Differences in codon bias and GC content contribute to the balanced expression of TLR7 and TLR9', *Proceedings of the National Academy of Sciences*, 113(10), pp. E1362–E1371. doi: 10.1073/pnas.1518976113.
- Niks, R. E. and Rubiales, D. (2002) 'Potentially durable resistance mechanisms in plants to specialised fungal pathogens', pp. 201–216.
- O'Connell, R. J. and Panstruga, R. (2006) 'Tête à tête inside a plant cell: Establishing

- compatibility between plants and biotrophic fungi and oomycetes', *New Phytologist*, 171(4), pp. 699–718. doi: 10.1111/j.1469-8137.2006.01829.x.
- Ökmen, B. *et al.* (2018) 'Mining the effector repertoire of the biotrophic fungal pathogen *Ustilago hordei* during host and non-host infection', *Molecular Plant Pathology*, 19(12), pp. 2603–2622. doi: 10.1111/mpp.12732.
- Park, E. *et al.* (2018) 'Plant–microbe interactions: organelles and the cytoskeleton in action', *New Phytologist*, 217(3), pp. 1012–1028. doi: 10.1111/nph.14959.
- Park, H. S. *et al.* (2019) 'Calcium-Calmodulin-Calcineurin Signaling: A Globally Conserved Virulence Cascade in Eukaryotic Microbial Pathogens', *Cell Host and Microbe*. Elsevier Inc., 26(4), pp. 453–462. doi: 10.1016/j.chom.2019.08.004.
- Payandeh, J., Pfoh, R. and Pai, E. F. (2013) 'The structure and regulation of magnesium selective ion channels', *Biochimica et Biophysica Acta (BBA) - Biomembranes*. Elsevier B.V., 1828(11), pp. 2778–2792. doi: 10.1016/j.bbamem.2013.08.002.
- Pisat, N. P., Pandey, A. and MacDiarmid, C. W. (2009) 'MNR2 regulates intracellular magnesium storage in *Saccharomyces cerevisiae*', *Genetics*, 183(3), pp. 873–884. doi: 10.1534/genetics.109.106419.
- Plücker, L. (2017) *Analysing the infection biology of the Brassicaceae smut Thecaphora thlaspeos* Master Thesis. Heinrich-Heine-University Düsseldorf.
- Plücker, L. *et al.* (2021) 'Genetic Manipulation of the Brassicaceae Smut Fungus *Thecaphora thlaspeos*', *Journal of Fungi*, 7(1), p. 38. doi: 10.3390/jof7010038.
- Pollard, M. *et al.* (2008) 'Building lipid barriers: biosynthesis of cutin and suberin', *Trends in Plant Science*, 13(5), pp. 236–246. doi: 10.1016/j.tplants.2008.03.003.
- Poloni, A. and Schirawski, J. (2016) 'Host specificity in *Sporisorium reilianum* is determined by distinct mechanisms in maize and sorghum', *Molecular Plant Pathology*, 17(5), pp. 741–754. doi: 10.1111/mpp.12326.
- Lo Presti, L. *et al.* (2015) 'Fungal Effectors and Plant Susceptibility.', *Annual review of plant biology*, 66, pp. 513–545. doi: 10.1146/annurev-arplant-043014-114623.
- Provart, N. J. *et al.* (2016) '50 years of Arabidopsis research: Highlights and future

- directions', *New Phytologist*, 209(3), pp. 921–944. doi: 10.1111/nph.13687.
- Qi, M. *et al.* (2019) 'Candidate Effectors From *Uromyces appendiculatus*, the Causal Agent of Rust on Common Bean, Can Be Discriminated Based on Suppression of Immune Responses', *Frontiers in Plant Science*, 10(October). doi: 10.3389/fpls.2019.01182.
- Quamme, G. A. (2010) 'Molecular identification of ancient and modern mammalian magnesium transporters', *American Journal of Physiology - Cell Physiology*. doi: 10.1152/ajpcell.00124.2009.
- Rago, A. M. *et al.* (2017) 'Peanut Smut: From an Emerging Disease to an Actual Threat to Argentine Peanut Production', *Plant Disease*, 101(3), pp. 400–408.
- Ramanadane, K. *et al.* (2022) 'Structural and functional properties 1 of a magnesium transporter of the SLC11/NRAMP family', *eLife*, 11, pp. 1–29. doi: 10.7554/eLife.74589.
- Ramos-Alonso, L. *et al.* (2020) 'Iron Regulatory Mechanisms in *Saccharomyces cerevisiae*', *Frontiers in Microbiology*, 11(September), pp. 1–8. doi: 10.3389/fmicb.2020.582830.
- Rauwane, M. E. *et al.* (2020) 'Pathogenicity and virulence factors of *Fusarium graminearum* including factors discovered using next generation sequencing technologies and proteomics', *Microorganisms*, 8(2). doi: 10.3390/microorganisms8020305.
- Redkar, A., Jaeger, E. and Doehlemann, G. (2018) 'Visualization of Growth and Morphology of Fungal Hyphae in planta Using WGA-AF488 and Propidium Iodide Co-staining', *Bio-Protocol*, 8(14), pp. 1–7. doi: 10.21769/bioprotoc.2942.
- Reza, M. H. *et al.* (2016) 'Magnesium uptake by cora transporters is essential for growth, development and infection in the rice blast fungus *magnaporthe oryzae*', *PLoS ONE*, 11(7), pp. 1–30. doi: 10.1371/journal.pone.0159244.
- Romani, A. and Scarpa, A. (1992) 'Regulation of cell magnesium', *Archives of Biochemistry and Biophysics*, 298(1), pp. 1–12. doi: 10.1016/0003-9861(92)90086-C.
- Rosenbaum, D. M., Rasmussen, S. G. F. and Kobilka, B. K. (2009) 'The structure

and function of G-protein-coupled receptors', *Nature*, 459(7245), pp. 356–363. doi: 10.1038/nature08144.

Routledge, S. J. *et al.* (2015) 'The synthesis of recombinant membrane proteins in yeast for structural studies', *Methods*. Elsevier Inc., 95(2015), pp. 26–37. doi: 10.1016/j.ymeth.2015.09.027.

Roy, A. *et al.* (2020) 'Calcium signaling is involved in diverse cellular processes in fungi', *Mycology*. Taylor & Francis, 12(1), pp. 1–15. doi: 10.1080/21501203.2020.1785962.

Sacristán, S. and García-Arenal, F. (2008) 'The evolution of virulence and pathogenicity in plant pathogen populations', *Molecular Plant Pathology*, 9(3), pp. 369–384. doi: 10.1111/j.1364-3703.2007.00460.x.

Sambrook, J. - Fritsch, E.F. - Maniatis, T. (1989) *Molecular Cloning. A laboratory Manual*. Second Edi. Cold Spring Harbor: Cold Spring Harbor Laboratory Press.

Savary, S. *et al.* (2019) 'The global burden of pathogens and pests on major food crops', *Nature Ecology and Evolution*. Springer US, 3(3), pp. 430–439. doi: 10.1038/s41559-018-0793-y.

Saville, B. J., Donaldson, M. E. and Doyle, C. E. (2012) 'Investigating Host Induced Meiosis in a Fungal Plant Pathogen', in Swan, A. (ed.) *Meiosis - Molecular Mechanisms and Cytogenetic Diversity*. London: IntechOpen, p. 52. doi: 10.5772/30032.

Schoen, T. (2017) *The role of sugar transporters in virulence of the phytopathogenic fungus Thecaphora thlaspeos*. Heinrich-Heine-Universität.

Schuler, D. *et al.* (2015) 'Hxt1, a monosaccharide transporter and sensor required for virulence of the maize pathogen *Ustilago maydis*', *New Phytologist*, 206(3), pp. 1086–1100. doi: 10.1111/nph.13314.

Schulz, B. *et al.* (1990) 'The b alleles of *U. maydis*, whose combinations program pathogenic development, code for polypeptides containing a homeodomain-related motif.', *Cell*, 60(2), pp. 295–306. doi: 10.1016/0092-8674(90)90744-Y.

Sharma, R. *et al.* (2014) 'Gene Loss rather than gene gain is associated with a host

jump from monocots to dicots in the smut fungus *melanopsichium pennsylvanicum*', *Genome Biology and Evolution*, 6(8), pp. 2034–2049. doi: 10.1093/gbe/evu148.

Škerle, J. *et al.* (2020) 'Membrane Protein Dimerization in Cell-Derived Lipid Membranes Measured by FRET with MC Simulations', *Biophysical Journal*, 118(8), pp. 1861–1875. doi: 10.1016/j.bpj.2020.03.011.

Smith, R. L., Thompson, L. J. and Maguire, M. E. (1995) 'Cloning and characterization of MgtE, a putative new class of Mg²⁺ transporter from *Bacillus firmus* OF4', *Journal of Bacteriology*, 177(5), pp. 1233–1238. doi: 10.1128/jb.177.5.1233-1238.1995.

Snetselaar, K. M. (1993) 'Infection of Maize Stigmas by *Ustilago maydis*: Light and Electron Microscopy', *Phytopathology*, p. 843. doi: 10.1094/phyto-83-843.

Snetselaar, K. M. and Mims, C. W. (1992) 'Sporidial Fusion and Infection of Maize Seedlings by the Smut Fungus *Ustilago Maydis*', *Mycologia*, 84(2), pp. 193–203. doi: 10.1080/00275514.1992.12026126.

Southern, E. M. (1975) 'Detection of specific sequences among DNA fragments separated by gel electrophoresis', *Journal of Molecular Biology*, 98(3), pp. 503–517. doi: 10.1016/S0022-2836(75)80083-0.

Spanu, P. D. and Panstruga, R. (2017) 'Editorial: Biotrophic Plant-Microbe Interactions', *Frontiers in Plant Science*, 8(February), pp. 1–4. doi: 10.3389/fpls.2017.00192.

Spanu, P. and Kämper, J. (2010) 'Genomics of biotrophy in fungi and oomycetes-emerging patterns', *Current Opinion in Plant Biology*. Elsevier Ltd, 13(4), pp. 409–414. doi: 10.1016/j.pbi.2010.03.004.

Sponder, G. *et al.* (2010) 'Lpe10p modulates the activity of the Mrs2p-based yeast mitochondrial Mg²⁺channel', *FEBS Journal*, 277(17), pp. 3514–3525. doi: 10.1111/j.1742-4658.2010.07761.x.

Sponder, G. *et al.* (2013) 'The G-M-N motif determines ion selectivity in the yeast magnesium channel Mrs2p.', *Metallomics: integrated biometal science*, 5(6), pp. 745–52. doi: 10.1039/c3mt20201a.

- Steinberg, G. (2007) 'On the move: endosomes in fungal growth and pathogenicity', 5(April), pp. 309–316.
- Stockenhuber, R. *et al.* (2015) 'Efficient detection of novel nuclear markers for Brassicaceae by transcriptome sequencing', *PLoS ONE*, 10(6), pp. 1–19. doi: 10.1371/journal.pone.0128181.
- Strouse, C. E. (1974) 'The Crystal and Molecular Structure of Ethyl Chlorophyllide a ·2H₂O and Its Relationship to the Structure and Aggregation of Chlorophyll a', *Proceedings of the National Academy of Sciences*, 71(2), pp. 325–328. doi: 10.1073/pnas.71.2.325.
- Sugai, K. *et al.* (2020) 'High humidity causes abnormalities in the process of appressorial formation of blumeria graminis f. Sp. hordei', *Pathogens*, 9(1). doi: 10.3390/pathogens9010045.
- Szegedy, M. A. and Maguire, M. E. (1999) 'The CorA Mg²⁺ transport protein of Salmonella typhimurium. Mutagenesis of conserved residues in the second membrane domain', *Journal of Biological Chemistry*. © 1999 ASBMB. Currently published by Elsevier Inc; originally published by American Society for Biochemistry and Molecular Biology., 274(52), pp. 36973–36979. doi: 10.1074/jbc.274.52.36973.
- Tan, K. *et al.* (2009) 'Structure and electrostatic property of cytoplasmic domain of ZntB transporter', *Protein Science*, 18(10), pp. 2043–2052. doi: 10.1002/pro.215.
- Tanaka, S. *et al.* (2014) 'A secreted Ustilago maydis effector promotes virulence by targeting anthocyanin biosynthesis in maize', *eLife*, 3, p. e01355. doi: 10.7554/eLife.01355.
- Tanaka, S. *et al.* (2018) 'Neofunctionalization of the secreted Tin2 effector in the fungal pathogen Ustilago maydis', *Nature Microbiology*. doi: 10.1038/s41564-018-0304-6.
- Tang, R.-J. *et al.* (2022) 'Conserved mechanism for vacuolar magnesium sequestration in yeast and plant cells', *Nature Plants*. Springer US. doi: 10.1038/s41477-021-01087-6.
- Terfrüchte, M. *et al.* (2013) 'Establishing a versatile Golden Gate cloning system for genetic engineering in fungi', *Fungal Genetics and Biology*, 62, pp. 1–10. doi:

10.1016/j.fgb.2013.10.012.

Timmusk, S. *et al.* (2017) 'Perspectives and challenges of microbial application for crop improvement', *Frontiers in Plant Science*, 8(February), pp. 1–10. doi: 10.3389/fpls.2017.00049.

Tong, M. Y. *et al.* (2020) 'Identification and functional analysis of the CorA/MGT/MRS2-type magnesium transporter in banana', *PLoS ONE*, 15(10 October), pp. 1–18. doi: 10.1371/journal.pone.0239058.

Toruño, T. Y., Stergiopoulos, I. and Coaker, G. (2016) 'Plant-Pathogen Effectors: Cellular Probes Interfering with Plant Defenses in Spatial and Temporal Manners', *Annual Review of Phytopathology*, 54, pp. 419–441. doi: 10.1146/annurev-phyto-080615-100204.

Tsuba, M. *et al.* (2002) 'Chemical factors of the leaf surface involved in the morphogenesis of *Blumeria graminis*', *Physiological and Molecular Plant Pathology*, 60(2), pp. 51–57. doi: 10.1006/pmpp.2002.0376.

Vanky, K. (2004) 'Taxonomic studies on ustilaginomycetes - 24', *Mycotaxon -Ithaca Ny-*, 89, pp. 55–118.

Vollmeister, E. *et al.* (2012) 'Fungal development of the plant pathogen *Ustilago maydis*', *FEMS Microbiology Reviews*, 36(1), pp. 59–77. doi: 10.1111/j.1574-6976.2011.00296.x.

De Waard, M. *et al.* (1997) 'Direct binding of G-protein', *Nature*, 385(6615), pp. 446–450. doi: 10.1038/385446a0.

Wachek, M. *et al.* (2006) 'Oligomerization of the Mg²⁺-transport proteins Alr1p and Alr2p in yeast plasma membrane', *FEBS Journal*, 273(18), pp. 4236–4249. doi: 10.1111/j.1742-4658.2006.05424.x.

Wahl, R. *et al.* (2010) 'A novel high-affinity sucrose transporter is required for virulence of the plant pathogen *Ustilago maydis*', *PLoS Biology*, 8(2). doi: 10.1371/journal.pbio.1000303.

Walker, C. J. and Weinstein, J. D. (1991) 'Further characterization of the magnesium chelatase in isolated developing cucumber chloroplasts: Substrate specificity,

- regulation, intactness, and ATP requirements', *Plant Physiology*, 95(4), pp. 1189–1196. doi: 10.1104/pp.95.4.1189.
- Walters, D. R., McRoberts, N. and Fitt, B. D. L. (2008) 'Are green islands red herrings? Significance of green islands in plant interactions with pathogens and pests', *Biological Reviews*, 83(1), pp. 79–102. doi: 10.1111/j.1469-185X.2007.00033.x.
- Wang, E. *et al.* (2012) 'A common signaling process that promotes mycorrhizal and oomycete colonization of plants', *Current Biology*. Elsevier Ltd, 22(23), pp. 2242–2246. doi: 10.1016/j.cub.2012.09.043.
- Wang, Q. M. *et al.* (2015) 'Multigene phylogeny and taxonomic revision of yeasts and related fungi in the Ustilaginomycotina', *Studies in Mycology*. ELSEVIER B.V., 81, pp. 55–83. doi: 10.1016/j.simyco.2015.10.004.
- Wang, Z. *et al.* (2020) 'Magnesium Fertilization Improves Crop Yield in Most Production Systems: A Meta-Analysis', *Frontiers in Plant Science*, 10(January), pp. 1–10. doi: 10.3389/fpls.2019.01727.
- Weiberg, A. *et al.* (2013) 'Fungal small RNAs suppress plant immunity by hijacking host RNA interference pathways', *Science*, 342(6154), pp. 118–123. doi: 10.1126/science.1239705.
- Weiland, P. and Altegoer, F. (2021) 'Identification and Characterization of Two Transmembrane Proteins Required for Virulence of *Ustilago maydis*', *Frontiers in Plant Science*, 12(May). doi: 10.3389/fpls.2021.669835.
- Wicker, T. *et al.* (2013) 'The wheat powdery mildew genome shows the unique evolution of an obligate biotroph', *Nature Genetics*. Nature Publishing Group, 45(9), pp. 1092–1096. doi: 10.1038/ng.2704.
- Wiermer, M., Feys, B. J. and Parker, J. E. (2005) 'Plant immunity: The EDS1 regulatory node', *Current Opinion in Plant Biology*, 8(4), pp. 383–389. doi: 10.1016/j.pbi.2005.05.010.
- Wolpert, T. J., Dunkle, L. D. and Ciuffetti, L. M. (2002) 'Host-selective toxins and avirulence determinants: What's in a name?', *Annual Review of Phytopathology*, 40, pp. 251–285. doi: 10.1146/annurev.phyto.40.011402.114210.

- Xiao, S. *et al.* (2005) 'The atypical resistance gene, RPW8, recruits components of basal defence for powdery mildew resistance in Arabidopsis', *Plant Journal*, 42(1), pp. 95–110. doi: 10.1111/j.1365-313X.2005.02356.x.
- Yamaguchi-Iwai, Y. *et al.* (1996) 'Iron-regulated DNA binding by the AFT1 protein controls the iron regulon in yeast', *EMBO Journal*, 15(13), pp. 3377–3384. doi: 10.1002/j.1460-2075.1996.tb00703.x.
- Yang, L. N. *et al.* (2021) 'Pathogen-Mediated Stomatal Opening: A Previously Overlooked Pathogenicity Strategy in the Oomycete Pathogen *Phytophthora infestans*', *Frontiers in Plant Science*, 12(July), pp. 1–14. doi: 10.3389/fpls.2021.668797.
- Zacharias, D. A. *et al.* (2002) 'Partitioning of lipid-modified monomeric GFPs into membrane microdomains of live cells', *Science*, 296(5569), pp. 913–916. doi: 10.1126/science.1068539.
- Zelman, A. K. *et al.* (2012) 'Evolutionary and structural perspectives of plant cyclic nucleotide-gated cation channels', *Frontiers in Plant Science*, 3(MAY), pp. 1–13. doi: 10.3389/fpls.2012.00095.
- Zhang, B. *et al.* (2000) 'The role of Mg²⁺ cofactor in the guanine nucleotide exchange and GTP hydrolysis reactions of Rho family GTP-binding proteins', *Journal of Biological Chemistry*. © 2000 ASBMB. Currently published by Elsevier Inc; originally published by American Society for Biochemistry and Molecular Biology., 275(33), pp. 25299–25307. doi: 10.1074/jbc.M001027200.
- Zhang, Y. and Skolnick, J. (2005) 'TM-align: A protein structure alignment algorithm based on the TM-score', *Nucleic Acids Research*, 33(7), pp. 2302–2309. doi: 10.1093/nar/gki524.
- Zhou, F. *et al.* (2004) 'High humidity suppresses ssi4-mediated cell death and disease resistance upstream of MAP kinase activation, H₂O₂ production and defense gene expression', *Plant Journal*, 39(6), pp. 920–932. doi: 10.1111/j.1365-313X.2004.02180.x.

7 Supplements

17 Nov 2017

Alignment Results

Data Name: Align Multi Pit1 Um Pit1 reference
 Description: Global Protein alignment, 6 sequences
 File Name: C:\Users\Lesley\Go...\Align Multi Pit1 Um Pit1 reference.am4

Alignment: Global Protein alignment against reference molecule
 Parameters: Scoring matrix: BLOSUM 62

Reference molecule: Pit1 U-maydis, Region 1 to 435
 Number of sequences to align: 6
 Total length of aligned sequences with gaps: 977 aas
 Settings: Similarity significance value cutoff: >= 60%

Summary of Percent Matches:

Ref:	Pit1 U-maydis	1 to	435	(435 aa)	--
2:	Pit1 A-flocculos	1 to	738	(738 aa)	22%
3:	Pit1 T-thlaspeos	1 to	678	(678 aa)	23%
4:	Pit1 M-pennsylva	1 to	425	(425 aa)	64%
5:	Pit1 S-reilianum	1 to	423	(423 aa)	69%
6:	Pit1 P-hubeiensi	1 to	444	(444 aa)	69%

```

Pit1 U-maydis      1 merhdgeeyipaifggpphasqvislmkfsgetttwnlpimlaqally
Pit1 A-flocculos  1 mtrhdgssqvpfiiferg-pnvrqilalqdyaldqiwnnaplvlsqalll
Pit1 T-thlaspeos  1 mvrhdgselipvlfdsh-pkpsqlltlqtfaieqvwwnapivvsqalll
Pit1 M-pennsylva  1 merhdgseylpyifgse-phgsqvlalmrfsqeattwnlpmliaqtlly
Pit1 S-reilianum  1 mhrhdgteyvsaifagqpphapqvialmrmtqelttwnlpiaaqtllv
Pit1 P-hubeiensi  1 mqrhdgqeyipgvfantaphpsqvislirfsqenttwnlpmtiaqtlly

Pit1 U-maydis      51 eivrtypaelrmlhrfgrkhpnmaeiffilikyltifavifdilvtet
Pit1 A-flocculos  50 evlkrtpaeaamlrriyvrrkklhlaemffsikytsllsvilttlvqlt
Pit1 T-thlaspeos  50 eivrtypaelamfgriykrkpniaellfftikytsllavvvtiivqlt
Pit1 M-pennsylva  50 eivrtypaeirmlmrvyqrkknmaeiffvlikyltliavicdilvtet
Pit1 S-reilianum  51 eivrtypaemrmltrlvqrkknmaeiffvlikylalvavtldilvmmt
Pit1 P-hubeiensi  51 eivrtypaefrmvslvqrkhpnmaveffilikylcliauvldilvtet

Pit1 U-maydis      101 aartdfdcrsawwtstfyfmcstlvfcvlgwrariifrtsqvaswsls
Pit1 A-flocculos  100 vpgtdarcmafswasniltfaictlvvatiawrtsiifhrsrrvlallg
Pit1 T-thlaspeos  100 vpsmgnqcnalswvssiltfaictlvvitlawrnyiihlhrshrvlialc
Pit1 M-pennsylva  100 aaksdlacrwwawtstfyflcstlvfcvlgwrariifrtkrklatylit
Pit1 S-reilianum  101 aprtdfdcrsawwtstlyfvcstlvfcvlgwrariifrtcrvasylla
Pit1 P-hubeiensi  101 aarsdadcsawwtstlyfacstlvfavvswrariifrtsniaswvlg

Pit1 U-maydis      151 glmgqfavamwtnryvdkadaltpagtcapaaqvh-adasqrnaalqlh
Pit1 A-flocculos  150 gllvqvgltawavinyrtpialpnlgcapqgtnhkadps-----
Pit1 T-thlaspeos  150 glvidqililtgwavnnyrtpvllpnlgca-aidvr-v-rshkpa-----
Pit1 M-pennsylva  150 glvgqlaiamwantriskadalspagtcapaaqvh-gspdd-neslhih
Pit1 S-reilianum  151 glvgqfsvamwtntrvskadaltpagtcapaaqvh-g-gpnanaaltik
Pit1 P-hubeiensi  151 glsvqfaiamwtnryvdkadaltpagtcapssqvh-stpssnpalhlh

```

```

Pit1 U-maydis          200 wqsstfwflllyntifessilmacciklrktssgpgs--ltkiakvlfn
Pit1 A-flocculos     191 felstfwyvllynalfdlamvvssarlwqsargplg--farvssllfan
Pit1 T-thlaspeos     192 welstfwyvlfnclfdlvmvasssyqlwrsarsplg--farisallfn
Pit1 M-pennsylva     198 wqsstfwfllfyntifdlailliaccrlrktssgpng--ltqiakvlfin
Pit1 S-reilianum     199 wqsstfwflllyntlfesavmlaccvrlkrtssgpmg--ltqiakvlfvn
Pit1 P-hubeiensi     200 wqsstywflllyntvfeslimmaccwklkntssgpngvgltrianvlfdn

Pit1 U-maydis          248 vhythagvetcnvielvmllgwtslppvhitsiaiqivvglqmligeqe
Pit1 A-flocculos     239 vhyaicadvvnlvvelvtilgfrgsvpsyqylviaiaigmgvmqmliteqe
Pit1 T-thlaspeos     240 ihyalcvdlsnmielvailayrdvipdyqflniaigamtgmqlliseqn
Pit1 M-pennsylva     246 vhyivavetcnlltvvmlmgwasklppvhstsiaiqivvglqmligeqe
Pit1 S-reilianum     247 vhythagvetcnfvvelvmllgwasslppvhmtsiaiqivvglqmligeqe
Pit1 P-hubeiensi     250 vhythagvetcnvisaimlmgwpts lppvhmtsiaiqivvglqmligeqe

Pit1 U-maydis          298 vys-----pt-----csql-sys-----
Pit1 A-flocculos     289 vya-----pr-----gatvasynfplqsiggshhgggg-
Pit1 T-thlaspeos     290 vynrqgtsaptynlpllesrglgsgctav-gsstisivarkgpsvsavaa
Pit1 M-pennsylva     296 vys-----ps-----csrv-tys-----
Pit1 S-reilianum     297 vys-----ps-----csty-s-s-----
Pit1 P-hubeiensi     300 vys-----pt-----csgm-tfs-----

Pit1 U-maydis          310 -----q--ys--sdsqg-----vi--
Pit1 A-flocculos     317 -----a--vg-ggggggsgcatsagfahgggagstslssaqlrk--
Pit1 T-thlaspeos     339 arkatvq--ke--sdaeq-----magv
Pit1 M-pennsylva     308 -----tggfs--snngs-----ys--
Pit1 S-reilianum     308 -----g--ya--stngt-----yv--
Pit1 P-hubeiensi     312 -----a--yststng-----yv--

Pit1 U-maydis          320 -----nkh--haat-----s
Pit1 A-flocculos     355 -----skh--hada-----t
Pit1 T-thlaspeos     358 vsiafdlrsersihtplpfsdredcaersmpppplpskn-gestndtips
Pit1 M-pennsylva     320 -----kph--hnat-----
Pit1 S-reilianum     318 -----nkh--htat-----s
Pit1 P-hubeiensi     323 -----nkh--htas-----d

Pit1 U-maydis          328 ssngtfstpertsly-----vkrpgtgtv-----
Pit1 A-flocculos     363 smgsiatlnmttlsepdeprmrvtasfersvdhprsgtpapfseksapp
Pit1 T-thlaspeos     406 stkgptnlssnatai-----gnrcskrlft-----
Pit1 M-pennsylva     327 ssnasfsspnhsly-----vkrpgtantg-----
Pit1 S-reilianum     327 ssn-ftapgrtly-----vkrpgtant-----
Pit1 P-hubeiensi     332 ssnithslpgralsy-----vkrpgtanta-----

Pit1 U-maydis          353 -----adigc
Pit1 A-flocculos     413 apvagqdlvlsmttittatsyadpdgktapslaftrlrqzrhasdggi
Pit1 T-thlaspeos     431 -----pdssr
Pit1 M-pennsylva     352 -----tdvts
Pit1 S-reilianum     -----
Pit1 P-hubeiensi     357 -----tdggf

Pit1 U-maydis          359 das-----gggqhgrkgt-----
Pit1 A-flocculos     463 ddsldddddddldkqspkergavvphgpgagtggglgrkgt-----
Pit1 T-thlaspeos     437 dvallr-----tggmdgrkneggvminstr
Pit1 M-pennsylva     358 e-----yrgrkgt-----
Pit1 S-reilianum     350 -----dtgyparknt-----
Pit1 P-hubeiensi     363 gesrvvg-----aggkhgrkgt-----

```

```

Pit1 U-maydis          372 ----fs-----sissvpayvkan---p---
Pit1 A-flocculos      503 ----gavkelehtcgngepvkdhkgigidvddykshassd---dtrem
Pit1 T-thlaspeos      463 tqtidfsh-----ststlsaydvdn---d---
Pit1 M-pennsylva      366 ----fs-----sissvpayvks---p---
Pit1 S-reilianum      360 ----fs-----scssvpayvrs---p---
Pit1 P-hubeiensi      380 ----fs-----sissipayvksigigga---

Pit1 U-maydis          388 vet-----vspqm-----psk---a
Pit1 A-flocculos      545 vdl-----adpavsrsssfssssssassftlsgcpppskvfa
Pit1 T-thlaspeos      485 sesyrsmlhhaqdvsv-----pls--l
Pit1 M-pennsylva      381 tde-----lapql-----ppk--s
Pit1 S-reilianum      376 eel-----aapqp-----ppk--s
Pit1 P-hubeiensi      399 ded-----vapqv-----pak--g

Pit1 U-maydis          401 sqsiyk----revvtvdmsspvp---p---pg-----pspap
Pit1 A-flocculos      583 tsspttt----ttvetskplapqppbcdgp---rgiegrrapsip
Pit1 T-thlaspeos      510 agtpggrtissageangppnspsrp---plrshtpi-----pylpp
Pit1 M-pennsylva      393 --tvnmk----qevqvsidmspvp---q-----sg-----atnva
Pit1 S-reilianum      388 --tiqyr----qdvvtvdmvgqcp---l---pa-----haqaa
Pit1 P-hubeiensi      411 --piqfr----qdvqvtvdaspvhp---s---agg-----aapp

Pit1 U-maydis          -----
Pit1 A-flocculos      -----
Pit1 T-thlaspeos      550 ltghpyqrrprtassstasssispsytrpqtasssvatahategvdieye
Pit1 M-pennsylva      -----
Pit1 S-reilianum      -----
Pit1 P-hubeiensi      -----

Pit1 U-maydis          -----
Pit1 A-flocculos      -----
Pit1 T-thlaspeos      600 vdeesetesrragratgtsaataaagrgededaetsmssrfsadephlr
Pit1 M-pennsylva      -----
Pit1 S-reilianum      -----
Pit1 P-hubeiensi      -----

Pit1 U-maydis          431 -----papym-----
Pit1 A-flocculos      623 -----hpbqlldhpytqrpdrppasapasslaslshsskq
Pit1 T-thlaspeos      650 kgsilasmggkvpapfkgvkgkldslrgrs-----
Pit1 M-pennsylva      421 -----dgpfq-----
Pit1 S-reilianum      416 -----pappmpyl-----
Pit1 P-hubeiensi      440 -----papym-----

Pit1 U-maydis          -----
Pit1 A-flocculos      662 raaavivhldvdasdeharaphghrqrerdgetspgsafsvdgahr
Pit1 T-thlaspeos      -----
Pit1 M-pennsylva      -----
Pit1 S-reilianum      -----
Pit1 P-hubeiensi      -----

Pit1 U-maydis          -----
Pit1 A-flocculos      712 lrhvggsvqslkqtvrerldsiraral
Pit1 T-thlaspeos      -----
Pit1 M-pennsylva      -----
Pit1 S-reilianum      -----
Pit1 P-hubeiensi      -----

```

Figure 7-1 Pit1 protein alignment

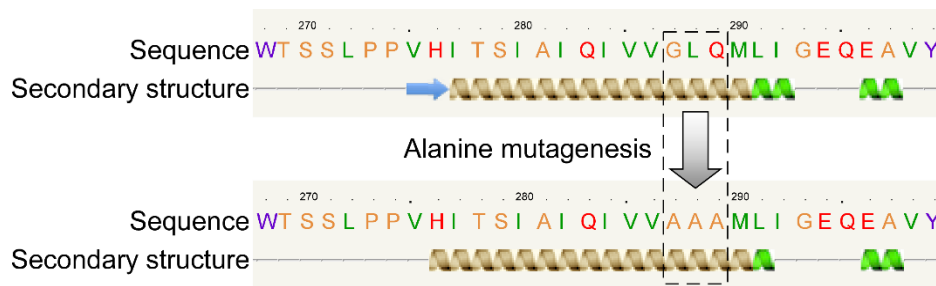


Figure 7-2 Section of the Pit1 secondary structure prediction before and after alanine mutagenesis of the GLQ motif using the Phyre2 algorithm (Kelly et al., 2015). Exchange of the GLQ motif with alanine does not affect the predicted alpha helix conformation of the protein.

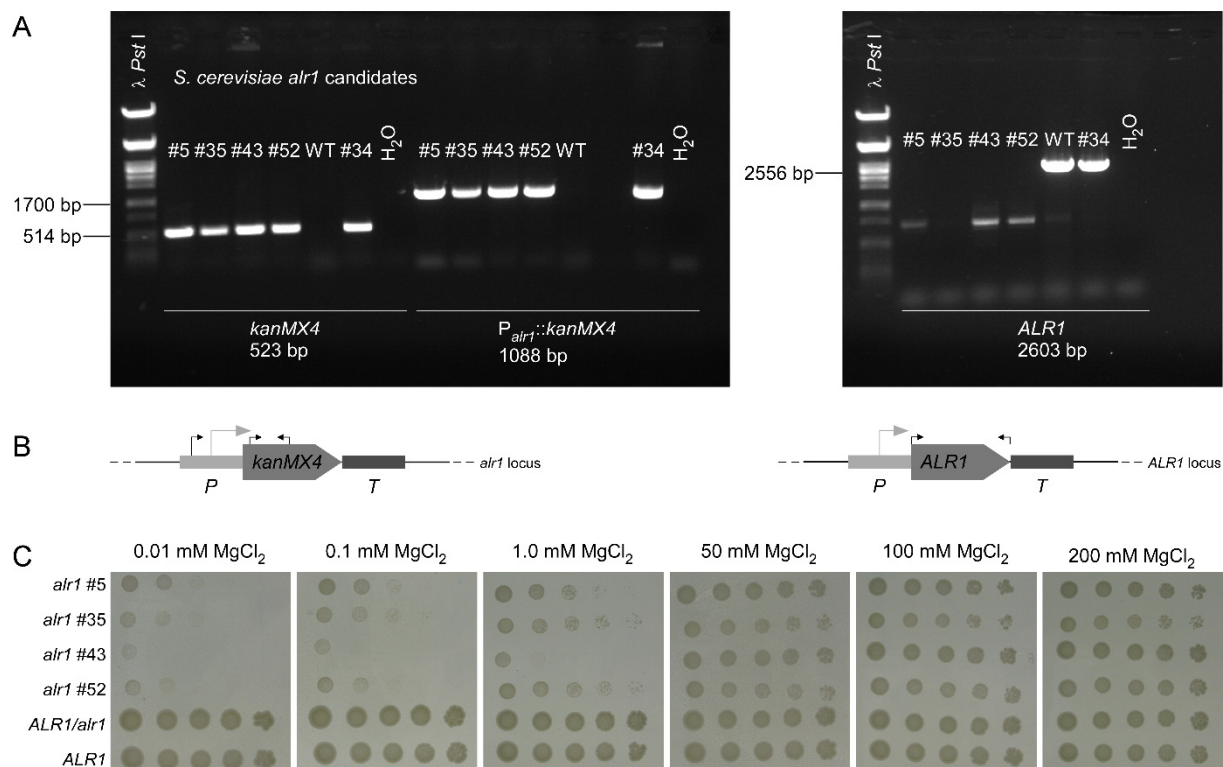


Figure 7-3 Confirmation of haploid *S. cerevisiae alr1* candidates after isolation from random sporulation of an *ALR1/alr1* *S. cerevisiae* strain (Euroscarf Accession number: Y26280).

A: Verification of insertion of the *kanMX4* resistance marker into the *ALR1* open reading frame in *S. cerevisiae alr1* candidates via colony PCR. Amplified was a fragment of the resistance marker *kanMX4* (523 bp), a fragment spanning the *ALR1* promoter and the *kanMX4* marker to test for correct insertion of the marker into the *ALR1* ORF (1088 bp) and the *ALR1* ORF (2603 bp) in the *alr1* candidates #5, #34, #35, #43, #52 and a haploid *ALR1* WT strain (CEN.PK2-1C). The candidates #5, #35, #43 and #52 show the expected bands for a haploid *alr1* strain with correct insertion of the *kanMX4* marker into the *ALR1* ORF, while #34 is still diploid (*ALR1/alr1*).

B: Model of the *ALR1* WT locus and the *alr1* locus after insertion of *kanMX4* into the *ALR1* ORF. Black arrows indicate the position of forward and reverse primers to amplify the fragments in A.

C: *S. cerevisiae alr1* candidates show a Mg^{2+} dependent growth phenotype. The diploid *ALR1/alr1* progenitor strain, the haploid *ALR1* WT and the *alr1* candidates confirmed in colony PCR were grown in serial dilutions on synthetic defined medium (SD medium) supplemented with $MgCl_2$ in the concentrations indicated. The *alr1* candidates #5, #35, #43 and #52 showed a Mg^{2+} dependent growth defect between 0.01 mM and 1 mM $MgCl_2$ in comparison to the WT strains *ALR1/alr1* and *ALR1*. Between 50 mM and 200 mM the *alr1* strains grew like WT.

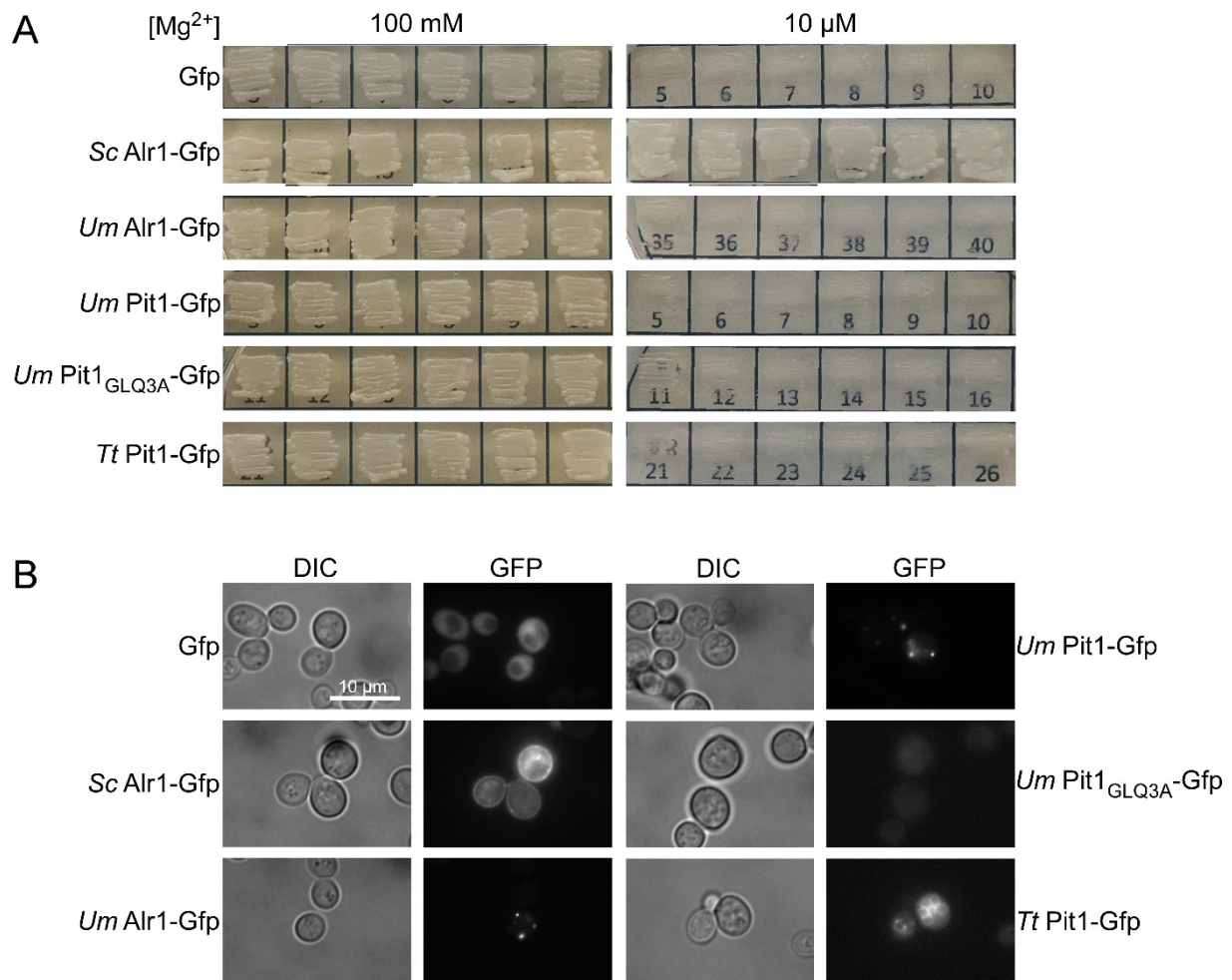
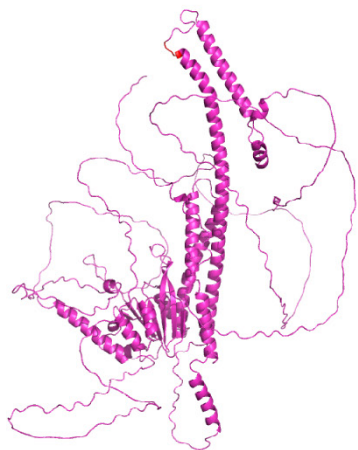


Figure 7-4 Complementation analysis of *S. cerevisiae alr1* deletion strain with *ScALR1-GFP*, *Umalr1-gfp*, *Umpit1-gfp*, *Umpit1_{GLQ3A}-gfp*, *Ttpit1-gfp* and an empty vector control expressing cytosolic Gfp.

A: Ten transformants for each construct were patched on SD-His supplemented with 100 mM or 10 μ M MgCl₂ (6/10 candidates are depicted here). None of the constructs restored growth of the *alr1* deletion strain on 10 μ M MgCl₂ except for *ScALR1-GFP*.

B: Microscopy of three transformants per construct revealed that *Sc Alr1-Gfp* localizes to the plasma membrane, but all other fusion proteins mislocalize to other cellular compartments. In case of the *Umpit1_{GLQ3A}-gfp* construct the fusion protein is not even expressed. Microscopy was performed once. Intensities for the GFP channel are optimized for each image and not comparable between each other.

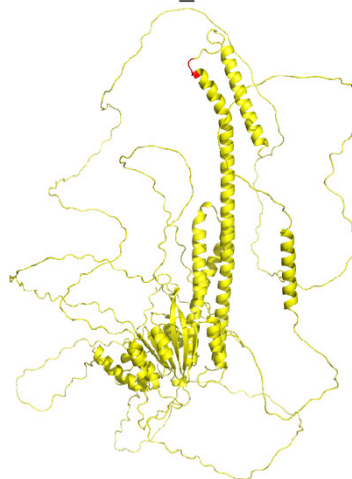
S. cerevisiae ALR1p



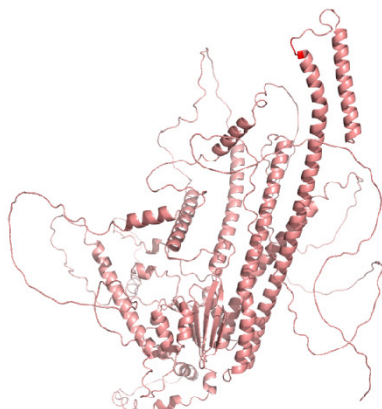
S. cerevisiae ALR2p



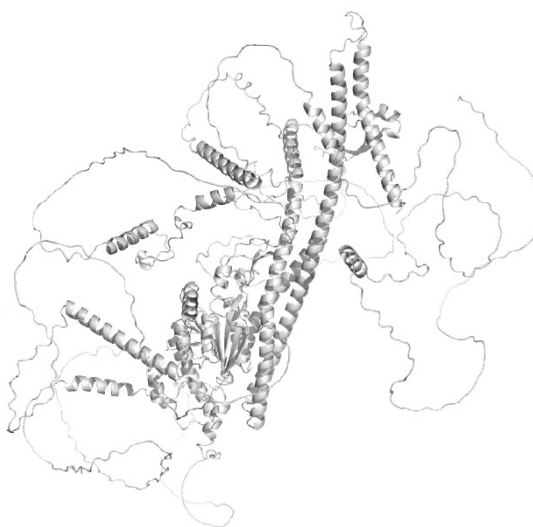
UMAG_00361



S. cerevisiae MNR2p



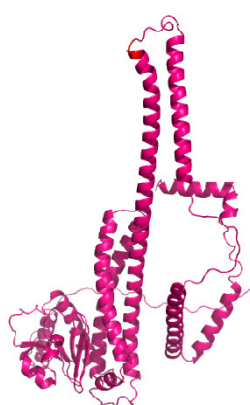
UMAG_10049



S. cerevisiae LPE10p



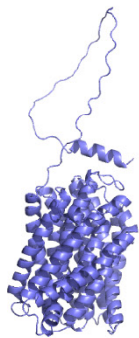
S. cerevisiae MRS2p



UMAG_10884



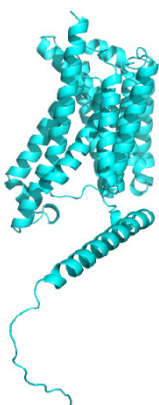
H. sapiens SLC41 3X1



UMAG_00219



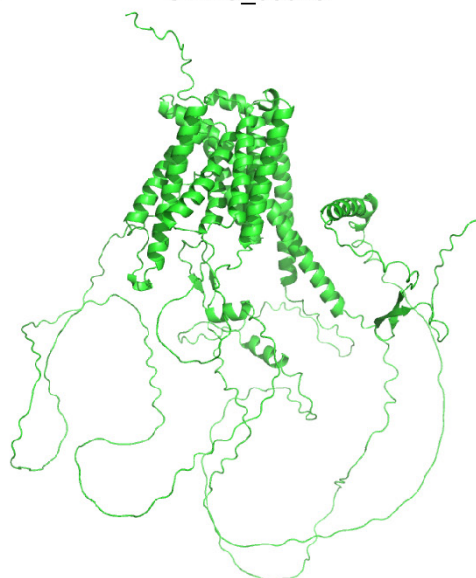
H. sapiens NIPA2 a



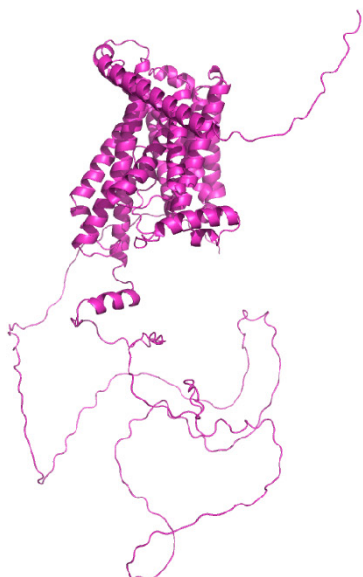
H. sapiens NIPA-like 2 a



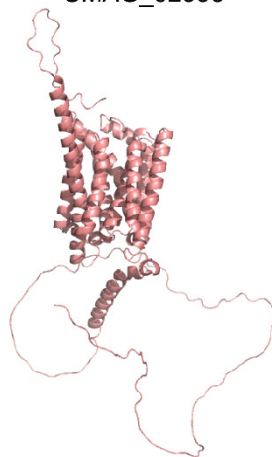
UMAG_03028



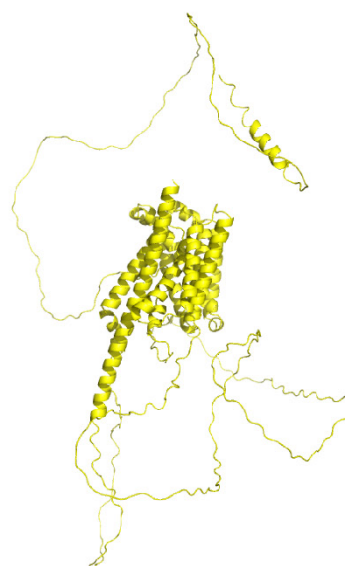
UMAG_01797



UMAG_02993



UMAG_02316



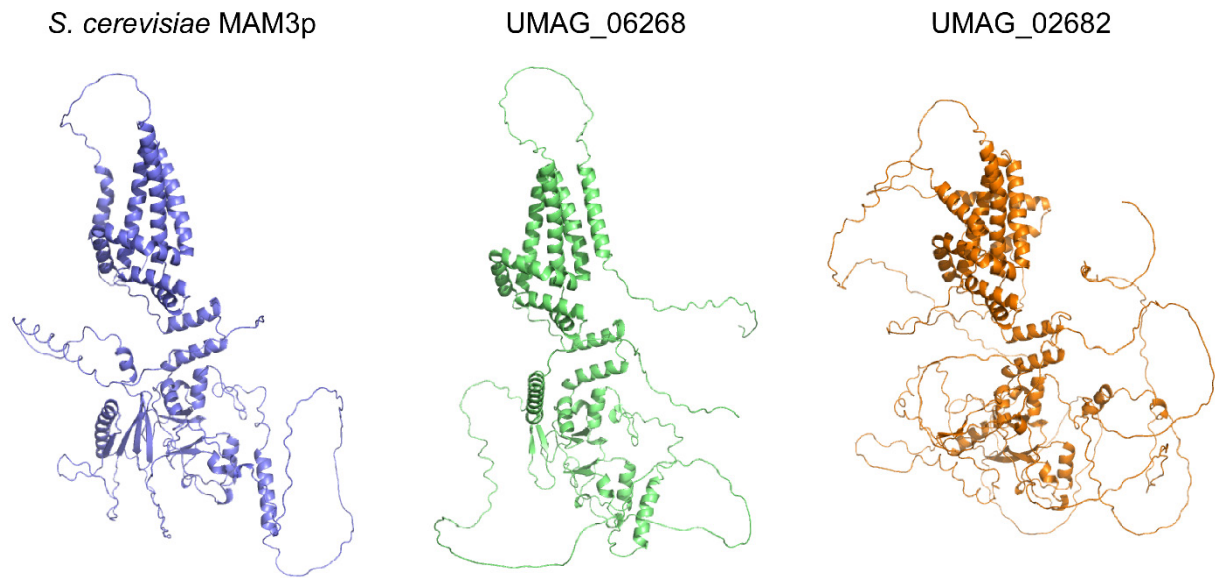


Figure 7-5 Protein structure predictions of the complete *U. maydis* Mg²⁺ transporter repertoire and their closest characterized homologue of *S. cerevisiae* or *H. sapiens* generated with AlphaFold2 (Jumper *et al.*, 2021). The GMN motifs of the CorA-type Mg²⁺ transporters are marked in red.

	Mam3-like	MgtE	Nipa1	Nipa2	Nipa3	Nipa4	Mnr2	Alr1	Mrs2/Lpe10	Mam3
<i>Saccharomyces cerevisiae</i>							●	●	●	●
<i>Candida albicans</i>					●	●	●	●	●	●
<i>Magnaporthe oryzae</i>			●	●	●	●	●	●	●	●
<i>Neurospora crassa</i>			●	●	●	●	●	●	●	●
<i>Botrytis cinerea</i>			●	●	●	●	●	●	●	●
<i>Aspergillus nidulans</i>			●	●	●	●	●	●	●	●
<i>Piriformospora indica</i>		●	●	●	●	●	●	●	●	●
<i>Ustilago maydis</i>	●	●	●	●	●	●	●	●	●	●
<i>Pseudozyma hubeiensis</i>	●	●	●	●	●	●	●	●	●	●
<i>Sporisorium reilianum</i>	●	●	●	●	●	●	●	●	●	●
<i>Sporisorium scitamineum</i>	●	●	●	●	●	●	●	●	●	●
<i>Ustilago hordei</i>	●	●	●	●	●	●	●	●	●	●
<i>Ustilago bromivora</i>	●	●	●	●	●	●	●	●	●	●
<i>Melanopsychium pennsylvanicum</i>	●	●	●	●	●	●	●	●	●	●
<i>Anthracoystis flocculosa</i>	●	●	●	●	●	●	●	●	●	●
<i>Thecaphora thlaspeos</i>	●	●	●	●	●	●	●	●	●	●
<i>Homo sapiens</i>		●	●	●	●	●			●	●

Figure 7-6 Conservation of the Mg²⁺ transporter repertoire of *U. maydis* in other fungi and *H. sapiens*. Putative homologues of the *U. maydis* Mg²⁺ transporters were identified in the listed asco- and basidiomycetes as well as *H. sapiens* via protein BLAST search.

Table 7-1 Overview about the structural similarity of potential *U. maydis* Mg²⁺ transporters (query) and their respective homologs (reference protein) according to sequence- and structure-based alignment. (RMSD = root-mean-square deviation of atomic positions)

Query	Reference protein	Sequence-based alignment		Structure-based alignment			
		Pymol RMSD [Å]	Pymol aligned atoms	Pymol RMSD [Å]	Pymol aligned atoms	TM align RMSD [Å]	TM align aligned residues
UMAG_00219	SLC41A3	2.004	311/657	2.172	1795/2356	3.55	428/657
UMAG_10049	<i>S. cerevisiae</i> MNR2p	38.026	725/969	10.433	1498/1699	6.63	572/969
UMAG_10049	<i>S. cerevisiae</i> Alr1p	41.705	622/859	20.161	1015/1221	5.76	476/859
UMAG_00361	<i>S. cerevisiae</i> Alr1p	10.674	430/859	1.299	1826/2147	4.48	433/859
UMAG_00361	<i>S. cerevisiae</i> Alr2p	38.421	582/858	1.166	1730/2163	4.69	431/858
UMAG_00361	<i>S. cerevisiae</i> MNR2p	26.05	564/881	2.055	1321/1764	5.25	503/881
UMAG_10884	<i>S. cerevisiae</i> LPE10p	1.229	263/413	1.090	1381/2002	3.14	356/413
UMAG_10884	<i>S. cerevisiae</i> MRS2p	1.403	261/470	1.213	1565/2003	3.49	345/470
UMAG_01797	<i>H. sapiens</i> NIPA2 a	1.428	173/657	1.537	1791/2105	2.33	308/360
UMAG_01797	<i>H. sapiens</i> NIPA-like 2 a	1.944	238/657	2.999	1330/1853	3.25	315/383
UMAG_03028	<i>H. sapiens</i> NIPA2 a	3.808	202/823	1.574	698/866	3.49	303/360
UMAG_03028	<i>H. sapiens</i> NIPA-like 2 a	5.230	202/823	1.920	744/995	4.43	330/383
UMAG_02316	<i>H. sapiens</i> NIPA2 a	1.019	194/653	1.353	1230/1807	2.52	311/360
UMAG_02316	<i>H. sapiens</i> NIPA-like 2 a	1.013	220/653	1.397	1168/1739	2.29	303/383
UMAG_02993	<i>H. sapiens</i> NIPA2 a	4.849	270/476	5.479	1834/2159	4.96	286/360
UMAG_02993	<i>H. sapiens</i> NIPA-like 2 a	4.727	254/476	5.651	1650/1786	5.66	302/383
UMAG_06268	<i>S. cerevisiae</i> MAM3p	3.995	374/645	1.477	2238/2446	4.07	445/645
UMAG_02682	<i>S. cerevisiae</i> MAM3p	6.905	356/706	1.188	1119/1366	4.18	402/706

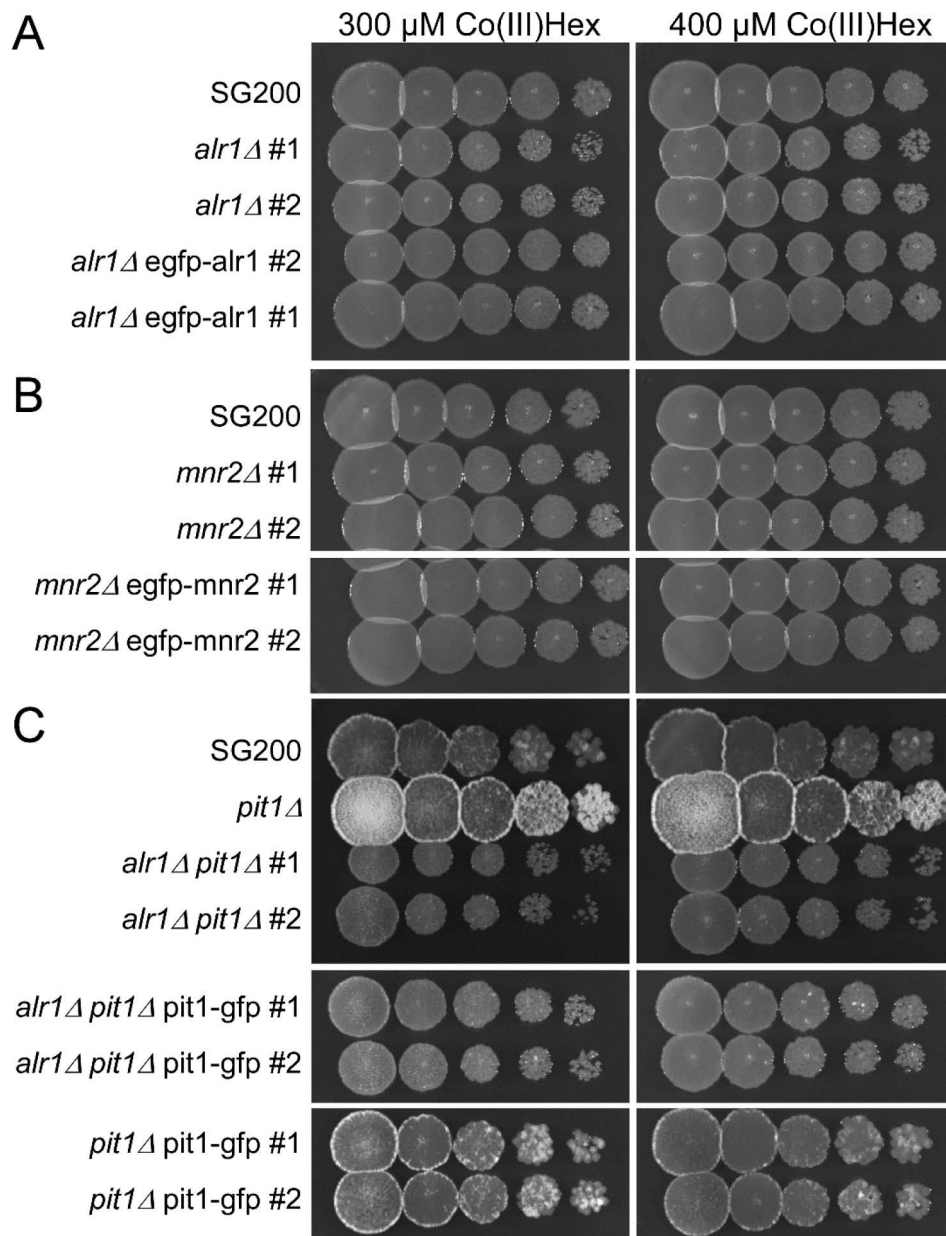


Figure 7-7 Growth of CorA-type Mg^{2+} transporter deletion mutants and complementation strains is not impaired in presence of the CorA-type Mg^{2+} transporter inhibitor hemaammin-cobalt(III)-chloride (Co(III)Hex).

A: SG200, *alr1Δ* and *egfp-alr1* complementation strains were grown in serial dilutions on YEPS light complex medium supplemented with 20 mM $MgCl_2$ and 300 μM or 400 μM Co(III)Hex. None of the strains show a growth reduction. The experiment was performed once.

B: SG200, *mnr2Δ* and *egfp-mnr2* complementation strains were grown in serial dilutions on YEPS light complex medium supplemented with 20 mM $MgCl_2$ and 300 μM or 400 μM Co(III)Hex. None of the strains show a growth reduction. The experiment was performed once.

C: SG200, *Pit1Δ*, *alr1Δ pit1Δ*, *pit1-egfp* over expression strains and *alr1Δ pit1Δ pit1-egfp* complementation strains were grown in serial dilutions on YEPS light complex medium supplemented with 20 mM $MgCl_2$ and 300 μM or 400 μM Co(III)Hex. None of the strains show a growth reduction. The experiment was performed once.

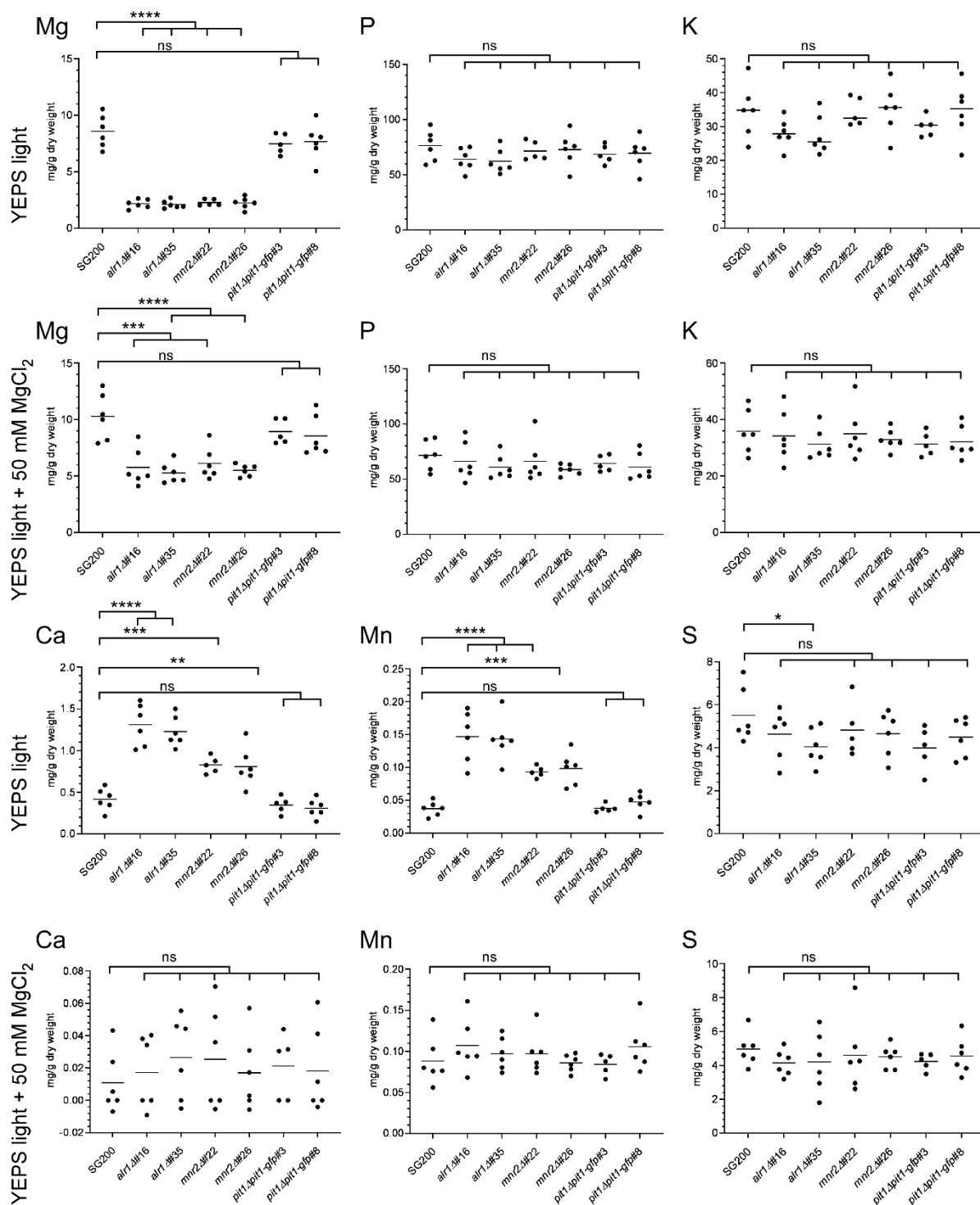


Figure 7-8 Analysis of the Mg, P, K, Ca, Mn and S composition of Mg²⁺ transporter mutants and Pit1-Gfp overexpression strains.

SG200, *alr1Δ*, *mnr2Δ* and Pit1-Gfp overexpression strains were pregrown in YEPS light supplemented with 50 mM MgCl₂ and subsequently shifted to standard YEPS light or YEPS light supplemented with 50 mM MgCl₂ complex medium for 8 h. The element composition of the cells was analysed using ICP-MS. For each element the concentration is given for every strain. Significance of differences between the respective strain and SG200 is indicated above (multiple unpaired t test comparisons calculated with Prism8 software).

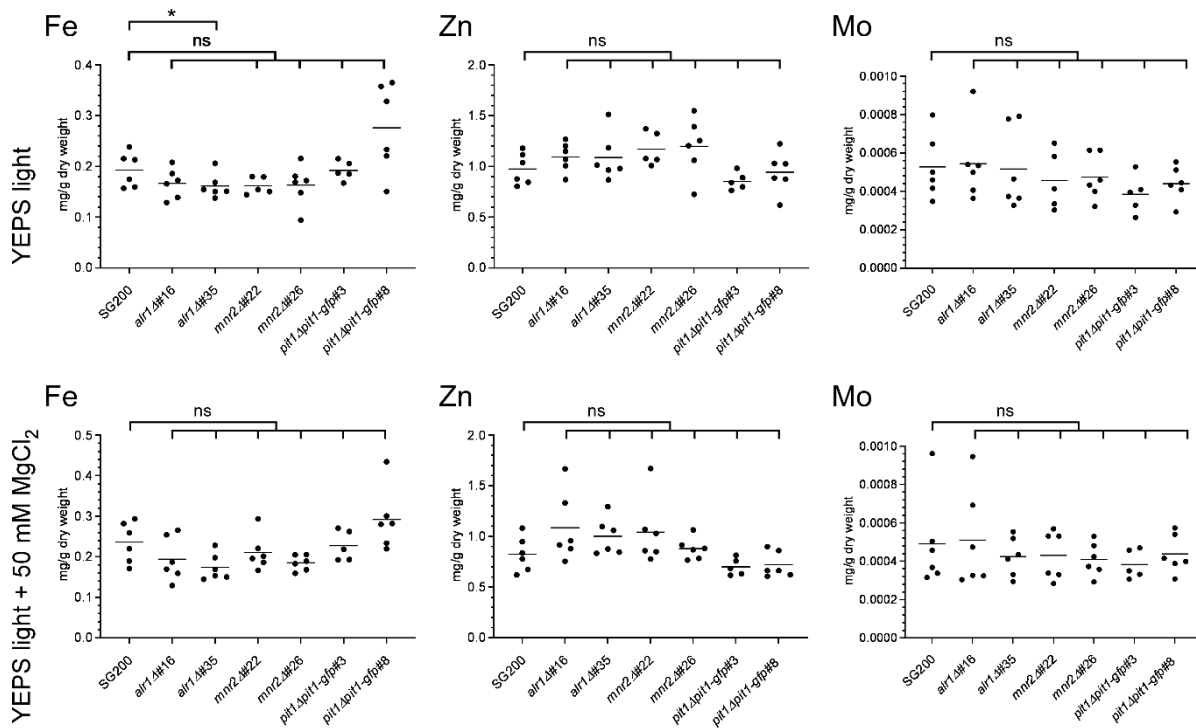


Figure 7-9 Analysis of the Fe, Zn and Mo composition of Mg^{2+} transporter mutants and Pit1-Gfp overexpression strains.

SG200, *alr1Δ*, *mnr2Δ* and Pit1-Gfp overexpression strains were pregrown in YEPS light supplemented with 50 mM $MgCl_2$ and subsequently shifted to standard YEPS light or YEPS light supplemented with 50 mM $MgCl_2$ complex medium for 8 h. The element composition of the cells was analysed using ICP-MS. For each element the concentration is given for every strain. Significance of differences between the respective strain and SG200 is indicated above (multiple unpaired t test comparisons calculated with Prism8 software).

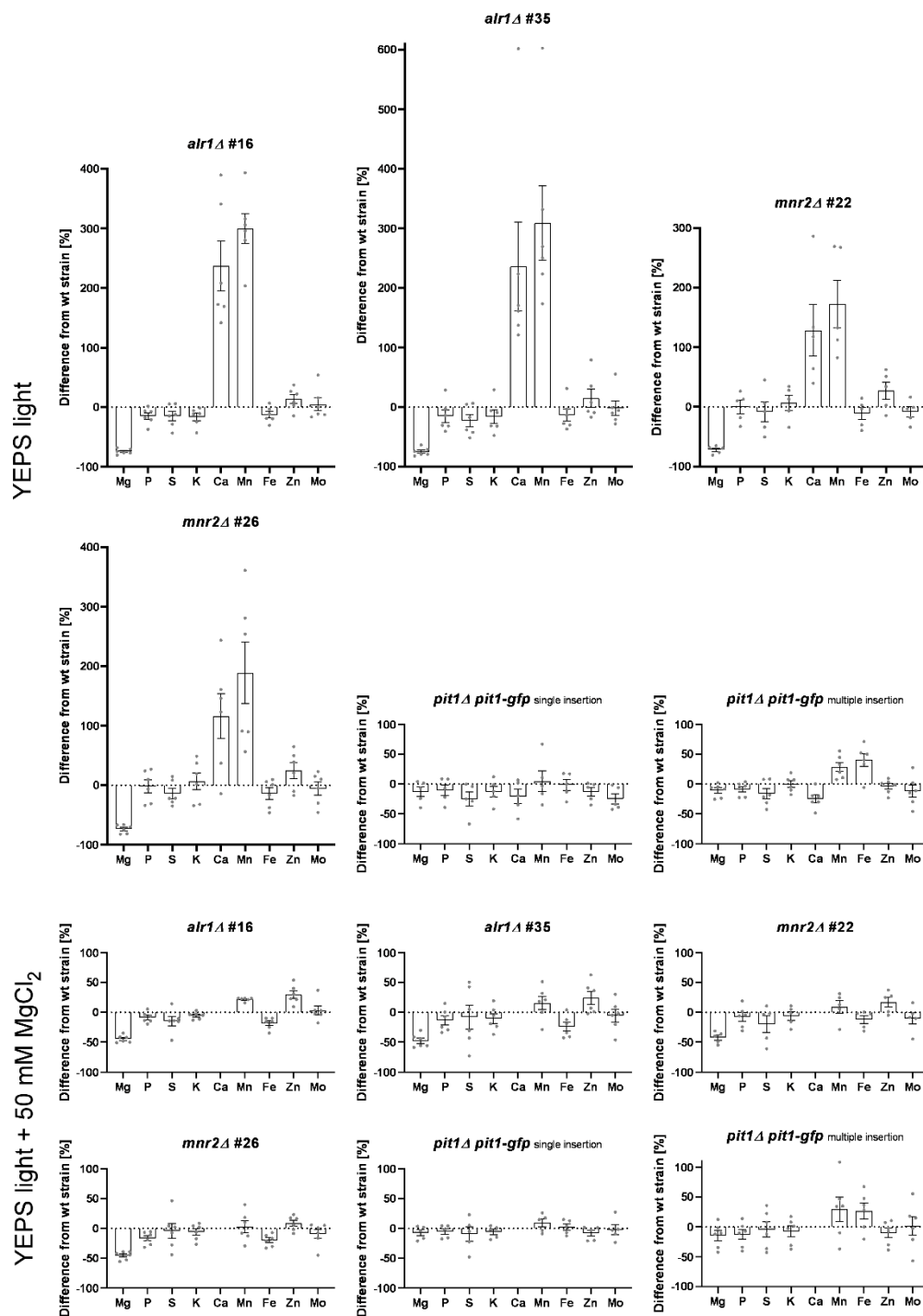


Figure 7-10 Analysis of the Mg, P, K, Ca, Mn, S, Fe, Zn and Mo composition of Mg^{2+} transporter mutants and Pit1-Gfp overexpression strains.

SG200, *alr1Δ*, *mnr2Δ* and Pit1-Gfp overexpression strains were pregrown in YEPS light supplemented with 50 mM $MgCl_2$ and subsequently shifted to standard YEPS light or YEPS light supplemented with 50 mM $MgCl_2$ complex medium for 8 h. The element composition of the cells was analysed using ICP-MS. For each strain, the difference of each element from the WT strain SG200 is shown. Mean values and SEM of six biological replicates are shown as well as the individual data points.

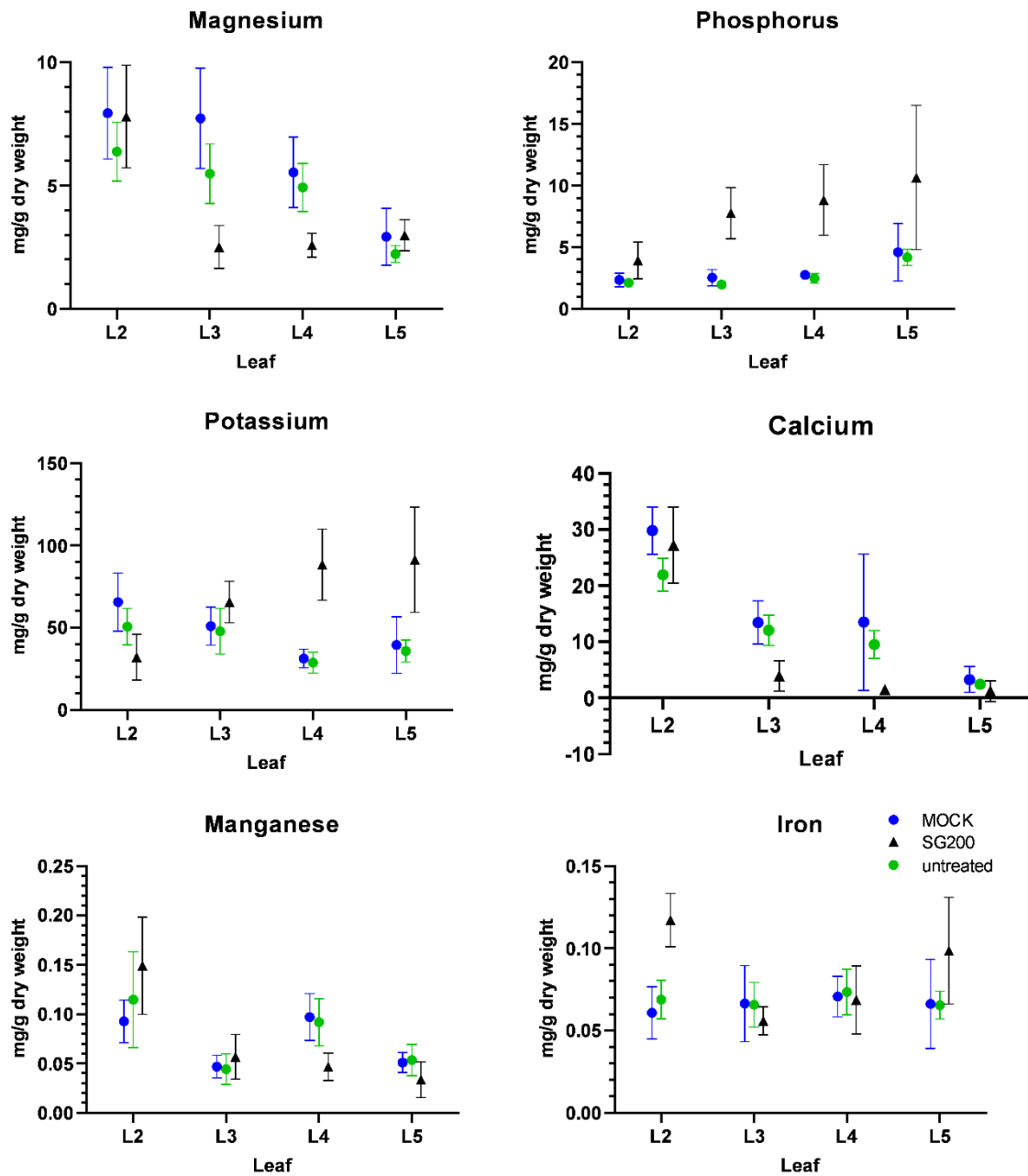


Figure 7-11 Analysis of the Mg, P, K, Ca, Mn and Fe composition of *Zea mays* Golden Bantam leaves after SG200 infection and MOCK treatment in comparison to untreated plants from one infection experiment. From 10 plants for each treatment the leaves L2-L5 were sampled and their elemental composition analysed via ICP-MS. Mean values and standard deviation are shown for each element and treatment.

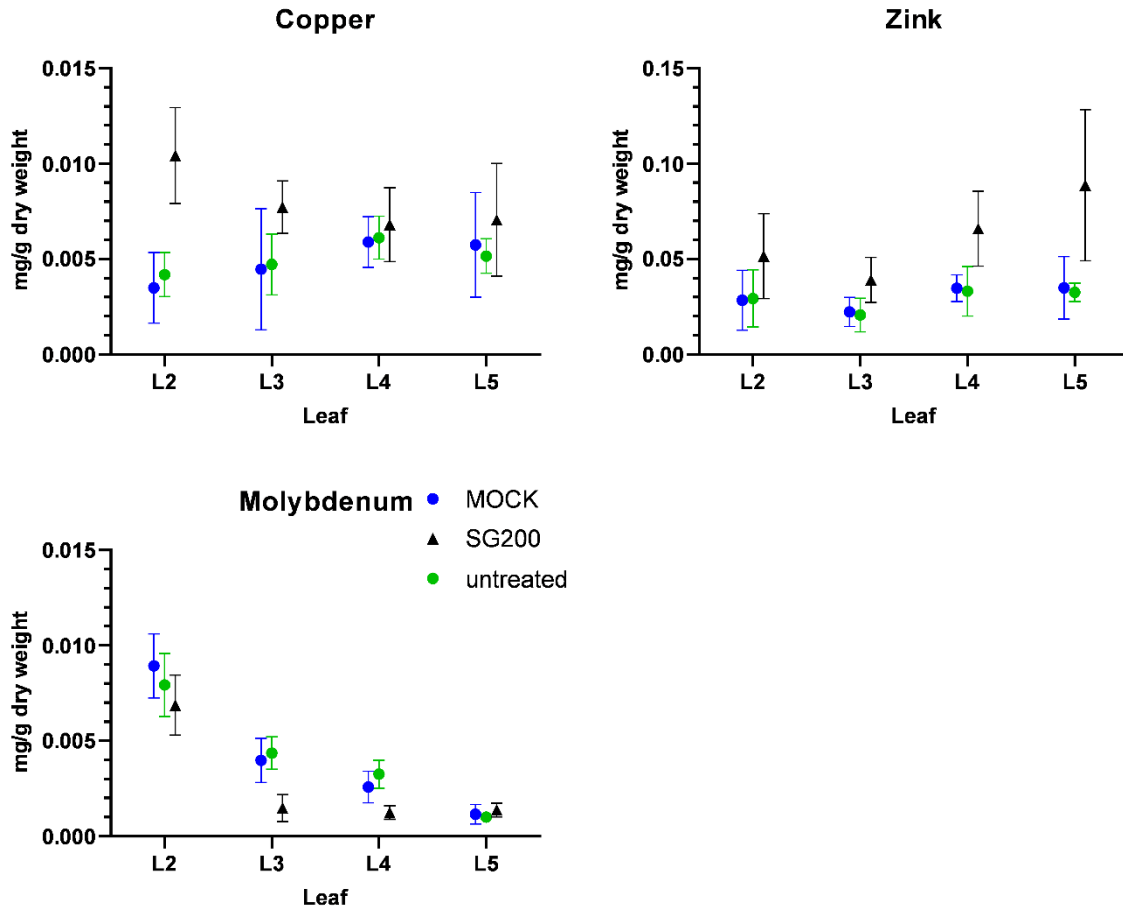


Figure 7-12 Analysis of the Cu, Zn and Mo composition of *Zea mays* Golden Bantam leaves after SG200 infection and MOCK treatment in comparison to untreated plants from one infection experiment. From 10 plants for each treatment the leaves L2-L5 were sampled and their elemental composition analysed via ICP-MS. Mean values and standard deviation are shown for each element and treatment.

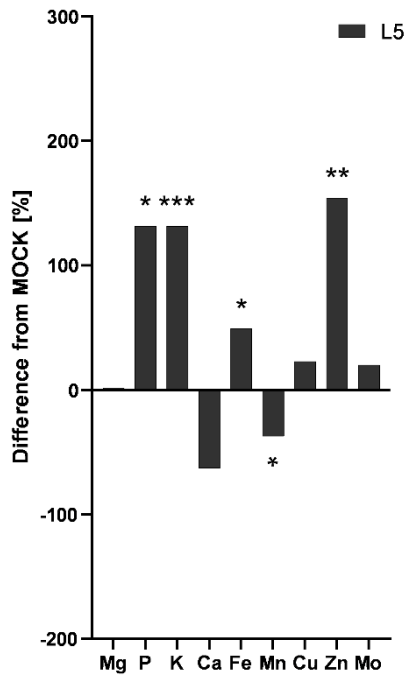


Figure 7-13 Element composition of *Zea mays* Golden Bantam leaves after SG200 infection and MOCK treatment in comparison to untreated plants from one infection experiment. Differences in element composition in % of SG200 infected L5 leaves in comparison to MOCK treated leaves. The level of significance is indicated by (*) above or below the respective bar (unpaired t test).

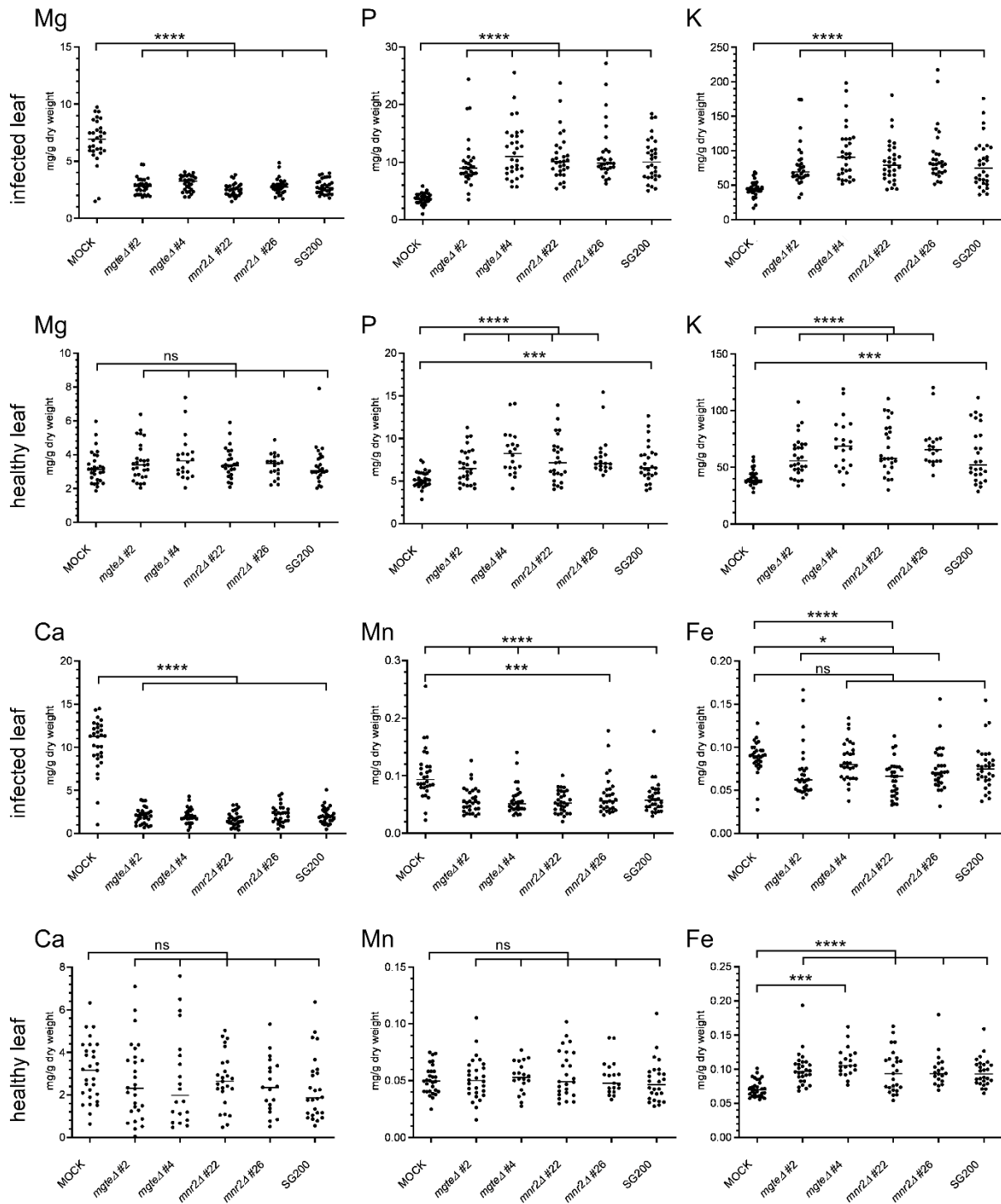


Figure 7-14 Analysis of the Mg, P, K, Ca, Mn and Fe concentration in Zea mays Golden Bantam leaves infected with SG200, *mgtE1* or *mnr21* in comparison to MOCK treated leaves. Scatter plots of three independent infection experiments with 10 biological replicates per experiment. Significance of differences between the respective strain and MOCK is indicated above (multiple unpaired t test comparisons calculated with Prism8 software).

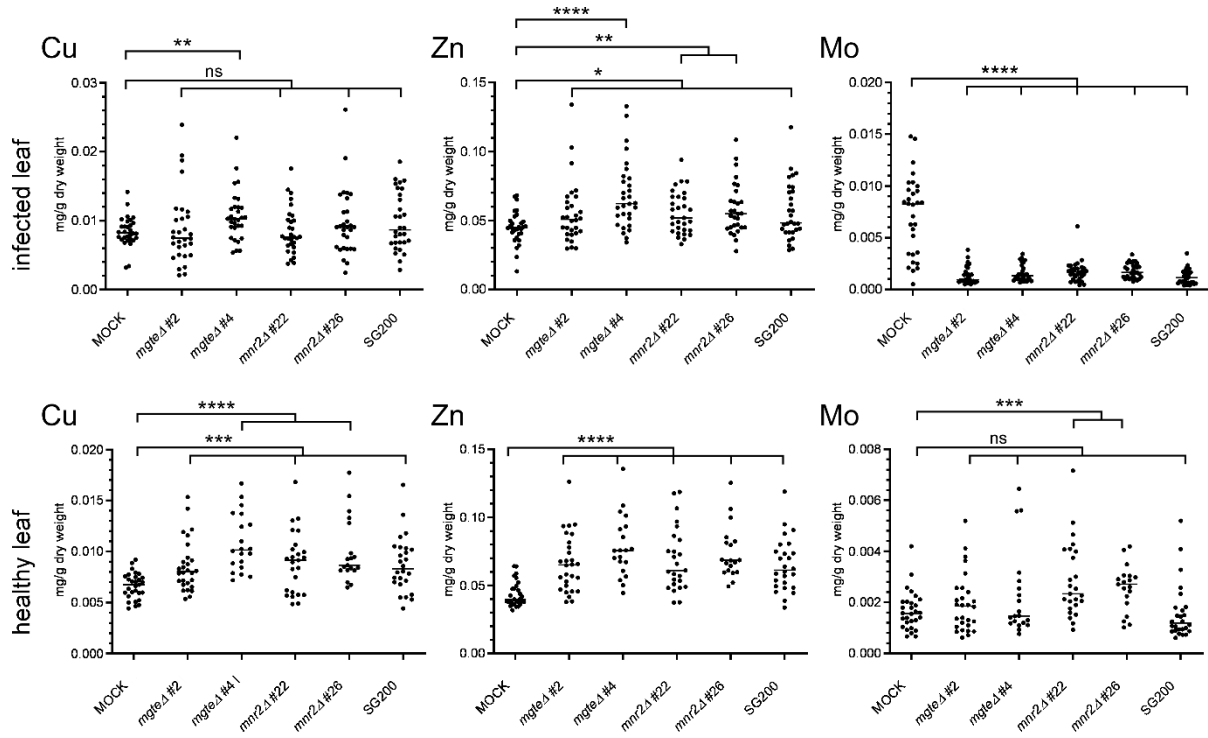


Figure 7-15 Analysis of the Cu, Zn and Mo concentration in *Zea mays* Golden Bantam leaves infected with SG200, *mgtEΔ* or *mnr2Δ* in comparison to MOCK treated leaves. Scatter plots of three independent infection experiments with 10 biological replicates per experiment. Significance of differences between the respective strain and MOCK is indicated above (multiple unpaired t test comparisons calculated with Prism8 software).

8 Acknowledgements

Ein herzliches Dankeschön an Michael für seine Unterstützung ein eigenes Projektthema in meine Doktorarbeit einzubringen und weiterzuentwickeln. Gleiches gilt auch Vera, die mich stets gefördert und gefordert hat und mein wissenschaftliches Arbeiten sehr geprägt hat. Vielen Dank auch für euer Engagement und eure Unterstützung bei meinen Bemühungen Familie und Wissenschaft miteinander zu vereinbaren.

Herzlich bedanken möchte ich mich auch bei Prof. Dr. Laura Rose für die Übernahme des Zweitgutachtens und die konstruktiven Diskussionen während der Committee-Meetings.

Außerdem möchte ich mich bei der Graduiertenschule iGRADplant bedanken, dass ich als assoziiertes Mitglied von den vielen Fördermöglichkeiten profitieren und an zahlreichen Veranstaltungen teilnehmen durfte.

Ein großes Dankeschön auch an alle aktuellen und ehemaligen RAB-Attack Mitglieder und das Mibi3 Team für all eure Hilfe, die freundschaftlich-familiäre Atmosphäre und die anregenden Diskussionen. Ohne euch hätte es deutlich weniger Spaß gemacht!

Sabrina, Karo und Peter, vielen Dank, dass ihr meine Arbeit als HiWis unterstützt habt, ihr wart eine enorme Hilfe.

Vielen herzlichen Dank auch an das gesamte Institut für die tolle Zusammenarbeit, die Unterstützung bei der einen oder anderen Frage, die vielen interessanten Gespräche und die tolle Atmosphäre.

Ein riesiges Dankeschön an meine Familie und ganz besonders an Martin, dafür, dass du mich stets unterstützt und mir mit so viel Verständnis für eine so lange Zeit den Rücken freigehalten hast, damit ich meine Ziele erreichen kann.

Statutory declaration

I hereby declare that this dissertation is the result of my own work, taking into account the “Rules and Principles for Safeguarding and Good Scientific Practice at Heinrich Heine Universität Düsseldorf”. This dissertation has not been submitted in the same or similar form to other institutions. I have not previously failed a doctoral examination procedure.

Eidesstattliche Erklärung

Ich versichere an Eides Statt, dass die Dissertation von mir selbstständig und ohne unzulässige fremde Hilfe unter Beachtung der „Grundsätze zur Sicherung guter wissenschaftlicher Praxis an der Heinrich-Heine-Universität Düsseldorf“ erstellt worden ist. Die Dissertation wurde in ihrer jetzigen oder ähnlichen Form noch bei keiner anderen Hochschule eingereicht. Ich habe zuvor keine erfolglosen Promotionsversuche unternommen.

Düsseldorf, September 2022

Lesley Plücker